

NOTE TO USERS

This reproduction is the best copy available.

UMI[®]

Micro cantilever based rheology of liquids

Ramin Motamedi

A Thesis

In the Department

of

Mechanical and Industrial Engineering

Presented in Partial Fulfilment of the Requirements

For the Degree of Doctor of Philosophy (Mechanical Engineering) at

Concordia University

Montreal, Quebec, Canada

August 2009

© Ramin Motamedi, 2009



Library and Archives
Canada

Published Heritage
Branch

395 Wellington Street
Ottawa ON K1A 0N4
Canada

Bibliothèque et
Archives Canada

Direction du
Patrimoine de l'édition

395, rue Wellington
Ottawa ON K1A 0N4
Canada

Your file *Votre référence*
ISBN: 978-0-494-71150-7
Our file *Notre référence*
ISBN: 978-0-494-71150-7

NOTICE:

The author has granted a non-exclusive license allowing Library and Archives Canada to reproduce, publish, archive, preserve, conserve, communicate to the public by telecommunication or on the Internet, loan, distribute and sell theses worldwide, for commercial or non-commercial purposes, in microform, paper, electronic and/or any other formats.

The author retains copyright ownership and moral rights in this thesis. Neither the thesis nor substantial extracts from it may be printed or otherwise reproduced without the author's permission.

AVIS:

L'auteur a accordé une licence non exclusive permettant à la Bibliothèque et Archives Canada de reproduire, publier, archiver, sauvegarder, conserver, transmettre au public par télécommunication ou par l'Internet, prêter, distribuer et vendre des thèses partout dans le monde, à des fins commerciales ou autres, sur support microforme, papier, électronique et/ou autres formats.

L'auteur conserve la propriété du droit d'auteur et des droits moraux qui protègent cette thèse. Ni la thèse ni des extraits substantiels de celle-ci ne doivent être imprimés ou autrement reproduits sans son autorisation.

In compliance with the Canadian Privacy Act some supporting forms may have been removed from this thesis.

While these forms may be included in the document page count, their removal does not represent any loss of content from the thesis.

Conformément à la loi canadienne sur la protection de la vie privée, quelques formulaires secondaires ont été enlevés de cette thèse.

Bien que ces formulaires aient inclus dans la pagination, il n'y aura aucun contenu manquant.


Canada

ABSTRACT

Micro Cantilever Based Rheology of Liquids

Ramin Motamedi, Ph.D.
Concordia University, 2009

In this work the objective was to extract the properties of high viscosity liquids using the vibrational response of the micro cantilevers utilized in the atomic force microscopes (AFM). Such an aim could not be achieved using thermal excitation of the cantilever because the energy given to the cantilever in this method is not enough to allow it to have a recognizable response. Instead we proposed the frequency sweep and step excitation techniques and we proved that they can be used to overcome such a limitation. These two methods are considered as two specific types of the acoustic excitation technique. The application of acoustic excitation to the cantilever in liquid resulted in many spurious peaks in the response, which make it impossible to identify the original cantilever response. Therefore, the first step of this study was to understand the real factors leading to this effect and to improve the design of the fluid cell. After achieving such a goal, we focused on the extraction of the fluid properties by comparing the theoretical analysis with the experimentally obtained results. During our study we implemented the previously established theory for the frequency sweep and we managed to develop the theory for the step excitation technique by ourselves. We proved that although both methods are successful in analysing high viscosity liquids, the step excitation technique was better than the frequency sweep method mainly in having an exact theoretical solution rather than a solution in the form of a series. This enabled us to increase the

accuracy of the theoretically obtained results by diminishing the truncation error. In addition, for determination of the fluid properties from the frequency sweep data, three different methods were proposed. These were to determine the properties of the fluids through the whole frequency range using the phase response or the amplitude response or by using both responses at each excitation frequency. Finally, we explained how to extend our work in order to serve for the studies being made on the non-Newtonian fluids and we also mentioned few guidelines to help in focusing such efforts to achieve the best results expected.

Dedicated to my Mom Goli and Dad Masoud.

ACKNOWLEDGMENTS

I first take this opportunity to express my appreciation to my advisor, Dr. Paula Wood-Adams, for believing in me and for her continuous support during my research. Her useful and practical suggestions made accomplishment of this work possible.

I would like to thank my parents and my sister. Without their support, encouragement and patience, I would not be able to succeed in my studies.

A special thanks goes to Hany Gomaa who provided invaluable assistance in completion of this work.

Last but not least, I want to thank my colleagues and friends Sina Chaeichain, Mohsen Jalali, Arkadz Fatseyeu, Yury Yuryev, Wang Heng and Nithya Subramanian for their productive criticism and also for providing a nice environment to work with.

Table of Contents

List of Figures	x
List of Tables	xvi
List of Symbols	xvii
Chapter 1 Introduction and Literature Review	1
1.1) Different Applications of AFM	2
1.2) Different Techniques for Cantilever Excitation	4
1.3) Spurious Peaks in Frequency Response of Acoustic Excitation	8
1.4) Modeling of Cantilever Vibration in Viscous Fluids	12
1.5) Measurements of Rheological Properties Using AFM Cantilever ..	28
Chapter 2 Theory	36
2.1) Transverse Vibration of a Cantilever	37
2.2) Hydrodynamic Drag Force	42
2.3) Different Types and Kinematics of Excitation	48
2.3.1) Thermal Noise	48
2.3.2) Frequency Sweep	51
2.3.3) Step Excitation	54
Chapter 3 Experimental Setup, Sample Preparation and Data Processing	60
3.1) Experimental Setup	60
3.1.1) Atomic Force Microscope (AFM)	62
3.1.2) Signal Generator	63
3.1.3) Data Acquisition (DAQ)	64

3.1.4)	Cantilever Material and Dimensional Properties	65
3.2)	Sample Preparation	67
3.3)	Signal Processing	73
Chapter 4	Critical Issues in the Design of Fluid Cells and Tip Holders	79
4.1)	The Holding Mechanism of Cantilever Chip in the Fluid Cell	81
4.2)	The Fluid-Borne Excitation	83
4.3)	The Location of Piezo Element	85
4.4)	Supporting and Gluing the Piezo to the Tip Holder	90
Chapter 5	Experimental Results for Different Excitation Techniques	94
5.1)	Averaging of Data	94
5.2)	Checking the Concentration Changes Over Time	98
5.3)	Reproducibility of the Experiments Respect to Both FS and SE	103
5.4)	Linearity With Respect to the Drive Amplitude for FS and SE	105
5.5)	Confirmation of Linear Viscoelasticity by Examining Higher Harmonics	110
5.6)	Discussion of the Experimental Results	117
5.7)	Discussion on the Theoretical Results	131
5.8)	Finding the Properties of Newtonian Fluids from Their FS Experimental Data	133
5.9)	Extending the Micro Cantilever Based Rheometry to Non- Newtonian Fluids	143
Chapter 6	Conclusions, Contributions, Future Works	151
6.1)	Conclusions	151

6.2) Contributions	153
6.3) Future Works	154
References	156
Appendix A	164
Appendix B	166
Appendix C	169
Appendix D	171
Appendix E	173
Appendix F	178
Appendix G	180
Appendix H	182
Appendix I	188
Appendix J	196
Appendix K	202
Appendix L	210
Appendix M	220
Appendix N	226
Appendix O	234

List of Figures

Figure 1.1	Schematic of the major excitation techniques	5
Figure 1.2	Schematic of different minor excitation techniques	7
Figure 1.3	Typical response of a cantilever in liquid environment	9
Figure 1.4	A schematic drawing of a cantilever, with a rectangular cross section, while oscillating in a medium at the 5 th mode of vibration	17
Figure 1.5	A schematic drawing of a cylindrical tube of viscous fluid surrounding concentrically a vibrating cylindrical cantilever	20
Figure 2.1	Free-body diagram of an element of length dx	37
Figure 2.2	The first three mode shapes for a beam with one end fixed and other end free	40
Figure 2.3	A circular cylinder oscillating transversely along a diameter	43
Figure 2.4	Theoretical response of a silicone cantilever which is excited thermally	51
Figure 2.5	Theoretical response of a silicone cantilever which is excited with a frequency sweep	54
Figure 2.6	Theoretical responses of a silicone cantilever to step excitation	58
Figure 3.1	Schematic of experimental setup	61
Figure 3.2	Optical system of the AFM	63
Figure 3.3	PCI-5402 - Signal Generator	64
Figure 3.4	PCI-6132 - Multifunction DAQ (S series)	65
Figure 3.5	CLFC-NOBO tipless cantilever from Veeco	66
Figure 3.6	Density of glycerin-water solution in terms of its concentration at	68

temperature of 26 °C	
Figure 3.7 Viscosity of glycerin-water solution in terms of its concentration at temperature of 26 °C	68
Figure 3.8 Linear Viscoelastic Properties for 8.5% PS solution, 25 °C	71
Figure 3.9 Linear Viscoelastic Properties for 12% PS solution, 25 °C	71
Figure 3.10 Linear Viscoelastic Properties for 16% PS solution, 25 °C	72
Figure 3.11 Linear Viscoelastic Properties for 25% PS solution, 25 °C	72
Figure 3.12 The algorithm of the LabVIEW code written for controlling the signal generator and the DAQ hardware and also for analyzing the recorded data	73
Figure 3.13 The front panel of the virtual instrument developed by the LabVIEW ...	75
Figure 4.1 Schematic of a fluid cell from Veeco (MTFML model)	80
Figure 4.2 Schematic of a regular tip holder from Veeco (MMMC model)	80
Figure 4.3 Frequency responses with different cantilever base and clip positions (in water)	82
Figure 4.4 Repeatability of the frequency response of a cantilever when glued to the fluid cell (in water)	83
Figure 4.5 Cross section of the fluid cell defined in Figure 2 (a) before modification and (b) after modification	84
Figure 4.6 Frequency responses of the cantilever in 50% glycerine-water solution before (black line) and after (gray line) installing the reservoir	85
Figure 4.7 Cantilever response in three solutions of glycerine and water; a) measured by AFM optics, b) determined theoretically	87

Figure 4.8 Fluid cell frequency responses when containing solutions of glycerine and water	88
Figure 4.9 Fluid cell frequency responses obtained from excitation of two different cantilevers in 75% glycerine-water solution	89
Figure 4.10 Two common mechanisms for supporting the piezo; a) gluing and b) clamping	91
Figure 4.11 The effect of utilizing different mechanism of supporting the piezo on the thermal noise response of long cantilever which was immersed in water	92
Figure 5.1 The effect of vector averaging on data records for step excitation of 50% glycerine-water solution in time domain	95
Figure 5.2 The effect of RMS on averaging data records for thermal noise of 50% glycerin-water solution in frequency domain	96
Figures 5.3 Vector averaging (a) and RMS averaging (b) for the damped part of step excitation for 50% glycerine-water solution	97
Figure 5.4 The schematic of the modified cantilever holder which shows the interface between the examined fluid and the surrounding air	99
Figure 5.5 Thermal noise responses of a cantilever in 25% glycerin-water solution over time	99
Figure 5.6 Thermal noise responses of a cantilever in 50% glycerin-water solution over time	100
Figure 5.7 Thermal noise responses of a cantilever in 75% glycerin-water solution over time	100

Figure 5.8 Thermal noise responses of a cantilever in 50% glycerin-water solution over time	102
Figure 5.9 Resonant frequency shift because of concentration change over time for %50% glycerin-water solution	103
Figure 5.10 The inclination of the cantilever for the first modes of vibration	104
Figure 5.11 Linearity with respect to the drive amplitude for the frequency sweep test. For this test the long cantilever was immersed in water	106
Figure 5.12 Linearity with respect to the drive amplitude for the step excitation test. For this test the long cantilever was immersed in glycerin	107
Figure 5.13 Linearity with respect to the drive amplitude for the frequency sweep test. For this test the long cantilever was immersed in 16% PS/DEP	108
Figure 5.14 Linearity with respect to the drive amplitude for the step excitation test. For this test the long cantilever was immersed in 8.5% PS/DEP	109
Figure 5.15 Appearance of peaks at harmonics of excitation frequency for long cantilever surrounded by air	113
Figure 5.16 Appearance of peaks at harmonic frequency of excitation frequency for long cantilever immersed in water	114
Figure 5.17 Appearance of peaks at harmonic frequency of excitation frequency for long cantilever immersed in 16% PS solution	115
Figure 5.18 Linear relationship between the magnitudes of the peaks, located at excitation frequency and its harmonics, and the driving amplitudes for 16% PS solution	116
Figure 5.19 Thermal noise for long cantilever immersed in water	117

Figure 5.20 Thermal noise for medium cantilever immersed in water	119
Figure 5.21 Thermal noise for long cantilever immersed in 50% glycerine-water	119
Figure 5.22 Amplitude response of frequency sweep excitation for the long cantilever immersed in water	122
Figure 5.23 Phase response of frequency sweep excitation for the long cantilever immersed in water	122
Figure 5.24 Comparison of the amplitude responses of several long cantilevers, which are all immersed in water	124
Figure 5.25 Unwrapped phase response for long cantilever immersed in water	125
Figure 5.26 Unwrapped phase drift of the AFM for drive amplitude of 10 (V)	126
Figure 5.27 Unwrapped phase response which the effect of phase drift is removed. The long cantilever was used for this result and the surrounding fluid is water	127
Figure 5.28 The response of the long cantilever which is immersed in water to the step excitation (a) in the frequency domain and (b) in the time domain ..	129
Figure 5.29 Illustration of the original and noiseless experimental data for the long cantilever which is immersed in water	135
Figure 5.30 Measured and real density of glycerine-water solutions using long and medium cantilevers	136
Figure 5.31 Measured and real viscosity of glycerine-water solutions using long and medium cantilevers	137
Figure 5.32 Error between the measured and real properties of glycerine-water solutions using long and medium cantilevers	138

Figure 5.33.Determined properties of water at each frequency of excitation using the long cantilever	142
Figure 5.34 The comparison between the frequency sweep responses of the long cantilever immersed in %16 PS/DEP solution as a non-Newtonian fluid and immersed in water and pure glycerine as two Newtonian fluids	145
Figure 5.35 The comparison between the theoretical and experimental responses of frequency sweep excitation for the long cantilever immersed in %16 PS/DEP solution	147
Figure 5.36 The comparison between the theoretical and experimental responses of frequency sweep excitation for the medium cantilever immersed in %16 PS/DEP solution	148

List of Tables

Table 2.1 The values of some important parameters of cantilever vibration for the first six modes of vibration	41
Table 3.1 Properties of Newtonian fluids at 26 °C which were examined in this project	69
Table 3.2 Properties of non-Newtonian fluids at 25 °C which were examined in this project	70

List of Symbols

A	– cross section area
A_{FS}	– amplitude of cantilever base oscillation in frequency sweep excitation
A_{noise}	– the averaged value of noise floor
A_{SE}	– amplitude of cantilever base oscillation in step excitation
b	– cantilever width
C	– separated variable in time space which is transformed in Fourier domain
C^*	– overlap concentration
C_∞	– characteristic ratio
c	– separated variable in time space
D	– diameter of the circular beam
d	– damping coefficient
E	– Young's modulus
F_B	– the applied force on cantilever because of Brownian motion
F_d	– drag force
F_{drive}	– driving force
F_{hydro}	– hydrodynamic force
f	– frequency
f_{ref}	– reference frequency
G_d	– dynamic modulus

I	– moment of inertial
K_0	– modified Bessel function of the third kind
K_1	– modified Bessel function of the third kind
K_B	– Boltzmann's constant
L	– cantilever length
l	– carbon-carbon bond length
M	– internal moment
M_w	– weight averaged molecular weight
N_A	– Avogadro's number
n	– number of monomers in the chain
P	– stress tensor
R	– radius
R_g	– radius of gyration
Re	– Reynolds number
r	– radial coordinate
T	– absolute temperature
t	– time
U_0	– velocity amplitude of a circular beam
u	– velocity of a circular beam
V	– internal shear force
v	– fluid velocity

\hat{W}	– relative motion of the cantilever to the movement of its base in frequency domain
w	– relative motion of the cantilever to the movement of its base in time domain
x	– spatial coordinate along the length of the cantilever
Y	– displacement in the y direction in the frequency domain
\hat{Y}_b	– displacement of cantilever base in the frequency domain
y	– displacement and cantilever deflection in the y direction in the time domain
y_b	– displacement of cantilever base in the time domain
α	– modal parameter
β	– modal parameter
Γ	– hydrodynamic function
γ_0	– strain amplitude
γ	– strain
δ	– mechanical loss angle , thickness of the layer of fluid surrounding the cantilever at which the velocity has decreased by $1/e$
θ	– tangential coordinate
λ	– modal parameter
μ	– viscosity
ρ	– density
σ	– stress
τ	– a function defined for calculation of Ω
ϕ	– separated variable in spatial space
ψ	– stream function

Ω	– correction function
ω	– angular frequency
ω_0	– excitation frequency
$\omega_{vac,1}$	– fundamental resonant frequency of the cantilever in vacuum
c	– cantilever
$circ$	– circular cross section
exp	– experimental
f	– fluid
Im	– Imaginary part of a complex number
i	– mode number
j	– mode number
m	– harmonic number
Re	– real part of a complex number
r	– radial component
$rect$	– rectangular cross section
$theo$	– theoretical
y	– y direction
θ	– tangential component
\wedge	– stand for a transformed Fourier variable

Chapter 1

Introduction and Literature Review

The atomic force microscope (AFM) was invented in 1986 by Gerd Binnig et al¹. It originated from the scanning tunnelling microscope (STM) which was a Nobel Prize winning invention in physics. With the help of the AFM, the surface of samples can be imaged with a resolution on the order of fractions of nanometers which is 1000 times more than any optical diffraction limit. The AFM was originally designed based on its operation in contact mode meaning that the height image of the sample can be obtained by monitoring and calibrating the deflection of the micro-cantilever as it moves on the sample surface. The cantilever deflection is typically measured by optical or by electrical means. Because of the destructive effect of this mode on the surface of soft samples, the next generation of the AFMs had the tapping mode, also called the dynamic mode. In this mode, the micro-cantilever is excited such that it oscillates at a frequency close to its primary natural frequency and by monitoring the amplitude of vibration, as the cantilever scans the sample surface, the height image is produced.

Besides imaging, many other applications have been developed for the AFM since its invention. In this project we focused on one of these applications which is the measurement of rheological properties of fluids on the micro scale. This chapter is dedicated to the previously related works in this field and provides background for understanding the rest of the work. The content of this part is structured as follows. First, we describe different applications of AFM. After that some common techniques for

exciting the AFM cantilevers were explained. Then it is followed by introducing the difficulties of the acoustic excitation, which is our preferred excitation method, in a liquid environment. The development in modeling of cantilever frequency response is presented next, and finally, we focus on the microcantilever based rheological measurements as one of the recent applications of the AFM.

1.1) Different applications of AFM

Although the AFM was originally designed for the purpose of imaging surfaces, its high sensitivity in detecting forces, on the order of picoNewtons, made it applicable for the measurement of atomic interaction forces, magnetic forces, electric forces, friction forces, and also in the investigation of mechanical properties and structures of soft materials at the nanometer scale. In contrast to the STM, that can be used only for conductive surfaces, the AFM enables the scientists to investigate and scan, in atomic scale, both conductive and isolative surfaces of samples ranging from metallic and inorganic materials to polymeric and biological materials. Introducing the tapping (dynamic) mode for AFM and the invention of some accessories, including the fluid cell, also expanded the applicability of the instrument for imaging of more delicate materials in their natural environment^{2,3,4}. In the tapping mode, lateral forces which can cause scratches and the removal of weakly attached molecules on the surface are reduced considerably. Beside force measurement and imaging, many other applications were developed in which the AFM can be used as a sensor. For example, its use as a temperature sensor, gas sensor, spectrometer, calorimeter, environmental sensor,

microbalance, stress detector, or even as an electrochemical electrode were just a few applications that Berger et al⁵ reviewed in detail.

One of the applications of AFM that has received a lot of attention recently, is measuring the rheological properties of fluids^{6,7}. The physics behind this application is that the oscillatory behavior of the AFM cantilevers depends strongly on the properties of the medium in which they are vibrating. For example, the resonant frequencies and quality factors (i.e. the sharpness of the peaks) in the frequency response of the cantilever reduce in liquids compared to those of the cantilever in air. Therefore, by observing these changes in vibrational characteristic of the cantilever, one can determine the properties of the fluid. The important advantages of this technique are, primarily, the small quantity of the fluid (on the order of micro litre) and the relatively compact apparatus required for the measurement, secondarily, local measurements of non-homogenous fluids, and finally, in some cases faster measurement of rheological properties compared to the conventional methods. However, the use of the AFM in dynamic mode is challenging in liquid media because of the complex hydrodynamic force acting on the cantilever. Also several factors that originate from the design of the cantilever holder significantly affect the frequency response. Therefore, understanding the influence of each of these factors is necessary for the reliable operation of the AFM in liquid media. This issue comprises part of the current work however the main focus is the extension of this technique for high viscosity Newtonian fluids and the investigation of the applicability of this method for non-Newtonian fluids.

1.2) Different techniques for cantilever excitation

For the various applications of the AFM, there are many different techniques to excite the micro-cantilever. Since the main differences in these techniques are due to the types of driving force, the response of the cantilever strongly depends on the chosen excitation technique, especially when it is used in a liquid environment. The three major types are thermal excitation, magnetic excitation and acoustic excitation, which are shown schematically in Figure 1.1 and explained briefly in the following paragraphs.

In thermal excitation^{8,9} (Figure 1.1 a), the cantilever response is the result of random collisions due to the Brownian motion of the surrounding fluid molecules. In this technique, the cantilever is excited directly and consequently a smooth vibration response, related only to the properties of the cantilever and the fluid, is observed. Moreover, this technique provides the smallest possible oscillation at a given temperature which is useful in imaging of very smooth surfaces. But knowing that the thermal driving force is stochastic in nature, we comprehend that this method is not helpful in determining any information concerning the cantilever phase response, and for example it cannot be used to measure any surface mechanical properties. However, the main applications of this technique are to estimate the cantilever resonant frequency and to measure the rheological properties of low viscosity Newtonian fluids.

Another direct excitation method is the magnetic excitation technique^{10,11,12} (Figure 1.1 b), which provides a smooth vibration response as well. For such a technique, a micro-cantilever is magnetized either by attaching a magnetic particle¹¹ to it or by coating it with a magnetic material¹², then it is stimulated by an external varying magnetic field. This gives one the flexibility of using many types of cantilevers in many different

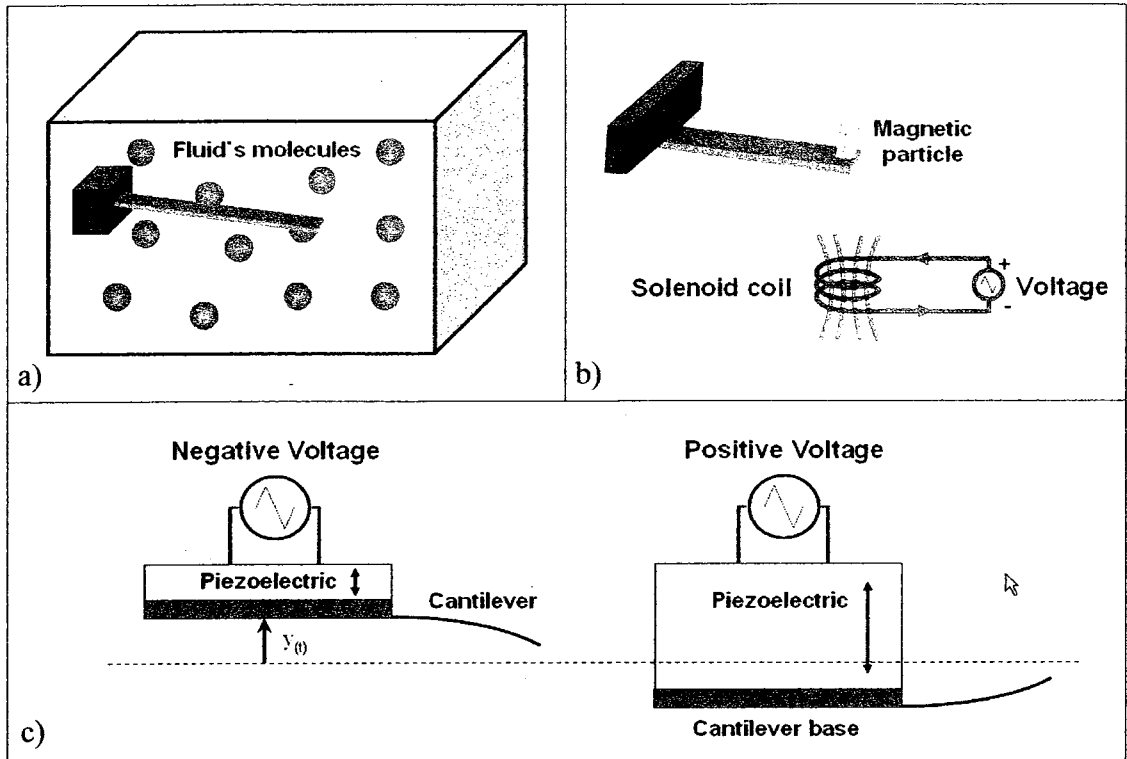


Figure 1.1 Schematic of the major excitation techniques. a) thermal noise b) magnetic excitation c) acoustic excitation.

environments. However such coating changes the cantilever vibration properties. Moreover, the vibration properties of the cantilever can be affected also by the changes in its mass as the magnetized cantilever absorbs some magnetic particles from the surrounding environment over time. Finally, the fluid will be heated as a result of using the magnetic field which affects the fluid's rheological properties.

In the case of acoustic excitation⁴ (Figure 1.1 c), the cantilever is excited through movement of its base by a piezoelectric actuator. This is an indirect method, meaning that the driving force is applied to the cantilever indirectly through its base. The actuator is usually placed directly under the cantilever chip in the tip holder that is used in air or vacuum, while it is usually located away from the cantilever base in the fluid cell which is used for liquid media. As will be explained in detail later on, the response of the

cantilever to acoustic excitation in a liquid environment contains many spurious peaks which do not correspond to the natural frequencies of the cantilever and are rather related to the design of the fluid cell.

In addition to the techniques mentioned above, there are several other excitation techniques of minor importance which are clarified in Figure 1.2. For example, Scherer et al¹³ proposed a technique (Figure 1.2 a) that uses electrostatic forces for cantilever actuation. In this method, an electric field is applied between the AFM cantilever tip and a sharpened steel electrode. Such a technique allows the exertion of a point force on the cantilever and the freedom of choosing any arbitrary function for the applied force. Moreover, the response of the cantilever, which was measured using a laser Doppler vibrometer (LDV), proved to show no extra spurious peaks. However, this technique can only be used for a conductive cantilever that is immersed in a non conductive medium such as a dielectric liquid or gas. These disadvantages were resolved by the acoustic radiation pressure method (Figure 1.2 b), proposed by Degertekin et al¹⁴. This is done by, applying a localized force via a pressure wave, focused on the cantilever tip, produced by a micro machined acoustic transducer. This technique is mainly used for characterizing the cantilever and measuring its frequency response while giving an additional flexibility to be applied to many cantilevers of arbitrary shape and material. Another technique was introduced by Buguin et al¹⁵ (Figure 1.2 c), which resembles the previously introduced magnetic excitation technique in its method of operation only. Here the AFM cantilever is forced to oscillate by passing an AC current through it while putting it in a permanent magnetic field, and as a result, the resulting Lorentz forces cause the cantilever to vibrate. This method has the additional advantage of its cantilever being in a pure unmodified

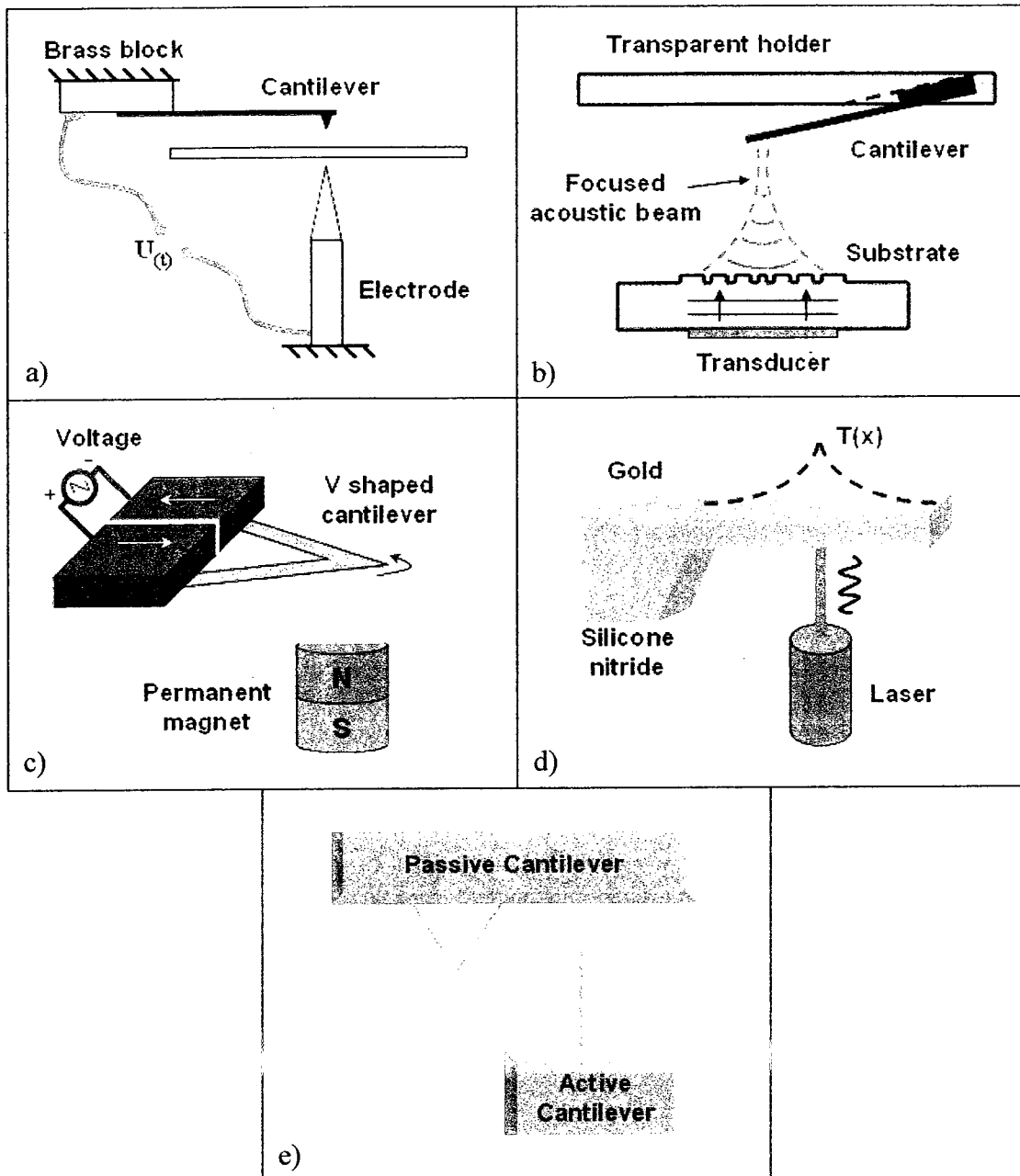


Figure 1.2 Schematic of different minor excitation techniques. a) electrostatic excitation b) acoustic radiation pressure excitation c) magnetic (Lorenz forces) excitation d) photothermal excitation e) fluid driven excitation.

state, unlike the magnetic excitation where the cantilever had to be coated by magnetic material or a magnetic glued particle. However, the cantilever again must also be conductive and this method is only limited to the V shaped cantilevers because they can

provide a closed circuit. The photothermal technique (Figure 1.2 d) is an additional method that was introduced by Ratcliff et al¹⁶, where they used a modulated laser on a metal coated cantilever which allowed for bending because of different thermal expansion coefficients of the metal and the core material. The regular optical system of the AFM was used in order to measure the cantilever vibrations. But again such a technique was restricted to bi-material cantilevers only¹⁷. Last but not least, was the technique introduced by Volkov et al¹⁸ (Figure 1.2 e), which used fluid force, in the vicinity of the cantilever, as its excitation method. Such a technique uses two different cantilevers, one passive and the other active. The piezo on the active cantilever is used to drive the fluid in vicinity of the passive cantilever whose vibration is continuously monitored. In this way, it was shown that many of the spurious peaks appearing in the acoustic excitation method no longer exist. Moreover, cantilevers of many materials, types and shapes can be used.

1.3) Spurious peaks in frequency response of acoustic excitation

Among the three main excitation techniques, acoustic excitation is thought to be the preferable one although the thermal and magnetic driving methods produce smoother cantilever responses. This is mainly because the cantilever used for this technique does not need any modification and special coating and its amplitude of vibration is big enough for different application of the AFM. Moreover, the later two techniques require additional hardware such as a signal conditioner, a data acquisition system, special cantilevers, and a magnetic field system making the two techniques more complex and

costly. However the most important disadvantage of acoustic excitation, as mentioned before, is that the response of the cantilever in a liquid environment usually contains many spurious peaks which do not correspond to the natural frequencies of the cantilever (see Figure 1.3). Therefore many investigations have been carried on to understand the nature of these redundant peaks and to improve the acoustic excitation technique^{4,12,19-24}.

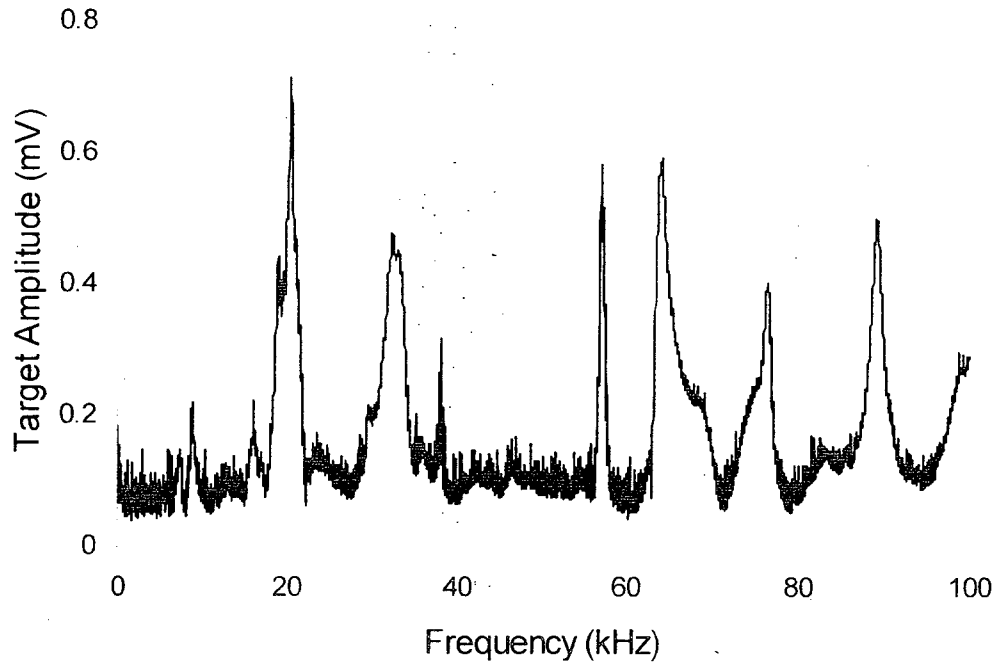


Figure 1.3 Typical response of a cantilever in liquid environment within a fluid cell.

Putman et al⁴, who were the pioneers in introducing tapping mode atomic force microscopy in liquid media, were faced with these extra frequency peaks for the first time. They realized that any changes in the liquid cell system, such as changing its geometry, its material, the working liquid, and more importantly the amount of liquid, affect the positions and amplitudes of the resonances. Schaffer et al¹⁹ observed experimentally the same frequency response dependency upon the fluid cell system's

geometrical and material design issues. Based on their observations of the responses of different cantilevers in the same liquid environment, Schaffer et al¹⁹ proposed the hypothesis that “the cantilever response spectrum is the product of a fluid drive spectrum, which depends only on the cantilever module and fluid, and the thermal noise spectrum, which depends only on the cantilever and fluid”. Their hypothesis was supported by measuring the fluid drive spectra of three different cantilevers in the same environment and showing that their shapes are very similar. Moreover, they showed experimentally that the mode shapes of the vibrating cantilever are independent of the fluid drive spectrum and depend only on the vibrational characteristics of the cantilever in the fluid. Other researchers, who used different types of AFMs and fluid cells which in some cases were made in-house, also reported the appearance of spurious peaks^{12,20,21}. For example, Xu et al²² used an Agilent AFM with a modified fluid cell in order to apply different types of excitations to the micro cantilevers and measure their responses under identical conditions. For acoustic excitation, they also observed the spurious peaks in the response of the cantilever and based on their theory, which will be explained in the next section, they determined the fluid drive spectrum. Xu et al²² reached a similar conclusion as Schaffer et al¹⁹ in that the response of cantilever in acoustic excitation is the result of two mechanisms: a) structure-born excitation and b) fluid-born excitation. The first mechanism is ideal acoustic excitation but when combined with the other mechanism, spurious peaks are observed in the cantilever response. Also, it was shown that Schaffer et al’s method¹⁹ for determination of the fluid-born excitation is as a special case in the analysis of Xu et al²² because Schaffer et al¹⁹ approximated the structure-born excitation with the thermal noise of the cantilever.

Even in other instruments with similar concept and mechanism for excitation of their cantilever, these redundant peaks appeared. Kirstein et al²⁰ observed such extra peaks in the frequency response of a circular cantilever in an in-house built near field optical microscope. They proved that these peaks are related to vibrations of some parts in the instrument. This was done by comparing the responses of a single cantilever in two different media, air and water, and observing the existence of some peaks at the same frequencies for both responses.

Although the effects of the various design problems on the cantilever response were previously recognized, the exact relationships were not understood and the early improvements of the frequency response based on control of these factors had not been considered. Instead efforts were focused on other approaches. Tamayo et al²³ mixed the standard driving signal with a feedback signal from the cantilever response such that they could increase the quality factor of the cantilever oscillations by up to three orders of magnitude. However their technique is very sensitive to viscosity variations and is, therefore, limited by small temperature fluctuations. Rogers et al²⁴ used another approach. They attached a piezoelectric microactuator over the axial surface of a microcantilever and insulated it from the conductive liquid medium using a fluoropolymer coating. In this way they could excite the microcantilever by applying a direct force, resulting in the disappearance of redundant peaks. However, this technique is no longer standard acoustic excitation and like the magnetic coated cantilevers, the vibrational properties and bending angle of their cantilevers are changed.

Because of the particular design of commercial fluid cells, it is impossible to apply ideal acoustic excitation to the cantilever resulting in an even more complicated

frequency response. As a part of this project, we apply some simple modifications to a widely used commercial fluid cell from Veeco²⁵ (MTFML model) in an effort to approximate ideal acoustic excitation and in this way investigate the frequency response of the cantilever in this cell without fluid born excitation and certain design related aspects. We will show that the vibration of the fluid cell body is the most significant disturbance in the observed frequency response.

In the next section, the development in the theory of cantilever frequency response will be summarized in order to provide a proper background for understanding the modeling used in the results and the other experimental parts.

1.4) Modeling of cantilever vibration in viscous fluids

The theoretical response of a vibrating AFM cantilever in vacuum is well known^{26,27}. However, the vibrational characteristics of such a cantilever will change considerably when it is immersed in a viscous fluid. Since the sensitivity of the AFM depends directly on the oscillatory behaviour of the cantilever, it is important to understand such phenomena.

The vibration of any solid body results in a flow in the surrounding fluid by dragging the fluid as it moves. This increases the effective mass of the moving body and as a result its resonance frequency decreases. The effective mass of such a body includes its actual mass and the mass of the moving fluid which is called the induced mass. In hydrodynamics the induced mass is referred to sometimes as the added mass or the virtual mass^{28,29,30}. On the other hand, the moving fluid contributes some damping effects

to the oscillatory behaviour of the body resulting in a decrease in its amplitude of oscillation. Solving the Navier-Stokes equations and continuity equation along with the equation of motion of the vibrating body in the fluid is vital in order to study such a phenomenon. Also for a long time it was of great interest to solve these equations to analyze practical applications, at the macroscale, such as for the design of ships or under water structures. These bodies were generally simulated using simple geometries such as a transversally oscillating cylinder²⁸ or a sphere oscillating along its diameter³⁰ in a viscous fluid.

Concerning the modeling of the oscillatory behavior of AFM cantilever beams when immersed in a fluid, two main theoretical approaches have been used: (1) the simple model of equivalent spring-mass-damper system and (2) the ‘‘hydrodynamic’’ functions methods. The development of these techniques will be explained in detail in the following paragraphs.

In 1992, Butt et al³¹ implemented a simplified model of a cantilever system to evaluate the scan speed limit for cantilevers in various fluids. This was achieved by assuming a massless cantilever with a spring constant of k and a mass point of m at its free end. Moreover, for the cantilever, they assumed a damping force that is proportional to the velocity of the free end with a proportionality constant d . In order to find this constant, they simulated the mass by a sphere of radius R . Based on the Stoke’s law, the applied drag force on a moving sphere which is immersed in a fluid is:

$$F_d = 6\pi R\mu \frac{dy}{dt} \quad \text{Equation (1.1)}$$

where μ is the viscosity of the fluid and y is the displacement of the sphere. Based on this, the damping coefficient d is equal to $6\pi R\mu$. In this way, they could couple the

damping effect of the surrounding fluid with the response of the cantilever. Their approach was improved by Chen et al³² by considering two different cases of damping, first in gases and second in liquids. For gases, the Reynolds number is small, typically in the order of 10^{-2} , and as a result the drag force is proportional to the velocity of the sphere. Hence like Butt et al, they used the Stoke's law in their modeling. However, for liquids the typical values of density and viscosity are 1000 and 100 times greater than gases respectively, and the resonant frequency of the cantilever usually shifts three to five times less than in gases and as a result, the Reynolds number in liquids is not as small as that for gases. Therefore, the applied drag force could be found from:

$$F_d = \frac{2}{3} \pi \rho R^3 \frac{d^2 y}{dt^2} + 3 \pi R^2 \sqrt{2 \mu \rho \omega} \frac{dy}{dt} \quad \text{Equation (1.2)}$$

where ρ is the density of the liquid and ω is the angular frequency of the sphere oscillation. In Equation (1.2), the first term of the drag force is proportional to the acceleration and defines the added mass. In this model, beside the radius of the sphere, another parameter was defined that depends on the size of the cantilever. These geometrical parameters are constant for each cantilever and once they are determined, by fitting the model to a set of experimental resonance peak data, they can be used to predict the behavior of the cantilever in other fluids. With this method, the cantilever beam is modeled as a one-dimensional simple harmonic oscillator and only the first mode of vibration can be predicted. Chen et al³² also used a variational method, for the equation of motion of the cantilever, to approximate the higher modes of vibration from the first mode. Later on, this work was verified experimentally by Oden et al³³. They implemented their study on several cantilevers of two shapes, V-shaped and rectangular cantilevers, while oscillating in different fluids, such as air and glycerol/water mixtures.

These fluids were chosen to cover a wide range of viscosities. Their experimental results demonstrated a good agreement with the theoretical model for low viscosity liquids but the theory was incapable of predicting the experimental values for higher viscosity liquids.

An apparently more realistic model for the oscillatory behavior of cantilever beams in viscous fluids was proposed by Kokubun et al³⁴. They modeled the cantilever by a string of spheres of radius R equal to one half of the width of the cantilever, and they approximated the applied drag force at each point of the cantilever by that on a sphere which vibrates with the same amplitude of the cantilever. Their method consists of a very complicated analysis in order to predict the frequency response of the cantilevers; however after determining the frequency response, calculating the resonant frequency and the quality factor at each mode of vibration are straight forward. Similar to the method proposed by Chen et al³², again in this method we need to find some physical parameters by fitting the model to the experimental values. Hirai et al³⁵ verified this model by achieving a good agreement with the experimental results for the peak amplitudes at resonant frequencies; however they discovered that this model is overestimating the value of the applied drag force.

In an additional attempt to determine the higher modes of vibration, Salapaka et al³⁶ used a more accurate method that is not based on the sphere approach but instead employed the multi mode model directly for the analysis of the oscillatory behavior of the cantilever. Again this method requires finding an experimental parameter from the first mode of vibration which was then utilized to find higher modes of vibration. They also applied the same assumption of the damping force being proportional to the velocity of

the cantilever in their technique, which limits the usage of this technique only for gases, which usually have low Reynolds number. This was proved experimentally for air during their study.

The key point for the equivalent spring-mass-damper or simply the sphere approach is to find the equivalent sphere radius or some other physical parameters from experimental values of the fundamental mode of vibration. These parameters are essential for predicting the behavior of the cantilever at higher modes of vibrations. The dependency of the radius of the equivalent sphere upon the cantilever geometrical parameters and the nature of the material used has been studied by many researchers^{32,37,38,39,40}, however the results obtained were inconsistent. Therefore, it could be concluded that it is impossible to evaluate the radius of the equivalent sphere before determining the fitting parameters. Although this method has been utilized in many research works, it proved to be misleading when the cantilever size or geometry is changed. In contrast to this approach, the real geometry of the cantilever is being used for modeling of its oscillatory behaviour in the hydrodynamic function approach. The hydrodynamic function method allows multimode analysis of the cantilever and as a result there is no need for experimental parameters to investigate the higher harmonics. The development of this approach is described next.

The simplest model which uses the actual geometry and dimensions of the cantilever was proposed by Weigert et al⁴¹. In their model, the resonant frequency of the cantilever was predicted by replacing the actual mass of the cantilever with its effective mass in the analysis of undamped cantilever vibration. For evaluation of the added mass at each mode of vibration, the mass of moving fluid (induced mass) is approximated with the

mass of the fluid in double cones around the nodes of vibration in vacuum. The height of the double cone is the same as the width of the cantilever and its maximum radius is equal to half of the distance between two neighbouring nodes, which is related to the wavelength of the n^{th} mode (Figure 1.4). They verified their model by experimentally determining the resonant frequencies of two dimensionally different rectangular cantilevers in air and water and found satisfactory results up to the 7th mode of vibration. However the discrepancy between theoretical and experimental results increases at the higher modes. Since the mass of moving fluid was not determined through solving of the Navier-Stokes equations in this model, the effect of the viscosity of the fluid cannot be taken into account.

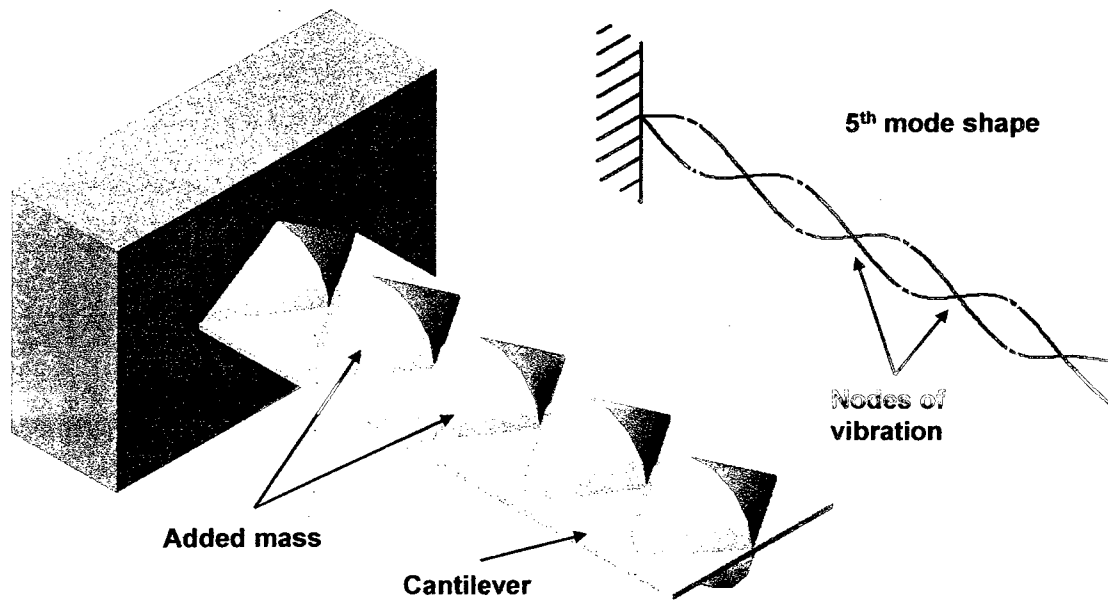


Figure 1.4 A schematic drawing of a cantilever, with a rectangular cross section, while oscillating in a medium at the 5th mode of vibration.

Elmer et al⁴² determined theoretically the shift in the resonant frequencies of rectangular cantilevers in the same way as Weigert et al⁴¹ using the concept of virtual mass. However, Elmer et al evaluated the virtual mass in a more logically accepted manner. The virtual mass was calculated by solving the hydrodynamic equations for the flow around the cantilever. Many assumptions were made to simplify the problem; mostly important are the assumptions of the fluid being inviscid and the length of the cantilever being infinite (2D flow around the cantilever). As a result of these assumptions, the drag force on the cantilever will only be due to the pressure difference between the upper and lower surface of the cantilever. This allowed for the determination of the pressure field around the cantilever through solving a simplified form of the Navier-Stokes equations, in which the viscous terms are neglected, namely the Euler equations. In order to find the accuracy of the model, they performed a series of experiments with different cantilevers immersed in different fluids. It was concluded that there was a systematic error in their proposed model. Moreover, the accuracy of their model was limited to the higher modes of vibration. The authors thought that the reason comes from the approximation of 2D flow induced a large error in the results for the first few modes however Maali et al⁴³ proved that in the higher modes of vibrations the third component of the flow is even more important than in the lower modes. Instead, the main reason seems to be the importance of the viscous dissipative effect on the lower modes of vibration which is neglected in this inviscid model. Nonetheless their model was still more accurate than Weigert et al's model⁴¹, in the prediction of the resonant frequencies, as was proven mathematically and experimentally.

The effect of viscosity on the cantilever response was considered in the modeling of Kirstein et al²⁰. Since the motion of the surrounding fluid is not instantaneous and has a phase shift comparing to the movement of the cantilever. they divided the applied drag force on the cantilever into two parts: one part is in phase with the motion of the cantilever and the second part is out of phase. The first part, which can also be considered in phase with the cantilever acceleration, is the inertial force; while the second part which has the same phase as the velocity of the cantilever is the damping force. In order to evaluate these forces, they defined two parameters: the added mass coefficient, C_m , and the fluid damping coefficient, C_v . These coefficients relate those forces to the acceleration and the velocity of the cantilever, respectively, and also link them to the volume of the fluid that moves with the cantilever. The coefficients were determined through solving the Navier-Stokes equations for the general case of a cylindrical cross section cantilever with diameter D which is confined concentrically by a cylindrical vessel of diameter D_0 that is filled with the fluid, as shown in Figure 1.5. It was found that these coefficients are dependent upon the Reynolds number. Then the problem was simplified for two practical cases of high Reynolds number and an infinite viscous fluid which is the case for the vibration of the cantilevers in fluid cells. It should be mentioned that the analysis of cylindrical cross section is important because it is the typical shape of cantilevers used for scanning near-field optical microscopes. However for the case of AFM cantilevers, the cross section is usually rectangular. For this case, Kirstein et al²⁰ highlighted two approaches for determining the coefficients. The first can be made through carrying out the analysis for a cantilever with an elliptical cross section in an elliptical coordinate system instead of the cylindrical one and the coefficients for the

rectangular cantilever will be approximated by the ones for a very flat elliptic cantilever. The other approach, which was verified roughly by the results of other researchers^{32,42}, was based upon modifying and rescaling of the Reynolds number as well as the parameters of C_m and C_v according to the new cantilever geometry.

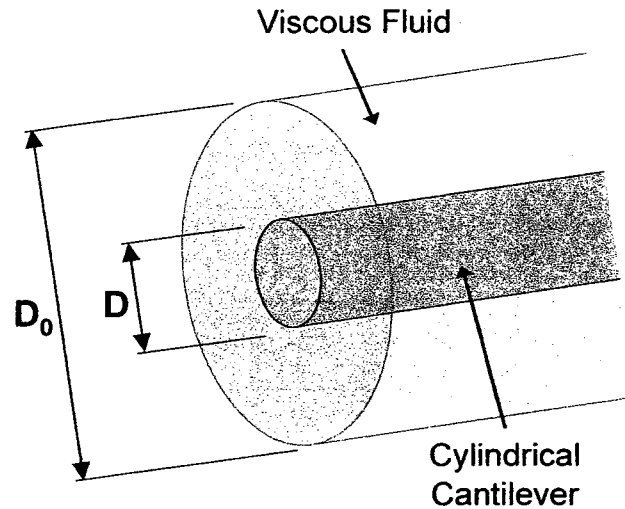


Figure 1.5 A schematic drawing of a cylindrical tube of viscous fluid surrounding concentrically a vibrating cylindrical cantilever

After evaluating the inertial and damping forces, they were implemented them in the governing equation for the cantilever vibration from which two equations for the shifted resonant frequencies and the quality factors of the cantilever in the fluid were derived. In these equations the most important parameter is the Reynolds number which depends on the frequency of the oscillation itself. Therefore these equations are implicit in terms of the resonant frequency and hence an iterative approach should be implemented to solve for the resonant frequency. The comparison of the theoretical and experimental results for this model indicated an accurate estimation of both resonant frequency and quality factor

for lower modes of vibration within an error of 1% and a systematic error for the higher modes which increases with mode number. The trend of this error with respect to the mode number is in contrast with the one generated by the models of Weigert et al and Elmer et al. This can be considered as an advantage of Kirstein et al's model because eventually in practice the lower modes of vibration are more important. In addition, this model can also be used to predict the quality factors, which describe the broadening of the resonant peaks.

Interestingly at the same time as Kirstein et al²⁰ presented their work, one of the fundamental contributions in this field was made by Sader⁹ who derived the general theoretical model for the frequency response of cantilever beams immersed in viscous fluids. In his model, the cantilever can have an arbitrary cross section, which should be uniform along its entire length. Also, it can be excited by any chosen driving force and the surrounding fluid can have any value for the density and the viscosity. This theory was developed mainly based upon the assumptions that the ratio of length to nominal width of the cantilever is very large and in addition the amplitude of vibration is much smaller than any of the cantilever's characteristic lengths. As a consequence of these assumptions, the resulting flow can be approximated by a 2D flow around the cantilever. Moreover, the nonlinear terms in the Navier-Stokes equations can be neglected, so that the hydrodynamic drag force can be considered to be a linear function of the cantilever displacement. Based upon the last conclusion, Sader⁹ used the following parametric equation to represent the applied drag force at point x on the length of the cantilever:

$$F_{hydro(x|\omega)} = \frac{\pi}{4} \rho \omega^2 b^2 \Gamma_{(\omega)} Y_{(x|\omega)} \quad \text{Equation (1.3)}$$

where ρ is the density of the fluid, ω and Y are the frequency and amplitude of cantilever oscillation respectively, $\Gamma_{(\omega)}$ is the hydrodynamic function and b is the width of the cantilever. The hydrodynamic function is a dimensionless function that represents the effect of the cross section shape and can be obtained either analytically or numerically from solving the Navier-Stokes equations for the flow. Because the cross section of cantilevers in most practical situations is either circular or rectangular, Sader⁹ presented the hydrodynamic functions for these two cases. He defined the hydrodynamic function analytically for the case of the circular cross section using previously obtained theoretical results for the drag force on a transversally oscillating cylinder²⁸. Then he proposed a numerically obtained correction function $\Omega(\omega)$, which should be multiplied to the hydrodynamic function of the circular cross section to rescale the values properly, for the rectangular cross section as shown in the following equation:

$$\Gamma_{rect}(\omega) = \Omega(\omega) \times \Gamma_{circ}(\omega) \quad \text{Equation (1.4)}$$

After that, Sader implemented the equation for the hydrodynamic drag force in the governing equation of the cantilever deflection. By applying the appropriate boundary conditions and also with the help of the theory of Green's function, he found the general solution for the cantilever deflection at each point of its length and at each frequency of excitation. Then, he simplified his model for the special case of thermal driving force because of the frequent use of this type of excitation in AFM applications. For this case, another formula was also derived for the inclination of the cantilever beam because, in most AFMs, the optical system measures the inclination of the cantilever rather than its deflection.

Sader⁹ also investigated the validity of approximating the thermal frequency response with the simple harmonic oscillation (SHO) model in the neighbourhood of a resonant peak, which is a technique that was used in many experimental cases. He showed that this approximation is reasonable only in the case of small dissipative effects in the fluid. Then he derived two formulas, based on his theoretical model, for expressing the resonant frequency and quality factor of the frequency response for the case of small dissipative effects in the fluid.

His theoretical model was validated experimentally by Chon et al⁴⁴ through a series of experiments with several rectangular cantilevers that had different aspect ratios and were immersed in different fluids. They showed qualitatively that the effect of viscosity can not be neglected in the analysis of AFM cantilevers. This was done by measuring the frequency responses of a cantilever in acetone and 1-butanol. These fluids have almost the same density but their viscosities differ by an order of magnitude. As a result of this difference in the viscosity, both the resonant frequencies and the breadths of their peaks were different. This result is in contrast with the one reported by Chu et al⁴⁵ for the vibration of macro scale cantilever beams in viscous fluids. Such a distinction can be explained by focusing on the difference between the relative importance of fluid damping in the macro and micro scales. Where during macro scale analysis, the fluid damping is negligible compared to the internal losses of the cantilever, it is significant in the case of the micro scale.

Chon et al⁴⁴ also checked the sensitivity of the Sader's model to the uniformity of the cantilever cross section and the material properties. For this purpose, they chose two sets of cantilevers, one that had very precise geometries and uniform material properties and

the other did not. These two sets were called calibrated and practical cantilevers respectively. Comparison of their experimental results with the Sader's theoretical model indicated that the sensitivity of the model to the uniformity of geometrical and material properties is small and therefore the model can be used for practical cantilevers as long as the aspect ratio of the cantilever is large.

Although Sader's theory was significantly improved over previous models of oscillatory behavior of AFM cantilever in fluid, his model is restricted to the assumption of 2D flow of an incompressible fluid around the cantilever. To satisfy this assumption, the distance between two adjacent nodes of vibration should greatly exceed the nominal width of the cantilever. Therefore, for a cantilever with a finite length, his model is limited practically for prediction of the fundamental resonant frequency and its first few harmonics. In the higher modes of vibration the axial flow, which is the 3rd component of the flow, is not negligible compared to the other components of the flow, and as a result, the model introduces a considerable error in prediction of the experimental frequency response. This was proved experimentally by Maali et al⁴³ who investigated the oscillatory behavior of an AFM cantilever immersed in air and water up to the 8th mode of vibration. Beside the experimental results, they also showed the effect of the axial flow by solving the 3D Navier-Stokes equations numerically for the oscillation of the cantilever in a viscous fluid. In this case, the numerically predicted viscous damping coefficient and the added mass were closer in value to the experimentally determined results.

It should be emphasized that all the above mentioned models are for flexural vibration of the cantilever, while the cantilever can exhibit longitudinal and torsional vibrations

also. For the case of longitudinal vibration, almost none of the commercial AFMs are capable of measuring the related deformations. Therefore, there has not been any need to model the behaviour of the cantilever for this type of vibration. For the case of torsional vibration, regular AFMs can determine the amount of deflection angle at each point of the cantilever; so Green et al⁴⁶ extended Sader's approach for this type of vibration. Similarly, they solved the elastomechanical governing equation for the deflection angle of the cantilever at the same time with the Navier-Stokes equations for the fluid. They also specified the torsional hydrodynamic function for both circular and rectangular cantilevers that can be used to evaluate the hydrodynamic torque on the cantilever. They found that the modal frequencies for torsional vibration are much higher than for flexural vibration. Their model could not predict the cantilever behaviour at higher modes of vibration very well due again to the assumption of 2D flow around the cantilever.

Regarding this inaccuracy, Eysden et al⁴⁷ improved their models by finding analytically more realistic hydrodynamic functions that take into account the 3D flow around the cantilever. These hydrodynamic functions depend not only upon the Reynolds number of the system but also upon the vibration modes. However, the final formulas obtained for these functions are very complicated and numerical values are presented to facilitate their usage.

It should be mentioned that despite of the discrepancy of Sader's model with experimental results at higher modes of vibration, this model is well accepted and widely used among the researchers in this field for many reasons. First it provides the whole frequency response of the cantilever and does not need *a priori* information about the experimental results. Second, in most of the AFM applications and related investigations,

only the fundamental resonant frequency or at most its first few harmonics are needed. Third, the simplicity of his model and its accuracy are well balanced, and finally, the measurement system of regular AFMs provides more reliable data for flexural vibration than for torsional vibration. Here we focus on Sader's model and determine accurately its applicability limits.

More recently, in another attempt to model the oscillatory behaviour of the cantilever in viscous fluids, Xu and Raman²² derived simple formulas based on transfer functions to describe the response of the AFM cantilevers to thermal, magnetic and ideal acoustic excitations as they were defined in section 1.2 (Acoustic excitation is ideal when the base of the cantilever is moved in a controlled manner). The hydrodynamic function used for their analysis is that of Sader⁹. Comparing these theoretical responses in the neighbourhood of fundamental resonant frequency indicated that although their peak frequencies are close to each other, the peak frequency of the ideal acoustic excitation is slightly higher than that of the thermal excitation and also that the peak frequency of the magnetic excitation is slightly smaller than that of the thermal excitation. Moreover, they studied experimentally the responses of the cantilever to these excitation techniques in liquid media using an Agilent AFM and fluid cell. The system of the AFM was modified in a way that the switching between three excitation techniques could be done without changing the cantilever position and the laser alignment. Therefore their frequency responses could be compared under identical conditions. The experimental results for thermal and magnetic excitations showed that Xu et al's theoretical models can excellently predict the oscillatory behaviour of the cantilever in the region of the first mode of vibration. This includes the predictions of their peak frequencies and also the

non-zero amplitude of vibration for the magnetic excitation at very low frequencies. In the case of the acoustic excitation, they observed many spurious peaks in the response of the cantilever, which as mentioned before are not related to the true dynamics of the cantilever, and therefore they could not verify their model for this case very well. The only thing that followed their model was the zeroing trend of oscillation amplitude at very low frequencies. Finally regarding their model, it should be mentioned that the achieved accuracy was not very surprising because the hydrodynamic function, which was used in their analysis, only evaluates the drag force at the first few modes of vibration accurately.

Beside the above mentioned investigations regarding the frequency responses and vibrational characteristics, some studies have been carried on the other aspects of the cantilever oscillatory behavior in viscous fluids. For example, Green et al⁴⁸ examined the frequency response of a cantilever vibrating in the vicinity of a solid surface. The result of their study is practically important while doing experiments with liquids. This is because in practice for liquids we usually use the fluid cell which holds the cantilever just below its glassy surface. It was found that for a rectangular cantilever, the effect of approaching the cantilever to the surface is a broadening and shifting of the resonant peak to a lower frequency. However for most gases and fluids with typical properties that make the Reynolds number (defined as $Re = \rho b^2 \omega_{vac} / 4\mu$ where b is the width of the cantilever, ρ is the density of the fluid, μ is the viscosity of the fluid and ω_{vac} is the resonant frequency of the cantilever in vacuum) greater than one, if the distance between the cantilever beam and the solid surface is greater than the cantilever width then its

frequency response is unaffected and the models for the unbounded cantilevers can be applied here.

In another study, Jai et al.⁴⁹ showed that for cantilevers having low quality factors, the displacement of the cantilever base is comparable to the cantilever oscillation amplitude in the acoustic excitation technique. Consequently, for this type of excitation, the free end of the cantilever has a movement equal to the summation of the base displacement and the cantilever oscillation amplitude.

As an overview on the development of the theoretical models of cantilever oscillatory behavior in viscous fluids, it can be noticed that the very early studies of this subject matter were focused on the determination of the cantilever vibrational characteristics such as resonant frequency. However, after achieving these goals over time, the direction of these studies were turned to the estimation of the whole range of frequency response of the cantilever for different methods of excitation.

1.5) Measurements of rheological properties using AFM cantilevers

The fact that immersing a micro cantilever in a fluid changes its oscillatory behaviour led many researchers to evaluate the vibrational characteristics of cantilever beams based on the knowledge of both their material and geometrical properties as well as the surrounding fluid properties, as summarized in the previous sections. From another point of view, determining the fluid properties by observing the changes in vibrational behaviour is another application for the AFM which was firstly introduced by Oden et

al³³. The determination of the fluid properties by this method is useful in many fields such as microfluidic systems because only a small amount of fluid, in the order of microliters, is required.

The microcantilever based rheological measurement technique was originally developed in order to determine the viscosity of liquids only. The initial efforts in this area were based on very simple and quite inaccurate models as the development was taking place in parallel with the development of models of the vibrational behaviour of the cantilever. For example Oden et al³³ and Ahmed et al⁵⁰ used the simple one dimensional sphere model, which was developed by Chen et al³², during their studies of the viscosity of water / glycerol solutions and other liquids. During their studies they actually did not extract the viscosity of such liquids directly; instead they compared both experimental and theoretical resonant frequencies of a thermally excited AFM cantilever for the tested liquids. In this way, they found the sensitivity of the technique for different viscosities and Oden et al³³ showed that one cantilever can be used to measure a broad range of viscosity from 10^{-2} up to 10^2 mPa.s. Furthermore, Ahmed et al⁵⁰ proved that such a method can be used for online measurement of fluids' viscosities during a chemical reaction or at the physical state of a biological system. This was done by monitoring the change of the cantilever resonant frequency over time for the hydrolysis of herring sperm DNA. Later on, Bergaud et al²¹ used the more precise hydrodynamic function model of Sader⁹ for the viscosity measurements. Five different composite cantilever beams, that had silicon cores and a thin gold coating, were excited acoustically in water and ethanol using an in-house made AFM. They developed a MATLAB code to extract the viscosity of the tested liquids from the experimentally obtained resonant

frequency. Because Sader's model is more accurate for the lower modes of vibration, they used only the first and second resonant frequencies in their computations. The calculated viscosities were compared with the real viscosities of the liquids and the maximum error was around 25 percent. They also mentioned that any inaccuracy in the determination of the resonant frequency or the properties of the cantilever will be magnified considerably in the final result. Therefore the use of well characterised cantilevers and calibrating the whole AFM system before doing the experiment were highly recommended. Finally, it was noted that the applicability of this technique is in the limit of low dissipative effect otherwise there will be no resonant peak in the frequency response as was shown experimentally for silicone oil.

The next step in development of this technique was determining both viscosity and density of the fluid simultaneously which was achieved for the first time by Boskovic et al⁶. Their method was applicable for both gases and liquids having a wider range of viscosities and densities. Boskovic et al⁶ managed to determine these properties through the following procedure. First, they evaluated the resonant frequency ω_R and the quality factor Q of the resonance through fitting the formula for the amplitude frequency response of simple harmonic oscillation (SHO) to the neighbourhood of the resonant peak. Then the viscosity and density were determined by solving simultaneously the two equations for ω_R and Q which were derived by Sader⁹ from his theoretical model. The technique was verified by performing a series of experiments using a single micro cantilever which was thermally excited and immersed in different gases and liquids with known properties. Again because of the considerations regarding the accuracy of Sader's model, only the frequency responses around the fundamental resonant frequency were

used in the calculations. They achieved good agreement, with a maximum error less than 14%. It was shown that even fluids with similar properties could be recognized by this method however since the validity of the model used in this technique is in the limit of small damping and dissipative effect ($Q > 1$), highly viscous fluids can not be studied. Their method was also used by Hennemeyer et al⁷ to determine the properties of sugar solutions and then the results were compared with the real values for the verification of the technique. Hennemeyer et al⁷ also found that a very slow steady flow around the cantilever does not change its frequency response. This indicated that the micro cantilevers can be used as an online rheological measuring tool during production processes too.

In the previous method, the determination of viscosity and density was based on two vibrational characteristics, the resonant frequency and the quality factor which could be evaluated if the resonant peak appears in the frequency response. Therefore, the applicability of the method is limited for low viscosity fluids. Recently, Belmiloud et al⁵¹ proposed a different approach which is not restricted to the resonance phenomena. In their method, the phase frequency response was measured as well as the amplitude frequency response. Having these two measured values, Belmiloud et al evaluated the inertial (added mass) and the dissipative (damping coefficient) parts of the applied drag force at each frequency. These terms were determined analytically based on the knowledge of the fluid and the cantilever properties by other researchers previously. By equalling the experimentally and theoretically obtained values of added mass and damping coefficient and then solving them simultaneously, they could predict the viscosity and density of the fluid at each frequency. In this method, there is no restriction

for the viscosity of the fluid because, even without the appearance of resonance, the frequency responses of the cantilever are different in distinct fluids. Their method was experimentally (less than %1) verified by extracting the viscosity and density of silicone oils (viscosities ranging from 10 to 30000 cP) using a magnetically excited cantilever. In their experiments, no resonant peak was observed for fluids with the viscosity greater than 100 cP because of the large dissipative effects. The calculated values for viscosities were in good agreement with the known values and also showed the frequency independent behaviour of Newtonian fluids. However for densities, the inaccuracy of the values was explained by the inability of the theoretical model to estimate small inertial effects for high viscosity fluids (low Reynolds number). Later on, Belmiloud et al⁵² extended their method for viscoelastic fluids which exhibit frequency dependency in their properties. An educated guess of $G = i\omega\eta$ was assumed for the shear modulus of the fluid in order to replace the viscosity in the hydrodynamic function. Knowing that $G = G' + iG''$, they derived two equations which relate the fluid's storage and loss modulus to the added mass and the damping coefficient at each frequency. They followed their theory with some qualitative experiments in order to show the frequency dependency of fluid properties in the frequency response of the cantilever. It was observed that the cantilever had a resonant frequency, even in a compact gel, because of its low viscosity at high frequencies. Although the estimation of the drag force based on the assumption of $G = i\omega\eta$ is not valid in terms of a proper constitutive equation, their approach and results were encouraging to expand this technique for rheological measurements with complex fluids.

It should be noted that all the above methods require knowledge about the dimensions, material properties and vacuum resonant frequency of the cantilever. The accuracy of these data directly determines the accuracy of the viscosity measurements. The suppliers of AFM micro cantilevers usually provide only nominal dimensions and a range for the resonant frequency and spring constant of the cantilevers. Consequently, many investigations have been conducted on the calibration of the cantilevers^{53,54,55}. Unfortunately, these methods are too complicated and very time consuming. Moreover, the chance of breaking the cantilever is high during these calibration processes. As a result of these difficulties, some attempts were made to assess the required information from the oscillation of the cantilever in a reference fluid with known properties. In this regard, Boskovic et al⁶ rearranged the Sader's formulas for ω_R and Q to obtain the vacuum resonant frequency ω_{vac} and the mass per unit length μ of the cantilever. Air was chosen as the reference fluid and ω_R and Q were determined experimentally and then inserted into the equations in order to get ω_{vac} and μ , however the width of the cantilever was still needed for the rest of calculations.

In another attempt, Papi et al⁵⁶ approximated the vacuum resonant frequency with the resonant frequency of the cantilever in air, as it was shown that the difference between these two is less than few percent⁴⁴. Also they used a simple analytical approximation for the hydrodynamic function which was proposed by Maali et al⁴³. Combining these approximations with the Sader's formula for the resonant frequency, Papi et al derived an equation for the viscosity of the fluid in terms of the resonant frequencies of the cantilever in the fluid and air as well as two other parameters of α and β which include all the geometrical and material properties of the cantilever. Their experimental results

showed that, for different cantilevers and fluids, the variation of α is considerable while for β is not. They proposed to use a reference fluid to find α and a fixed value for β based on the average of their experiments. Later on, Papi et al⁵⁷, in another study, used the same approach for the old simple model of sphere and in this way they also could relate the sphere's equivalent parameters to the geometrical and material parameters of the cantilever. Although their method could be easily extended for determination of both viscosity and density, it seems that their technique is based on many approximations and can not grantee good accuracy for all situations.

As a general comment, one common source of error in methods that are based on the resonance phenomena is that the experimental resonant frequency is determined at the point of maximum amplitude of vibration irregardless of the technique for excitation of the cantilever. As it was mentioned in the previous section, Xu et al²² showed that, for liquids, the frequency of maximum oscillation in thermal excitation is slightly greater than the magnetic excitation and also less than the acoustic excitation. Therefore, the more precise way of determining the rheological properties is through considering the theoretical response of the cantilever based on the type of excitation. Moreover in this way, the rheological study of the fluids will not be restricted to the low viscosity fluids that let the appearance of resonant peak in the cantilever frequency response. In this study, we focus mainly on the acoustic excitation technique because of its vast use among the AFM users. After recognizing the disturbing factors in the frequency response of the cantilever in acoustic excitation and improving the design of the fluid cell in this respect, we applied this technique for the measurements of high viscosity Newtonian fluids and compared the results, wherever it was possible, with the results of thermal noise

technique. Then it was shown that this method can be extended for polymer solutions which are non-Newtonian liquids and different approaches were suggested for deriving theoretical models to predict the frequency response of the cantilever.

In the next chapter, the required theories for the analysis of the experimental results are provided.

Chapter 2

Theory

In this chapter, we present the mathematical models for oscillatory behavior of the AFM cantilever immersed in a viscous fluid and excited by Brownian motion of surrounding fluid (thermal noise), sinusoidal excitation of the cantilever base (frequency sweep) and step excitation of the cantilever base. To this end, we construct the governing equation of the cantilever deflection in section 2.1. After that, the applied hydrodynamic drag force on the cantilever is derived and in section 2.3 we derive the model for these excitation techniques. The following assumptions have been used through these analyses. It should be mentioned that in most of practical cases, the following criterions are satisfied by AFM cantilevers.

- (1) The cantilever has a uniform cross section over its entire length;
- (2) The cantilever is made from an isotropic linearly elastic material and its internal friction is negligible;
- (3) The ratio of length to width of the cantilever is very large;
- (4) The amplitude of vibration of the cantilever is very small;
- (5) The surrounding fluid is incompressible and Newtonian;
- (6) All torsional effects in the cantilever are negligible.

2.1) Transverse vibration of a cantilever

The cantilever used in the AFM is a beam with one end fixed and the other end free that vibrates transversally. Vibrational analysis of such beam is a classical problem which can be found in many vibration textbooks^{26,27}. Because of its importance in our theoretical derivations, such analysis is presented next.

Figure 2.1 shows a free-body diagram of an element of length dx with internal, external and inertial forces and moments on it. The balance conditions for forces and moments in the y direction for this element are:

$$\sum F_y = 0: \quad -\frac{\partial V}{\partial x} dx - \rho_c A dx \frac{\partial^2 y}{\partial t^2} + F(x,t) dx = 0 \quad \text{Equation (2.1)}$$

$$\sum M = 0: \quad -V dx + \frac{\partial M}{\partial x} dx \approx 0 \quad \text{Equation (2.2)}$$

where y is the cantilever deflection, E is Young's modulus of the cantilever, I is the moment of inertial of the cantilever, ρ_c is the density of the cantilever, L is the length of the cantilever, A is the cross section area of the cantilever, F is the external applied force per unit length, x is the spatial coordinate along the length of the cantilever, and t is time.

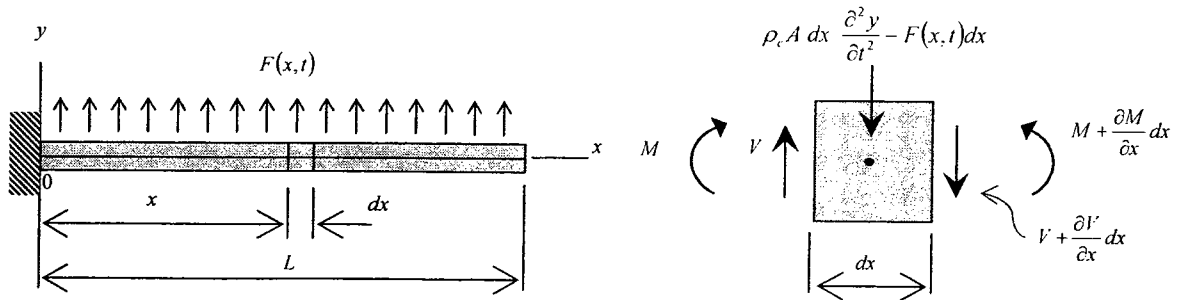


Figure 2.1 Free-body diagram of an element of length dx .

Substituting Equation (2.2) into Equation (2.1) and using the flexural theory $M = EI(\partial^2 y / \partial x^2)$, we obtain:

$$\frac{\partial^2}{\partial x^2} \left(EI \frac{\partial^2 y}{\partial x^2} \right) + \rho_c A \frac{\partial^2 y}{\partial t^2} = F(x, t) \quad \text{Equation (2.3)}$$

In the case of an isotropic elastic beam with a uniform cross section over its entire length, the flexural rigidity EI does not vary with x , therefore, Equation (2.3) can be simplified to:

$$EI \frac{\partial^4 y}{\partial x^4} + \rho_c A \frac{\partial^2 y}{\partial t^2} = F(x, t) \quad \text{Equation (2.4)}$$

In Equation (2.4), the external applied force $F_{(x,t)}$ consists of two parts; one part is the hydrodynamic force $F_{hydro(x,t)}$ due to the relative motion of the surrounding fluid and the other part is driving force $F_{drive(x,t)}$ that causes the oscillation of the cantilever. Thus, we can write:

$$EI \frac{\partial^4 y}{\partial x^4} + \rho_c A \frac{\partial^2 y}{\partial t^2} = F_{hydro(x,t)} + F_{drive(x,t)} \quad \text{Equation (2.5)}$$

This is the governing equation for the deflection of the cantilever. For the AFM cantilevers, the boundary conditions of this equation usually are:

$$\text{At fixed end } (x=0): \quad \begin{cases} y = 0 \\ \frac{\partial y}{\partial x} = 0 \end{cases} \quad \text{Equation (2.6)}$$

$$\text{At free end } (x=L): \quad \begin{cases} M = 0 \Rightarrow \frac{\partial^2 y}{\partial x^2} = 0 \\ V = 0 \Rightarrow \frac{\partial^3 y}{\partial x^3} = 0 \end{cases} \quad \text{Equation (2.7)}$$

Our goal is to derive the theoretical response of the AFM cantilever to thermal and acoustic excitations. For such an analysis, the modal functions of undamped free vibration ($F_{(x,t)} = 0$) of the cantilever are useful. This is mainly because of the particular format of the hydrodynamic and driving forces which will be explained in the next sections. For the case of free vibration, the governing equation of cantilever deflection is simplified to:

$$EI \frac{\partial^4 y}{\partial x^4} + \rho_c A \frac{\partial^2 y}{\partial t^2} = 0 \quad \text{Equation (2.8)}$$

This is a partial differential equation which can be solved using the separable variable method; that is, we assume:

$$y = c(t)\phi(x) \quad \text{Equation (2.9)}$$

Implementing the Equation (2.9) into Equation (2.8) will result in two ordinary differential equations in the form of:

$$\phi'''' - \lambda^4 \phi = 0 \quad \text{Equation (2.10)}$$

$$\ddot{c} + \omega^2 c = 0 \quad \text{Equation (2.11)}$$

where λ and ω have the following relation with the other parameters:

$$\omega = \lambda^2 \sqrt{\frac{EI}{\rho_c A}} \quad \text{Equation (2.12)}$$

We are interested in solving Equation (2.10) because it defines the modal shape of the cantilever. The general solution for this differential equation is in the form of:

$$\phi = A_1 \sin \lambda x + A_2 \cos \lambda x + A_3 \sinh \lambda x + A_4 \cosh \lambda x \quad \text{Equation (2.13)}$$

It is more convenient to write this equation in the following equivalent form:

$$\begin{aligned} \phi = & A_1'(\cos \lambda x + \cosh \lambda x) + A_2'(\cos \lambda x - \cosh \lambda x) \\ & + A_3'(\sin \lambda x + \sinh \lambda x) + A_4'(\sin \lambda x - \sinh \lambda x) \end{aligned} \quad \text{Equation (2.14)}$$

Now the boundary conditions should be applied. From the first two conditions, we conclude that $A_1' = A_3' = 0$ and the remaining two conditions will lead to the following equation for λ :

$$\cos \lambda L \cosh \lambda L + 1 = 0 \quad \text{Equation (2.15)}$$

This equation has infinite number of roots which can be calculated numerically. The first six positive roots, which are related to the first six mode of vibration, are summarized in Table 2.1. For the larger roots, the approximate values of the following equation may also be used:

$$\lambda_i L \approx \left(i - \frac{1}{2} \right) \pi \quad \text{Equation (2.16)}$$

Each of these roots defines one mode shape for the cantilever. Figure 2.2 shows the first three mode shapes for cantilever vibration.

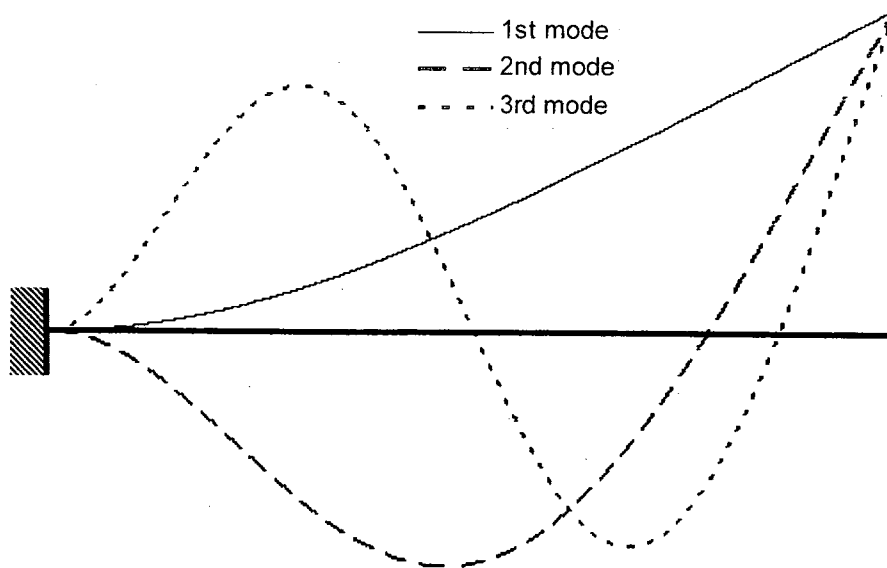


Figure 2.2 The first three mode shapes for a beam with one end fixed and other end free.

These roots also determine the resonant frequencies at each mode of vibration. Using Equation (2.12):

$$f_i = \frac{\omega_i}{2\pi} = \frac{\lambda_i^2}{2\pi} \sqrt{\frac{EI}{\rho_c A}} \quad \text{Equation (2.17)}$$

and, for example for the fundamental resonant frequency, we have:

$$f_1 = \frac{1}{2\pi} \left(\frac{1.875}{L} \right)^2 \sqrt{\frac{EI}{\rho_c A}} = \frac{3.515}{2\pi} \sqrt{\frac{EI}{\rho_c AL^4}} \quad \text{Equation (2.18)}$$

It should be also mentioned that the functions ϕ_i have the orthogonality property, that is:

$$\int_0^L \phi_i \phi_j dx = \begin{cases} \alpha_i L & (i = j) \\ 0 & (i \neq j) \end{cases} \quad \& \quad \int_0^L \phi_i''' \phi_j dx = \int_0^L \phi_i'' \phi_j'' dx = \begin{cases} \lambda_i^4 \alpha_i L & (i = j) \\ 0 & (i \neq j) \end{cases} \quad \text{Equation (2.19)}$$

where α_i can be any constant however in the analysis of cantilever vibration, it is common that the value of α_i is determined based on normalizing the function ϕ_i in the way that $\phi_i(L) = 1$. Also the parameter β_i , defined in the Equation (2.20), is important.

$$\beta_i L = \int_0^L \phi_i dx \quad \text{Equation (2.20)}$$

In Appendix A (pages 164-165), a MATLAB code for determination of α_i and β_i is presented and in Table 2.1, their values for the first six modes of vibration are summarized.

Mode number, i	1	2	3	4	5	6
$\lambda_i L$	1.8751	4.694	7.855	10.996	14.137	17.279
α_i	0.25000	0.25003	0.24990	0.24980	0.25008	0.24989
β_i	0.39150	-0.21701	0.12721	-0.09086	0.07074	-0.05785

Table 2.1 The values of some important parameters of cantilever vibration for the first six modes of vibration

The final issue of this section is transferring the governing equation for the deflection of the cantilever and its boundary conditions from the time domain to the frequency domain. This is done by taking the Fourier transform of Equations (2.5), (2.6) and (2.7) giving:

$$EI \frac{d^4 \hat{Y}_{(x|\omega)}}{dx^4} - \rho_c A \omega^2 \hat{Y}_{(x|\omega)} = \hat{F}_{hydro(x|\omega)} + \hat{F}_{drive(x|\omega)} \quad \text{Equation (2.21)}$$

and

$$\hat{Y}|_{x=0} = \frac{\partial \hat{Y}}{\partial x} \Big|_{x=0} = \frac{\partial^2 \hat{Y}}{\partial x^2} \Big|_{x=L} = \frac{\partial^3 \hat{Y}}{\partial x^3} \Big|_{x=L} = 0 \quad \text{Equation (2.22)}$$

where ω is the radial frequency and the symbol ' $\hat{}$ ' denotes the transformed function.

2.2) Hydrodynamic drag force

No matter what type of excitation technique is used, the vibration of an AFM cantilever in any medium other than vacuum results in a drag force on the cantilever. Therefore, in order to continue our analysis, we need to have a general mathematical form for this hydrodynamic force. Here, we follow the approach of Sader⁹ who scaled the hydrodynamic drag force for a circular cross section beam to a rectangular one.

Based on the third assumption that was mentioned at the beginning of this chapter, the hydrodynamic drag force on each point of the cantilever can be approximated by the hydrodynamic force that would be applied on an infinitely long rigid beam that oscillates transversely with the same amplitude, $\hat{Y}_{(x|\omega)}$, in the fluid. The reason is that, for such a situation, the variation of the velocity field along the length of the beam is less than over

the cross section plane. Therefore the 3D problem can be simplified to 2D. For a circular cylinder beam oscillating transversely with amplitude much smaller than its diameter (see Figure 2.3), the hydrodynamic drag force was first calculated by Stokes in 1851. Because of its importance, his theory is presented first.

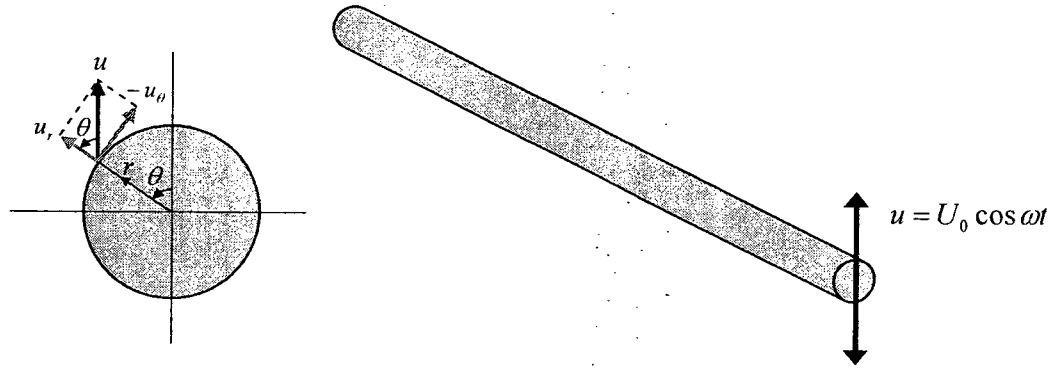


Figure 2.3 A circular cylinder oscillating transversely along a diameter

Let us assume that the velocity of such a beam is:

$$u = U_0 \cos \omega t = U_0 e^{i\omega t} \quad \text{Equation (2.23)}$$

and because of the particular geometry of the beam, we write the momentum equations for the surrounding fluid in the cylindrical coordinate system:

$$\begin{aligned} \frac{\partial v_r}{\partial t} + v_r \frac{\partial v_r}{\partial r} + \frac{v_\theta}{r} \frac{\partial v_r}{\partial \theta} - \frac{v_\theta^2}{r} &= -\frac{1}{\rho_f} \frac{\partial p}{\partial r} + \frac{\mu_f}{\rho_f} \left(\nabla^2 v_r - \frac{v_r}{r^2} - \frac{2}{r^2} \frac{\partial v_\theta}{\partial \theta} \right) \\ \frac{\partial v_\theta}{\partial t} + v_r \frac{\partial v_\theta}{\partial r} + \frac{v_\theta}{r} \frac{\partial v_\theta}{\partial \theta} + \frac{v_r v_\theta}{r} &= -\frac{1}{\rho_f} \frac{\partial p}{r \partial \theta} + \frac{\mu_f}{\rho_f} \left(\nabla^2 v_\theta + \frac{2}{r^2} \frac{\partial v_r}{\partial \theta} - \frac{v_\theta}{r^2} \right) \end{aligned} \quad \text{Equation (2.24)}$$

In Equation (2.24), v_r and v_θ are radial and tangential components of the fluid velocity, ρ_f and μ_f are the density and viscosity of the fluid and ∇^2 is defined as:

$$\nabla^2 \equiv \frac{\partial^2}{\partial r^2} + \frac{1}{r} \frac{\partial}{\partial r} + \frac{1}{r^2} \frac{\partial^2}{\partial \theta^2} \quad \text{Equation (2.25)}$$

For such a moving body, the boundary conditions of the fluid are zero velocity at infinity and the beam velocity on the cylinder, that is:

$$\text{At infinity} \quad \begin{cases} v_r|_{r \rightarrow \infty} = 0 \\ v_\theta|_{r \rightarrow \infty} = 0 \end{cases} \quad \text{Equation (2.26)}$$

$$\text{At the cylinder} \quad \begin{cases} v_r|_{r=\frac{D}{2}} = U_0 e^{i\omega t} \cos \theta \\ v_\theta|_{r=\frac{D}{2}} = -U_0 e^{i\omega t} \sin \theta \end{cases} \quad \text{Equation (2.27)}$$

Because the amplitude of vibration is small, the nonlinear terms in the momentum equations can be neglected. Therefore:

$$\begin{aligned} \frac{\partial v_r}{\partial t} &= -\frac{1}{\rho_f} \frac{\partial p}{\partial r} + \frac{\mu_f}{\rho_f} \left(\nabla^2 v_r - \frac{v_r}{r^2} - \frac{2}{r^2} \frac{\partial v_\theta}{\partial \theta} \right) \\ \frac{\partial v_\theta}{\partial t} &= -\frac{1}{\rho_f} \frac{\partial p}{r \partial \theta} + \frac{\mu_f}{\rho_f} \left(\nabla^2 v_\theta + \frac{2}{r^2} \frac{\partial v_r}{\partial \theta} - \frac{v_\theta}{r^2} \right) \end{aligned} \quad \text{Equation (2.28)}$$

In order to solve these differential equations, we can define the stream function in the cylindrical coordinate system as:

$$\begin{aligned} v_r &= \frac{1}{r} \frac{\partial \psi}{\partial \theta} \\ v_\theta &= -\frac{\partial \psi}{\partial r} \end{aligned} \quad \text{Equation (2.29)}$$

and by eliminating the pressure term from the momentum equations, we find the following equation for the stream function:

$$\left(\nabla^2 - \frac{\rho_f}{\mu_f} \frac{\partial}{\partial t} \right) \nabla^2 \psi = 0 \quad \text{Equation (2.30)}$$

This equation has the solution of:

$$\psi = \psi_1 + \psi_2 \quad \text{Equation (2.31)}$$

where ψ_1 and ψ_2 satisfy the following equations:

$$\nabla^2 \psi_1 = 0 \quad \text{Equation (2.32)}$$

$$\left(\nabla^2 - \frac{\rho_f}{\mu_f} \frac{\partial}{\partial t} \right) \psi_2 = 0 \quad \text{Equation (2.33)}$$

Solving the above equations will result in the following functions for ψ_1 and ψ_2 :

$$\begin{cases} \psi_1 = \frac{A}{r} e^{i\omega t} \sin \theta \\ \psi_2 = B K_1 \left(r \sqrt{i \frac{\rho_f \omega}{\mu_f}} \right) e^{i\omega t} \sin \theta \end{cases} \quad \text{Equation (2.34)}$$

where $i = \sqrt{-1}$ and the coefficients of A and B are obtained by applying the boundary conditions giving:

$$A = \frac{D^2}{4} U_0 \left(1 + \frac{2 K_1(\sqrt{i \text{Re}})}{\sqrt{i \text{Re}} K_0(\sqrt{i \text{Re}})} \right) \quad \text{Equation (2.35)}$$

$$B = \frac{2U_0}{\sqrt{i \text{Re}} K_0(\sqrt{i \text{Re}})} \quad \text{Equation (2.36)}$$

In the above equations, the functions K_0 and K_1 are modified Bessel functions of the third kind and Re is the Reynolds number which for this geometry is defined as follows:

$$\text{Re} = \frac{\rho_f \omega D^2}{4\mu_f} \quad \text{Equation (2.37)}$$

The applied hydrodynamic drag force on the beam per unit length can be calculated from the following equation using the stress tensor:

$$F_{hydro} = \frac{D}{2} \int_0^{2\pi} (p_{rr} \cos \theta - p_{r\theta} \sin \theta) d\theta \quad \text{Equation (2.38)}$$

where p_{rr} and $p_{r\theta}$ are defined as:

$$\begin{cases} p_{rr} = -p + 2\mu_f \frac{\partial v_r}{\partial r} \\ p_{r\theta} = \mu_f \left(r \frac{\partial}{\partial r} \left(\frac{v_\theta}{r} \right) + \frac{1}{r} \frac{\partial v_r}{\partial \theta} \right) \end{cases} \quad \text{Equation (2.39)}$$

The following expression for F_{hydro} is then obtained:

$$F_{hydro} = -\frac{\pi}{4} \rho_f D^2 U_0 i\omega \Gamma_{circ}(\omega) e^{i\omega t} \quad \text{Equation (2.40)}$$

where $\Gamma_{circ}(\omega)$ is called the hydrodynamic function for the circular beam and defined as:

$$\Gamma_{circ}(\omega) = 1 + \frac{4K_1(\sqrt{i\text{Re}})}{\sqrt{i\text{Re}} K_0(\sqrt{i\text{Re}})} \quad \text{Equation (2.41)}$$

It should be mentioned that because of the consistency with the definition of the Fourier transform which is:

$$\hat{X} = \int_{-\infty}^{+\infty} x e^{-i\omega t} dt \quad \text{Equation (2.42)}$$

it is more convenient to consider a velocity having a time dependency of $\exp(-i\omega t)$ for the circular beam. In this case, the determined hydrodynamic function is the conjugate of Equation (2.41), which is:

$$\Gamma_{circ}(\omega) = 1 + \frac{4iK_1(-i\sqrt{i\text{Re}})}{\sqrt{i\text{Re}} K_0(-i\sqrt{i\text{Re}})} \quad \text{Equation (2.43)}$$

Knowing that the displacement of the beam is the integral of its velocity, we can write:

$$y = \int u \, dt = \int U_0 e^{i\omega t} \, dt = \frac{U_0}{i\omega} e^{i\omega t} \quad \text{Equation (2.44)}$$

And by comparing the above equation with Equation (2.40), the hydrodynamic drag force can be written in the form of:

$$F_{hydro} = \frac{\pi}{4} \rho_f D^2 \omega^2 \Gamma_{circ}(\omega) y \quad \text{Equation (2.45)}$$

Therefore if we stay within the region of validity of our assumptions, for the vibration of an elastic circular beam, the hydrodynamic drag force on point x of the beam and at the frequency ω will be:

$$\hat{F}_{hydro(x|\omega)} = \frac{\pi}{4} \rho_f \omega^2 D^2 \Gamma_{circ}(\omega) \hat{Y}_{(x|\omega)} \quad \text{Equation (2.46)}$$

Such an approach can be used for any geometry but an analytical result is not always guaranteed. For a rectangular cross section beam, Sader⁹ used the same formula as Equation (2.46) for the applied hydrodynamic drag force on the beam but he substituted the width of the cantilever, b , instead of the diameter of the cylinder, D , and also scaled the hydrodynamic function of the circular cross section, $\Gamma_{circ}(\omega)$, to the rectangular one, $\Gamma_{rect}(\omega)$, by using a correction factor as indicated in the following equations:

$$\hat{F}_{hydro(x|\omega)} = \frac{\pi}{4} \rho_f \omega^2 b^2 \Gamma_{rect}(\omega) \hat{Y}_{(x|\omega)} \quad \text{Equation (2.47)}$$

$$\Gamma_{rect}(\omega) = \Omega(\omega) \times \Gamma_{circ}(\omega) \quad \text{Equation (2.48)}$$

For determination of this correction factor, Sader⁹ solved the Navier-Stokes equations for the surrounding fluid of the rectangular cross section beam numerically and then he performed a nonlinear least-squares fit to the ratio of the numerically obtained hydrodynamic function data of a rectangular beam to the analytically obtained

hydrodynamic function of a circular beam. The resultant expression for $\Omega(\omega)$, which is valid for the Reynolds range of $[10^{-6}, 10^4]$, is:

$$\Omega(\omega) = \Omega_{\text{Re}}(\omega) + i \Omega_{\text{Im}}(\omega) \quad \text{Equation (2.49)}$$

where

$$\begin{aligned} \Omega_{\text{Re}}(\omega) = & (0.913242 - 0.48274 \tau + 0.46842 \tau^2 - 0.12886 \tau^3 \\ & + 0.044055 \tau^4 - 0.0035117 \tau^5 + 0.00069085 \tau^6) \\ & \times (1 - 0.56964 \tau + 0.48690 \tau^2 - 0.13444 \tau^3 \\ & + 0.045155 \tau^4 - 0.0035862 \tau^5 + 0.00069085 \tau^6)^{-1} \end{aligned} \quad \text{Equation (2.50)}$$

and

$$\begin{aligned} \Omega_{\text{Im}}(\omega) = & (-0.024134 - 0.029256 \tau + 0.016294 \tau^2 \\ & - 0.00010961 \tau^3 + 0.000064577 \tau^4 - 0.000044510 \tau^5) \\ & \times (1 - 0.59702 \tau + 0.55182 \tau^2 - 0.18357 \tau^3 \\ & + 0.079156 \tau^4 - 0.014369 \tau^5 + 0.0028361 \tau^6)^{-1} \end{aligned} \quad \text{Equation (2.51)}$$

and in the above equations τ and Re are defined as:

$$\tau = \log_{10}(\text{Re}) \quad \text{Equation (2.52)}$$

$$\text{Re} = \frac{\rho_f \omega b^2}{4 \mu_f} \quad \text{Equation (2.53)}$$

2.3) Different types and kinematics of excitation

2.3.1) Thermal noise

The driving force for the thermally excited cantilever is the result of collisions of surrounding fluid molecules to the cantilever or the Brownian motion of the fluid. Because of the random nature of Brownian motion, it is obvious that the magnitude of

this force is independent of the position on the length of the cantilever. However Paul et al⁵⁸ showed that this force is frequency dependant and its spectral density is not white. They determined its magnitude based on the fluctuation-dissipation theorem, that is:

$$F_B(\omega) = 4K_B T \left(\frac{\pi}{4} \rho_f b^2 \right) \omega \Gamma_{\text{Im } rect}(\omega) \quad \text{Equation (2.54)}$$

where K_B is the Boltzmann's constant, T is the absolute temperature, and $\Gamma_{\text{Im } rect}(\omega)$ indicates the imaginary part of the hydrodynamic function $\Gamma_{rect}(\omega)$.

Following the approach made by Xu et al²² for the theoretical response of a thermally excited cantilever, we could write the governing equation of the cantilever deflection as follows:

$$EI \frac{d^4 \hat{Y}_{(x|\omega)}}{dx^4} - \rho_c A \omega^2 \hat{Y}_{(x|\omega)} = \hat{F}_{hydro(x|\omega)} + \hat{F}_B(\omega) \quad \text{Equation (2.55)}$$

For the boundary conditions of:

$$\hat{Y}|_{x=0} = \frac{\partial \hat{Y}}{\partial x} \Big|_{x=0} = \frac{\partial^2 \hat{Y}}{\partial x^2} \Big|_{x=L} = \frac{\partial^3 \hat{Y}}{\partial x^3} \Big|_{x=L} = 0 \quad \text{Equation (2.56)}$$

the general solution for this equation is in the form of:

$$\hat{Y}_{(x|\omega)} = \sum_{i=1}^{\infty} C_i(\omega) \phi_i(x) \quad \text{Equation (2.57)}$$

where the mode shapes of $\phi_i(x)$ are defined in section 2.1. We are going to derive an equation for the coefficients of $C_i(\omega)$. By substituting Equations (2.47), (2.54) and (2.57) in to Equation (2.55), we have:

$$\begin{aligned} & \sum_{i=1}^{\infty} (EI C_i \phi_i'''' - \rho_c A \omega^2 C_i \phi_i) \\ & = \sum_{i=1}^{\infty} \left(\frac{\pi}{4} \rho_f \omega^2 b^2 \Gamma_{rect} C_i \phi_i \right) + 4K_B T \left(\frac{\pi}{4} \rho_f b^2 \right) \omega \Gamma_{\text{Im } rect} \end{aligned} \quad \text{Equation (2.58)}$$

Keeping in mind the orthogonality properties of $\phi_i(x)$, the following equation can be obtained by multiplying the above equation by $\phi_j(x)$ and integrating over the length of the cantilever:

$$\frac{C_i(\omega)}{K_B T} = \frac{4 \left(\frac{\pi}{4} \rho_f b^2 \right) \omega \Gamma_{\text{tm } \text{rect}}(\omega) \times \beta_i L}{EI \lambda_i^4 \times \alpha_i L - \omega^2 \left(\rho_c A + \frac{\pi}{4} \rho_f b^2 \Gamma_{\text{rect}}(\omega) \right) \times \alpha_i L} \quad \text{Equation (2.59)}$$

where α_i , β_i and λ_i are defined in Equations (2.15), (2.19) and (2.20) and their values for the first six modes of vibration are summarized in Table 2.1. Using Equation (2.59), we can find the coefficients of $C_i(\omega)$ at a given absolute temperature of T and consequently, the cantilever deflection can be determined using Equation (2.57). However, in most of AFMs, the measured value is the inclination of the cantilever rather than its deflection. Therefore in this case, the theoretical response would be the deferential of the Equation (2.57) respect to x that is:

$$\frac{\partial \bar{Y}_{(x|\omega)}}{\partial x} = \sum_{i=1}^{\infty} C_i(\omega) \frac{d\phi_i(x)}{dx} \quad \text{Equation (2.60)}$$

where both $C_i(\omega)$ and $\phi_i(x)$ are now known. In Appendix C (pages 169-170), a MATLAB code for producing the theoretical response of a thermally excited cantilever based on the given material and geometrical properties of both the cantilever and the surrounding fluid is presented and Figure 2.4 shows a typical theoretical response of such a cantilever. For this figure, it is assumed that the cantilever's material is silicon and its length, width and the thickness are 400, 30 and 2 μm respectively. Also it is assumed that the cantilever is immersed in water.

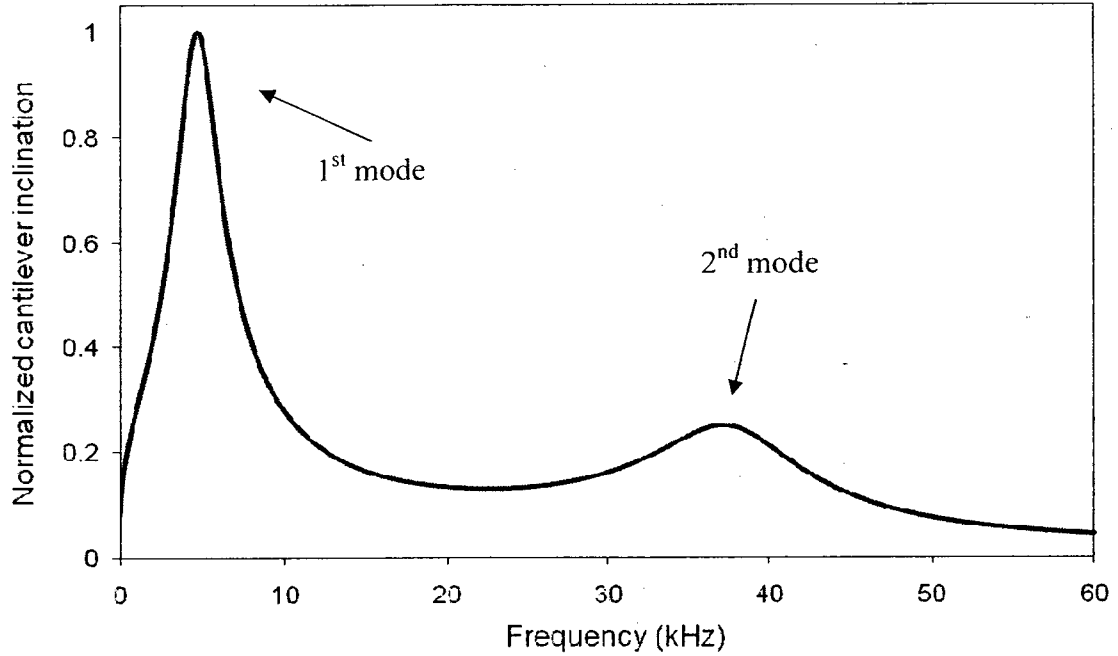


Figure 2.4 Theoretical response of a silicon cantilever which is excited thermally. The dimensions of the cantilever are $400 \times 30 \times 2 \mu\text{m}$ and the surrounding fluid is water. The response is normalized by the magnitude of the first mode peak.

2.3.2) Frequency sweep

The frequency sweep is in fact an acoustic excitation technique in which the base of the cantilever has the controlled motion of:

$$y_b(t) = A_{FS} \cos \omega_0 t \quad \text{Equation (2.61)}$$

where the angular frequency of ω_0 will change in the range of $[\omega_1, \omega_2]$ in n steps and at each step will stay constant for τ seconds. Also because the amplitude of vibration in acoustic excitation is much larger than the thermal excitation, the effect of Brownian driving force can be neglected compared to the hydrodynamic damping force here. Keeping this information in mind and following Xu et al's²² approach, the governing equation for the cantilever deflection and its boundary conditions become:

$$EI \frac{\partial^4 y_{(x,t)}}{\partial x^4} + \rho_c A \frac{\partial^2 y_{(x,t)}}{\partial t^2} = F_{hydro(x,t)} \quad \text{Equation (2.62)}$$

$$\begin{cases} y|_{x=0} = y_b(t) \\ \left. \frac{\partial y}{\partial x} \right|_{x=0} = \left. \frac{\partial^2 y}{\partial x^2} \right|_{x=L} = \left. \frac{\partial^3 y}{\partial x^3} \right|_{x=L} = 0 \end{cases} \quad \text{Equation (2.63)}$$

In the above equations, the $y_{(x,t)}$ is the absolute motion of the cantilever, however in the AFM, as mentioned before, the measured value is the slope of the cantilever. If we define the relative motion of the cantilever to the movement of its base as $w_{(x,t)}$, that is:

$$w_{(x,t)} = y_{(x,t)} - y_b(t) \quad \text{Equation (2.64)}$$

then the slope of the cantilever for both of these quantities is the same, that is:

$$\frac{\partial w_{(x,t)}}{\partial x} = \frac{\partial y_{(x,t)}}{\partial x} \quad \text{Equation (2.65)}$$

Therefore we can write the governing equation of the cantilever in terms of its relative motion, in the frequency domain, as:

$$EI \frac{d^4 \hat{W}_{(x|\omega)}}{dx^4} - \rho_c A \omega^2 \hat{W}_{(x|\omega)} = \hat{F}_{hydro(x|\omega)} + \rho_c A \omega^2 \hat{Y}_{b(\omega)} \quad \text{Equation (2.66)}$$

and the boundary conditions become:

$$\hat{W}|_{x=0} = \left. \frac{\partial \hat{W}}{\partial x} \right|_{x=0} = \left. \frac{\partial^2 \hat{W}}{\partial x^2} \right|_{x=L} = \left. \frac{\partial^3 \hat{W}}{\partial x^3} \right|_{x=L} = 0 \quad \text{Equation (2.67)}$$

In Equation (2.66), it is clear that the effect of considering a non-inertial reference frame which moves with the base of the cantilever is the appearance of an inertial term as an external driving force in governing equation. The solution for this differential equation is again in the form of:

$$\hat{W}_{(x|\omega)} = \sum_{i=1}^{\infty} C_i(\omega) \phi_i(x) \quad \text{Equation (2.68)}$$

and having the same approach as thermal noise, we obtain the following equation for the coefficients of $C_i(\omega)$ in terms of general form of $\hat{Y}_b(\omega)$:

$$\frac{C_i(\omega)}{\hat{Y}_b(\omega)} = \frac{\omega^2 \left(\rho_c A + \frac{\pi}{4} \rho_f b^2 \Gamma_{rect}(\omega) \right) \times \beta_i L}{EI \lambda_i^4 \times \alpha_i L - \omega^2 \left(\rho_c A + \frac{\pi}{4} \rho_f b^2 \Gamma_{rect}(\omega) \right) \times \alpha_i L} \quad \text{Equation (2.69)}$$

Knowing that the Fourier transform of $y_b(t) = A_{FS} \cos \omega_0 t$ is:

$$\hat{Y}_b(\omega) = \frac{1}{4\pi} A_{FS} [\delta(\omega - \omega_0) + \delta(\omega + \omega_0)] \quad \text{Equation (2.70)}$$

then the coefficient of $C_i(\omega_0)$ at the frequency of excitation will be:

$$\frac{C_i(\omega_0)}{A_{FS}} = \frac{\frac{1}{4\pi} \omega_0^2 \left(\rho_c A + \frac{\pi}{4} \rho_f b^2 \Gamma_{rect}(\omega_0) \right) \times \beta_i L}{EI \lambda_i^4 \times \alpha_i L - \omega_0^2 \left(\rho_c A + \frac{\pi}{4} \rho_f b^2 \Gamma_{rect}(\omega_0) \right) \times \alpha_i L} \quad \text{Equation (2.71)}$$

Now the inclination of the cantilever can be determined from:

$$\frac{\partial \hat{W}_{(x|\omega_0)}}{\partial x} = \sum_{i=1}^{\infty} C_i(\omega_0) \frac{d\phi_i(x)}{dx} \quad \text{Equation (2.72)}$$

In Appendix D (pages 171-172), a MATLAB code for producing the theoretical response of a cantilever for the case of the frequency sweep based on the given material and geometrical properties of both the cantilever and the surrounding fluid is presented and Figure 2.5 shows a typical theoretical response of such a cantilever. The assumed properties of the cantilever and the surrounding fluid are the same as in Figure 2.4.

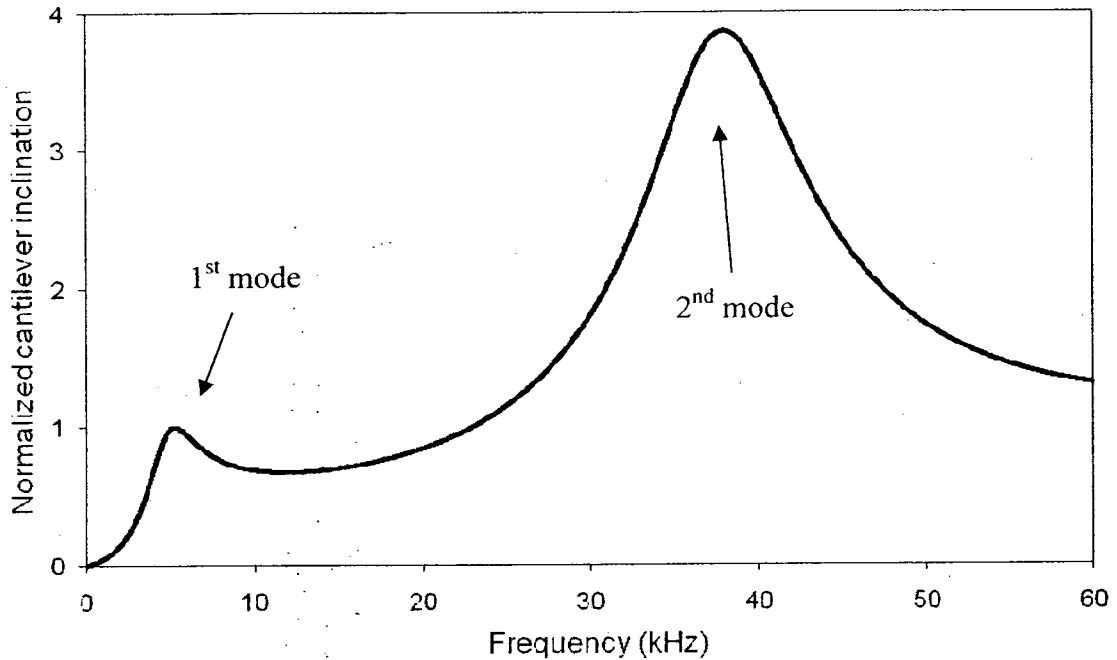


Figure 2.5 Theoretical response of a silicon cantilever which is excited with a frequency sweep. The dimensions of the cantilever are $400 \times 30 \times 2 \mu m$ and the surrounding fluid is water. The response is normalized by the magnitude of the first mode peak.

2.3.3) Step excitation

Like the frequency sweep, the step excitation is an acoustic excitation technique too; but here, the base of the cantilever has the motion of:

$$y_b(t) = \begin{cases} 0 & t < 0 \\ A_{SE} & t \geq 0 \end{cases} \quad \text{Equation (2.73)}$$

For this type of boundary condition usually the Laplace transform technique is being used but because we do not have any general formula for the hydrodynamic drag force of a cantilever that moves arbitrarily, this method is not applicable. Therefore, the specific form of the hydrodynamic drag force forced us to use the Fourier transform technique

here as well. As no solution for the step excitation was available in the literature, the following derivations represent one of the contributions of this thesis.

Two methods can be applied to solve the problem: (1) using a non-inertial reference frame or relative movement of the cantilever end to its base, which is the same approach that was used in modeling the frequency sweep and (2) using an inertial reference frame or absolute movement of the cantilever end.

In the first method, we can use the same derivation as the one used for the frequency sweep but we have to substitute the following equation, as the Fourier transform of Heaviside step function, instead of $\hat{Y}_b(\omega)$ in Equation (2.69):

$$F(\omega) = \frac{\delta(\omega)}{4\pi} - \frac{i}{\omega} \quad \text{Equation (2.74)}$$

Consequently, we have the following equation for $C_i(\omega)$ at all non-zero frequencies:

$$\frac{C_i(\omega)}{A_{SE}} = \frac{-i\omega \left(\rho_c A + \frac{\pi}{4} \rho_f b^2 \Gamma_{rect}(\omega) \right) \times \beta_i L}{EI \lambda_1^4 \times \alpha_i L - \omega^2 \left(\rho_c A + \frac{\pi}{4} \rho_f b^2 \Gamma_{rect}(\omega) \right) \times \alpha_i L} \quad \text{Equation (2.75)}$$

It should be mentioned that for the case of frequency sweep, the value of $\hat{Y}_b(\omega)$, which is the Fourier transform of cosine functions, is zero at all frequencies except the frequency of excitation and as a result, the coefficient of $C_i(\omega)$ is zero at all frequencies except the excitation frequency. Therefore the curve obtained for the theoretical response of a frequency sweep consists of the values of these non-zeros at each frequency of excitation, ω_0 . In other words, the presented curve in Figure 2.5 was constructed with the non-zeros points of many Fourier transforms curves each of which is related to one

frequency of excitation. However, the obtained curve for the case of the step excitation is the Fourier transform of the cantilever response itself.

Moving to the second method, we are considering both the inertial reference frame and the absolute motion of the cantilever. As a result, we are solving the following differential equation for the vibration of the cantilever in the frequency domain:

$$\frac{d^4 \hat{Y}_{(x|\omega)}}{dx^4} - B_{(\omega)}^4 \hat{Y}_{(x|\omega)} = 0 \quad \text{Equation (2.76)}$$

where

$$B_{(\omega)} = \lambda_1 \sqrt{\frac{\omega}{\omega_{vac,1}}} \left(1 + \frac{\pi \rho_f b^2}{4 \rho_c A} \Gamma_{rect}(\omega) \right)^{\frac{1}{4}} \quad \text{Equation (2.77)}$$

In the above equation, $\omega_{vac,1}$ is the fundamental resonant frequency of the cantilever in vacuum and has the following relation with the cantilever characteristics:

$$\omega_{vac,1} = \lambda_1^2 \sqrt{\frac{EI}{\rho_c A}} \quad \text{Equation (2.78)}$$

The boundary conditions in this situation are:

$$\begin{aligned} 1) \quad \hat{Y} \Big|_{x=0} &= \frac{\delta(\omega)}{4\pi} - \frac{i}{\omega} \\ 2) \quad \frac{\partial \hat{Y}}{\partial x} \Big|_{x=0} &= 0 \\ 3) \quad \frac{\partial^2 \hat{Y}}{\partial x^2} \Big|_{x=L} &= 0 \\ 4) \quad \frac{\partial^3 \hat{Y}}{\partial x^3} \Big|_{x=L} &= 0 \end{aligned} \quad \text{Equation (2.79)}$$

and the general solution for the Equation (2.76) is in the form of:

$$\hat{Y}_{(x|\omega)} = A_1(\cos B_{(\omega)}x + \cosh B_{(\omega)}x) + A_2(\cos B_{(\omega)}x - \cosh B_{(\omega)}x) + A_3(\sin B_{(\omega)}x + \sinh B_{(\omega)}x) + A_4(\sin B_{(\omega)}x - \sinh B_{(\omega)}x) \quad \text{Equation (2.80)}$$

Applying the first and second boundary conditions gives:

$$A_1 = \frac{\delta_{(\omega)}}{8\pi} - \frac{i}{2\omega} \quad \text{Equation (2.81)}$$

$$A_3 = 0$$

and from the third and fourth boundary conditions we will have:

$$A_2 = -A_1 \frac{\sin(B_{(\omega)}L)\sinh(B_{(\omega)}L)}{1 + \cos(B_{(\omega)}L)\cosh(B_{(\omega)}L)} \quad \text{Equation (2.82)}$$

$$A_4 = A_1 \frac{\sin(B_{(\omega)}L)\cosh(B_{(\omega)}L) + \cos(B_{(\omega)}L)\sinh(B_{(\omega)}L)}{1 + \cos(B_{(\omega)}L)\cosh(B_{(\omega)}L)}$$

Therefore by plugging the coefficient of A_1 , A_2 , A_3 and A_4 in Equation (2.80), we can find the theoretical deflection of the cantilever in the frequency domain. Again because the measured response in the AFM is the inclination of the cantilever, the associated theoretical value can be obtained by differentiating Equation (2.80) respect to x that is:

$$\frac{\partial \hat{Y}_{(x|\omega)}}{\partial x} = A_1 B_{(\omega)}(-\sin B_{(\omega)}x + \sinh B_{(\omega)}x) + A_2 B_{(\omega)}(-\sin B_{(\omega)}x - \sinh B_{(\omega)}x) + A_3 B_{(\omega)}(\cos B_{(\omega)}x + \cosh B_{(\omega)}x) + A_4 B_{(\omega)}(\cos B_{(\omega)}x - \cosh B_{(\omega)}x) \quad \text{Equation (2.83)}$$

It should be mentioned that the second method does not provide any equations for the individual modes of vibration but instead, it provides the exact solution and therefore does not carry any truncation error which always accompanies the solutions that are in the form of series. Figure 2.6 shows the theoretical response of a cantilever, which has the same properties as the cantilevers in Figure 2.4 and 2.5 including the surrounding

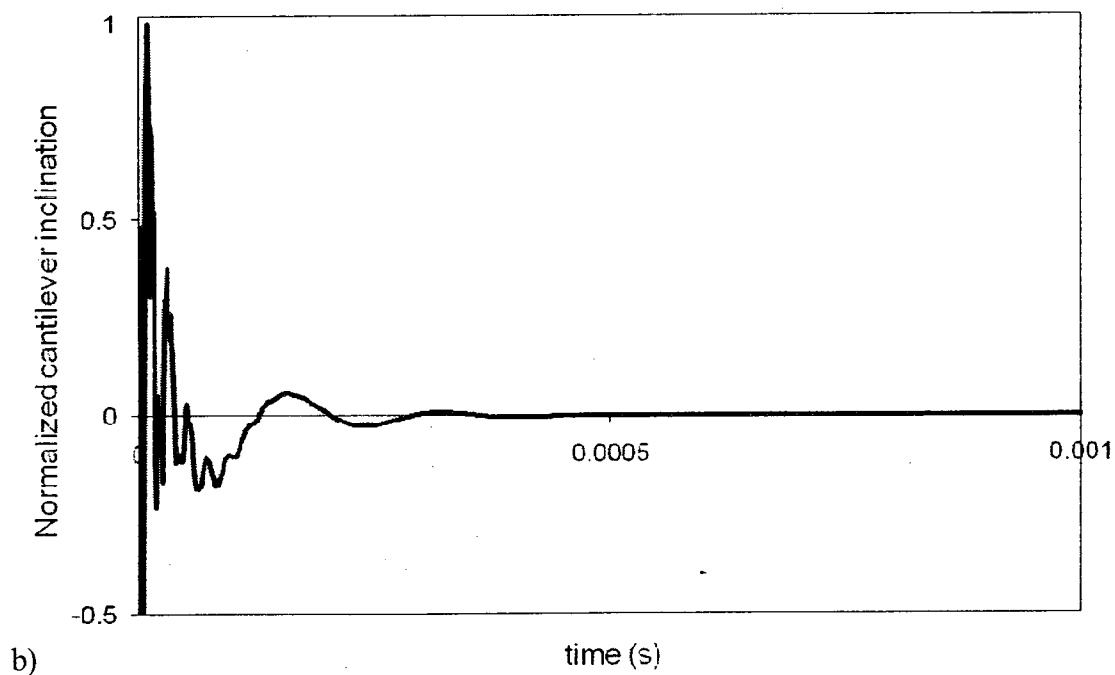
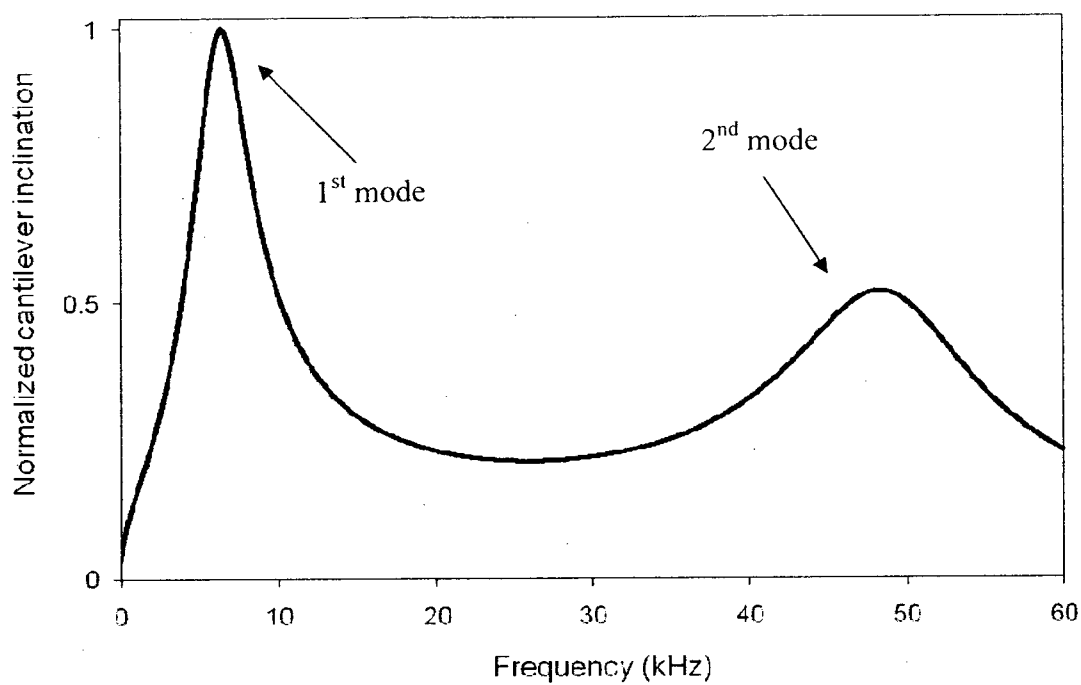


Figure 2.6 Theoretical responses of a silicon cantilever to step excitation. a) In the frequency domain and b) in the time domain. The dimensions of the cantilever are $400 \times 30 \times 2 \mu\text{m}$ and the surrounding fluid is water. The responses are normalized by the magnitude of the first peak.

fluid, to step excitation in both the frequency domain and the time domain. The results for the time domain is obtained numerically using inverse fast Fourier transform. In Appendix E (pages 173-177), a MATLAB code for producing the theoretical response of a cantilever to step excitation is presented.

Chapter 3

Experimental setup, sample preparation and signal processing

3.1) Experimental setup

Figure 3.1 shows the schematic of the experimental setup used in this project. A Digital Instruments Nanoscope III Multimode AFM was used for our experiments. Because the software of the instrument is designed only for the purposes of imaging and force measurements, our control on the input and output of the system was very limited. As a result, the system was modified from its normal configuration by adding a Signal Access Module (SAM) in order to have a direct access to signals between AFM head and controller. Among all of these signals only two of them are useful for our purpose; one is for the excitation of the cantilever (input signal) and the other one is for the vibrational response of the cantilever (output signal).

The input signal was produced by using a signal generator that gave the possibility of producing a signal with a variety of functions and the output signal was recorded using a data acquisition hardware. Both of these devices were controlled by the LabVIEW software⁵⁹. Also this software was used for most of analysis of the data.

Another modification in the system of the AFM was building a new stand for the AFM head. The shape and the supporting mechanism for the AFM head of the new stand

are similar to the original stand but its wall and top surface were made from transparent material which allowed us to track the laser spot for the alignment of the beam on the cantilever while the head was seated and the fluid was manipulated in the system. Also the top surface was coated with Teflon to provide a hydrophobic surface and prevent spreading of the fluid.

The final modification in the system of the AFM was for the tipholder which will be discussed in detail in chapter 4. In the following, a brief explanation about the principal of the AFM and also the specifications of the signal generator, data acquisition hardware and cantilevers, which were used in this project, are presented.

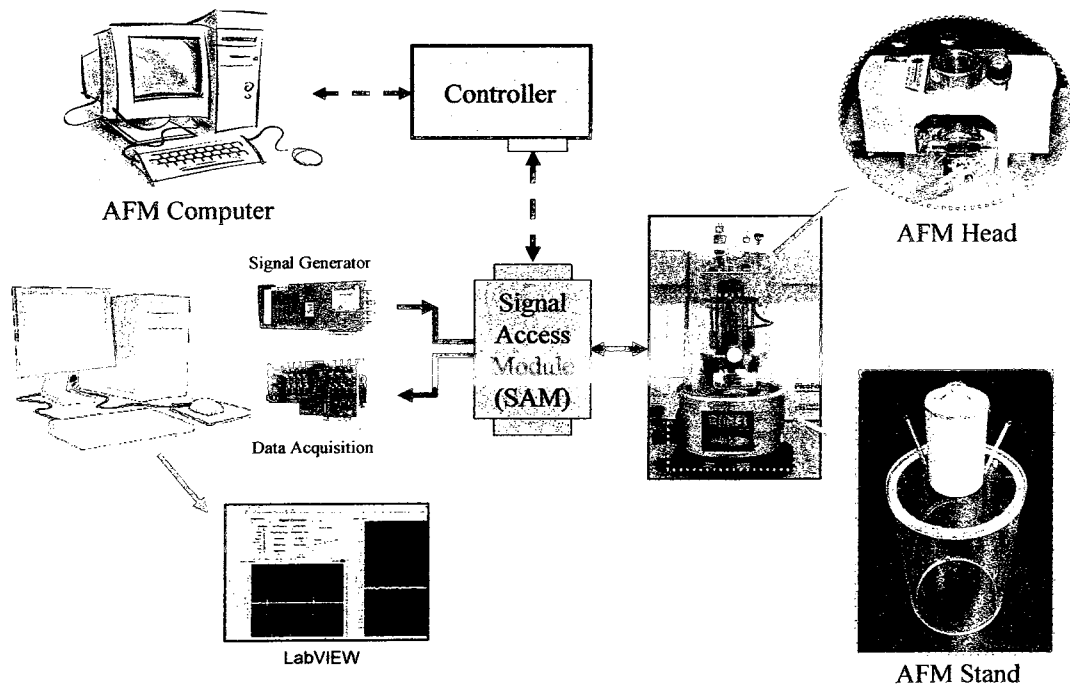


Figure 3.1 Schematic of experimental setup

3.1.1) Atomic Force Microscope (AFM)

As it was mentioned before, the AFM was originally invented for imaging purposes with resolution in the order of nanometers. The principal of the AFM simply consists of performing two operations at the same time. The first one is the scanning of the surface of the sample in the X and Y directions, using a cantilever with a sharp tip at its free end, and the second process is the measuring of the movement of the cantilever free end in the Z direction. These operations result in the representation of the complete topography of the sample surface. Concerning the scanning operation, there are generally two imaging modes; the static mode (also called contact mode) and a variety of dynamic or non-contact modes. In the dynamic modes, the cantilever oscillates at or close to its fundamental resonant frequency. There are many techniques developed for cantilever excitation, which were explained in details in chapter 1. Our AFM uses the acoustic excitation technique which is appropriate for our particular application.

Moving to the measuring of the cantilever movement, techniques such as optical interferometry, capacitive sensing, laser deflection and piezoresistive AFM cantilevers are developed. Among these techniques laser deflection, as is used in our AFM, is the most accurate. In this technique as shown in Figure 3.2, laser light from a solid state diode is reflected off the back of the cantilever and collected by a position sensitive detector (PSD) consisting of four closely spaced photodiodes whose output is collected by a differential amplifier. As a consequence of the angular displacement of the cantilever one photodiode gathers more light than the other photodiode, and this results in the production of an output signal that is proportional to the deflection of the cantilever.

Such a signal is produced from the difference between the photodiode signals when normalized by their sum. The accuracy of such a method allows measurement of deflections down to $<1\text{Å}$ and is limited by thermal noise.

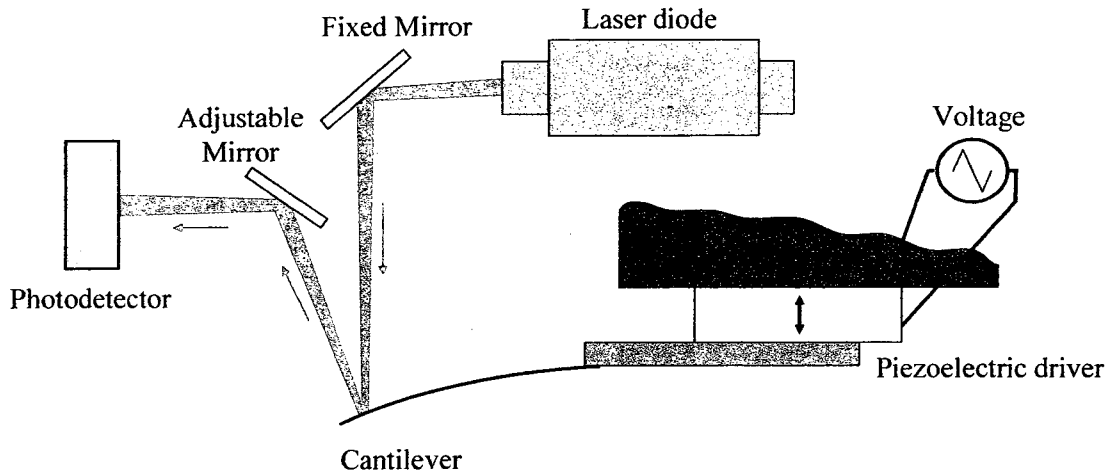


Figure 3.2 Optical system of the AFM

3.1.2) Signal generator

The piezo drive signal is generated using a signal generator from National Instruments that can be installed as a PCI board in nearly any up to date computer (see Figure 3.3). It has the ability to generate a signal with arbitrary function waveforms, but for few specific function waveforms, such as for the sine, square, triangle, noise, ramp and DC offset, it is already built-in inside the hardware. The signal generated using this device can have a voltage up to 10 volts peak-to-peak with a maximum frequency of 20 MHz. Its characteristics involve a 14 bit resolution and up to 100 MS/s of sample rate. Although it originally comes with its own software (NI FGEN soft front panel), it is

better controlled using the LabVIEW software when it is being used with the other electronic devices such as the data acquisition hardware. Finally, it is factory calibrated and also has onboard calibrator references that account for environmental effects on DC gain, offset and timing error. In our project for frequency sweep and step excitations we used the sine and square wave forms respectively. For the thermal noise no signal was applied to the piezo and the cantilever vibration observed was due to the Brownian motion of the surrounding fluid.

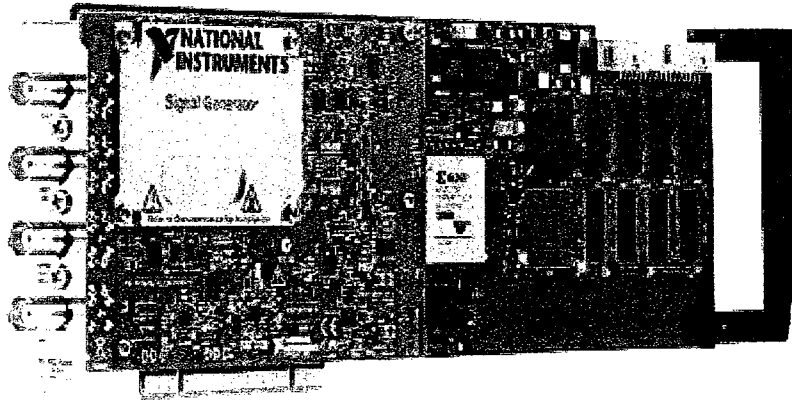


Figure 3.3 PCI-5402 - Signal Generator

3.1.3) Data Acquisition (DAQ)

The response signal from the photo detector was recorded using data acquisition hardware from National Instruments (see Figure 3.4) and similar to our signal generator it can be installed as a PCI board in nearly any up to date computer. This device has the ability of digitizing four signals simultaneously with a maximum sample rate up to 3 mega samples per second for each channel. It is also characterized by a 14 bit resolution

where a better input resolution can be obtained through selecting one of its four different input voltage ranges. Like the signal generator, it comes with its own software, but it is better operated with LabVIEW software in our case. Finally, it should be mentioned that both the signal generator and the data acquisition hardware were synchronized using a RTSI cable in order to have a direct control on the triggering of the devices when we are programming them in LabVIEW.

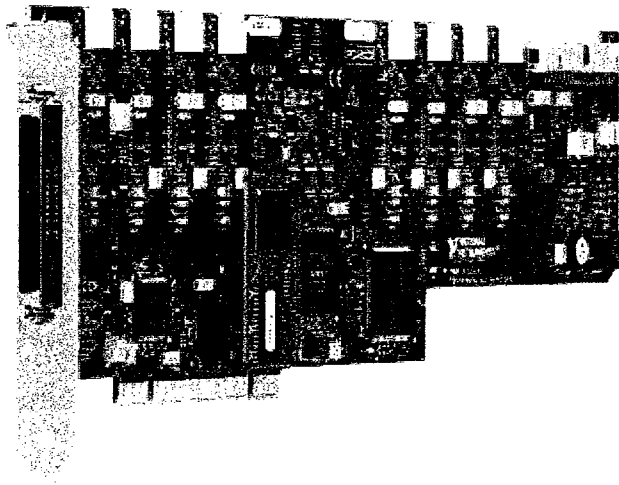


Figure 3.4 PCI-6132 - Multifunction DAQ (S series)

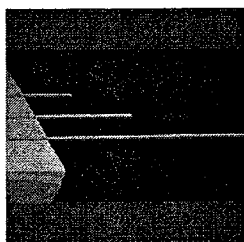
3.1.4) Cantilever material and dimensional properties

In general, most cantilevers that are available in the market are fabricated in two different methods. The cantilevers produced by the first method, called practical cantilevers, are made from low pressure chemical vapour deposition (LPCVD) of silicon nitrate which is coated with a layer of gold to improve its reflectivity. The second type, called calibrated cantilevers, is made from undoped and uncoated single crystal silicon

through a micromachining process. Because of the complexity in the fabrication process of these cantilevers, they are more expensive than the practical cantilevers.

Calibrated cantilevers have very precise dimensions and geometry and uniform material properties which are in accordance with the assumptions of the theory described in chapter 2. Moreover, the manufacturers of these cantilevers provide their dimensions with very precise tolerance (except for the thickness). In contrast, for the practical cantilevers, the manufacturers only provide the nominal values for the dimensions and as a result the user has to either accept huge errors in his results or measure the precise dimensions by himself using other techniques such as electron microscopy.

In this project, whenever the comparison between the experimental results and the theory was intended, calibrated cantilevers were used. For the qualitative experiments, which do not need the information about the cantilever's geometrical and material properties, practical cantilevers were used. For the calibrated cantilevers, the models used were the CLFC-NOBO tipless cantilevers from Veeco with the dimensions are indicated in Figure 3.5. Furthermore, these cantilevers, as mentioned earlier, are silicon with a modulus of 1.7×10^{11} Pa and a density of 2300 kg/m^3 . For practical cantilevers, their model and dimensions are mentioned in the text wherever they have been used.



	Length (μm)	Width (μm)	Thickness (μm)
Long	397	29	1.8 - 2.2
Medium	197	29	1.8 - 2.2
Short	97	29	1.8 - 2.2

Figure 3.5 CLFC-NOBO tipless cantilever from Veeco

Finally, the thickness of the calibrated cantilevers can be estimated from the resonant frequency of the cantilever under vacuum; however we used the resonant frequency of the cantilever in air as an approximation. It was reported that the error for such an approximation is less than 2%^{21,31,39,57}.

3.2) Sample preparation

In this project, both of Newtonian and non-Newtonian fluids were used in order to test the applicability of the proposed technique. The stress-strain rate behaviour of Newtonian fluids can be described simply by a constant parameter of viscosity. For this type of fluid, ethanol⁶⁰ and some solutions of glycerine⁶¹- water were chosen. The advantage of choosing glycerine-water solutions was providing a wide range of viscosity. Figures 3.6 and 3.7 show the density and viscosity of glycerine-water solutions in terms of their concentration at 26 °C. These graphs were generated from the more comprehensive information released by Dow Chemical Company^{62,63} on density and viscosity of the aqueous glycerine at different temperature and concentration (see Appendix F, pages 178-179)

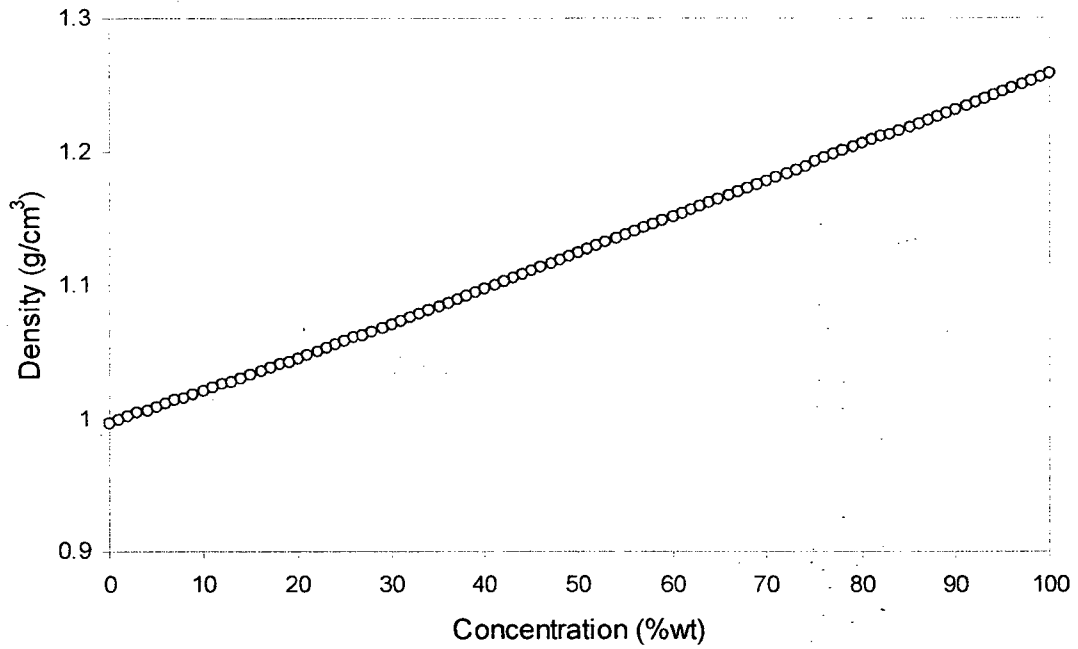


Figure 3.6 Density of glycerin-water solution in terms of its concentration at temperature of 26 °C

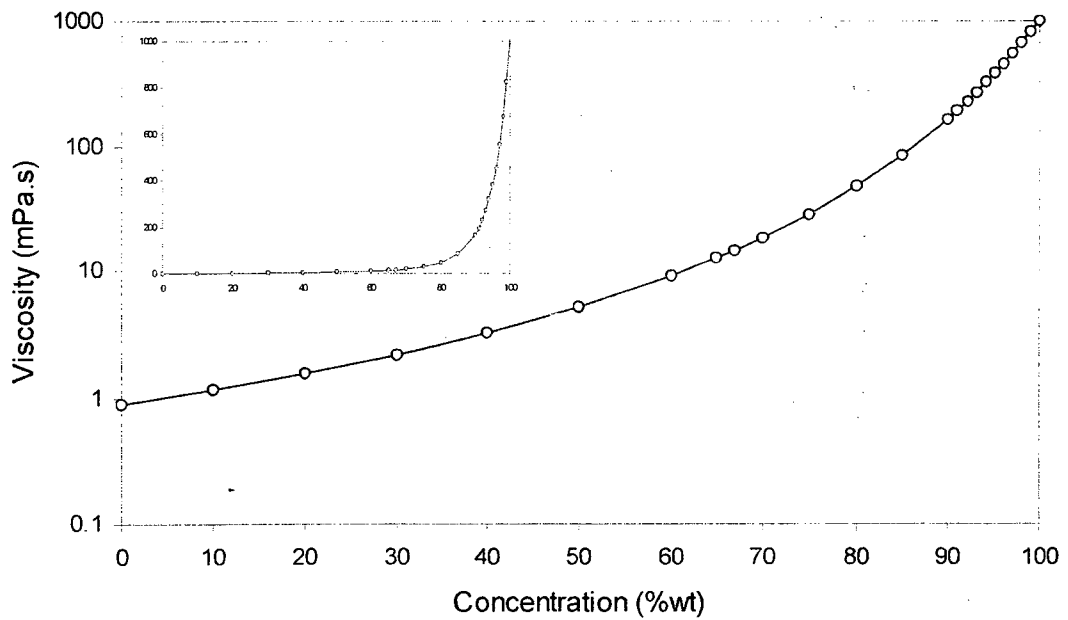


Figure 3.7 Viscosity of glycerin-water solution in terms of its concentration at temperature of 26 °C

These solutions were prepared by simply mixing water and glycerine according to the required weight fraction. Because of the possibility of change of concentration over time, fresh solutions were prepared for each series of tests and were kept in closed containers. Also in order to prevent any formation of bubbles around the cantilever during the experiment, the solutions were degassed by heating the closed container up to 70 °C and quickly cooling it right before the execution of the experiment. In Table 3.1, the properties of ethanol and the selected concentrations of the glycerine-water solutions are summarized.

Fluids	Ethanol	0% GW	25% GW	50% GW	60% GW	75% GW	80% GW	100% GW
Density (kg/m ³)	785	997	1058	1123	1151	1191	1205	1257
Viscosity (mPa.s)	1.08	0.88	1.82	4.93	8.634	26.92	44.38	931.2

Table 3.1 Properties of Newtonian fluids at 26 °C which were examined in this project.

In contrast to Newtonian fluids, non-Newtonian fluids such as polymer solutions exhibit complex behaviour as stress or strain is applied to them. They have both viscous and elastic properties. For this group, solutions of polystyrene⁶⁴ (PS) in diethyl phthalate⁶⁵ (DEP) were chosen because of the wide range of viscosity and elasticity that they can provide. The procedure for preparation of these solutions is as follows. First, for different concentrations of PS solutions, the required amount of PS and DEP were placed in a labelled container. Then the container along with its contents was weighed and its weight was recorded. In order to accelerate the dissolution of the PS in the DEP, dichloromethane⁶⁶ was added as a co-solvent. Next the container was sealed and stirred at room temperature for two days in order to have well-mixed and transparent solutions.

After that the seals were removed and the mixtures were exposed to the air in order for co-solvent to evaporate. The containers were weighed every day to check the amount of co-solvent left in the mixtures. After a few weeks, no change in the weight of containers was observed and their final weights became almost the same as their weights before adding the co-solvent. At this point, it was concluded that the dichloromethane was completely evaporated and the solutions were ready for the experiments.

The rheological properties of the solutions were measured using a rotational rheometer⁶⁷ at different temperatures and after that by applying the time-temperature superposition principle, their master curves were generated at 25 °C. Figures 3.8, 3.9, 3.10 and 3.11 show these master curves for the selected concentrations of the PS/DEP solutions and in Table 3.2, their densities and zero shear viscosities are summarized. It should be mentioned that pure DEP is a Newtonian fluid but because of consistency with the PS solutions, it is categorized in this group. Also the non-Newtonian behaviour of the 5% PS/DEP solution was out of the measuring range of the instrument and as a result, we only bring the value of its zero shear viscosity in Table 3.2. Finally the values of shifting factors a_T and b_T , used to generate the master curve for each concentration, are tabulated in Appendix G (pages 180-181)

Concentration (wt %)	0% PS/DEP	5% PS/DEP	8.5% PS/DEP	12% PS/DEP	16% PS/DEP	25% PS/DEP
Density (kg/m ³)	1120	1116.3	1113.7	1111.1	1108.2	1101.6
Zero shear viscosity (mPa.s)	13	138	524	1747	6311	99887

Table 3.2 Properties of non-Newtonian fluids at 25 °C which were examined in this project.

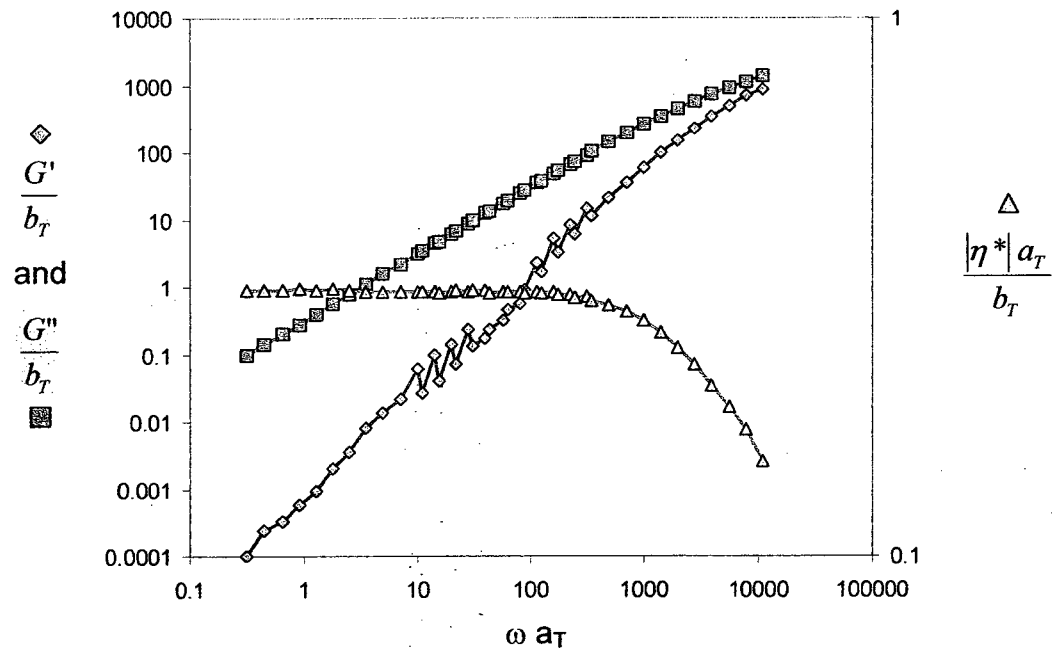


Figure 3.8 Linear Viscoelastic Properties for 8.5% PS solution, 25 °C

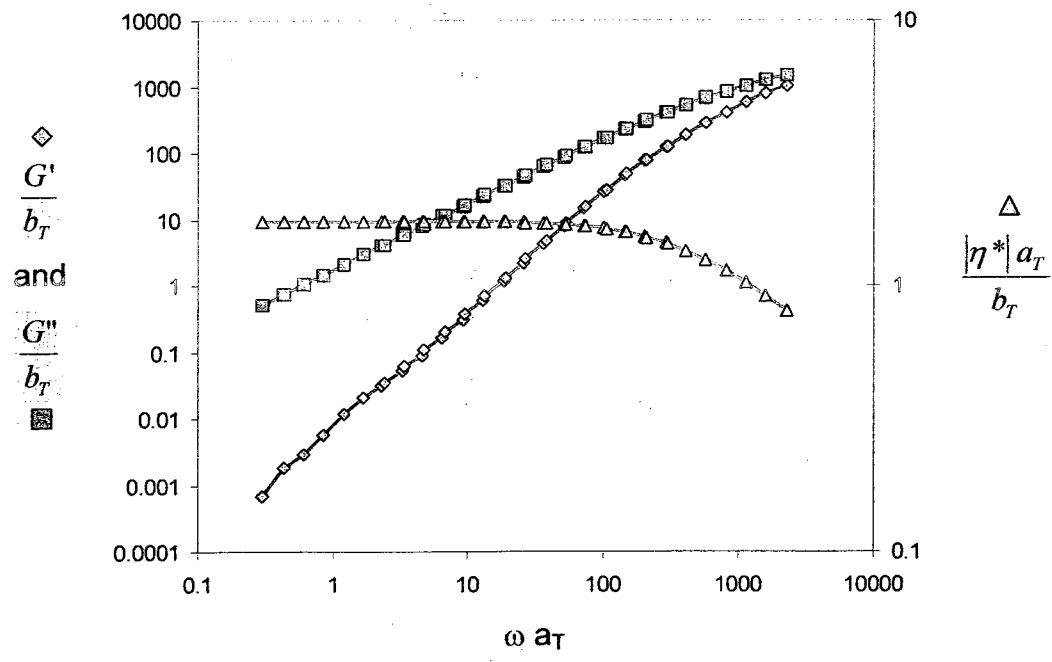


Figure 3.9 Linear Viscoelastic Properties for 12% PS solution, 25 °C

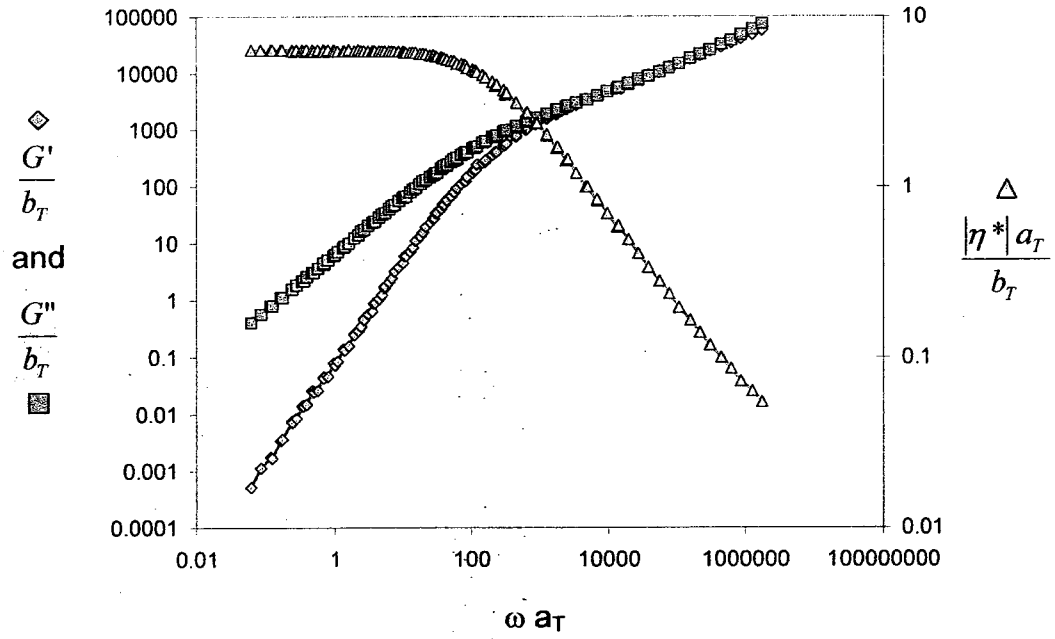


Figure 3.10 Linear Viscoelastic Properties for 16% PS solution, 25 °C

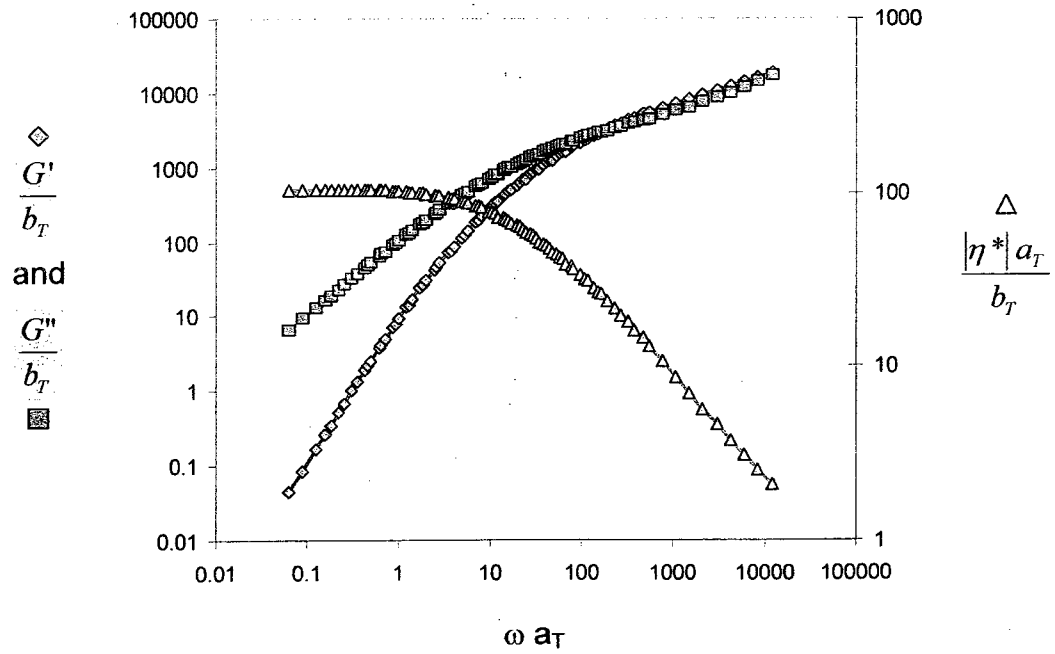


Figure 3.11 Linear Viscoelastic Properties for 25% PS solution, 25 °C

3.3) Signal processing

As it was mentioned before, the signal generator and the data acquisition hardware were controlled by the LabVIEW software. Also, this software was used for analysing the recorded data. In the following paragraphs we explain more about the code and parameters used for controlling both the hardware elements. Figure 3.12 illustrates the algorithm used in the code. It should be mentioned that the LabVIEW is a graphical programming language and it is used to generate a virtual instrument. The front panel of

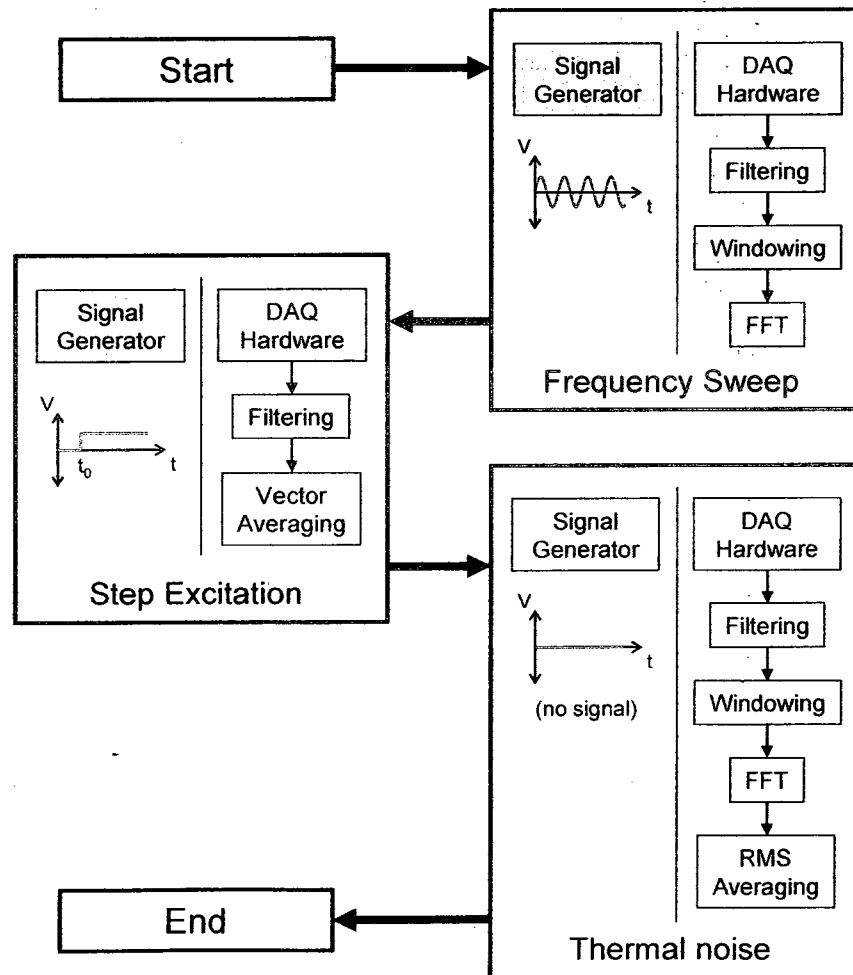


Figure 3.12 The algorithm of the LabVIEW code written for controlling the signal generator and the DAQ hardware and also for analyzing the recorded data

the virtual instrument for this project is shown in Figure 3.13 and the code is presented in Appendix H (pages 182-187).

In general, the three types of experiments that were performed in this project were the frequency sweep, the step excitation and the thermal noise. The general structure for the algorithm of the written LabVIEW code was determined based upon performing these three tests subsequently for each sample. However, as it will be explained in chapter 4, we have to change the tip holder for the thermal noise test. Therefore for each segment of the code, which is related to one test, an on/off key was incorporated in order to activate or deactivate the segment whenever it is required. Moreover, in all the tests the signal generator and the data acquisition hardware were programmed in such a way that they were triggered at the same time and worked together in parallel and also they were allowed to have different control parameters for each test.

For the frequency sweep test, the signal generator produces a sinusoidal signal whose frequency can change over a defined range in several steps. Therefore for this test, the applied signal to the piezo has three controlling parameters of start frequency, end frequency and the number of steps, in addition to its amplitude. For all the fluids, a frequency range of 0 to 60 kHz was selected because in such a range at least the first mode of vibration of all cantilevers could be observed. Concerning the number of steps, 600 steps were chosen in order to have the proper frequency resolution.

The signal applied to the piezo for the step excitation test, should be in the form of a Heaviside function, however for simplicity, the available predefined square waveform was selected and its frequency was adjusted in such a way that only the rising part of the signal, which is in the form of a Heaviside function, is applied to the piezo. Moreover,

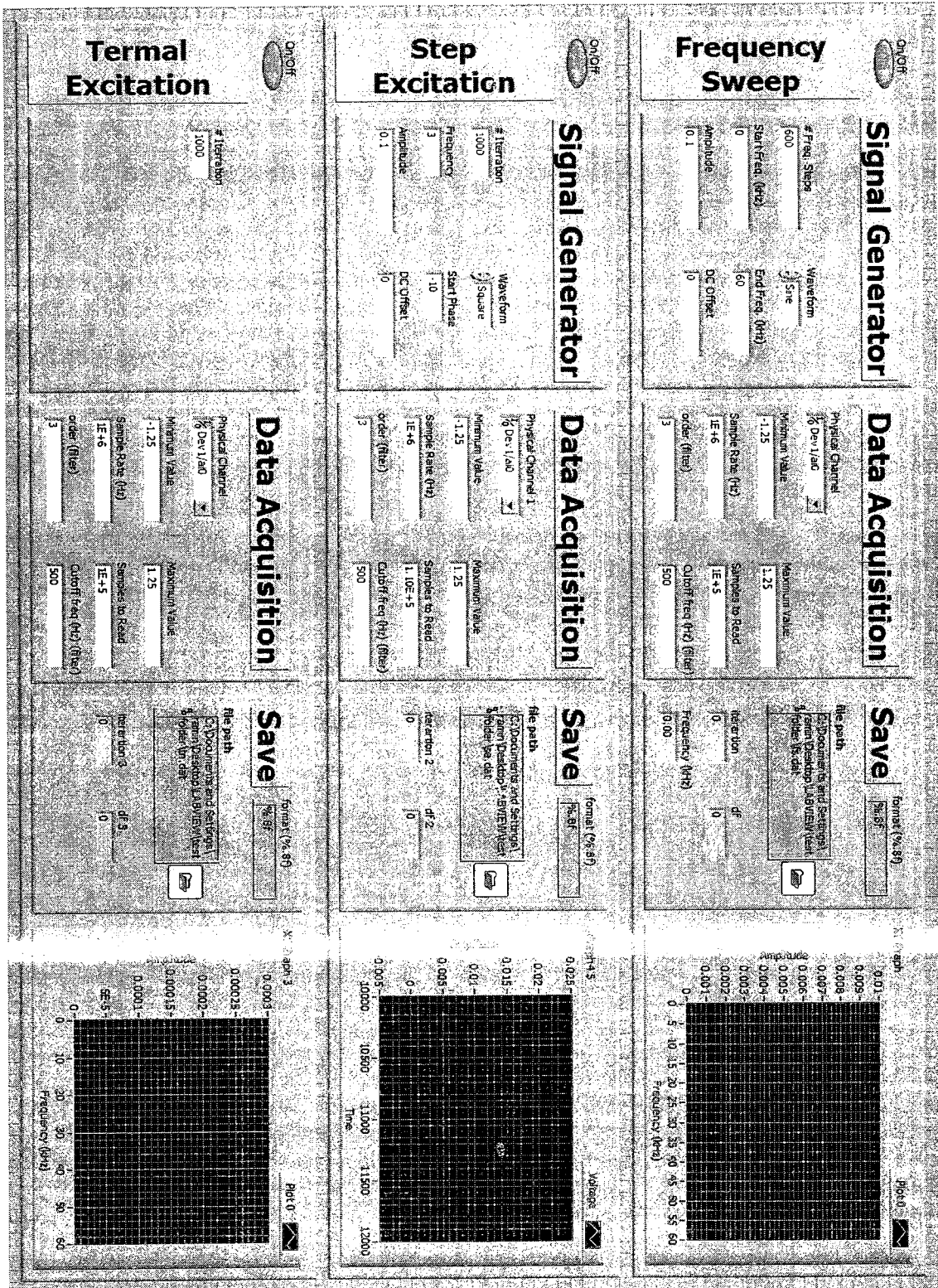


Figure 3.13 The front panel of the virtual instrument developed by the LabVIEW

an initial phase was added to the driving signal in order to excite the piezo after the overshooting effect of the filtering process on the response signal. Finally, due to the passive nature of the thermal excitation experiments, no signal was applied to the piezo while performing these tests.

Moving to the selected controlling parameters of the data acquisition hardware, the most important point in digitizing or sampling of an analogue signal is the selection of the sampling rate. It is vital because it determines the correct capturing of the signal shape and all its frequencies. Based upon the sampling theorem, in order to reconstruct the frequency content of the signal, the sampling rate should be more than twice the highest frequency contained in the signal. However in practice, in order to recognize frequencies and the amplitude of the signal, it is recommended to digitize signals at least with a frequency 10 times of the highest frequency of the signal. The maximum sampling rate for our data acquisition hardware is 3MHz but, the processing and hard drive recording speed of the computer, were the actual limiting factors for the sampling rate. Therefore, taking all factors into consideration, a sampling rate of 1 MHz was chosen for all the tests, which was more than enough to observe and construct the signal in the selected range of frequency for all the cantilevers in the liquids.

The other aspect of signal digitizing is the duration of the sampling or the number of recorded samples. This is important in determining the frequency resolution in the result of the fast Fourier transform (FFT) of the data. Hence, the duration of 0.1s is chosen, and with the sampling rate of 1 MHz, the frequency resolution of 10 Hz or 0.01 kHz was achieved. These parameters mentioned here were used for controlling the DAQ hardware

and were identical for all the tests. In the following paragraphs we will illustrate the process for analyzing the experimental data for each type of test.

First for the frequency sweep, a list of frequencies was defined for the signal generator to excite the cantilever base at those frequencies. At the same time, the cantilever response was recorded and then the high-pass filtering, windowing and FFT processes were applied on the recorded data. Using the result of the FFT, the amplitude and phase of vibration at the frequency of excitation were determined. Such a process was performed for all the listed excitation frequencies. Then from all of these results, two graphs showing the vibration amplitudes and phases in terms of the excitation frequencies were plotted. The high pass filtering process was performed in order to remove the DC offset of the signal and for this purpose a Butterworth filter of order three was used. The cut-off frequency of this filter was set to 500 HZ to also remove the noises which were observed at lower frequencies in the response. A Hanning window was the type of windowing process performed in order to minimize the spectral leakage of the FFT process.

Second for the step excitation, both the application of the signal to the piezo and the recording of the cantilever response were again done simultaneously. The process of filtering was done on the recorded data and after that the vector averaging was performed for one thousand sets of data. The filtering process was the same as for the frequency sweep experiment.

Finally for the thermal excitation we only used the data acquisition hardware to record the response of the cantilever due to the Brownian motion of the surrounding fluid and no signal was applied to the piezo. In this case, filtering, windowing and FFT were

performed on the recorded data with the same parameters and function as used before for the frequency sweep and step excitation. Then RMS averaging was performed on one thousand sets of data that were obtained from the FFT process. It should be mentioned that the effect of RMS and vector averaging on the experimental data will be explained in detail in chapter 5.

Chapter 4

Critical issues in the design of fluid cells and tip holders

Figure 4.1 shows the schematic of a commercial fluid cell which can be used for tapping mode, force modulation, and contact mode experiments in liquids. The main purpose of using the fluid cell is to insulate and separate the piezoelectric actuator from conductive fluids. In this cell which is made of glass, the microcantilever chip (1) is placed in a small groove close to the middle of the bottom of the fluid cell and is fixed to the cell by a clip and a spring (2). A silicone rubber o-ring is placed in the circular groove (3) around the cantilever to provide an enclosed fluid environment between the fluid cell and the scanner. Two channels (4) make the exchange of the enclosed liquid possible. The piezoelectric material used to excite the cantilever is located above one of supporting holes (5) and its wires pass through the fluid cell to the connecting chip (6). In this way, the whole electronic system is completely insulated from the fluid.

With this type of design, the entire fluid cell is vibrated in order to excite the cantilever (except for the thermal excitation experiments). This is in contrast to the regular tip holders used in air or vacuum, in which the piezoelectric actuator is located directly under the cantilever base causing only the cantilever to oscillate (see Figure 4.2). Although, these types of designs of fluid cells and tip holders are acceptable for many AFM applications, they introduce perturbations in the cantilever response in some application and processes, such as tuning of the cantilever, which deal with a range of

frequency in the dynamic AFM mode. This is because of some problems in the design of fluid cells and tip holders, which we discuss in detail in this chapter.

We begin our illustration with three problems that are related to the design of the fluid cell. After that we shift to a drawback with the regular tip holder in terms of the supporting mechanism of the piezo element.

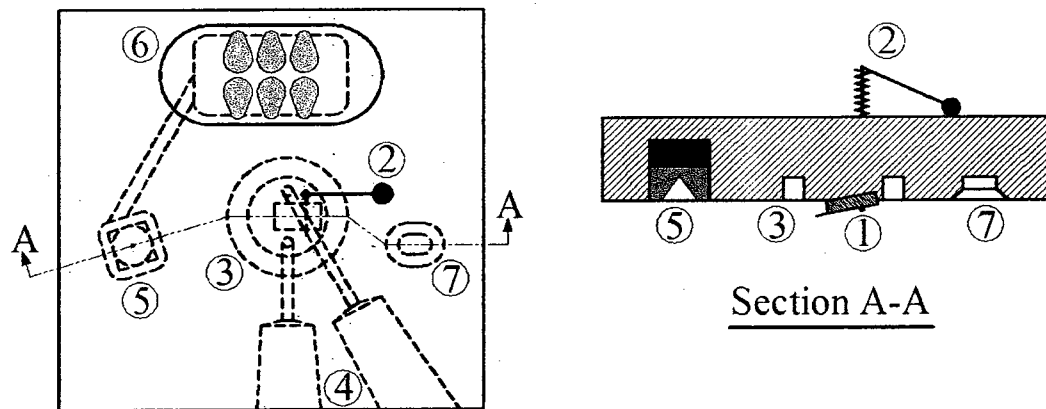


Figure 4.1 Schematic of a fluid cell from Veeco¹ (MTFML model). In this picture, (1) is the cantilever, (2) is the clip and spring, (3) is the circular groove for o-ring, (4) are the inlet and outlet channels for exchanging liquids, (5) is the moving support, (6) is the connecting chip, and (7) is the fixed support.

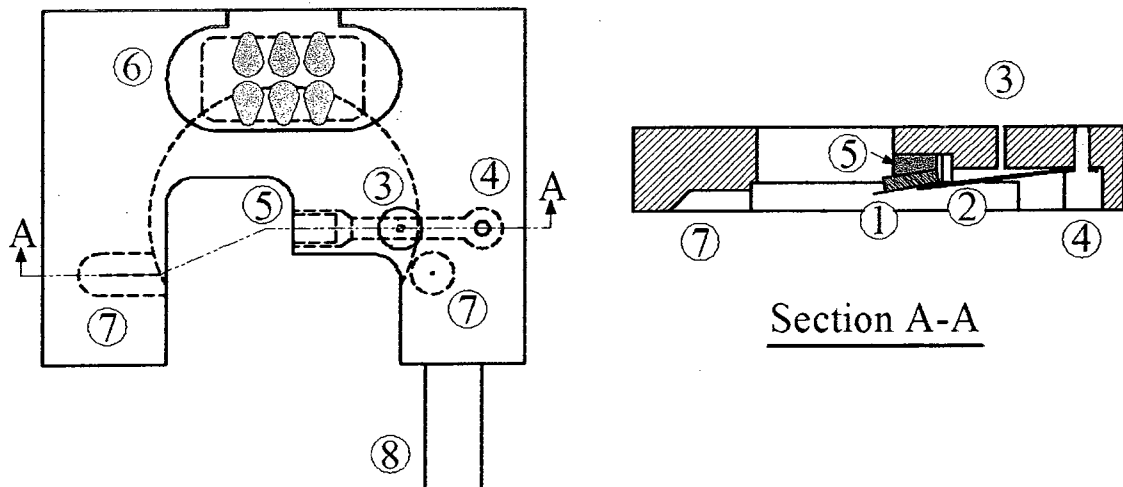


Figure 4.2 Schematic of a regular tip holder from Veeco¹ (MMMC model). In this picture, (1) is the cantilever, (2) is the clip and spring, (3) is the pin, (4) is the screw of the clip, (5) is the piezo element, (6) is the connecting chip, (7) are the supports and (8) is the handle.

4.1) The holding mechanism of the cantilever chip in the fluid cell

The first problem with the design of this fluid cell is its holding clip because first of all, its spring is not strong enough to secure the cantilever base tightly, and secondly it does not necessarily hold the cantilever such that its axis is perpendicular to the clip rod. Since the surface of the cantilever chip is sloped, any configuration other than perpendicular results in only a single point of contact, reducing the overall stability of the connection. Thirdly, the other end of the clip, which is above the fluid cell, can easily be moved or rotated during handling and mounting of the fluid cell on the AFM head thus changing the connection between the clip and the cantilever base. Moreover this can result in displacement of the cantilever chip in its groove and consequent misalignment of the laser beam from the AFM head. This is especially important because when the cantilever base moves to another position in its groove it creates a new vibrational system with a different frequency response. Therefore, the clip and spring system does not allow for reproducible experiments as shown in Figure 4.3. For these experiments the cantilever model used was the NSC12/tipless/Cr-Au from MikroMasch which is a practical cantilever and has nominal dimensions of 350 μm in length, 35 μm in width and a thickness of 2 μm . The fundamental resonant frequency of this cantilever in water is about 20 kHz. The position of this peak is unaffected by the cantilever chip location but its amplitude is significantly affected. We note that when attempting to study the rheological properties of fluids, both the shape and the location of the primary peak are important. Also, for the other system resonances in Figure 4.3, neither the position nor the amplitude of the peaks is constant and instead they strongly depend on the position

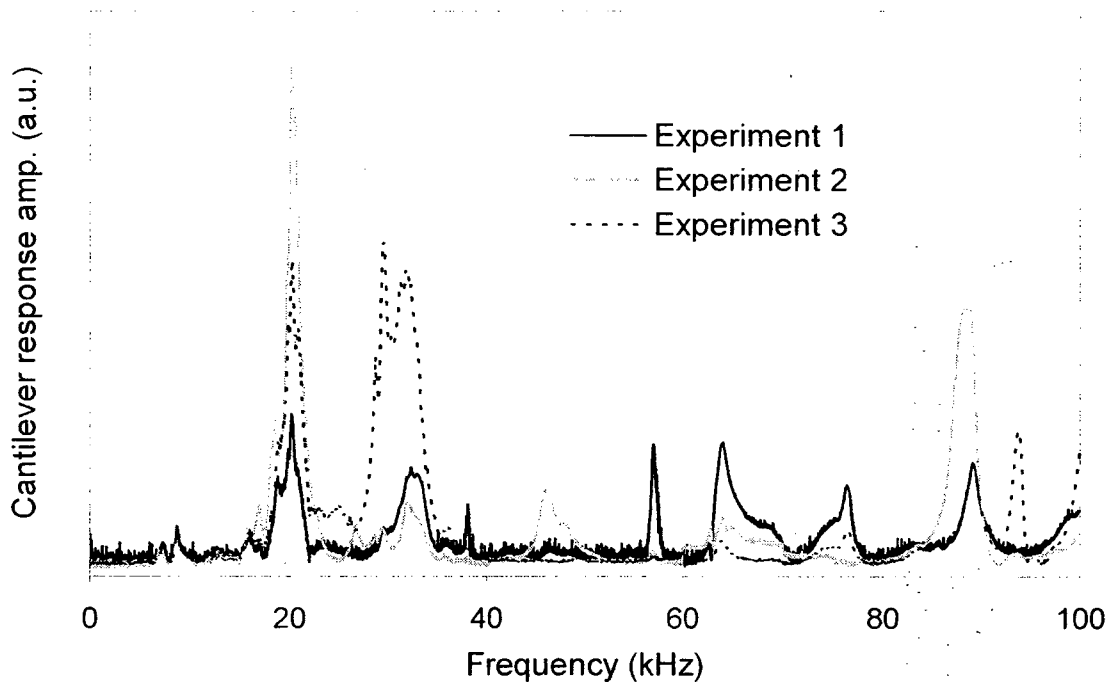


Figure 4.3 Frequency responses with different cantilever base and clip positions (in water)

of the clip and cantilever.

This problem was solved by removing the clip and gluing the cantilever base to the fluid cell using silicone glue⁶⁸. As a result of this modification, some redundant peaks associated with the clip and spring were eliminated from the frequency response of the system and the reproducibility of the experiments was improved. It should be mentioned that the problem of irreproducibility is not completely solved because the positioning of the fluid cell in the AFM head and also the force applied by the grip over the cell can not be exactly repeated manually. However, these are having relatively minor effects and by gluing the cantilever base to the fluid cell, we can improve the repeatability of the frequency response considerably. Figure 4.4 demonstrates the improvement in repeatability in the frequency response of a cantilever when glued to the fluid cell. For

these experiments another practical cantilever was used, namely the NSC12/tipless/Cr-Au from MikroMasch, which had nominal dimensions of 250 μm in length, 35 μm in width and a thickness of 2 μm . Such a change of cantilevers was needed due to the fragile nature of the cantilevers and the inability to repeat the same experiment again after the fluid cell was modified.

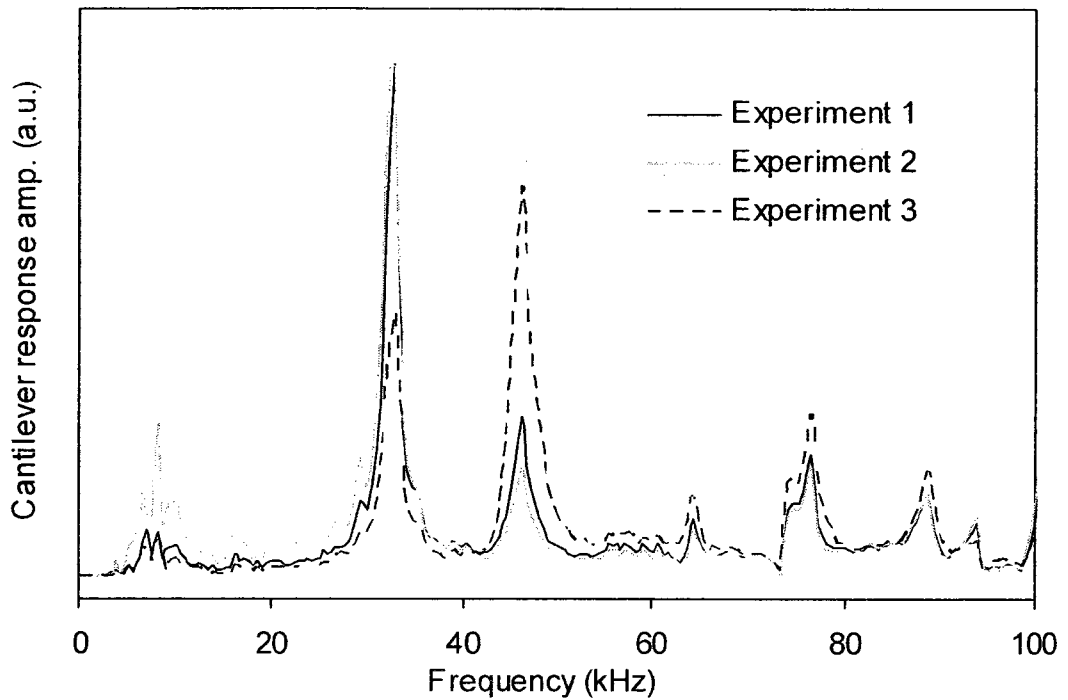


Figure 4.4 Repeatability of the frequency response of a cantilever when glued to the fluid cell (in water)

4.2) The fluid-borne excitation

The second problem arising from the design of the fluid cell is that it causes an unsteady, free surface flow of the fluid trapped between the cell and scanner (See Figure 4.5a). As mentioned previously, the piezoelectric actuator excites the cantilever through the movement of its base via vibration of the entire fluid cell. The large moving surface

of the fluid cell also generates an unsteady flow in the fluid which affects the vibration of the cantilever and is in fact another source of excitation for the cantilever. This means that the cantilever is excited not only by the movement of its base (structure-borne excitation), but also by the unsteady fluid motion (fluid-borne excitation) resulting in additional resonance peaks in the frequency response (see Figure 4.6). The same problem was encountered by Xu and Raman²² who used a different type of commercial fluid cell from Agilent.

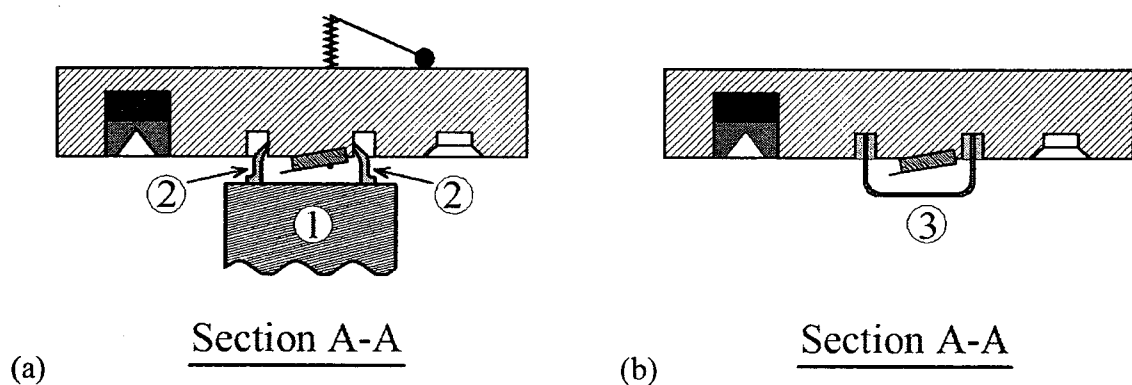


Figure 4.5 Cross section of the fluid cell defined in Figure 2 (a) before modification and (b) after modification. In this picture, (1) is the scanner, (2) is the o-ring, and (3) is the reservoir.

This problem can be solved by making a small fluid reservoir from glass and gluing it into the o-ring groove of the fluid cell as shown in Figure 4.5b. The reservoir can be filled and emptied using the inlet and outlet channels of the fluid cell. If the reservoir is filled completely with liquid, then the fluid inside the reservoir has almost the same velocity as the fluid cell. In other words, the relative motion of the fluid due to excitation of the fluid cell is very small and does not affect the vibration of the cantilever. Many of the spurious peaks in the frequency response of the cantilever then shrink. Figure 4.6 shows the frequency responses of a cantilever in a %50 glycerin-water solution with and

without the reservoir attached to the fluid cell. It should be emphasized that the fluid cell must be completely filled and free of bubbles and in order to accomplish this, the fluid must be degassed before filling the reservoir. For these experiments the long cantilever described in section 3.1.4 was used. The installation of the reservoir causes a shrinkage in the redundant peaks at 7, 9 and 27 kHz frequencies as shown by arrows on Figure 4.6.

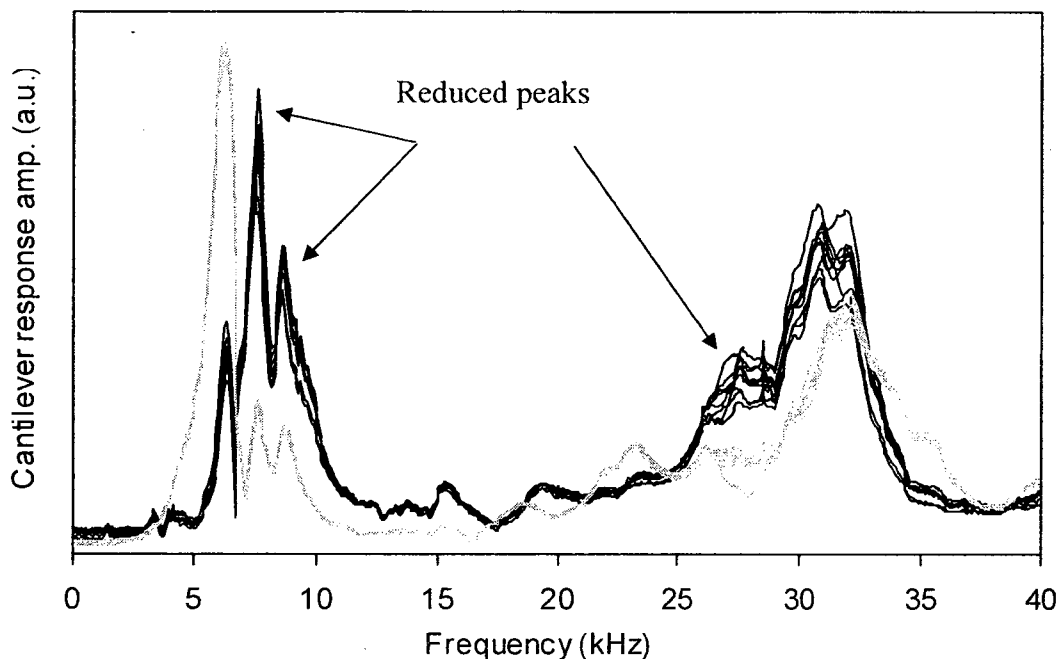


Figure 4.6 Frequency responses of the cantilever in 50% glycerin-water solution before (black line) and after (gray line) installing the reservoir. The cantilever is glued to the fluid cell.

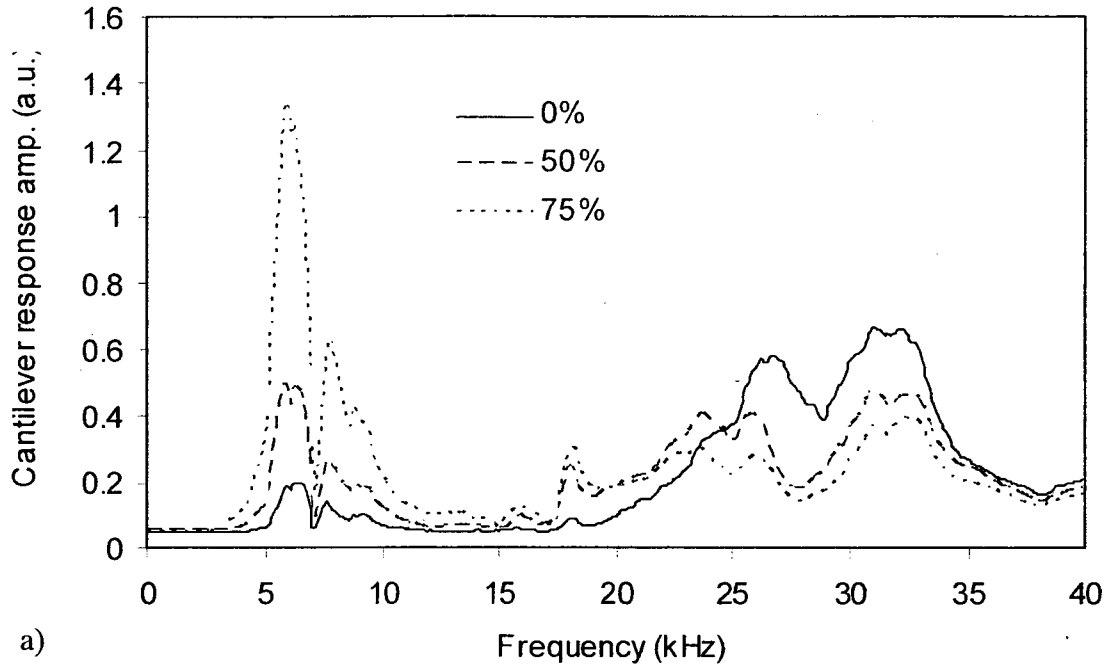
4.3) The location of piezo element

The last and most important problem with this fluid cell design is that the measured vibration response is the combination of the cantilever vibration and the fluid cell vibration. The response of the fluid cell itself to the excitation is frequency dependent and not the same as the movement of the piezoelectric actuator. This means that the driving

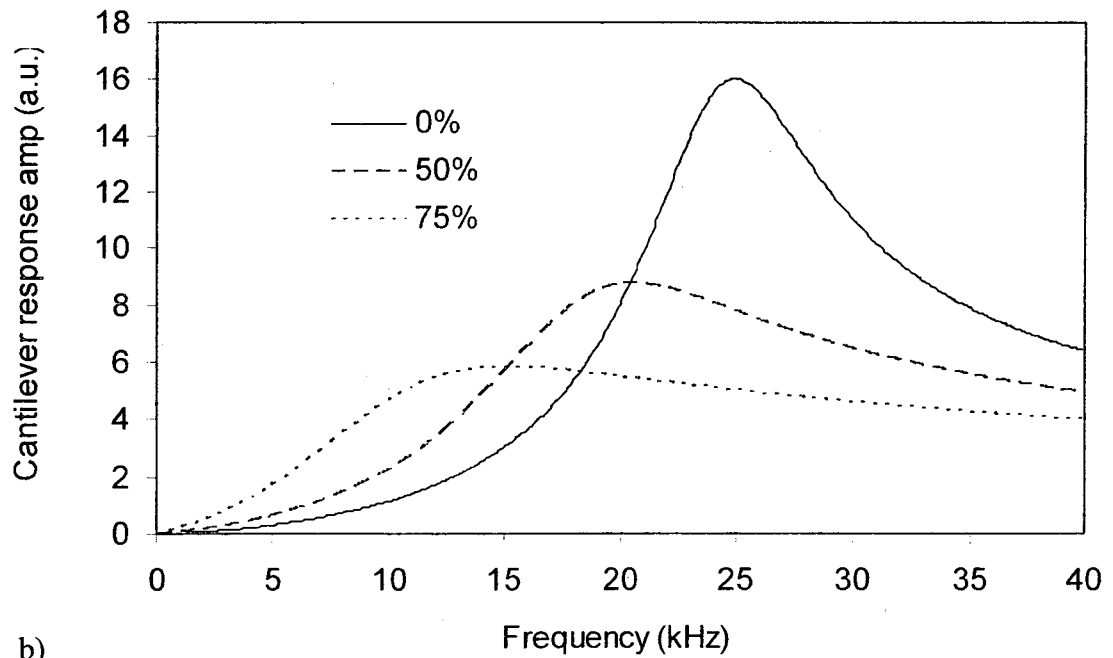
motion experienced by the cantilever is not the ideal constant amplitude sine wave. Therefore the presence of fluid cell and anything else between the piezoelement and the cantilever base make it impossible to measure the real frequency response of the cantilever.

In order to experimentally verify the above theory, we measured the response of a silicon microcantilever in three different solutions of glycerin and water using the modified fluid cell. Also after filling the reservoir, the inlet and outlet channels were blocked to prevent any evaporation. In this way we can be sure that fluid borne excitation of the cantilever is negligible. For this experiment, we used the medium cantilever described in section 3.1.4 and the properties of the surrounding liquids are summarized in Table 3.1. Figure 4.7a shows the cantilever responses observed by the AFM optics. The drive amplitude in all the experiments with liquids was the same and constant. Although the shapes of these responses are different, their peaks are at the same frequencies. On the other hand, Figure 4.7b shows the theoretical responses of such a cantilever in these liquids based on the theory presented in chapter 2, section 2.3.2. For the theoretical response, the cantilever base was forced with a displacement amplitude of one at all frequencies, $A_{FS} = 1$.

Comparing Figures 4.7a and 4.7b, one can find no similarity between the theoretical and experimental responses of the cantilever. However, when the experimental response in each liquid is divided by its ideal acoustic theoretical response, the results are the same for all liquids. These results, shown on Figure 4.8, are the response of the fluid cell at the cantilever base to the excitation from the piezoelement. These responses are similar because the vibrational characteristics of the fluid cell are mainly dependent upon the



a)



b)

Figure 4.7 Cantilever response in three solutions of glycerin and water; a) measured by AFM optics, b) determined theoretically

elasticity and mass of the fluid cell. And in our case the fluid mainly changes the mass of the fluid cell. However, since the densities of the fluids studied here are very close and

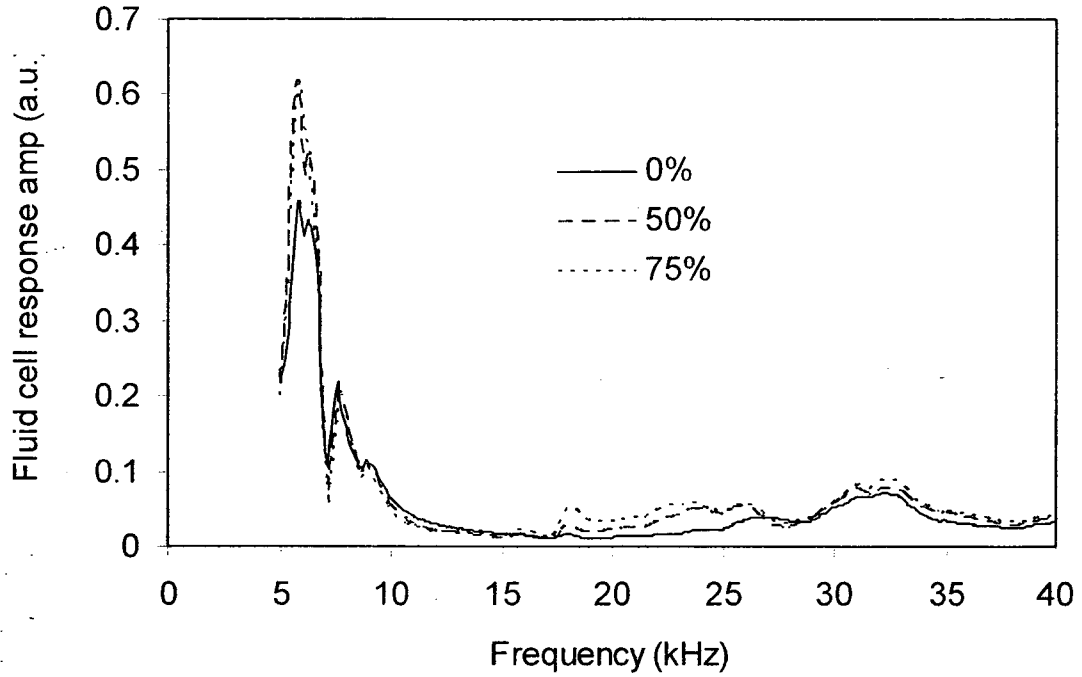


Figure 4.8 Fluid cell frequency responses when containing solutions of glycerin and water

since the volume of the reservoir is small, the total mass variation is negligible and therefore, the vibrational characteristics of the fluid cell are expected to be independent of the fluid it contains.

Based on the results shown on Figures 4.7 and 4.8, the experimental response to a specific excitation, $I(\omega_0)$, in the absence of fluid born excitation, can be written in the form of:

$$W_{\text{exp}}(x|\omega_0) = T_C(x|\omega_0) \times T_F(\omega_0) \times I(\omega_0) \quad \text{Equation (4.1)}$$

where $T_F(\omega_0)$ is defined as an experimentally obtained function that transfers $I(\omega_0)$ to the frequency response of the fluid cell itself, $T_C(x|\omega_0)$ is the transfer function for the ideal damped response of the cantilever, Equation (2.71), and together their product represents the experimental response of the cantilever $W_{\text{exp}}(x|\omega_0)$. Note that the cantilever

is excited by the function $A_{FS}(\omega_0) = T_F(\omega_0) \times I(\omega_0)$ illustrating that ideal acoustic excitation can only be achieved if the fluid cell is designed such that $T_F(\omega_0)$ is constant. To verify this, experiments were conducted using the long cantilever described in section 3.1.4 and the same fluid cell in 75% glycerin-water solution. The fluid cell transfer functions are identical for both cantilevers as illustrated in Figure 4.9.

Equation (4.1) can also be used to understand that the liquid damped dynamics of the cantilever, $T_C(x|\omega_0)$, act to amplify the dynamics of the fluid cell. When the cell is filled with air or another gas the damped cantilever response contains only sharp resonance peaks at higher frequencies and thus acts to filter out the dynamics of the cell itself.

The results presented here prove that with this type of fluid cell the frequency response is dominated by the dynamics of the cell itself rather than the cantilever. This

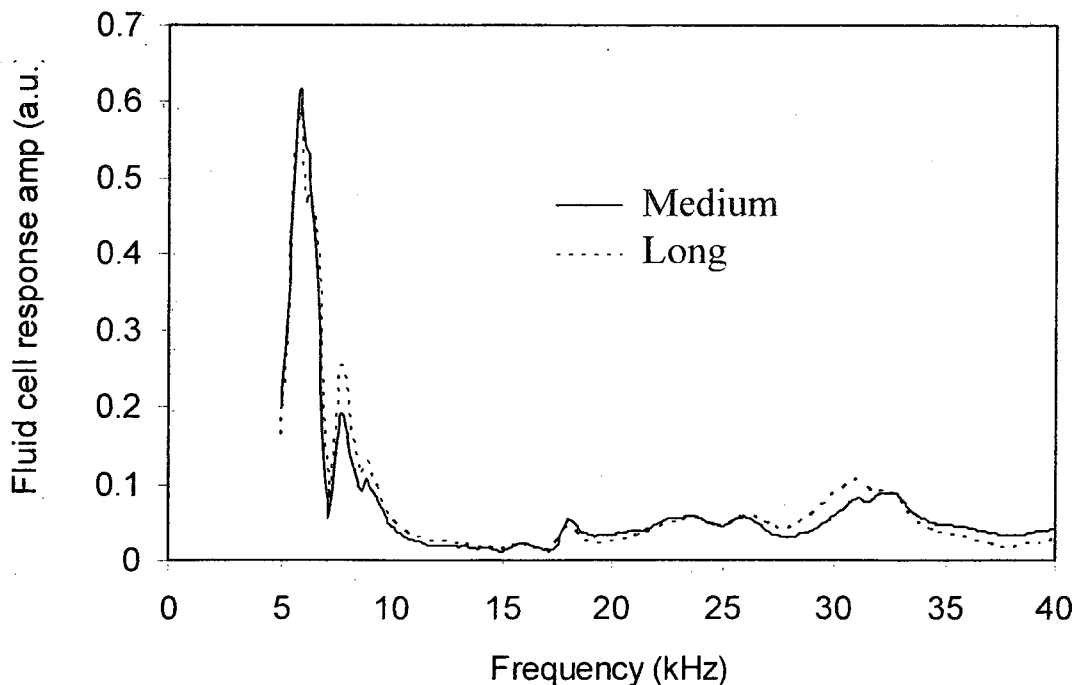


Figure 4.9 Fluid cell frequency responses obtained from excitation of two different cantilevers in 75% glycerin-water solution.

problem can only be solved by placing the piezoelectric actuator directly under the cantilever base as in the regular tip holders. Therefore, a regular commercial cantilever holder was modified to improve the acoustic excitation of cantilevers in liquids. The piezoelectric element was insulated by a thin film of Teflon and also a small piece of microscope glass was installed to cover the liquid just above the cantilever and the piezoelectric element. This glass and the glassy surface of AFM stand were also coated with Teflon in order to make them hydrophobic allowing the droplet to be contained by surface forces. In chapter 5, the experimental results obtained with this modified holder and also their comparison with the theoretical predictions are presented.

4.4) Supporting and gluing the piezo to the tip holder

So far we showed that there should not be any distance between the piezo and the cantilever base, meaning that the piezo must be located directly under the cantilever base. What we are expecting from the piezo is to produce a controlled movement for the cantilever base. For such a purpose, beside the voltage that we are applying to the piezo, the type of mechanism, that is being used to support the piezo to the body of the tip holder, is also important. Concerning the applied voltage, the signal generator that we used is very accurate and we have excellent control over the whole process. Moving to supporting the piezo, there are two common mechanisms used, which are shown in Figure 4.10. One of these mechanisms is to glue the piezo directly to the body of the tip holder and the second is to use a pair of clamps to hold the piezo on two pivots that are extended from the tip holder body. The gluing mechanism is usually used for tip holders

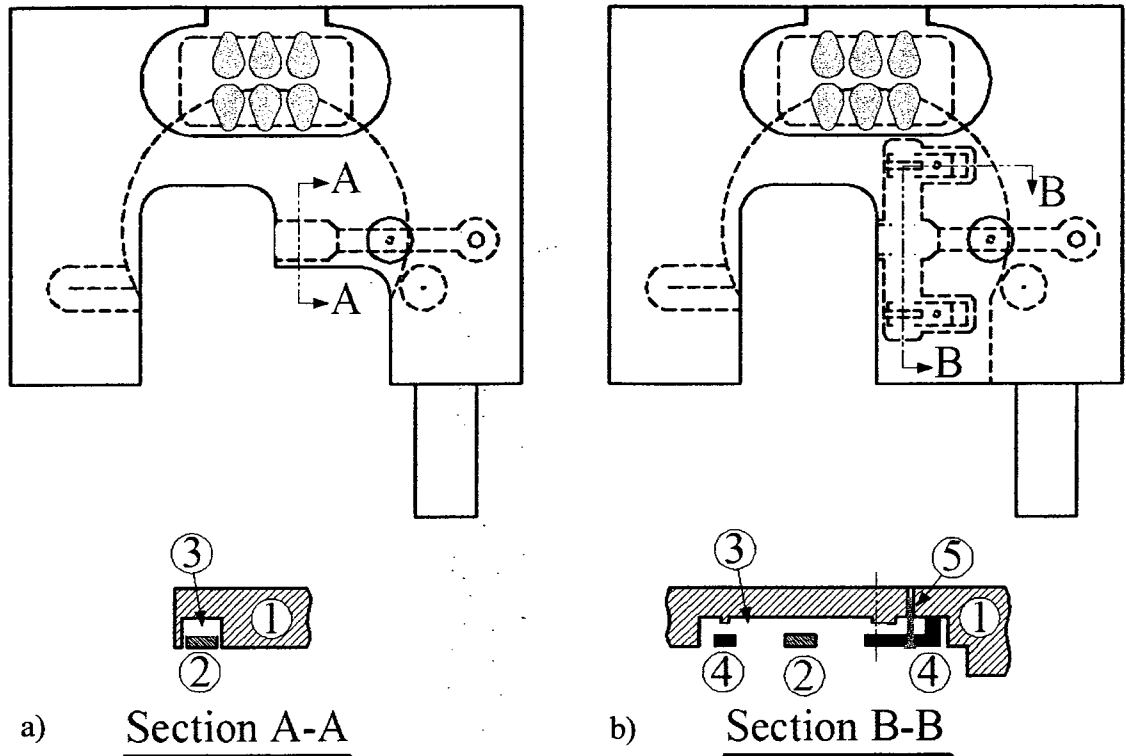


Figure 4.10 Two common mechanisms for supporting the piezo; a) gluing and b) clamping. In this picture, (1) is the stainless steel body of the tip holder, (2) is the cantilever seat, (3) is the piezo element, (4) are the clamps and (5) is the clamp's screw.

that have a small piezoelement while the clamping mechanism is used for holders having a large piezoelement, in the form of a bar that is employed to produce a large force. Each of these mechanisms has advantages and disadvantages which are discussed in the following paragraphs.

The advantage of the first mechanism for the piezo support is that the cantilever base movement is exactly equal to the expansion and contraction of the piezo as long as the piezo is attached to the tip holder body perfectly. However, over time these connections can be loosened for many reasons such as degradation of the glue or through washing of the tip holder with different solvents when changing the experimental fluid. Such loosening affects the noise floor, when we are using the AFM for thermal excitations,

causing a large increase in the value of the noise floor to the extent that sometimes the response of the cantilever can no longer be recognized (see Figure 4.11). Moreover, the noise floor values are neither stable nor repeatable and can also be frequency dependent. In contrast, in the other excitation techniques namely the frequency sweep and step excitation where we apply a signal to the piezo, the effect of changes in the noise floor on the cantilever response is not visible because for these cases the magnitude of the cantilever response is much greater than the magnitude of the noise floor.

In the clamping mechanism, the piezo is attached and kept tight to the body of the tip holder. Therefore in the thermal excitation a small, constant and repeatable value for the noise floor is observed. On the other hand in the frequency sweep and step excitation, the signal applied to the piezo causes its expansion and contraction and also the vibration of

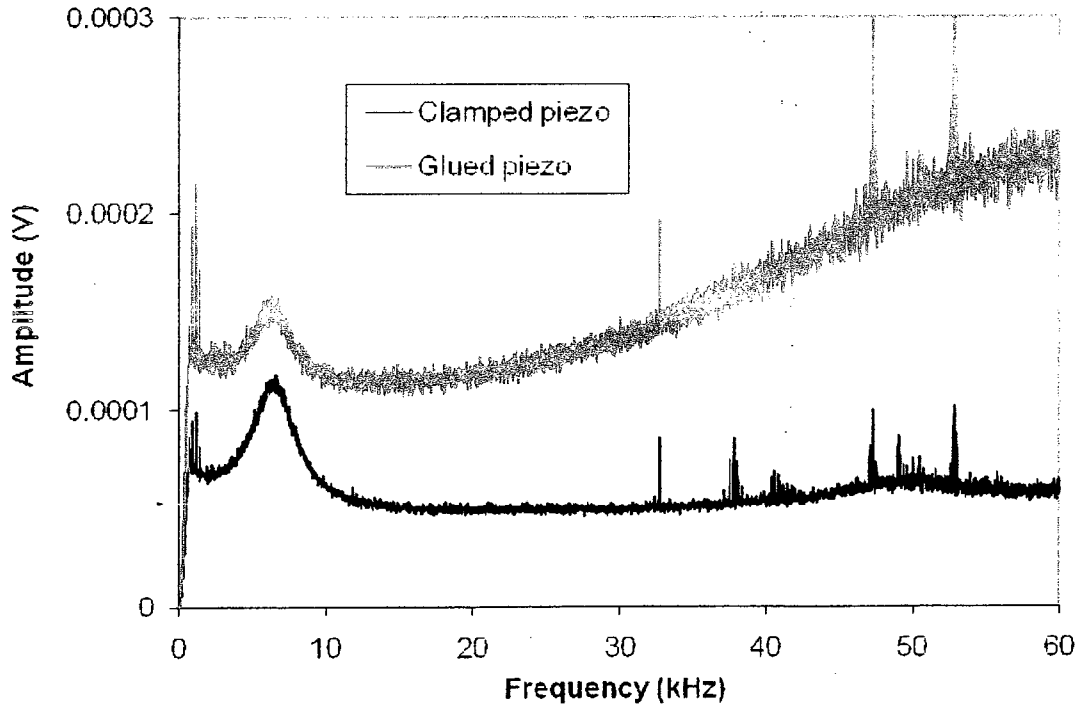


Figure 4.11 The effect of utilizing different mechanism of supporting the piezo on the thermal noise response of long cantilever which was immersed in water.

the piezo bar itself. This vibration is due to the large ratio of the length to the thickness of the piezo and also due to the free space underneath the piezo element because of the specific type of support used in this mechanism. Therefore the cantilever base, in this case, does not have a controlled movement and as a result in the cantilever response many spurious peaks appear.

In conclusion, for the frequency sweep and step excitation the gluing mechanism is preferred, while for the thermal noise the clamping mechanism is recommended. Moreover, we must emphasise that the critical design issues mentioned in this chapter refer to certain very commonly used fluid cells and tip holders which are manufactured by Veeco. However, there are several other manufacturers for the AFM and its accessories, such as Agilent and Nanotec companies, who employ different designs for the AFM which might not have such problems.

Chapter 5

Experimental results for different excitation techniques

The structure of this chapter, which presents the results of all experiments, consists of three parts. In the first part, we present the results of preliminary experiments such as averaging and reproducibility of the data. The second part focuses on the discussion of the experimental results for the Newtonian fluids and their comparison with theory for the different excitation techniques. Moreover two different approaches for extracting the properties of the fluids from the experimental data are proposed and the possible sources of errors are discussed. Finally in the third part, preliminary results for the non-Newtonian fluids are presented and potential approaches for extending the AFM cantilever techniques are introduced.

5.1) Averaging of data

Averaging is an important tool in signal processing and is usually used to reduce the noise effects. In spectral analysis, there are many types of averaging in which vector averaging and RMS averaging are the most important.

The vector average is simply the arithmetic mean of each of the real and imaginary parts of the FFT vector of the time domain data and consequently, its results are also complex numbers. Equation (5.1) shows the meaning of vector averaging mathematically:

$$Y_k = \langle X \rangle_k = \bar{X}_R + i \bar{X}_I \quad \text{Equation (5.1)}$$

In this equation, X_k and Y_k are the k^{th} instance of the input spectrum X and its averaged output Y respectively. Because the FFT is a linear transform, this kind of averaging is equivalent to the FFT of averaged data recorded in the time domain. As shown in Figure 5.1, vector averaging reduces the effects of white noise on the signal in the time domain. It also lowers the noise floor in the frequency domain. For this type of averaging, the

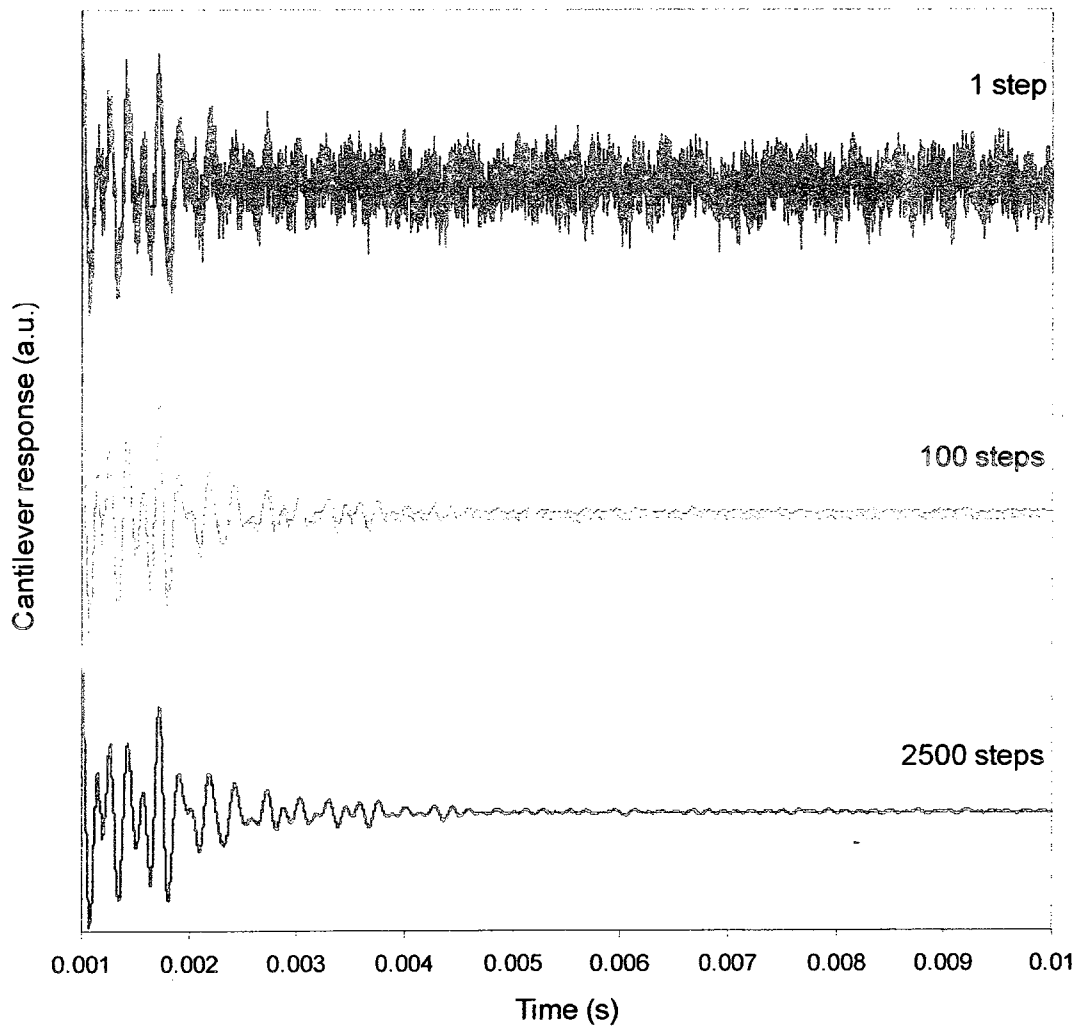


Figure 5.1 The effect of vector averaging on data records for step excitation of 50% glycerin-water solution in time domain

signal recording should be started at a consistent point in the periodic signal or in other words it must be triggered.

Recording of a signal starting at inconsistent points in a periodic signal results in phase noise in the FFT spectrum (see Figure 5.2). For this case, the RMS averaging can be used to reduce the effects of phase noise. The RMS averaging is the square root of averaged power spectra and returns a real spectrum. It can be expressed mathematically in the form of:

$$Y_k = \sqrt{\langle (X \text{ conj}(X)) \rangle_k} \quad \text{Equation (5.2)}$$

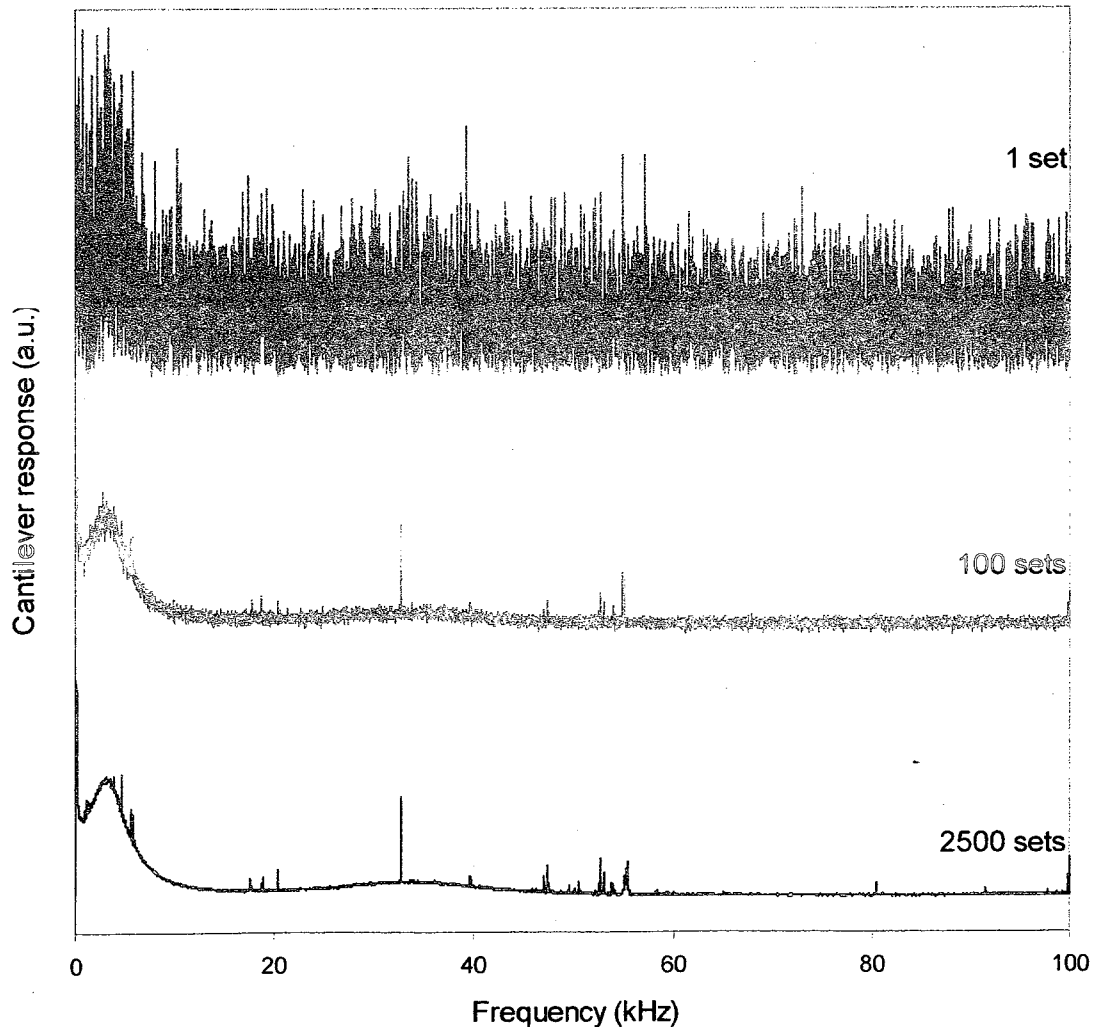
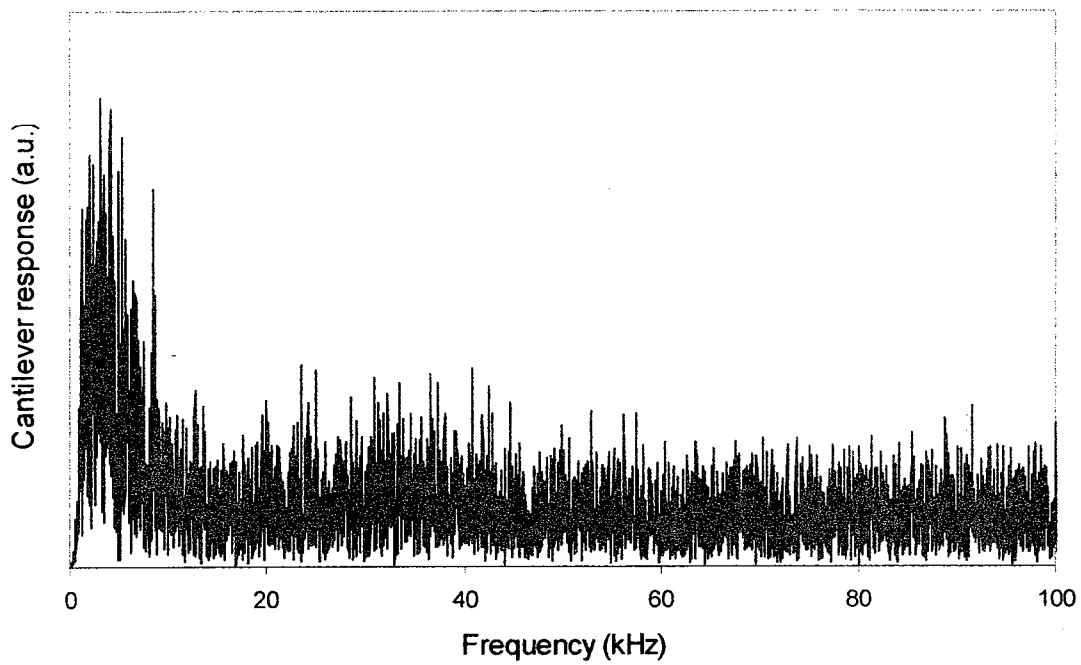
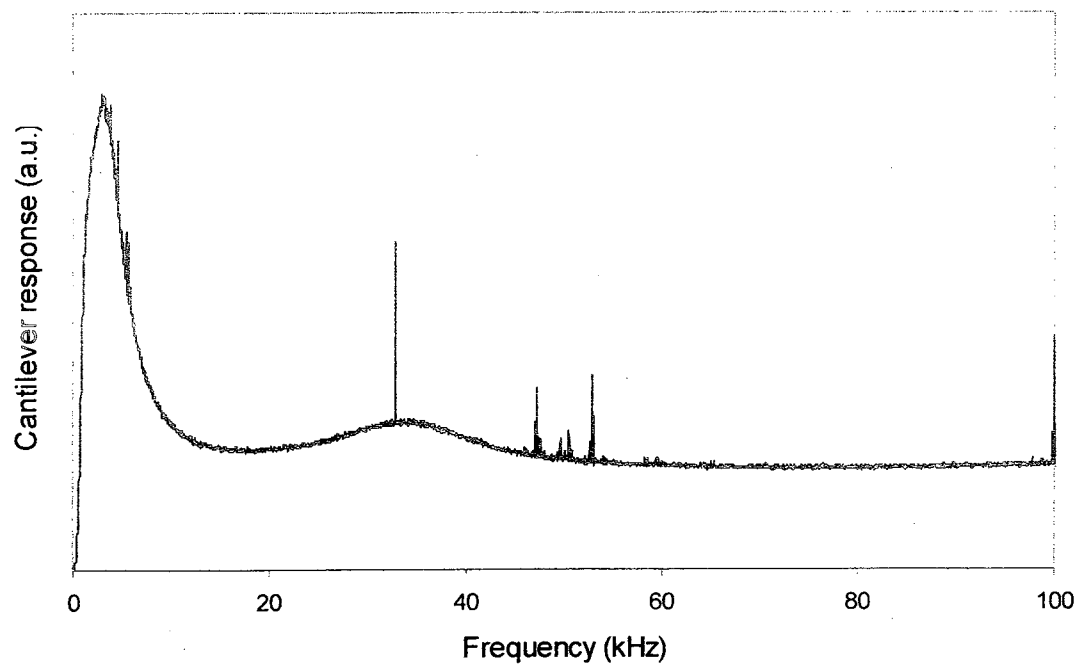


Figure 5.2 The effect of RMS on averaging data records for thermal noise of 50% glycerin-water solution in frequency domain



a)



b)

Figures 5.3 Vector averaging (a) and RMS averaging (b) for the damped part of step excitation for 50% glycerin-water solution

Because the power spectrum is the square of the magnitude of FFT spectrum and also the magnitude of FFT spectrum is independent of time shifts, RMS averaging eliminates any effect of phase variations or time dependency on the results however it can not reduce the noise floor.

In thermal noise, the signal is the result of the stochastic impact of fluid molecules to the cantilever and consequently it is not possible to start data acquisition at specific point in the periodic signal. On the other hand for the case of step excitation, data acquiring can be started exactly at the time of excitation and so triggering the signal is easy. Based on this, the appropriate method for thermal noise is RMS averaging and for step excitation is vector averaging. It should also be mentioned that after damping of the cantilever response to step excitation, the rest of the signal is thermal noise and although data acquisition was triggered for this case, vector averaging does not work properly for this part as Figure 5.3 shows on the previous page.

5.2) Checking the concentration changes over time

One important issue that can affect the interpretation of the experimental data is the change of concentration of the glycerine-water solutions over time. The reason for this change is that the liquid on the modified tip holder (see Figure 5.4) has an interface with the surrounding air and the water can be either evaporated from the solution or absorbed from the air because of humidity. The rate of each of these phenomena is not known however the overall changes can be investigated by observing the response of a cantilever in the solution over time. Three solutions of 25%, 50% and 75% glycerine-water were

chosen and the thermal noise signals were recorded every 10 minutes in each. The responses for the fresh solutions and after one and half hour are shown in Figures 5.5, 5.6 and 5.7.

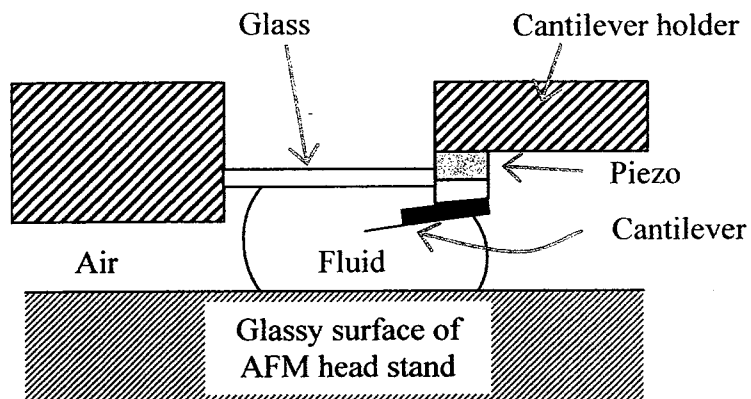


Figure 5.4 The schematic of the modified cantilever holder which shows the interface between the examined fluid and the surrounding air.

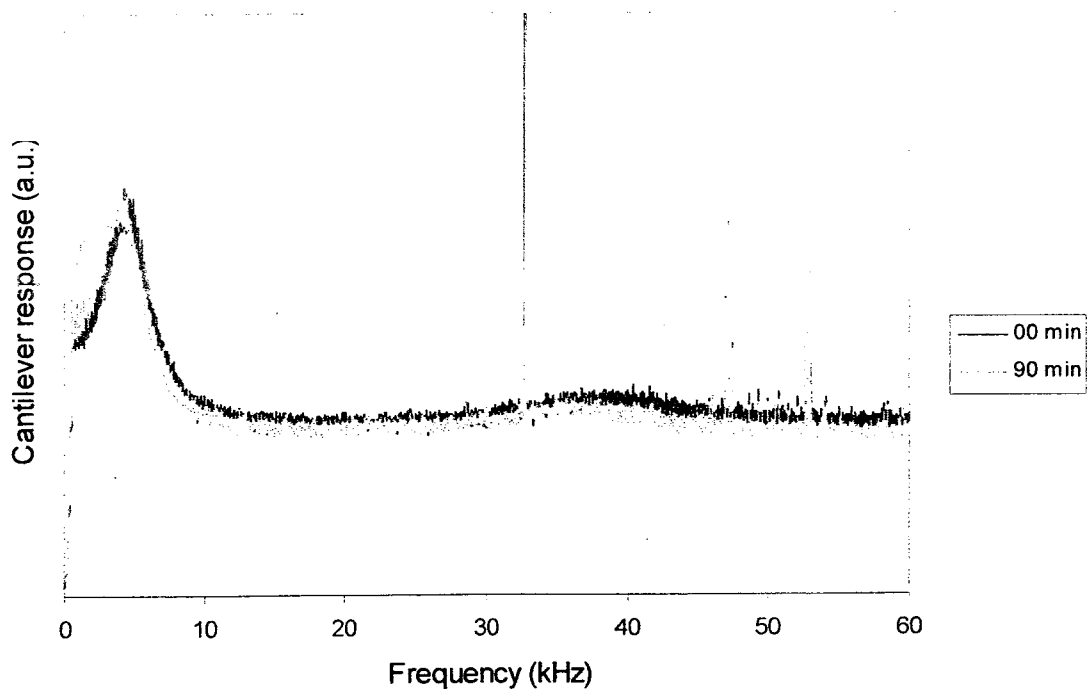


Figure 5.5 Thermal noise responses of a cantilever in 25% glycerin-water solution over time

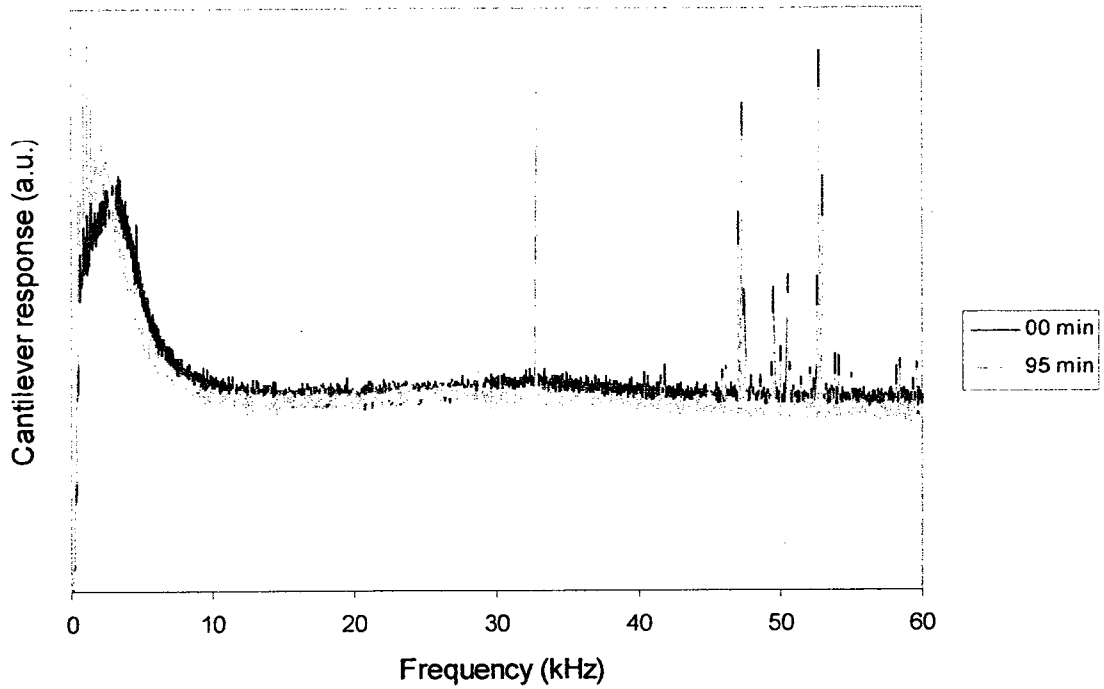


Figure 5.6 Thermal noise responses of a cantilever in 50% glycerin-water solution over time

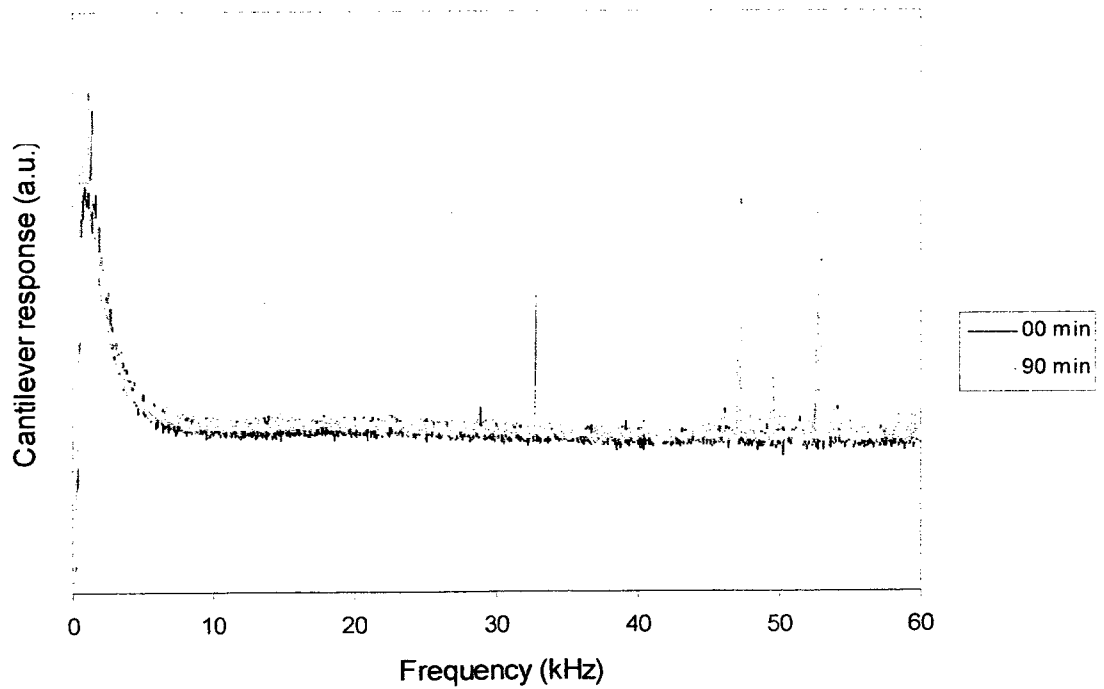


Figure 5.7 Thermal noise responses of a cantilever in 75% glycerin-water solution over time

Regarding to these figures, it should be mentioned that the peaks for the first two modes of vibration can be observed in the responses. The first modes, which have higher amplitudes, have frequencies less than 10 kHz and the second modes have frequencies between 10 and 50 kHz. As the glycerine concentration increases, the frequencies of these peaks decrease such that for 75% solution the first mode peak is about to disappear. Also the amplitude of the second mode decreases and becomes the same as the noise floor with increasing concentration. The other issue is the existence of some sharp peaks at very low frequencies and at around 33 and 50 kHz. These peaks appeared for all of the solutions at the same frequencies; therefore they are independent of fluid properties and are rather related to environmental or system noises. A more comprehensive discussion of the behaviour of the cantilever in thermal excitation is presented in section 5.6.

An analysis of the nature of the concentration change over time was done based on the shift of the first resonant frequency. From the previous figures, it can be noticed that the resonant frequencies decrease slightly as time passes. This indicates that some water evaporates from the solution over time. The other issue is the magnitude of the frequency shift for the different solutions after one and half hour. These shifts are 5 and 33 percent for 25% and 50% glycerine-water solutions respectively and almost zero for the 75% solution. The small frequency shift for 25% solution can be understood by considering that the properties of solutions at this concentration do not change significantly with a small change in concentration (see Figures 3.6 and 3.7). For the 75% solution, the lack of shift of frequency is likely due to the very low rate of evaporation at this concentration which means that one and half hour probably is not enough for a noticeable change in the properties of the fluid. However for the 50% glycerine-water solution the shift is

considerable and indicates that the change of concentration over time can be a potential source of error in interpretation of the experimental data. Therefore experiments with this solution should be done as quickly as possible. In this project, doing all necessary tests for one sample takes typically 20 minutes. In order to have an approximation of the frequency shift for our experiment for the worst case of 50% glycerine, we looked at the response of the cantilever over shorter periods (see Figure 5.8). It was found that the amount of frequency shift is almost linear with respect to time in the first 90 minutes as shown in Figure 5.9. From these results we could expect a frequency shift of around 7 percent for the 50% glycerine-water solution after 20 minutes of testing.

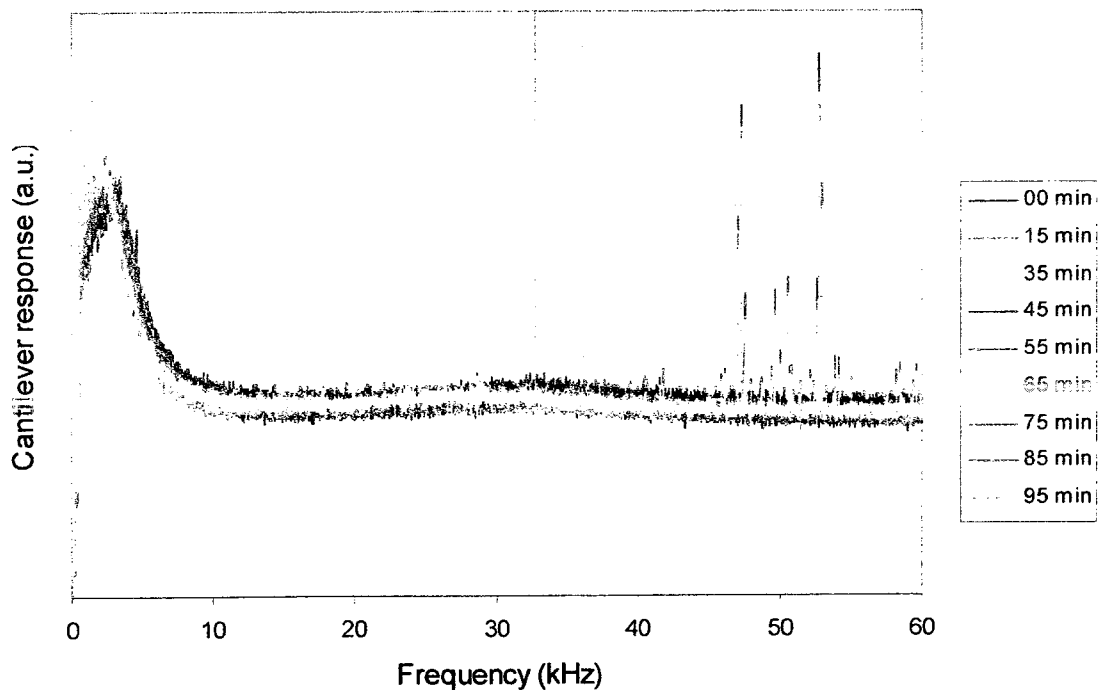


Figure 5.8 Thermal noise responses of a cantilever in 50% glycerine-water solution over time

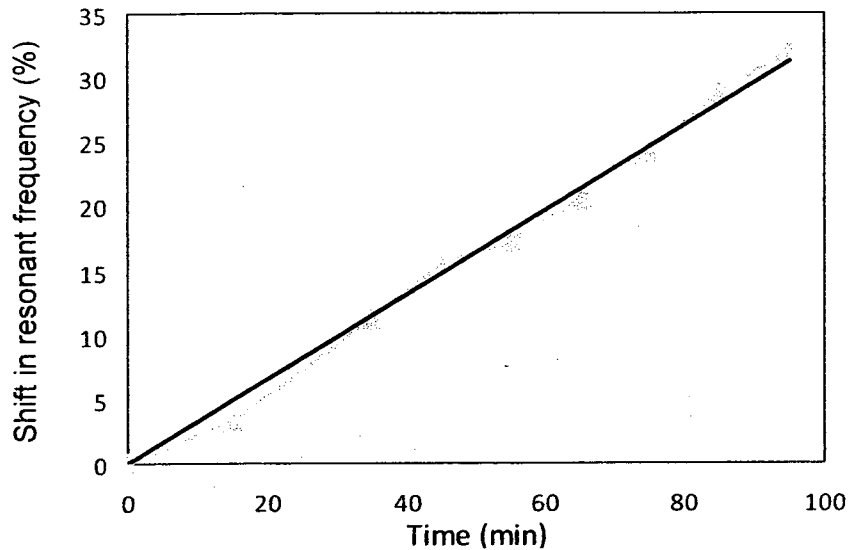


Figure 5.9 Resonant frequency shift because of concentration change over time for %50% glycerin-water solution.

5.3) Reproducibility of the experiments respect to both FS and SE

Reproducibility is one of the main principles of any scientific experiment. It can only be achieved under identical experimental conditions. We discussed in chapter 4 several factors that affected the reproducibility of the experiments with the fluid cell. Some of these factors included the change in the location of the laser spot on the cantilever beam as a result of laser realignment, the alteration in the route of the reflected laser beam because of the readjustment of the intermediate mirrors and the relocation of the cantilever chip on its seat. Such factors again hold for the modified tip holder and reduce reproducibility. Among the three above mentioned factors, the first mainly affects the shape of the cantilever response, which is the summation of all its modes of vibrations the effect of which depend on the position of the laser spot on the cantilever. This can be easily understood from Figure 5.10 where the inclination of the cantilever at each mode

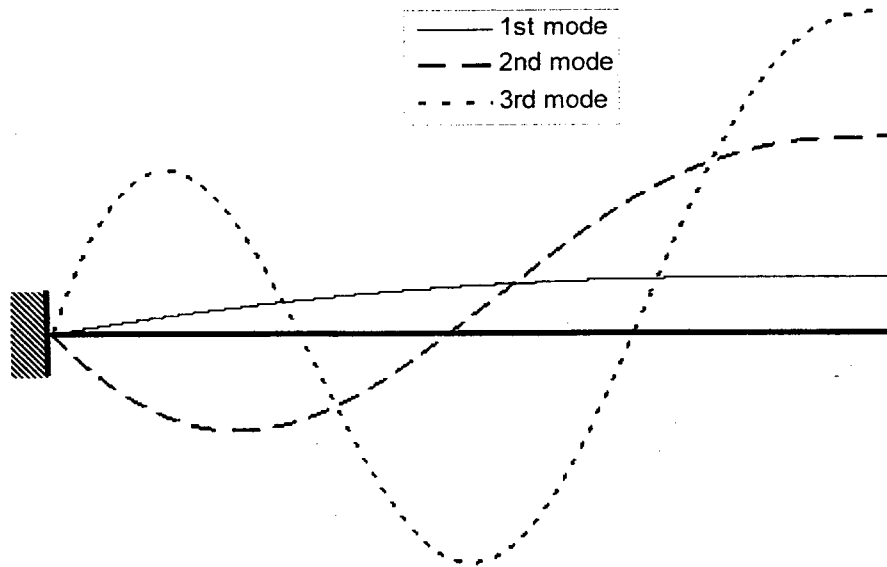


Figure 5.10 The inclination of the cantilever for the first modes of vibration.

of vibration is drawn. A small change in the location of the laser beam, along the length of the cantilever and near its free end, causes a severe change on the observed response especially at higher modes of vibration. The other factors do not affect the shape of the cantilever response instead they tend to scale the magnitude of vibration uniformly.

The method available for the alignment of the laser beam at the free end of the cantilever is not precise, as it depends upon the operator identifying the shadow of the cantilever. However, we tried to keep the same approach for aligning the laser on all the cantilevers in order to perform our experiments at the same condition. Moreover, we kept the settings of the optical system of the AFM the same for each fluid during the different types of experiments performed. All of which lead to obtaining reproducible results and meaningful comparisons between the data for different experiments. Furthermore, in order to compare the experimental results with the theory, the responses were normalized

mainly by the magnitude of the first mode peak and in this way the effects of the other factors and the need for calibration of the system were removed.

5.4) Linearity with respect to the drive amplitude for FS and SE

As a part of our initial experimentation, we investigated the effect of different drive amplitudes on the responses of the cantilever in the frequency sweep and step excitations. This was done for all of the fluids and without exception, it was observed that when the recorded response is divided by the value of drive amplitude, the results were the same. This means that the response of the cantilever has a linear relation with the drive amplitude at least over the studied range of voltage, (see for example Figures 5.11, 5.12, 5.13 and 5.14). For Newtonian fluids, such behaviour was expected in terms of the displacement of the cantilever base and the deflection or inclination of any point on the cantilever, as shown mathematically in chapter 2. However, in the AFM the input to the system is the voltage signal that is applied to the piezo element located underneath the cantilever base. Also the output of the system is the voltage produced by the photo detector that receives the reflection of the laser beam from the cantilever. Therefore, it can be concluded that the rest of the system which converts the voltage to the displacement and vice versa is linear also; these include the signal generator, the piezo element, the photo detector and the data acquisition hardware. For the non Newtonian fluids, the observed linearity in the results indicates that the experiments were carried out in the linear viscoelastic region of the fluid, meaning that the properties of the fluid are

independent upon the applied deformation and the rate of deformation. The unusual cantilever behaviour in the frequency sweep excitation will be discussed in section 5.6.

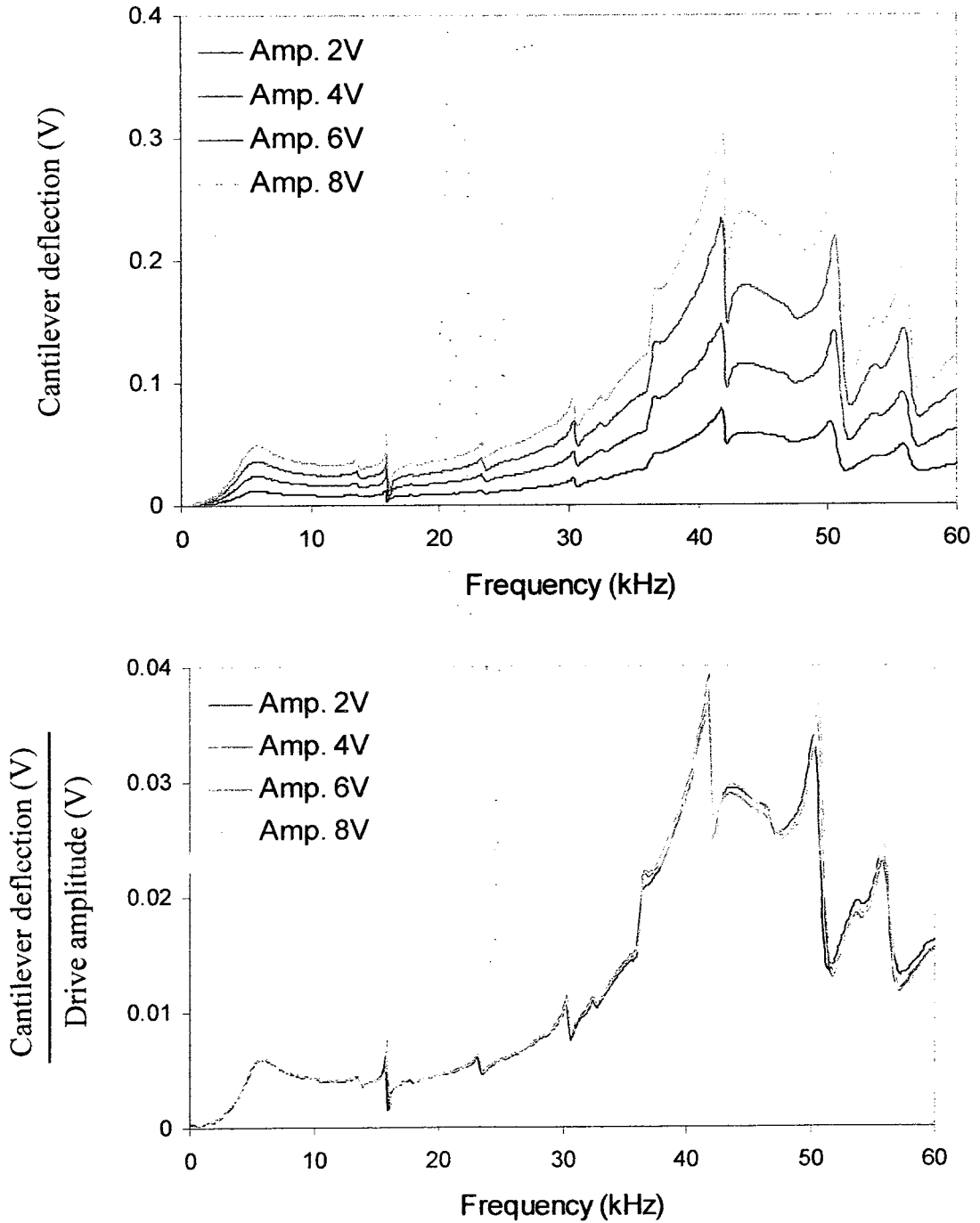


Figure 5.11 Linearity with respect to the drive amplitude for the frequency sweep test. For this test the long cantilever was immersed in water.

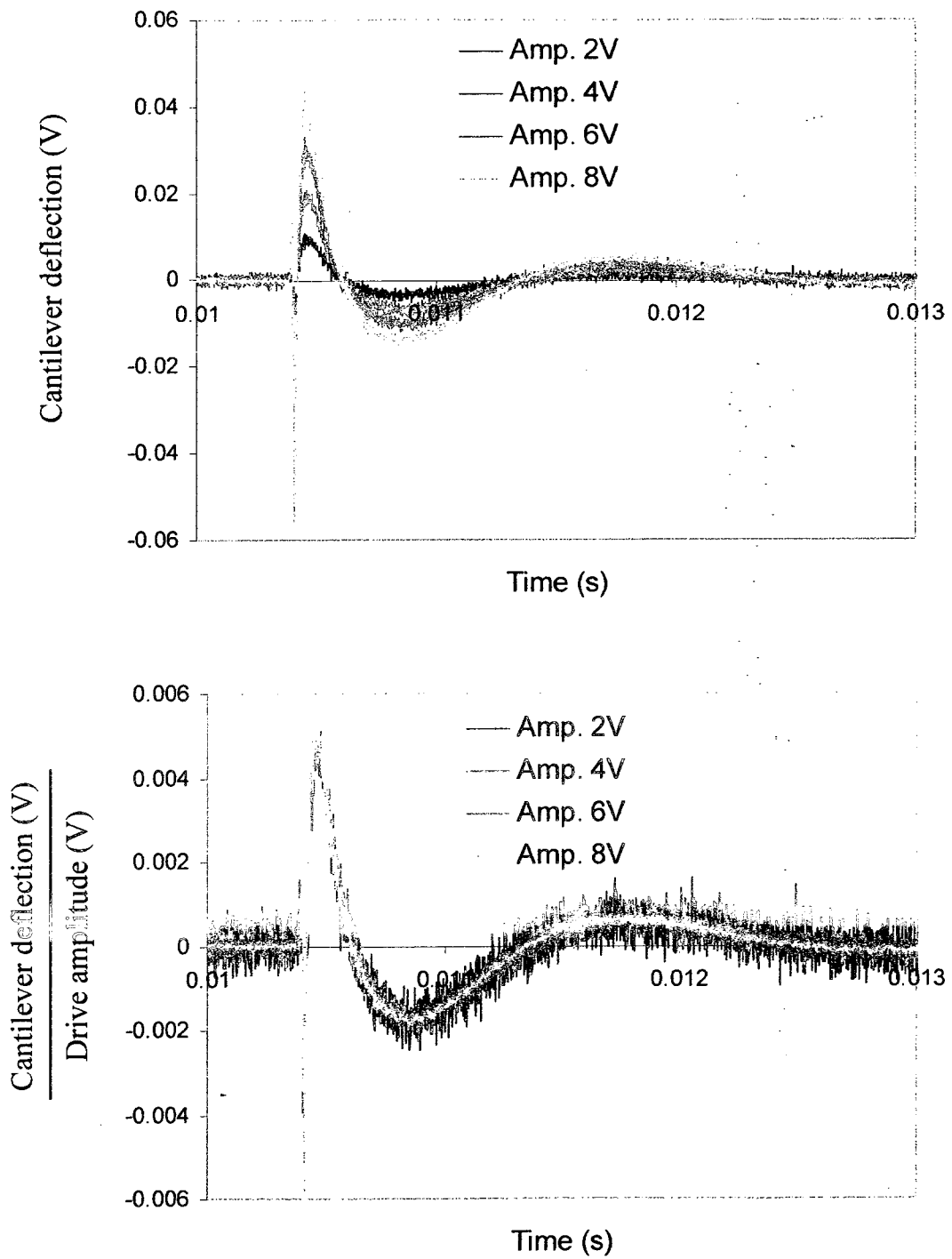


Figure 5.12 Linearity with respect to the drive amplitude for the step excitation test. For this test the long cantilever was immersed in glycerin.

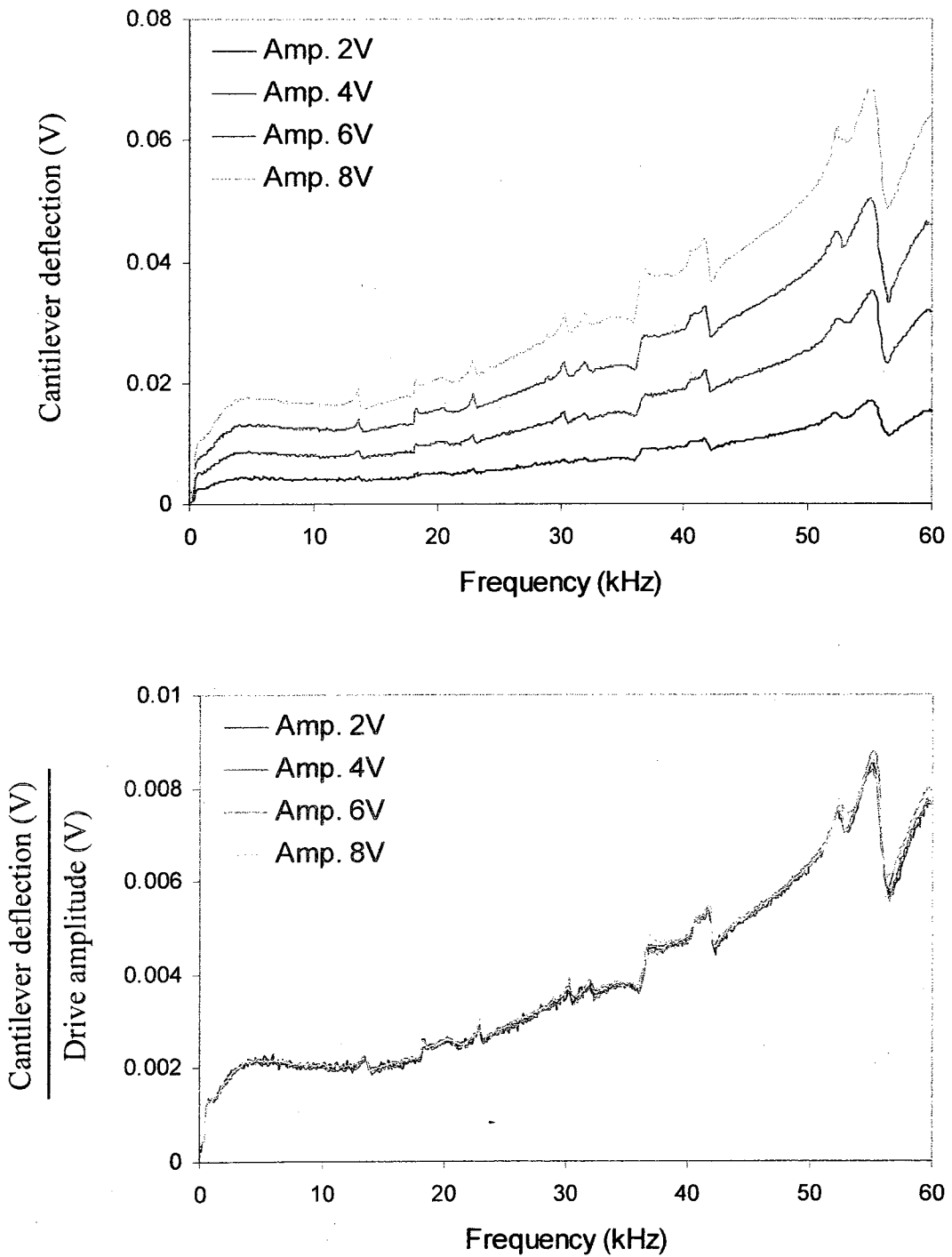


Figure 5.13 Linearity with respect to the drive amplitude for the frequency sweep test. For this test the long cantilever was immersed in 16% PS/DEP.

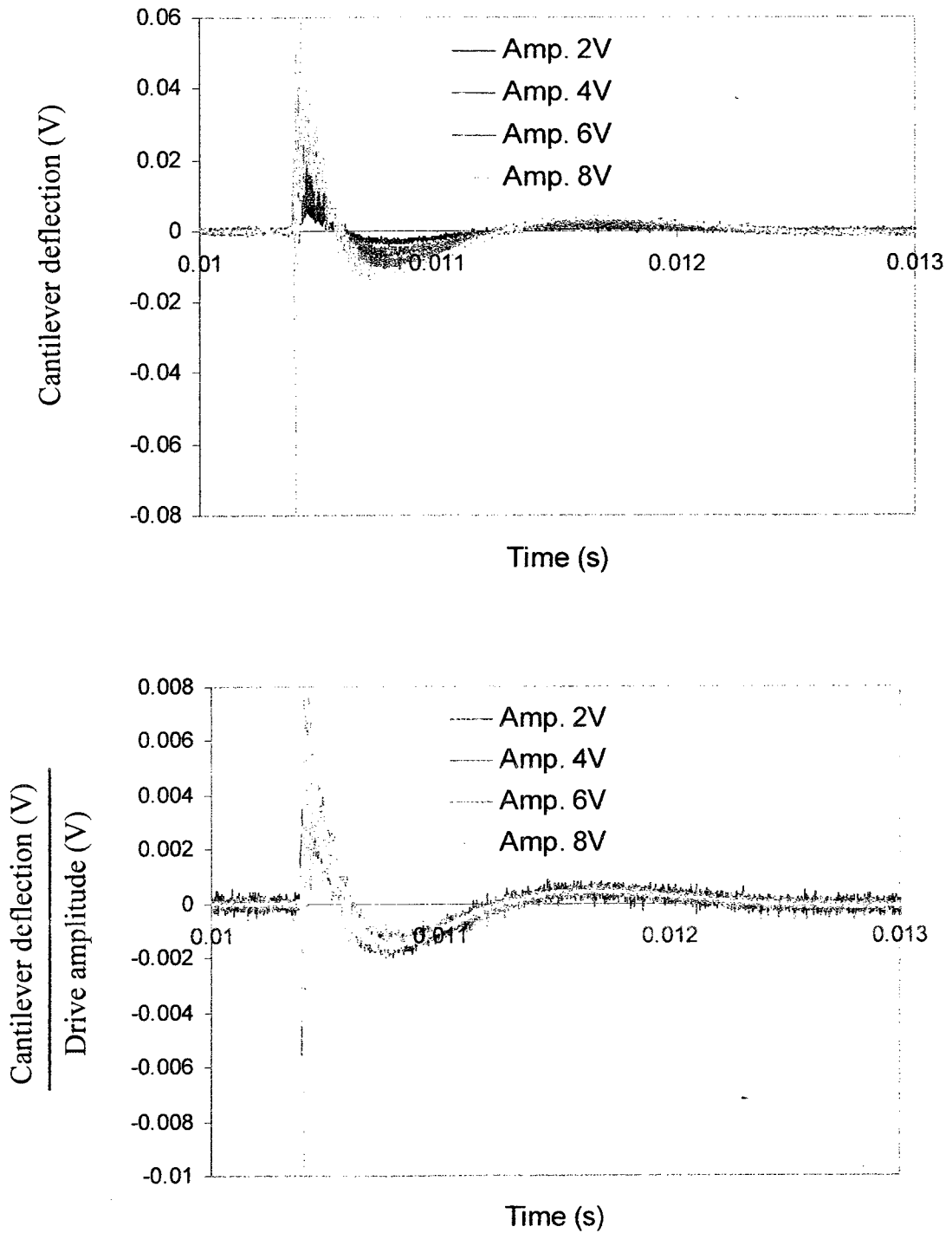


Figure 5.14 Linearity with respect to the drive amplitude for the step excitation test. For this test the long cantilever was immersed in 8.5% PS/DEP.

5.5) Confirmation of linear viscoelasticity by examining higher harmonics

In this section, we are again verifying the linearity of the polymer solution behaviour through a different type of experiment. For the standard oscillatory shear flow, there are some theories that predict the behaviour of the fluid and determine whether it is in the linear or nonlinear region. Knowing that the cantilever under study has an oscillatory movement which is some how similar to the standard oscillatory shear flow, we designed few experiments to use the standard oscillatory shear flow theories in order to verify the linearity of the non-Newtonian fluids. In this regards we are following the approach mentioned by Giacomin and Dealy⁶⁹.

In the standard oscillatory shear flow, a uniform sinusoidal strain with the frequency of ω and the amplitude of γ_0 is applied to the fluid as shown in the following equation:

$$\gamma(t) = \gamma_0 \sin(\omega t) \quad \text{Equation (5.3)}$$

For polymeric liquids, when the amplitude of this oscillatory strain is small, the linear viscoelastic properties could be observed in the fluid. In other words, the stress response of the fluid will be a sinusoidal function with the same frequency but shifted in phase. Also the amplitude of the stress would be proportional to the amplitude of the strain as illustrated in the following equation:

$$\sigma(t) = G_d \gamma_0 \sin(\omega t + \delta) \quad \text{Equation (5.4)}$$

In this equation, δ and G_d are called the mechanical loss angle and the dynamic modulus respectively. Therefore in the small amplitude oscillatory shear (SAOS) these two quantities are only function of the frequency and are independent of γ_0 that is $G_d(\omega)$ and $\delta(\omega)$.

In the case of large amplitude oscillatory shear, nonlinear viscoelastic behaviour will be exhibited by the polymeric fluids. In the nonlinear regime, the stress response is not sinusoidal but can be represented as a summation of an unlimited number of sinusoidal functions, where their frequencies are the odd harmonics of the strain frequency. This is described mathematically as:

$$\sigma(t) = \sum_{m=1, \text{odd}}^{\infty} \sigma_m \sin(m\omega t + \delta_m) \quad \text{Equation (5.5)}$$

In the above equation both σ_m and δ_m can be functions of both frequency and strain amplitude, that is $\sigma_m(\omega, \gamma_0)$ and $\delta_m(\omega, \gamma_0)$.

Based on these theories, we designed a set of experiments which are explained in the following few lines. First we excited the cantilever base at a specific frequency, and then the response of the cantilever was recorded. After that, the Fourier transform of this response was calculated and from its result it was checked whether the higher harmonics of the excitation frequency could be observed or not. It should be mentioned that, for this experiment, we used the tip holder with the large piezo bar that is suitable for the thermal noise excitation as was explained in chapter 4. This was done because it provided less noise floor than the other tip holder and also it made it possible to observe smaller peaks for the harmonics. These experiments were performed for both Newtonian and polymeric fluids and their results were compared to verify the linearity of the polymeric solution. For Newtonian fluids, air, water and 75% glycerine-water solution were used. For the polymeric fluids, 5% and 16% polystyrene-DEP solutions were used. Also for the excitations, three different frequencies of 7, 12 and 22 kHz were chosen. These frequencies were carefully chosen based on the sampling theory and also on the sampling

rate used for digitizing the signal, in order to capture higher vibration harmonics up to the fifth harmonic. Moreover, for the purpose of generality of the results, the frequencies were selected in order not to be multiples of each other. We chose different amplitudes of vibration, ranging from 0.1 to 10 volts.

Figure 5.15 shows the responses of the cantilever at different frequencies for different drive amplitudes in air. It was noticed that for high drive amplitudes, peaks at the harmonics of the excitation frequency appeared in the frequency response for both the odd and even harmonics. However for low drive amplitudes, only a peak for a fundamental excitation frequency was observed. If we consider the previous theory for this case, no harmonics should be observed in the response of the cantilever because air is a Newtonian fluid. However, such behaviour was also observed by Revenko et al¹², who excited the cantilever both magnetically and acoustically. They attributed the existence of such peaks to the inherent nonlinearity of the photodiode detector and the electronics of the microscope, which was used to measure the cantilever position. They also concluded that these peaks were not related to the motion of the cantilever because they appeared for both types of magnetic and acoustic excitations. Nevertheless, we still performed these experiments for water and the other solutions, including the polymeric fluids. Again we observed the harmonic peaks at high driving amplitudes only, as illustrated in Figures 5.16 and 5.17 for water and 16% PS solution. In this case, since there was no difference in behaviour between the polymeric and the Newtonian fluids, we could not consider this behaviour as an evidence of nonlinearity and it was concluded that we are still in the linear region.

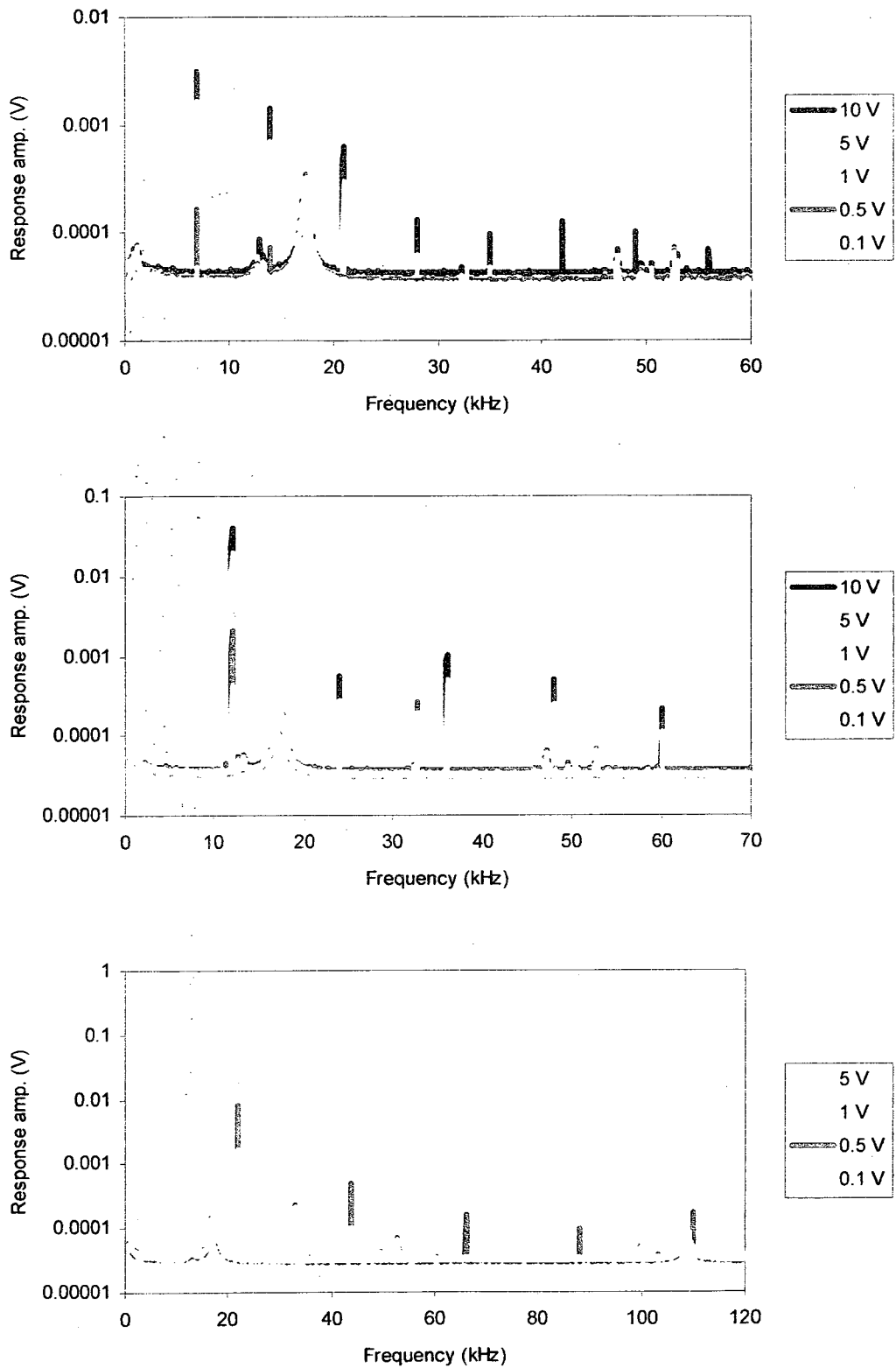


Figure 5.15 Appearance of peaks at harmonics of excitation frequency for long cantilever surrounded by air. Excitation frequencies are: a) 7 kHz, b) 12 kHz, c) 22 kHz

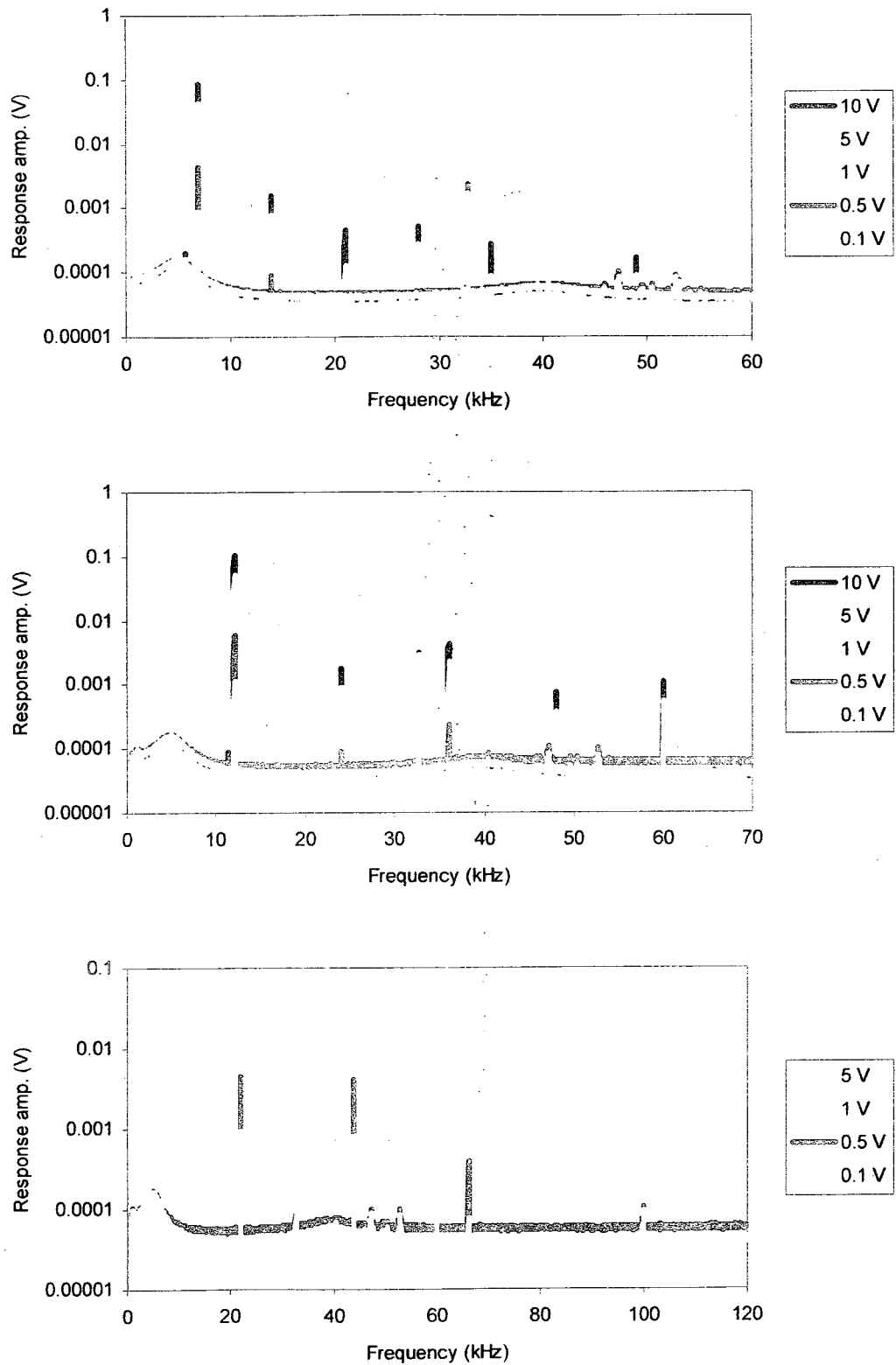


Figure 5.16 Appearance of peaks at harmonic frequency of excitation frequency for long cantilever immersed in water. Excitation frequencies are: a) 7 kHz, b) 12 kHz, c) 22 kHz

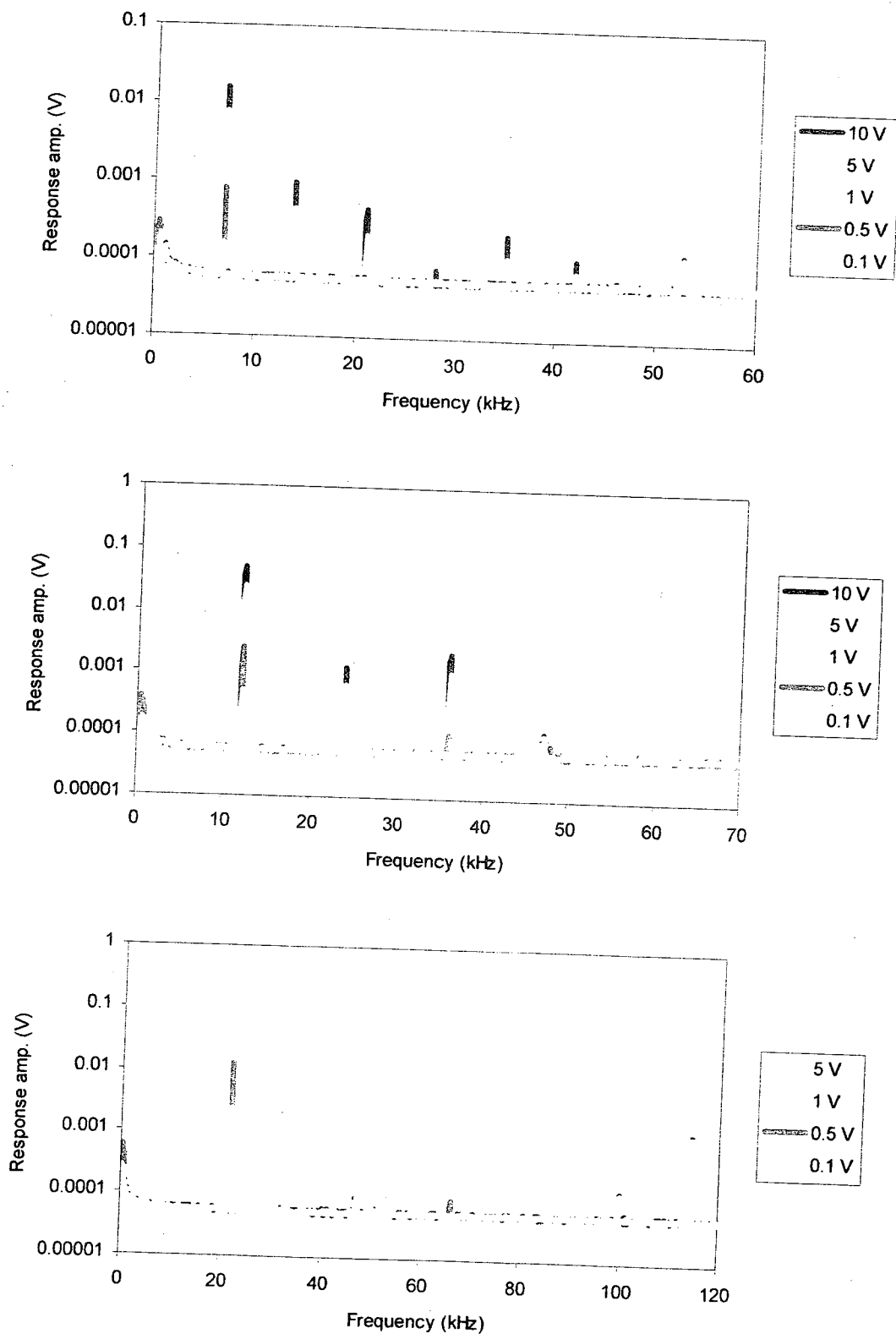


Figure 5.17 Appearance of peaks at harmonic frequency of excitation frequency for long cantilever immersed in 16% PS solution. Excitation frequencies are: a) 7 kHz, b) 12 kHz, c) 22 kHz

Monitoring the obtained values for the harmonics, there was no clear relationship between their magnitudes and the excitation frequencies. Moreover, there was no tendency between the magnitudes of the harmonics and the harmonic's number. However, it was noticed that there is a linear relationship between the magnitudes of these peaks and the driving amplitudes above 1 V, as for example shown in Figure 5.18 for 16% PS solution. It was also consistent with the previously obtained results for the linearity of the frequency sweep response, because the frequency sweep response was the magnitudes of the fundamental peaks in the defined range of frequency sweep. It should also be explained that the concluded linearity for the higher harmonics was based on a few driving amplitudes, mainly two, and was not as strong as the linearity of the fundamental peaks. We should also mention that such linearity for the magnitude of the peaks was observed for all the fluids.

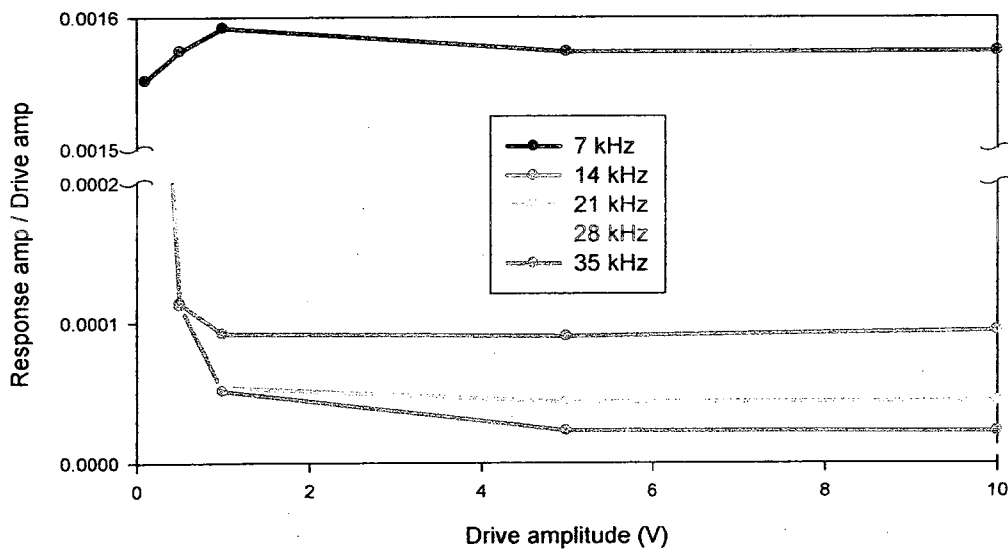


Figure 5.18 Linear relationship between the magnitudes of the peaks, located at excitation frequency and its harmonics, and the driving amplitudes for 16% PS solution

5.6) Discussion of the experimental results

In this section, we interpret the cantilever behaviour in response to thermal noise, frequency sweep and step excitation, mentioning all the advantages and disadvantages regarding each technique. During our discussion we often refer to the viscosity of the fluids as low, moderate or high viscosity. To be more precise we associate viscosity of water with the low viscosity, the viscosity of 75% glycerine-water solution with the moderate viscosity and the viscosity of pure glycerine with the high viscosity.

Starting with thermal excitation, Figure 5.19 shows the theoretical and experimental results for the amplitude response of the long cantilever immersed in water. The results are normalized with the value of the averaged noise floor. The figure also shows the theoretical results while adding the effect of the noise floor which was done using the

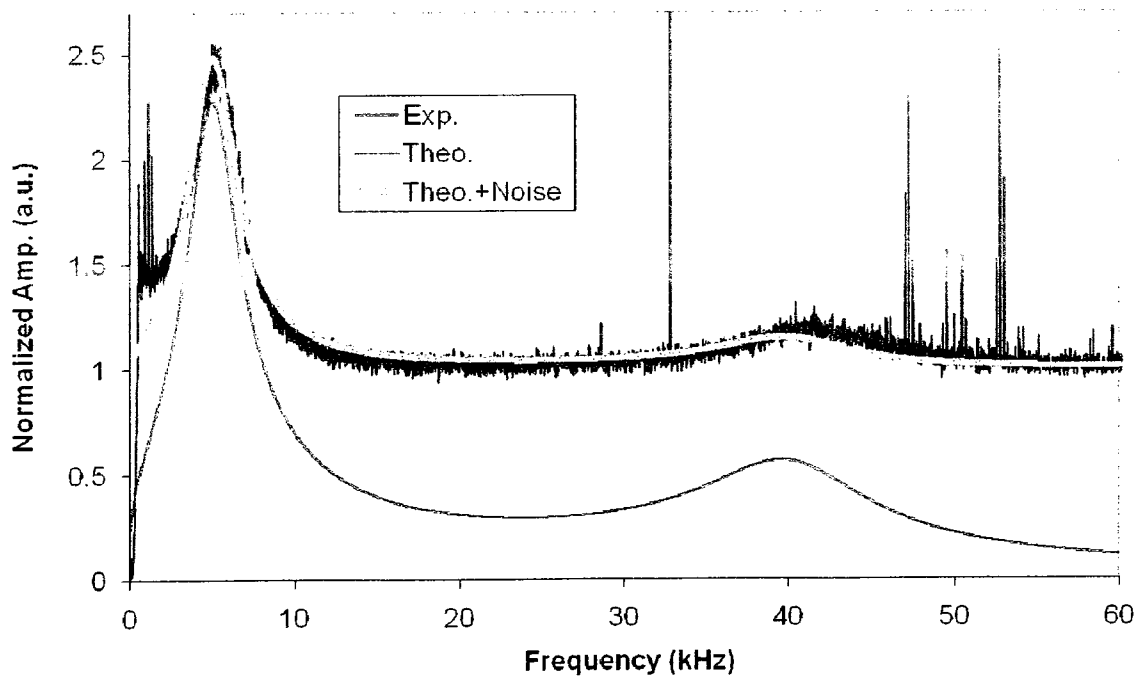


Figure 5.19 Thermal noise for long cantilever immersed in water

following equation:

$$Y_{theo-noise} = \sqrt{Y_{theo}^2 + A_{noise}^2} \quad \text{Equation (5.6)}$$

As it can be seen on this figure and in general for this type of excitation, if the investigated range of frequency is large enough to let us see a few modes of vibration, we can notice that the magnitude of the peaks for the lower modes of vibration are greater than the magnitude of the peaks for the higher modes of vibration. For example, the magnitude of the peak for the second mode of vibration is smaller than that for the first mode and larger than the magnitude of the peak for the third one.

The other issue is the effect of cantilever length and fluid viscosity on the cantilever vibration. For the assessment of the length variation, we need to compare the responses of two different cantilevers while immersed in the same fluid. However for investigating the effect of viscosity change, the comparison between the responses of one cantilever that is immersed in two different fluids is required. Figures 5.20 and 5.21 show the responses of medium cantilever immersed in water and the response of long cantilever immersed in 50% glycerine-water solution respectively. The comparison between Figures 5.19 and 5.20 indicates that the effect of utilizing a longer cantilever is the decrease of the resonance frequency of the cantilever at each mode of vibration. Also using a longer cantilever causes the peak to be sharper and larger in magnitude. On the other hand, the viscosity variation effect can be observed by comparing Figures 5.19 and 5.21. These figures show that the increase of fluid viscosity causes broadening of the peaks and a decrease in the frequencies of the modal peaks. This is because when the viscosity of the fluid increases, the damping effect and the added mass increases.

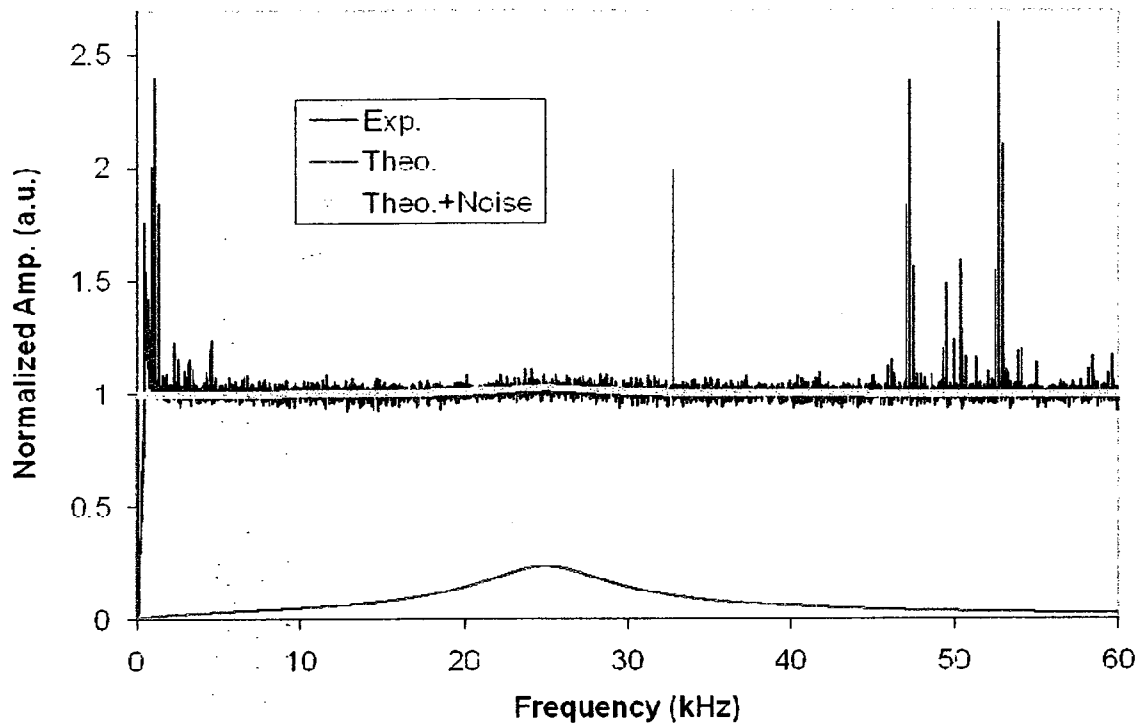


Figure 5.20 Thermal noise for medium cantilever immersed in water

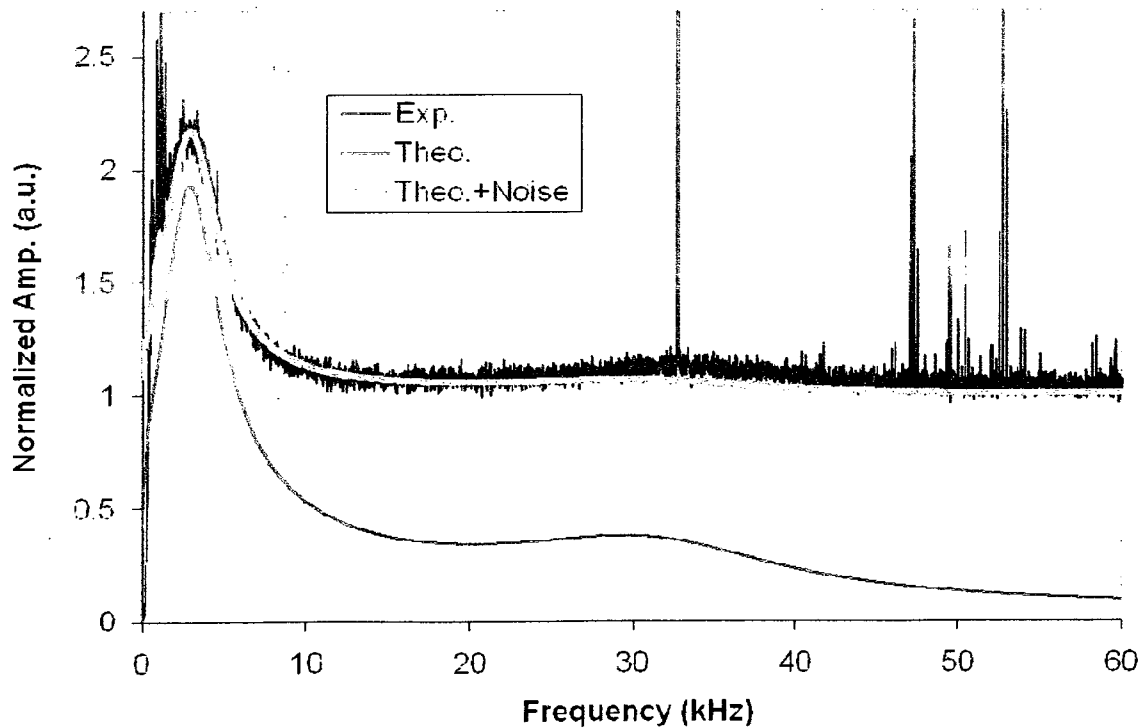


Figure 5.21 Thermal noise for long cantilever immersed in 50% glycerine-water

While keeping all the above mentioned factors in mind, it should be mentioned that the main advantage for the thermal excitation technique is the smooth response of the cantilever. This is mainly because there is no moving part in the AFM head except the cantilever in response to the thermal excitation. However, for such a technique there are two experimental limitations. First, we always observe a noise floor in the response the magnitude of which depends upon some environmental factors such as electrical noises, building vibrations and the surrounding sound noises. This noise limits the application of this technique to fluids in which a considerable part of the cantilever response is larger than the noise floor; in other words, when we have a large ratio of signal to noise. For example in Figure 5.19, the response around the first mode is more useful for the analysis than the response around the second mode. The second limitation is related to the filtering of the digitized signal. As it was mentioned in chapter 3, we performed a high-pass filtering with a cut-off frequency of 500 Hz for removing the DC value of the recorded signal. However, the effect of filtering on the results can be observed up to 2-3 kHz on the results. This causes the first peak for the response of the long cantilever, when immersed in a moderate or high viscosity fluid, to become useless because it is very close to the zero and as a result, it is altered by the filtering process. Also in such a situation, the second mode of vibration is also not usually visible. Therefore the the thermal noise response, in this case, does not show any features related to the properties of the fluid and the cantilever. On the other hand, when using shorter cantilevers we do not encounter any problems with the filtering process, because of the increase of the resonant frequency, but the magnitude of the model peaks are nearer to the noise floor.

As a result of these phenomena the applicability of this technique is limited to utilizing the long cantilever for the low viscosity fluid. This is because, for the other situations, the magnitude of the driving force due to the impact of the fluid molecules exhibiting Brownian motion is not enough to have a response greater than the noise floor. We can increase the amount of this force by increasing the temperature, however in this way the properties of the fluid will change. Therefore we need to provide the energy for the vibration of the cantilever in another way. This can be solved using the frequency sweep excitation or step excitation techniques which are explained next.

In the frequency sweep excitation, we can provide considerable amount of energy to cantilever by moving its base. As a result we can observe a response for the cantilever which has shorter length or is immersed in a higher viscosity medium. Figures 5.22 and 5.23 show the theoretical and experimental results for the amplitude and the phase of long cantilever vibration when it is immersed in water. Such graphs for the other fluids and cantilever are presented in Appendix I (pages 188-195).

Looking to the amplitude responses in this type of excitation, the general effects of variation of cantilever length and fluid viscosity on the frequency of the model peaks are similar to those observed in thermal noise. However, the higher modes of vibration have larger amplitudes than the lower modes of vibration for the range of low to moderate viscosities. This means that if a long cantilever is utilized in a moderate viscosity medium, although the usefulness of the first mode of vibration diminishes because of the interference with the effect of the filtering process, we can still use the response around the higher modes of vibration in our analysis. This is an advantage in comparison to the thermal noise, in which the ratio of signal to noise floor for the higher modes is not large.

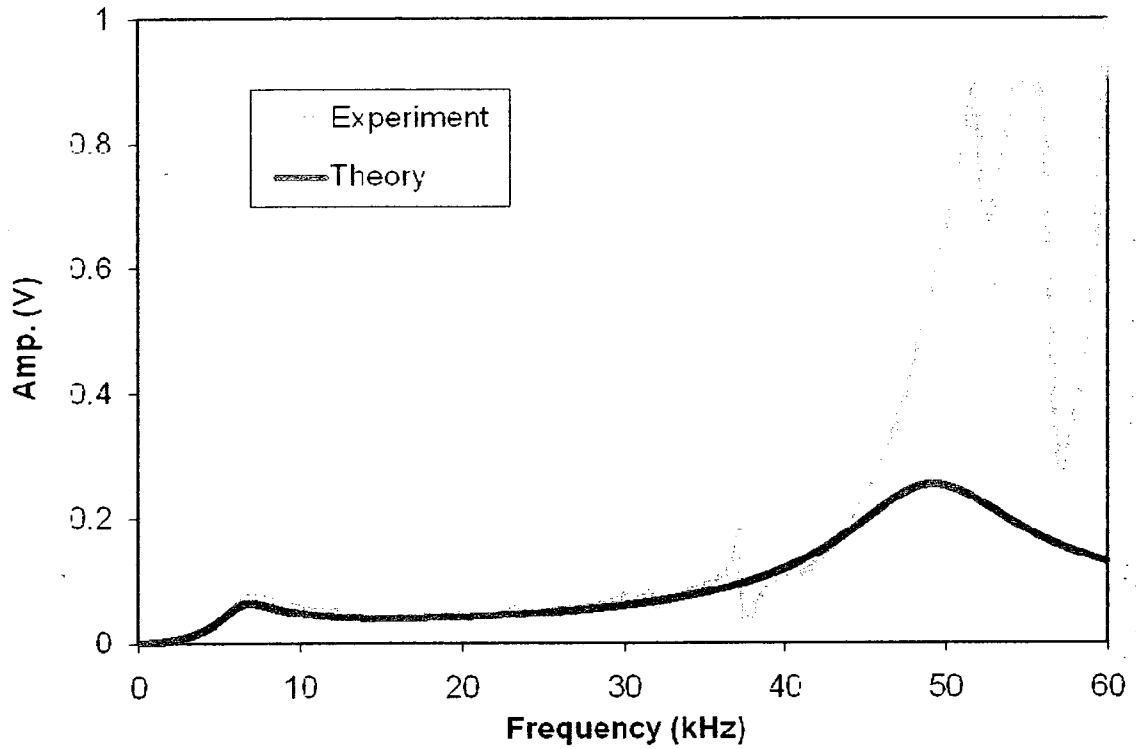


Figure 5.22 Amplitude response of frequency sweep excitation for the long cantilever immersed in water

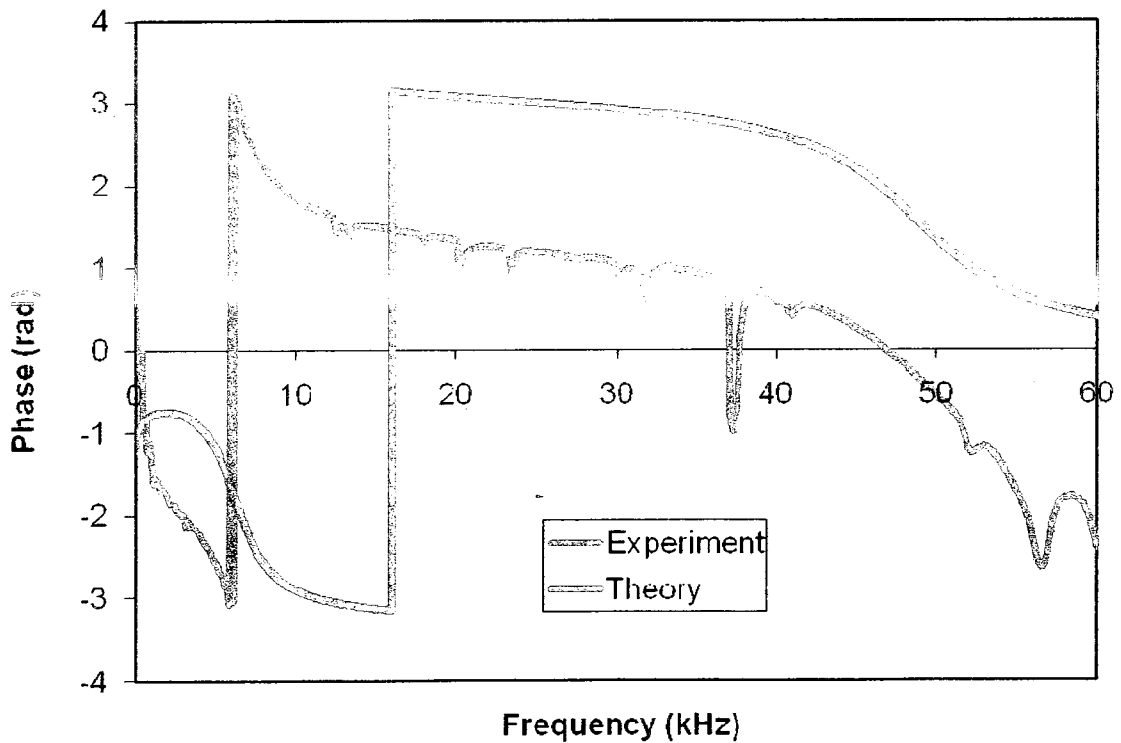


Figure 5.23 Phase response of frequency sweep excitation for the long cantilever immersed in water

On the other hand, the response of the cantilever for high viscosity fluids does not contain peaks and the variation of its shape becomes independent of fluid properties. In this case using a shorter cantilever could be helpful because all the peaks can be observed at higher frequencies. Therefore the applicable range of viscosity will increase in this type of excitation compared to the thermal noise type.

Looking again at the amplitude response in Figure 5.22, it can be noticed that there is a big deviation from the theoretical response between 40 and 60 kHz of frequency and also there are some noises at lower frequencies. In order to understand the reason for the deviation in behaviour in the above mentioned frequency range, the results of amplitude responses of several long cantilevers, which are all immersed in water, were compared and this is illustrated in Figure 5.24. It was observed that these responses are approximately similar in frequencies less than 40 kHz but have very different behaviour between 40 and 60 kHz. The small difference between the responses in first part of frequency range is related to the small differences of the cantilever thickness and scaling factor but this reason cannot be used for explaining the large deviation in the response between 40 and 60 kHz. It is more reasonable to relate this deviation to the environmental noises detected in this frequency range that were also observed in the thermal noise response as explained in section 5.2. Therefore, from now on we will only consider the response of the cantilever for frequencies less than 40 kHz in our analysis. As illustrated in Figure 5.22, there are also some small noises in the amplitude responses in the first part of frequency range. The peak around 37 kHz is related to the resonant frequency of the cantilever chip which was also observed by Han et al¹⁰. Based on this justification, the other peaks might be also related to the vibrations of the other moving parts in the

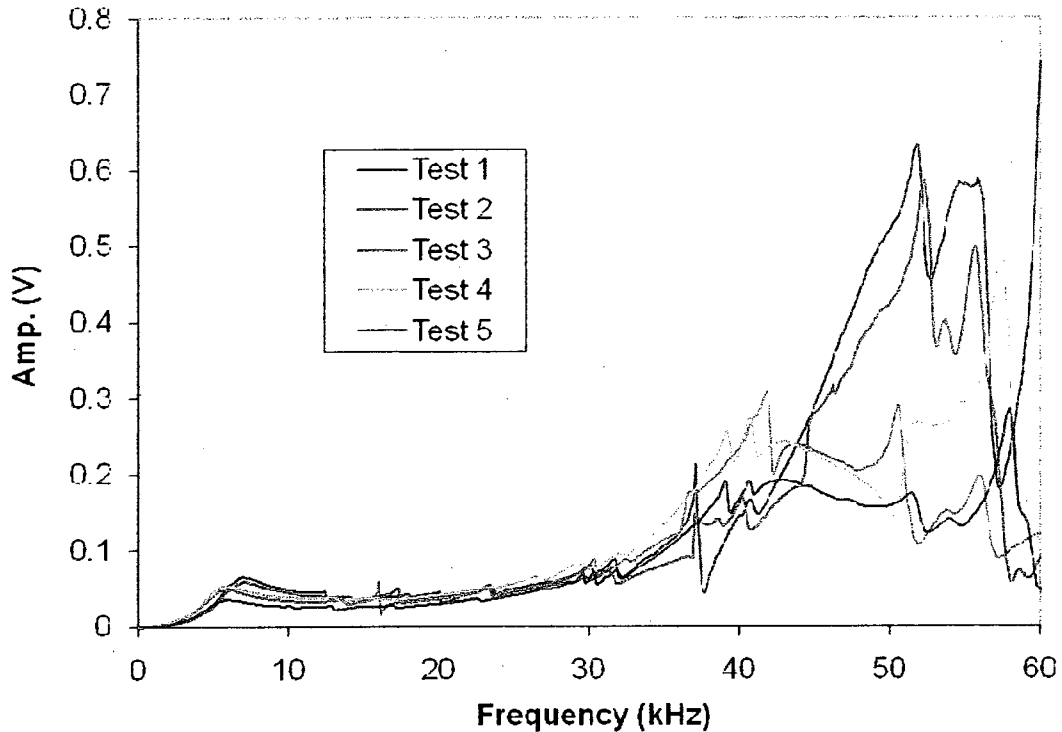


Figure 5.24 Comparison of the amplitude responses of several long cantilevers, which are all immersed in water

cantilever holder, such as the spring and clip in the holder. It should be mentioned that in order to get a very smooth response in this type of excitation, a very well designed holder is required that considers all of these vibrational aspects. Such optimization could be considered as future work for this project.

Referring to the phase response in Figure 5.23, it should be mentioned that the phase results are the inverse tangent of the ratio of the imaginary parts to the real parts of the Fourier transform results at each frequency. In general, the value of an inverse tangent is between π and $-\pi$, as shown in the figure. In this case when, for example, the phase of the cantilever response is going to be less than $-\pi$, a 2π will be added to it and the rest of the results continue starting from the value of π . This causes all the data to lie between π and $-\pi$ but a discontinuity in the results will appear. In order to remove these discontinuities

an unwrapping process was performed on the experimentally and theoretically obtained results so in this way we have a better view of the data. The result of such process on the data in Figure 5.23 is presented in the following figure.

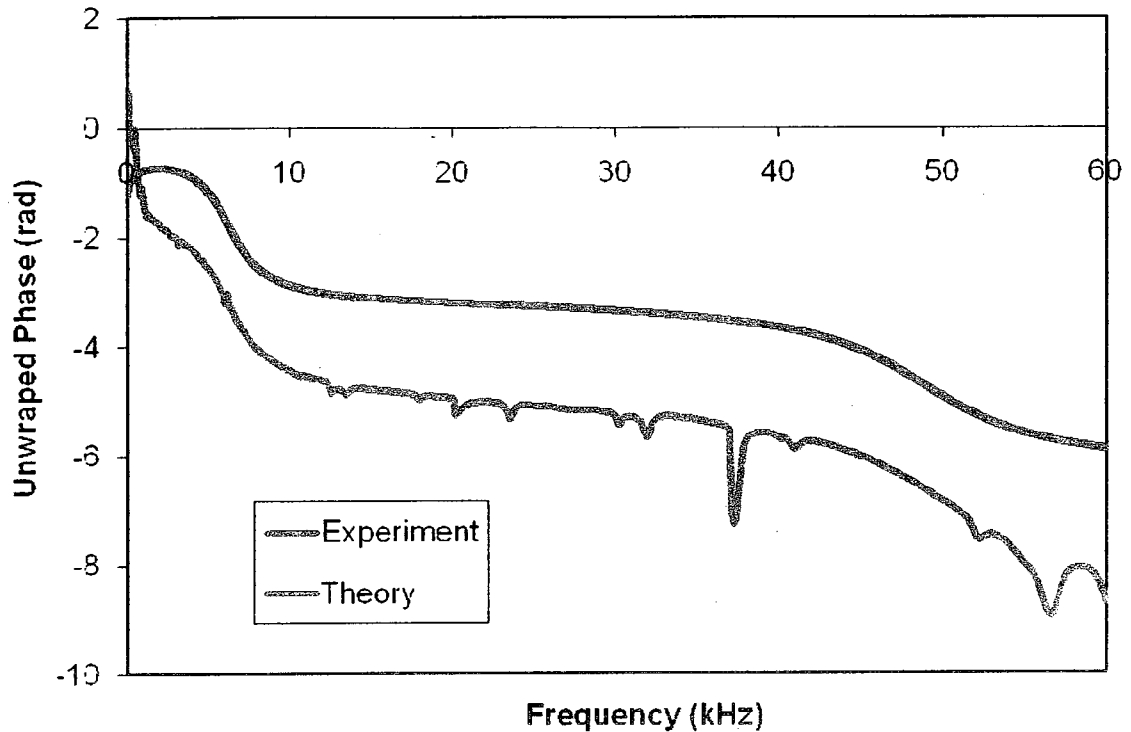


Figure 5.25 Unwrapped phase response for long cantilever immersed in water

The other issue concerning the phase response is the presence of a phase drift (see Figure 5.26) that the AFM machine exhibits without having any laser beam reaching the photo detector, which could be measured by removing the cantilever or unplugging the laser cable of the AFM head. The amount of this phase drift is not constant and depends upon the frequency of the driving signal. Moreover, for different drive amplitudes the shape of the phase drifts are the same but for low drive amplitudes they are much noisier. Basically, all drive amplitudes used for these experiments are much more than the values that are used normally for the imaging processes. As a result of using such high drive

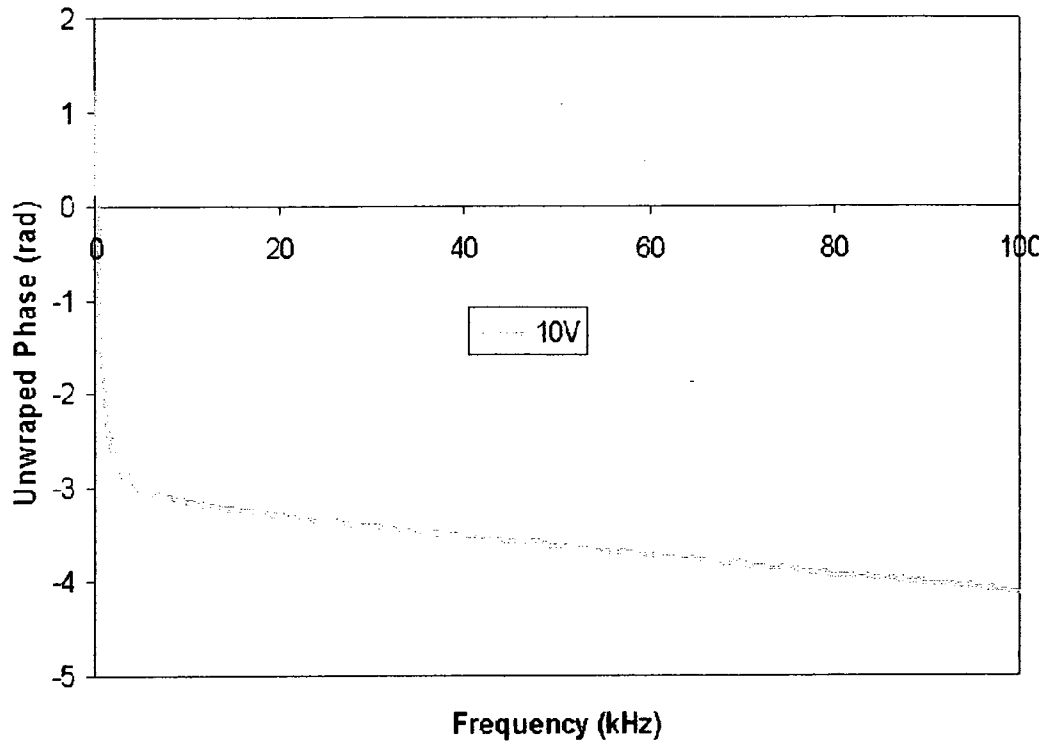


Figure 5.26 Unwrapped phase drift of the AFM for drive amplitude of 10 (V)

amplitudes, some issues regarding the grounding in the electronics of the AFM will happen, which could also be coupled with a capacitance effect. This will lead to noticeable reading of phase without a laser spot on the photo detector. So in order to see the results of the cantilever only, we subtract this imbedded drift and prevent it from affecting the output data, as shown in Figure 5.27. It should be mentioned that the difference between the theoretical and experimental result in this figure is around $\pi/2$ which is related to the implementation of sine instead of cosine or vice versa in the code used for the theoretical modeling.

Focusing on interpreting the experimental data from the physical point of view, it can be noticed that the phase response also shows the presence of different modes of vibration but in a different manner compared to the amplitude response. The amplitude

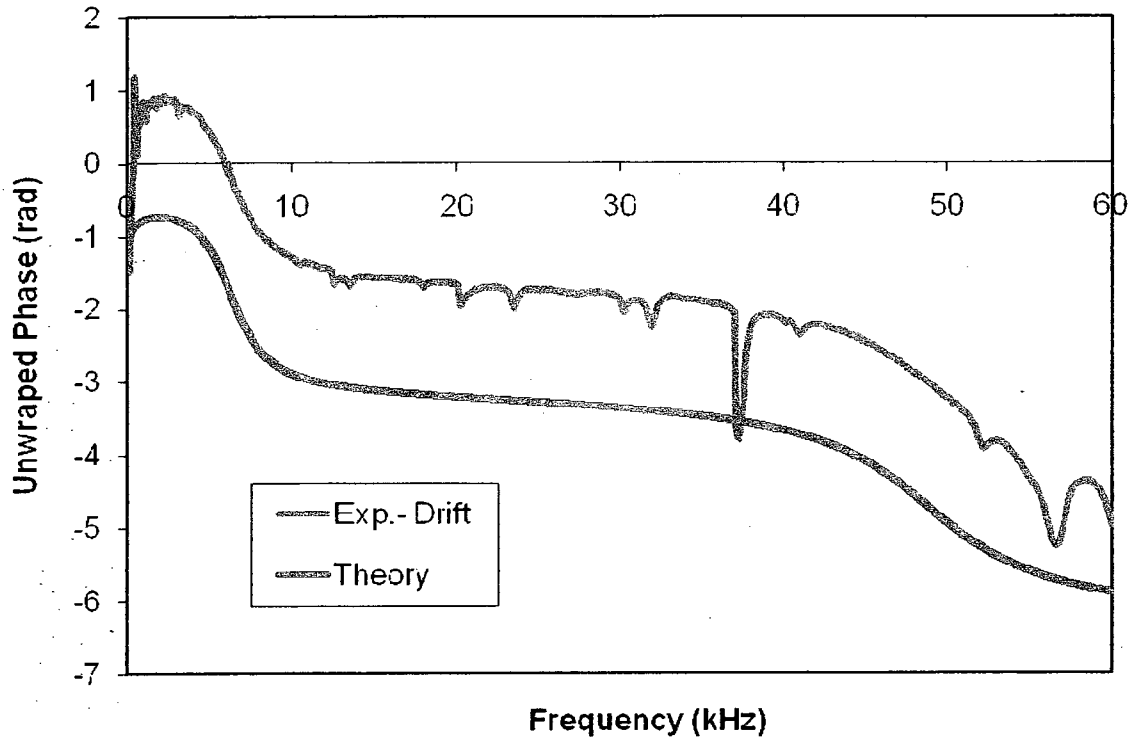


Figure 5.27 Unwrapped phase response which the effect of phase drift is removed. The long cantilever was used for this result and the surrounding fluid is water.

response exhibits such modes by the appearance of peaks, while the phase response displays them in the form of a significant decrease in the value of the phase, as shown in Figures 5.22 and 5.27 respectively. Moreover, for different modes of vibration, the amount of change in the value of the phase are the same for the phase response but for the amplitude response, as mentioned earlier, the higher modes have higher amplitudes.

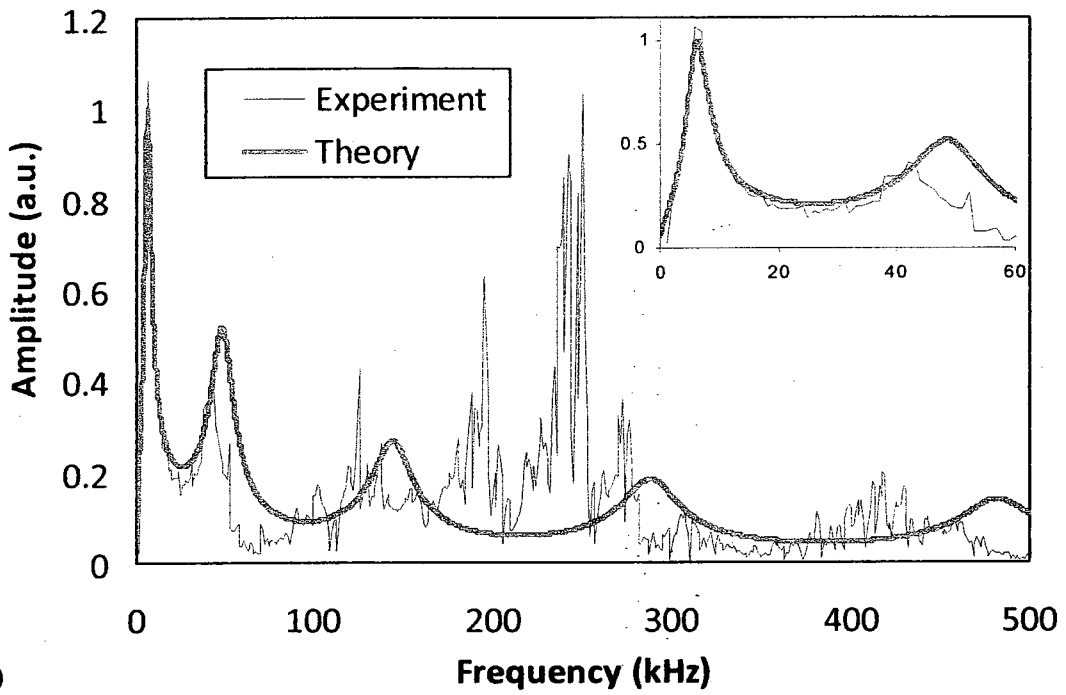
Furthermore, the effects of the cantilever length and fluid viscosity on the phase response are similar to those effects on the amplitude response. More precisely, we can observe that when the viscosity of the surrounding fluid increases or when a shorter cantilever is used, the resulting change in the value of the phase response occurs over a wider range of frequency and similarly the peaks in the amplitude response become broader and smoother. In addition, the value of frequency at which the peaks occur, in the

amplitude response, and the significant decrease occurs in the phase response, is shifted to a lower value as the viscosity of the fluid or the length of the cantilever increases.

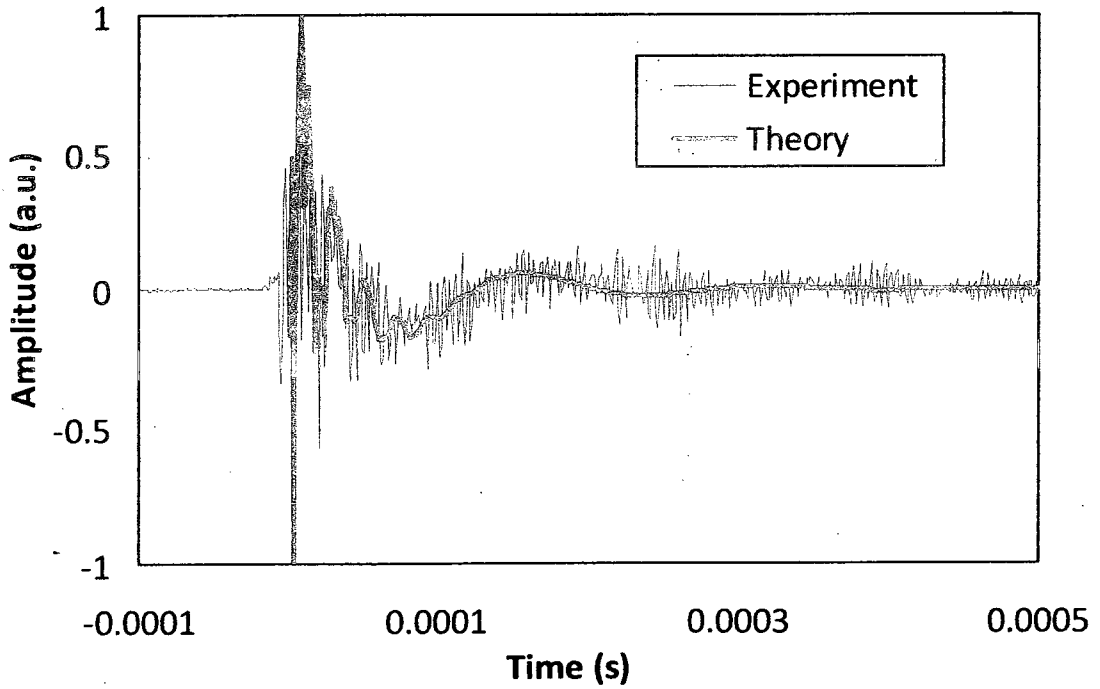
It should be mentioned that the noises appear in the phase response exactly at the same frequency as the noises in the amplitude response. However, the effects of these noises are a little different for both responses. For the phase response, the noise peaks cover a much narrower frequency band and deviate from the main trend only downwards; however, for the noises on the amplitude response, their effect is observed over a much broader frequency band and they are also found in both the upward and downward directions. This makes it easier to locate the noises and remove them from the data in the phase response as compared to the amplitude response. The phase response at the low frequency range of less than 3 kHz should also be neglected because the filtering process affects the phase response also.

In conclusion, both the amplitude and phase responses have the same information regarding the properties of the cantilever and its surrounding fluid. However the phase response is preferable for analyzing because the noises in this kind of response can be recognized and removed more effectively.

Moving to the last excitation technique, namely the step excitation, Figure 5.28 shows the response of long cantilever, immersed in water, in both the frequency and time domains. Similar results for the other cantilever and fluids are presented in Appendix J (pages 196-201). For this type of excitation, the response of the cantilever in the frequency domain is somehow similar to the thermal noise response. That is, the amplitude of the peak for the second mode is smaller than that of the first mode but greater than the third one. Moreover, the effects of changing the cantilever length and



a)



b)

Figure 5.28 The response of the long cantilever which is immersed in water to the step excitation (a) in the frequency domain and (b) in the time domain.

fluid viscosity, on the cantilever response, are similar to the ones described for frequency sweep and thermal noise. However, because of the large energy of excitation, the amplitude of vibration is much more than the value of noise floor and as a result it allowed us to observe the higher modes of vibration, up to the fifth. It was not feasible to observe them with thermal noise under the experimental conditions of our instrument.

Regarding the response of the cantilever in the time domain, it should be mentioned that it was constructed numerically using the inverse fast Fourier transform. In order to have such response for the same duration and resolution of the experimental response, that is the duration of 0.1 s with a resolution of 10^{-6} s , we calculated the cantilever response in the frequency domain up to 500 kHz with the resolution of 0.01 kHz using Equation (2.83). Then the results were transformed to the time domain using the IFFT in MATLAB. The results of this transformation were complex numbers and it should be admitted that we could not find any physical meaning for the imaginary parts so far. Nonetheless, the real parts predict the main features of the experimental response rather well. The main problem with the cantilever response, in the time domain, is that the effect of the filtering process on the results is difficult to identify. Therefore, in total the frequency domain is preferred for analysing the results.

By comparing between the frequency sweep excitation and the step excitation, we conclude that the later technique has three advantages. The main advantage is that we have an exact solution for the theoretical response rather than a solution in the form of a series. Therefore it does not have any truncation error regarding the series. The second advantage of this type of excitation is that the response around the first mode, which can be predicted more accurately by the theory than the higher modes, has higher magnitude

than the other features in the data. And finally, obtaining the total response takes less time in step excitation. The reason for the latest advantage is that in the frequency sweep excitation, the resolution of the data in frequency depends on the number and range of discrete frequencies used to drive the cantilever. Therefore, it is necessary to increase the number of measurement points and the overall measurement time in order to broaden the frequency range without reducing the resolution. However this is not the case for the step excitation because the range of the frequency and its resolutions depend on the sampling rate and duration for digitizing the signal which make the total acquisition time less.

5.7) Discussion on the theoretical results

As it was explained in the previous section, the higher modes of vibration affect the frequency response at lower frequencies when the viscosity of the solution or the length of the cantilever increases. On the other hand, the theoretical model for the applied drag force on the cantilever is not accurate for higher modes of vibration. The reason for this inaccuracy is that this model was derived based on the assumption of 2D flow for the surrounding fluid. But as mentioned in chapter 1, because of the considerable axial flow, this assumption is violated for the higher modes of vibration. Therefore, the main inconsistency between the theoretical and experimental results can be explained in this way for the long cantilever when it is immersed in high viscosity fluids.

The other issue, regarding the theoretical models for the different excitation techniques, is related to truncation in the series solutions. As we know, the theoretical response of the cantilever is the summation of all its modes of vibration. But the question

is “how many modes of vibration is required to represent the theoretical response in the selected range of frequency with a small truncation error?”. In order to answer such a question, we compared several simulations of the frequency sweep excitation that were obtained by applying different numbers of modes in the calculation. The result of such analysis is presented in Appendix K (pages 202-209). This comparison allowed some conclusions. First, the effect of the number of modes included on the phase response is less than on the amplitude response. Second, for the medium cantilever, the response is mainly around the first mode of vibration for all solutions. Moreover applying the 1st and 2nd modes is enough for representing the theoretical response in the range of 0 to 60 kHz except for pure glycerin which needs at least the first 4 modes. Finally, for the long cantilever, two modes of vibration can be observed for low concentration solutions and the effect of higher modes will appear as the concentration increases until the pure glycerin which even 9 modes of vibration are not enough for representing its theoretical response in the selected range of frequency.

It should be mentioned that, although for most cases using 4 modes of vibration was enough to represent the theoretical response; we implemented 9 modes of vibration for all cases when we wanted to obtain the theoretical responses for comparison with the experimental results. The reason for this was that in general using more numbers of modes introduces less error than not using them.

5.8) Finding the properties of Newtonian fluids from their FS experimental data

Two different approaches were applied in order to determine the properties of Newtonian fluids from the frequency sweep data. In general, the first one considers the whole frequency range and the viscosity and density are determined by finding the best fit of the theoretical response to either the amplitude or the phase experimental results. In the second approach, these properties are calculated at each frequency using the experimental values of both the amplitude and phase at that frequency. In the following paragraphs, the details of each approach and the results obtained are explained.

For the first approach, a MATLAB code was written to find the best fit between the theoretical and experimental results by implementing the nonlinear least-square regression criteria (see Appendix L, pages 210-219). The structure of this code was divided in two parts based on the type of the experimental data used. The first part, which uses the experimental amplitude response, determines the viscosity, density and the scaling factor for the best theoretical response. The reason for using the scaling factor in the calculation of this part was the lack of calibration coefficients for both the input and the output signals, which relate them to the movement of the base and the free end of the cantilever respectively. Similarly, a phase shift factor is determined in the second part of the code, which uses the phase response. In this case, the reason for implementing the phase shift factor is to account for the unknown value that by which the unwrapping process can shift the whole experimental phase response. It should also be mentioned that the noises in the experimental results were excluded from the experimental data for all the calculations. This was done by considering the noises observed on the phase response

diagram as our reference and excluding them from both the phase and amplitude responses, as illustrated in Figure 5.29.

The measured densities and viscosities are compared with their real values in Figures 5.30 and 5.31 respectively, at each concentration of glycerine-water solution for the long and medium cantilevers. The errors in these measured values are shown in Figure 5.32. By observing the error bars in Figure 5.32, one can notice three general different trends for the error, which are explained in the following pages.

The first trend is the increase of error as the concentration increases. The main reason for this, as mentioned earlier in the previous section, is related to the inaccuracy of the theoretical model for higher modes of vibration. This is because as the concentration of the glycerine-water solution increases, the viscosity increases and as a result we observe the effect of higher modes on the response. However there are some practical sources of errors too. It is well known that the properties of highly concentrated glycerine-water solutions, mainly their viscosities, strongly depend upon the fluid's temperature and also upon the accuracy of concentration of the prepared solution. In other words a small change in these two factors leads to a huge change in the properties of the solutions. Moreover, this dependency is significantly increased as the solutions become more concentrated. Consequently few sources of errors could occur. One of them could be the imprecise assumption of room temperature for the real value of the properties. The assumed room temperature was 26°C , which was almost the averaged temperature around the fluid; however this temperature was varying between 25°C and 27.5°C . Such variation gives misleading results and is a source of error. Another source of error is the local heating of the fluid around the cantilever. The given energy to the base of the cantilever

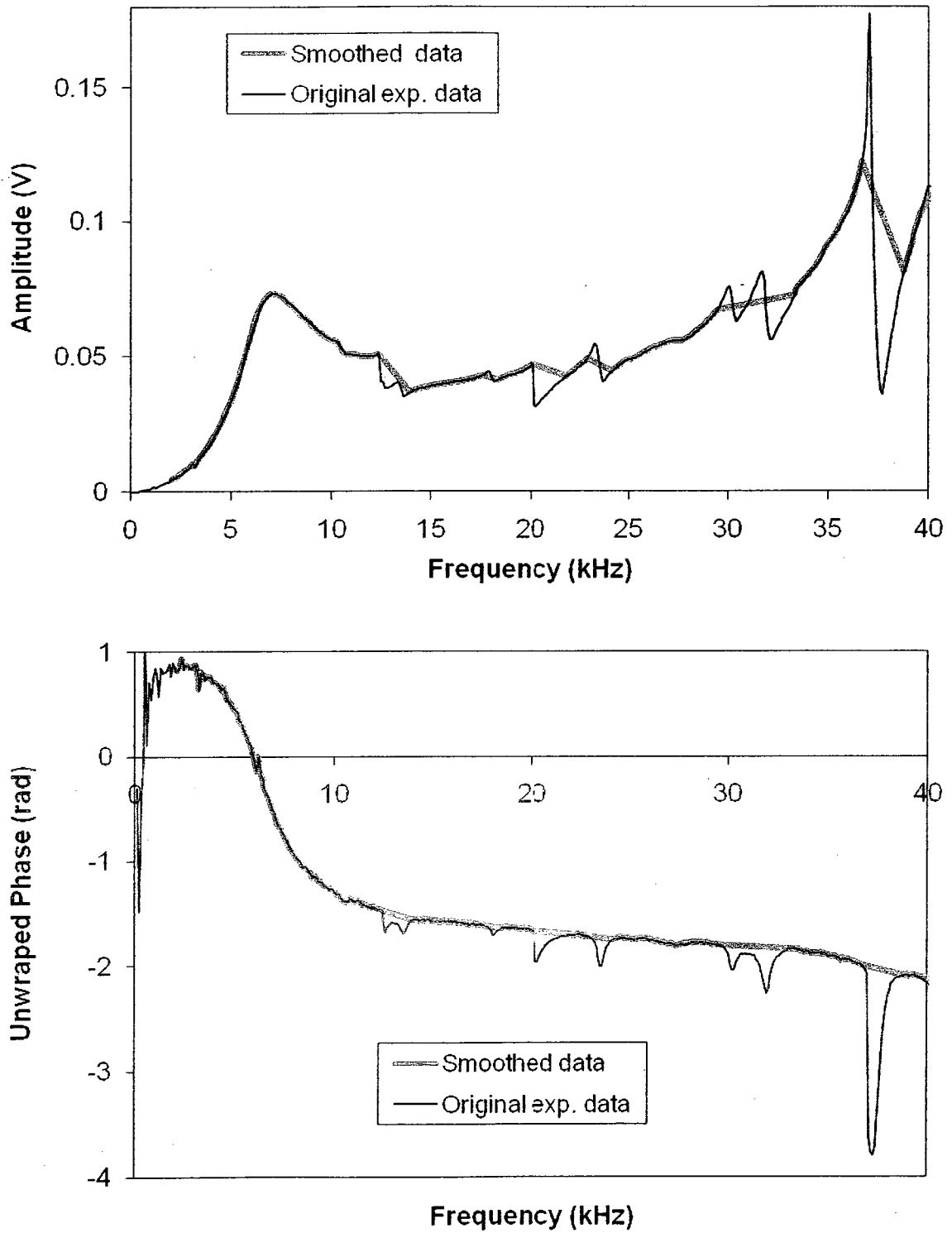


Figure 5.29 Illustration of the original and noiseless experimental data for the long cantilever which is immersed in water

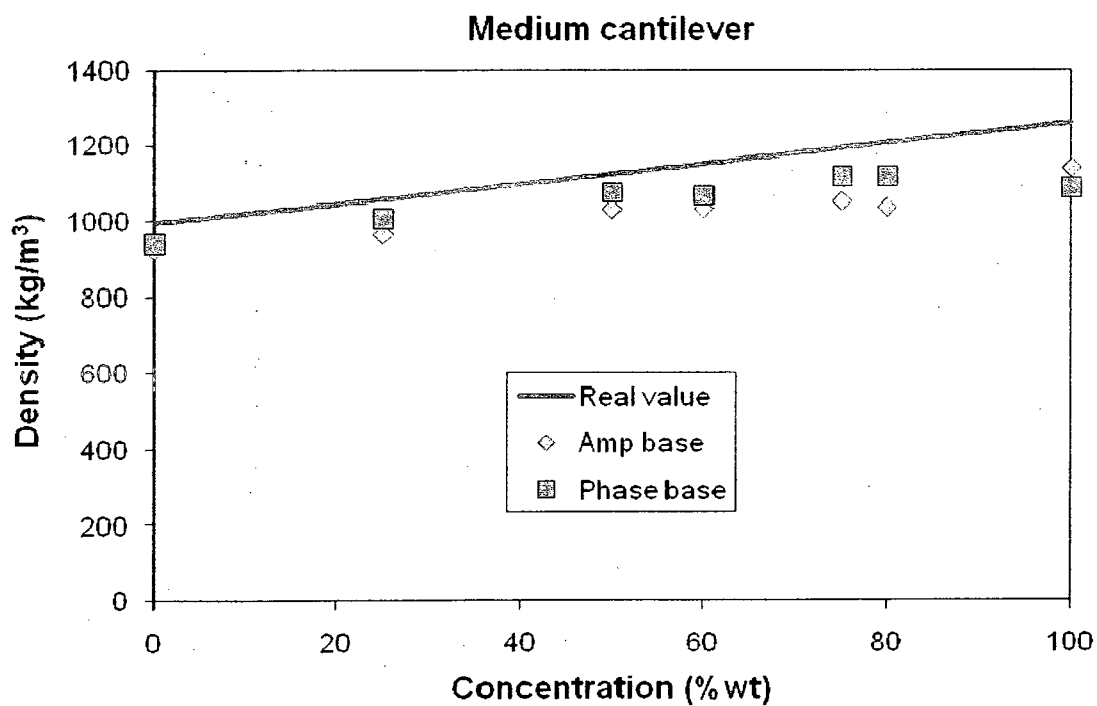
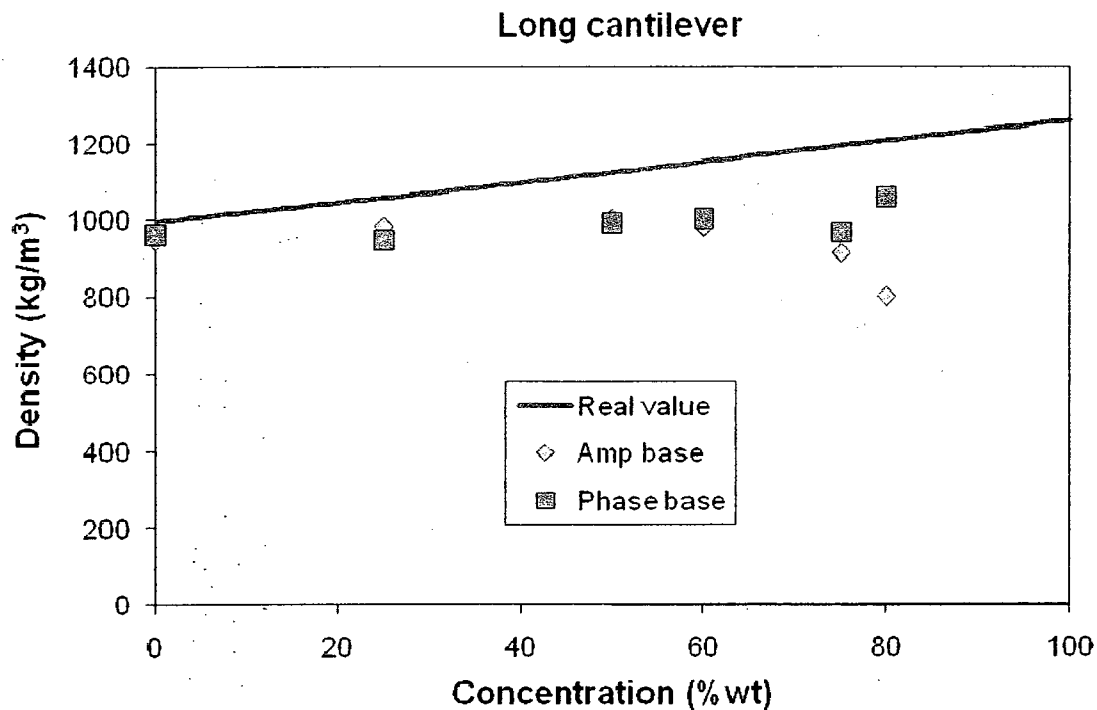


Figure 5.30 Measured and real density of glycerine-water solutions using long and medium cantilevers.

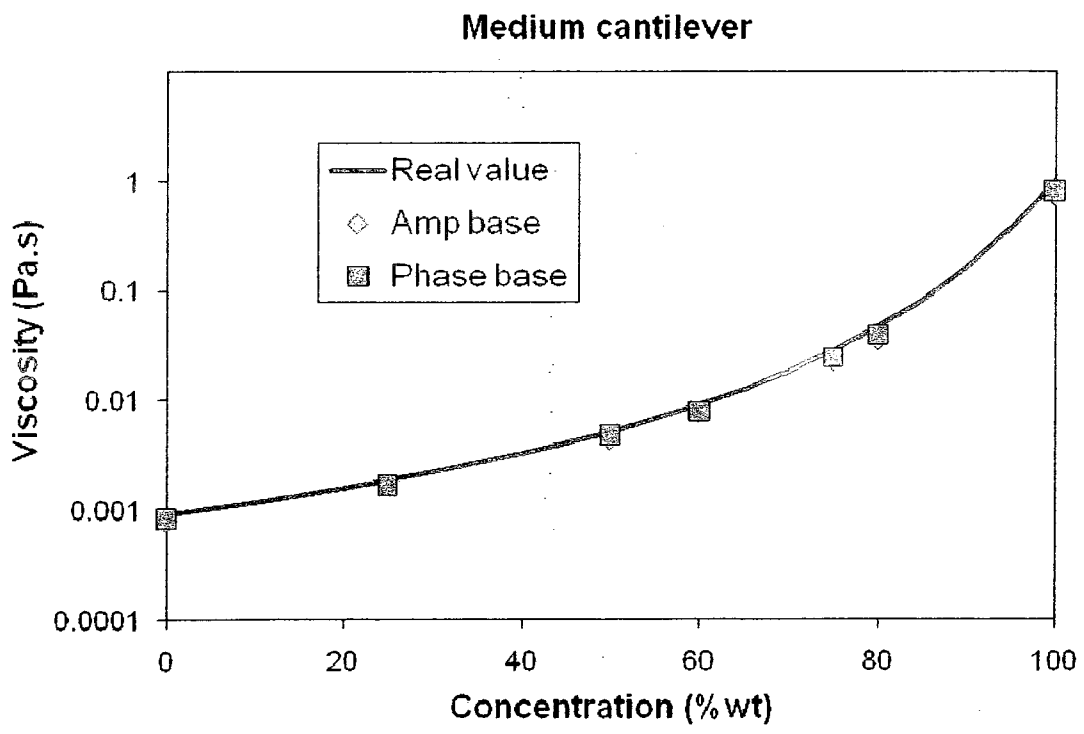
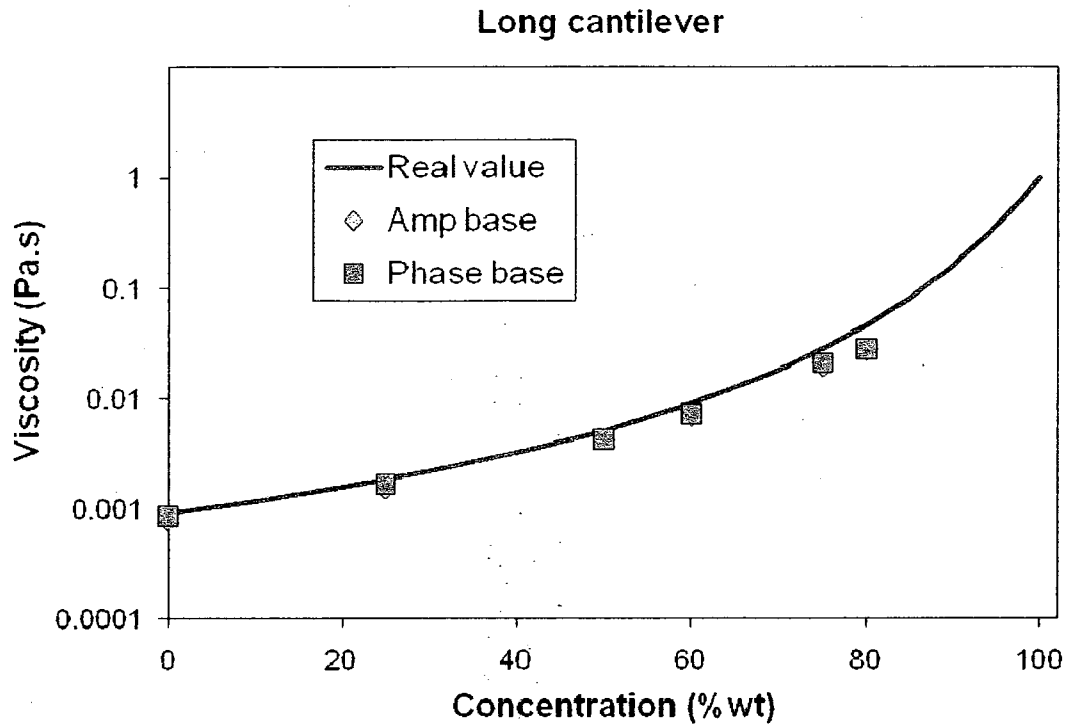


Figure 5.31 Measured and real viscosity of glycerine-water solutions using long and medium cantilevers.

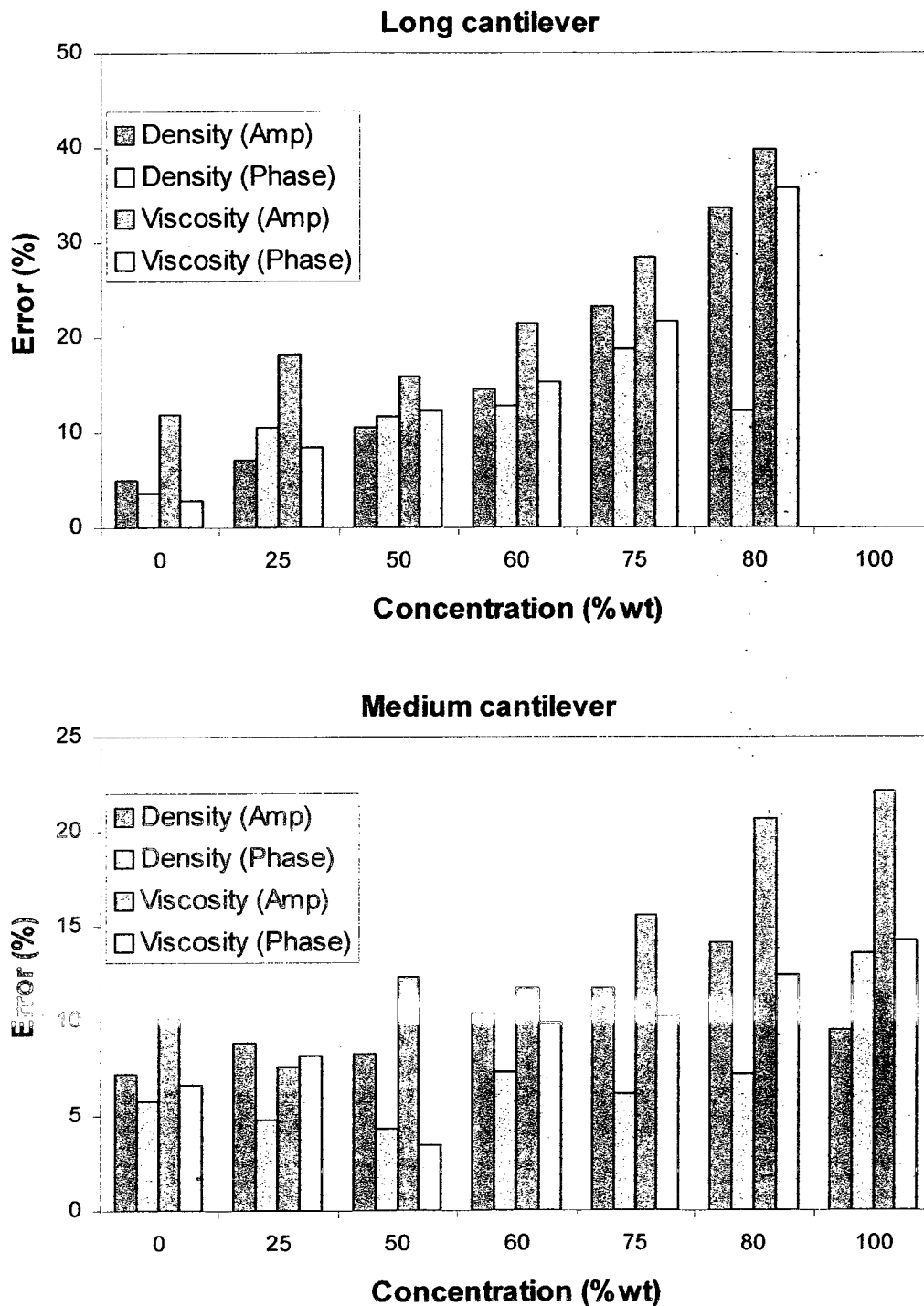


Figure 5.32 Error between the measured and real properties of glycerine-water solutions using long and medium cantilevers.

in this type of excitation dissipates through the fluid. Moreover the laser beam aligned on the cantilever tip heats the fluid in that region. These two factors increase the temperature of the nearby fluid and cause some deviations in the results from what are expected. It should be mentioned that the later factor was also reported by Hennemeyer et al⁷. Looking to the results indicates that most of the measured properties are less than their real values. This could also be a sign that the actual temperature of the fluid is higher than the assumed room temperature. Based on the determined viscosity from the phase response, it was found that the local heating causes an average increase of 3 °C in the temperature of the fluid surrounding the cantilever. Finally, any inaccuracy during the preparation of the correct concentration for the solutions could cause an error in the results. However, this source of error is less likely to occur because we used a very precise balance with 1 mg precision and for each concentration 25 g of solution were prepared, which increased the overall accuracy.

The second trend in the errors is related to the length of the cantilever. As the length of the cantilever increases, the effect of the higher modes will be observed on the response. Since the theoretical model for higher modes is inaccurate, the error of the result increases when we utilize the longer cantilever.

Lastly, the third trend in the errors is linked to the utilization of either the amplitude or phase response. It is noticed that using the phase response results in less error than when the amplitude response is implemented. First, this is because the noises affect the phase response less than the amplitude response and as a result, recognizing and deleting the noise from the experimental data is easier in the phase response. Second, this is also due to the fact that the theoretical response for the amplitude response is scaled while the

phase response is shifted. Based on the least square residual criterion of *nlinfit* command in the MATLAB code, the determined properties from the amplitude response have likely more error, if the scaling factor has an error. In other words, if both the scaling factor and the phase shifting factor had the same error value, the effect of the scaling factor error on the calculated properties is larger than the effect of the phase shifting factor error on the properties.

In conclusion, for the determination of the fluid's properties from the whole response, the results of phase responses are more reliable because their fitted curves represent both the values of experimental data and their trends while the fitted curves for the amplitude response just represent the trends and not the values of the experimental data.

Shifting to the second approach for the determination of the Newtonian fluids' properties, both the amplitude and the phase values must be employed at each frequency in order to obtain the properties. The major problem concerning this approach is the existence of more unknown variables than the known ones. At each frequency these unknowns are density, viscosity, the scaling factor for the amplitude response and the shifting phase factor for the phase response. So in order to solve such a problem, we define a reference frequency and we normalize both experimental and theoretical responses for the amplitude for the whole frequency range and we shift both experimental and theoretical phase response to zero, using their values at the reference frequency. Implementing such a technique, we are able to get rid of the unknown scaling factor and phase shift, this is shown mathematically in the following equations:

$$\begin{cases} F_{1(\rho,\mu)} = \frac{\text{Amp}_{\text{exp}}|_{@f}}{\text{Amp}_{\text{exp}}|_{@f_{\text{ref}}}} - \frac{\text{Amp}_{\text{theo}}|_{@f}}{\text{Amp}_{\text{theo}}|_{@f_{\text{ref}}}} = 0 \\ F_{2(\rho,\mu)} = \left[\text{Phase}_{\text{exp}}|_{@f} - \text{Phase}_{\text{exp}}|_{@f_{\text{ref}}} \right] - \left[\text{Phase}_{\text{theo}}|_{@f} - \text{Phase}_{\text{theo}}|_{@f_{\text{ref}}} \right] = 0 \end{cases} \quad \text{Equation (5.7)}$$

Moreover, in order to find the density and viscosity at each frequency, the above equations should be solved together. In order to find these properties, this algorithm was developed in a MATLAB code, which is shown in Appendix M (pages 220-225). The results obtained by this code are presented for the long cantilever immersed in water in Figure 5.33 and the results for the rest of the fluids and medium cantilever are shown in Appendix N (pages 226-233).

From these figures, it is obvious that the results are very sensitive to the noise and the trend in amplitude and phase responses. Also it was noted that the selection of reference frequency is very critical because it can change the results dramatically. In general, it was observed that the measured density has a smaller error than that the measured viscosity and wherever the amplitude of vibration is small, compared to the whole response, (mainly at low frequencies for medium cantilever and low viscosity fluids) the estimation of the properties has a larger error. Furthermore, the error around the reference frequency was found to be larger than the other parts, which is because of the sensitivity of the approach to the selected value.

At the end of this section it should be mentioned that for these types of experiments there are also three more general sources of error. The first one is the change in the concentration of the solutions over time that was explained in detail in section 5.2. And second, for the calculations of the theoretical model, the movement of free end of the cantilever was accounted, but in practice the laser cannot be exactly aligned at the free

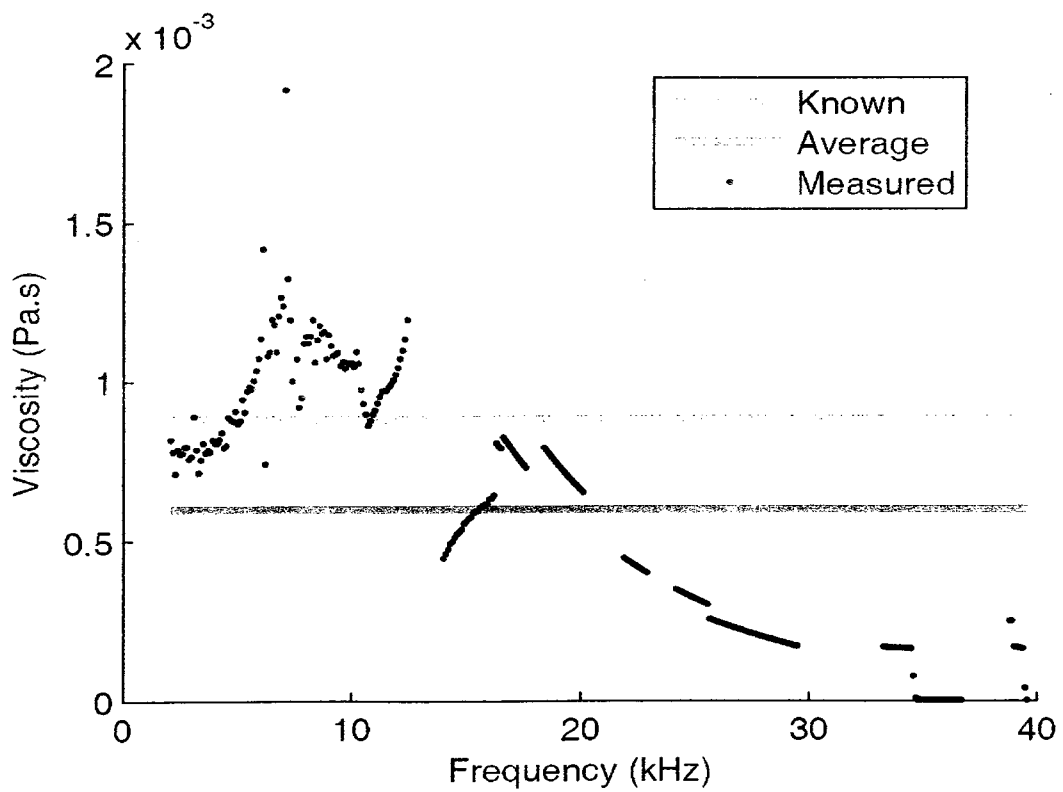
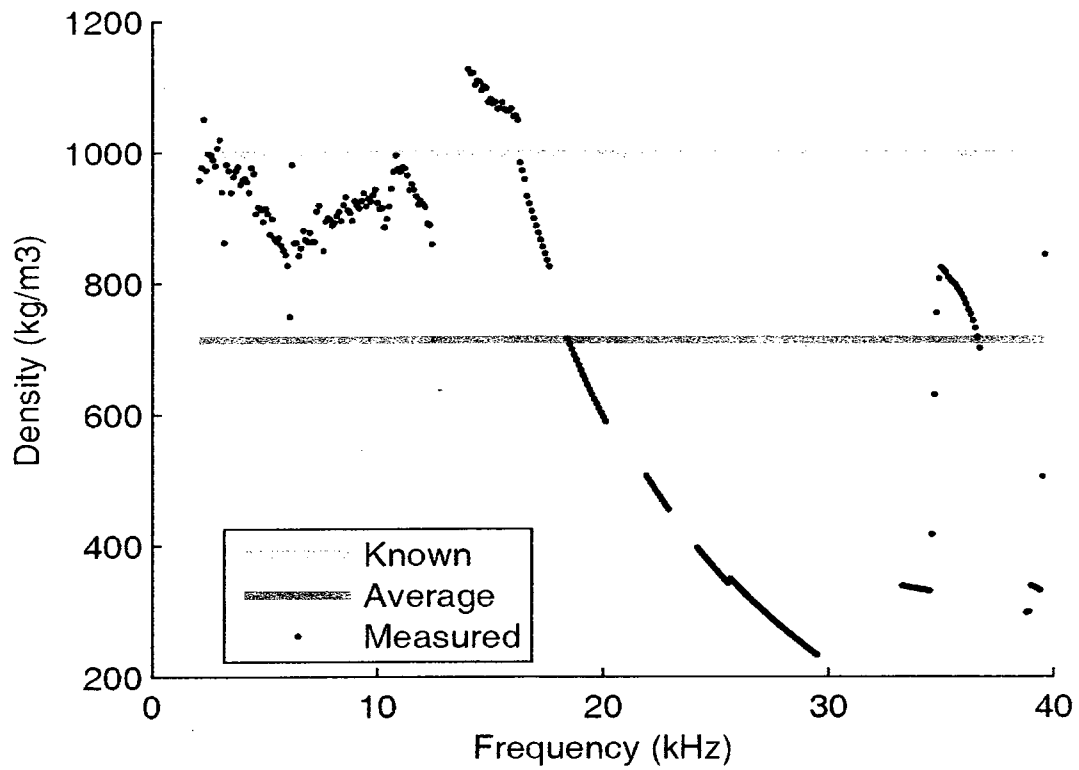


Figure 5.33. Determined properties of water at each frequency of excitation using the long cantilever.

end. As a result, the response of the cantilever at the higher modes, which depends more on the location of the laser (see Figure 5.10), cannot be predicted very well. Also because of the thickness of the laser beam, this error is increased for shorter cantilevers. Finally the third one is related to the uncertainty in estimation of the cantilever thickness using its resonant frequency in air.

5.9) Extending the micro cantilever based rheometry to non-Newtonian fluids

The second approach of the previous section gives the capability of measuring the fluid properties at each frequency of vibration. Such a capability, in spite of not being important for Newtonian fluids, opens a new application for the AFM to measure the properties of non-Newtonian fluids because of the dependency of their properties on the excitation frequency. However to utilize such an application for a non-Newtonian solution, the concentration of the solution should be more than the overlap concentration, C^* , in order to have a uniform fluid and to allow us to measure the bulk properties. Moreover, in the case of the solution concentration being less than C^* , it should be confirmed that the smallest dimension of the cantilever is much larger than the average distance between the polymer chains in the solution, otherwise the measured properties will not represent the bulk properties of the fluid. For the solutions of PS/DEP, diethyl phthalate is considered as a good solvent. However if we assume a theta solvent for the polystyrene, the values of overlap concentration, C^* , and the radius of gyration, R_g , are 0.43 g/mL and 11 nm respectively, which are obtained using the following equation⁷⁰:

$$C^* = \frac{M_w}{N_A R_g^3} = \left[\frac{n^{1/2} l C_\infty^{1/2}}{\sqrt{6}} \right]^{-3} \frac{M_w}{N_A} \quad \text{Equation (5.8)}$$

In the above equation, M_w is the weight averaged molecular weight, N_A is the Avogadro's number, n is the number of monomers in the chain, l is the carbon-carbon bond length and C_∞ is the characteristic ratio. In our study, the calculated value of C^* is greater than the concentration of all PS/DEP solutions used, however based on the calculated R_g , the averaged distance between two chains for the lowest concentration, that is %5 PS/DEP solution, is around 20 nm which is much smaller than the 2 μ m thickness of the cantilever used. Therefore, overly even for a theta solvent, which is associated with higher C^* and smaller R_g compared to a good solvent, we are always on the safe side.

Moving to the experimental results obtained for the non-Newtonian fluids, it should be mentioned that in the cantilever response we can observe that the viscosity decreases as the frequency increases. This is consistent with what was illustrated in the results obtained from the rotational rheometer and presented in chapter 3. For example in Figure 5.34, the responses of the long cantilever, which is immersed in water, %16 PS/DEP solution and pure glycerine, are compared. The zero shear viscosity of the %16 PS/DEP solution is around 6300 mPa.s, which is much higher than the viscosity of pure glycerine, which is around 900 mPa.s. However, as it can be noticed the frequency of the first peak for the %16 PS/DEP solution is more than that of the first peak for pure glycerine and less than that for water. This shows that at this range of frequency the viscosity of the polymer solution is in between the viscosities of water and glycerine, which is expected because the viscosity of this solution varies between 600 and 100 mPa.s, for the

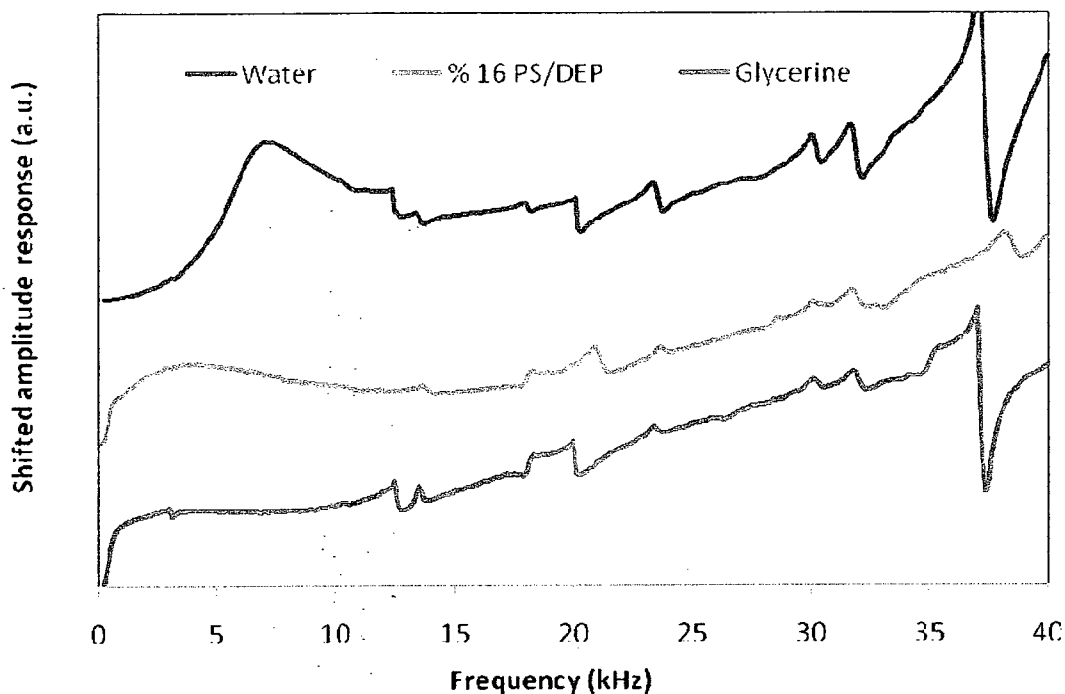


Figure 5.34 The comparison between the frequency sweep responses of the long cantilever immersed in %16 PS/DEP solution as a non-Newtonian fluid and immersed in water and pure glycerine as two Newtonian fluids.

frequency range of 2 to 50 kHz, as shown in Figure 3.10. Also, the decrease of viscosity can be recognized by observing that as the frequency increases the curvature of the cantilever response in the %16 PS/DEP solution becomes similar to the curvature of the cantilever response while immersed in water. Such cantilever behaviour at high frequencies can be explained by knowing that the PS solution behaves as a low viscosity fluid because of its high elastic properties at those frequencies. This allows the fluid to store a part of the cantilever energy when it is moving forward, which in its turn helps in the backward movement of the cantilever by releasing that energy. The experimental results obtained for the rest of non-Newtonian fluids are presented in Appendix O (pages 234-235).

Unfortunately the theory of chapter 2 is not useful for these non-Newtonian fluids for one main reason that is related to the assumptions used for the derivations of hydrodynamic drag force. Indeed, the hydrodynamic force was derived from the Navier-Stokes equations, which are the momentum equations after implementing the Newtonian constitutive equation. Such a constitutive equation generally is not valid for non-Newtonian fluids and as a result the presented theory in chapter 2 is not applicable here. It should be mentioned that basically there is not a general constitutive equation for all non-Newtonian fluids. So far some constitutive equations have been proposed for different kinds of non Newtonian fluids which in most cases have very complicated mathematical formula. As a result, implementing them in the momentum equations and using them for driving the hydrodynamic force most probably will not result in an exact analytical solution. In practice some researchers apply educated assumptions instead of the viscosity term in the equations to make it appropriate for the non Newtonian fluid. However, in most of the cases the equation does not obey the conservation of momentum and if the resultant formula works, it should be considered as an empirical equation. Going further in depth in developing the theory for non Newtonian is considered as the future work of this study, nonetheless we will explain few suggestions as the potential methods for approaching such a problem.

The first suggestion is to use the Generalized Newtonian constitutive equation. In such an equation, the viscosity of the fluid is considered as a function of the strain rate, and based on the Cox-Merz⁷¹ rule this viscosity is equal to viscosity which is a function of frequency and its frequency is equal to the strain rate. Using the obtained results of the rotational rheometer for %16 PS/DEP (see Figure 3.10), we calculated the theoretical

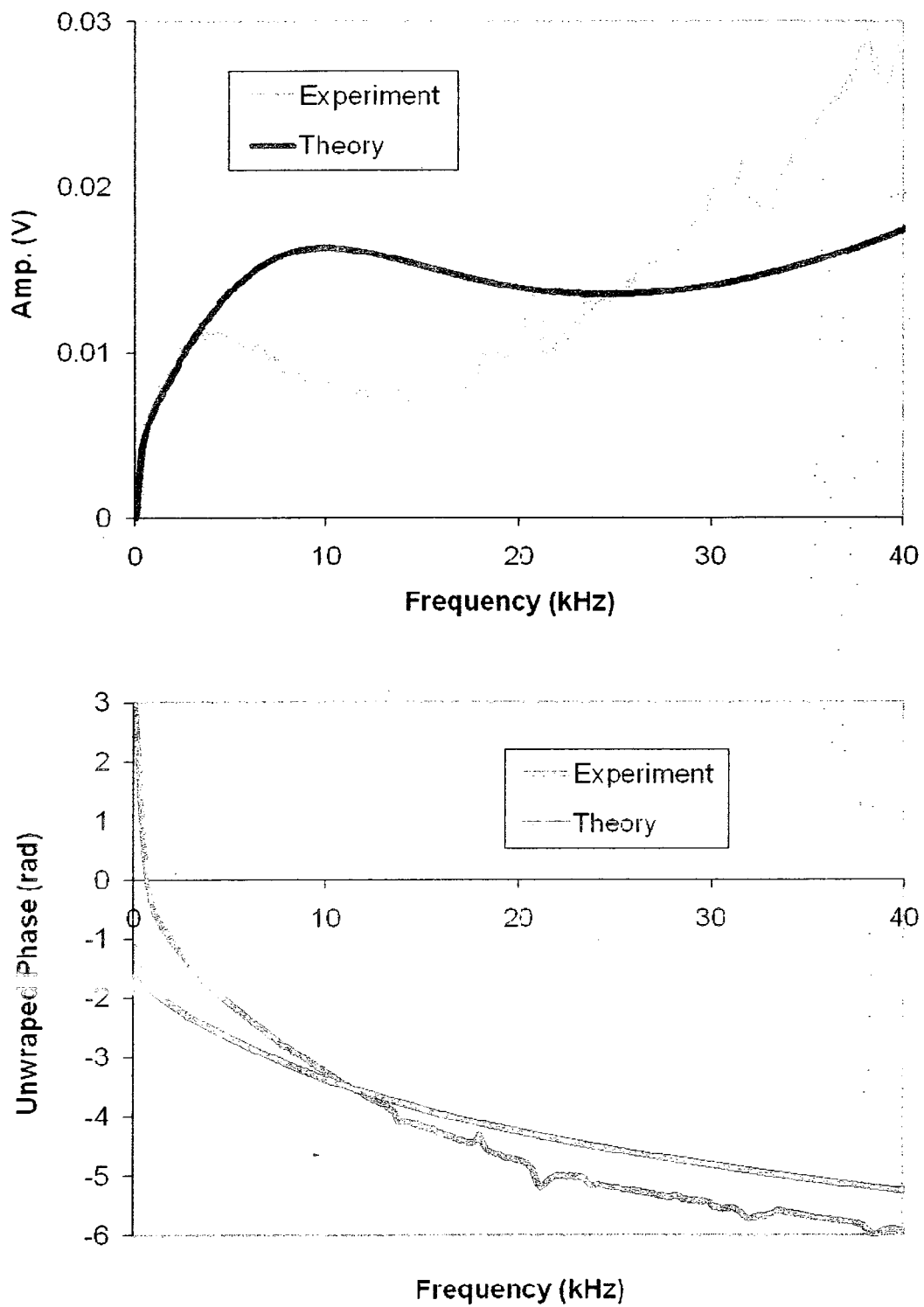


Figure 5.35 The comparison between the theoretical and experimental responses of frequency sweep excitation for the long cantilever immersed in %16 PS/DEP solution.

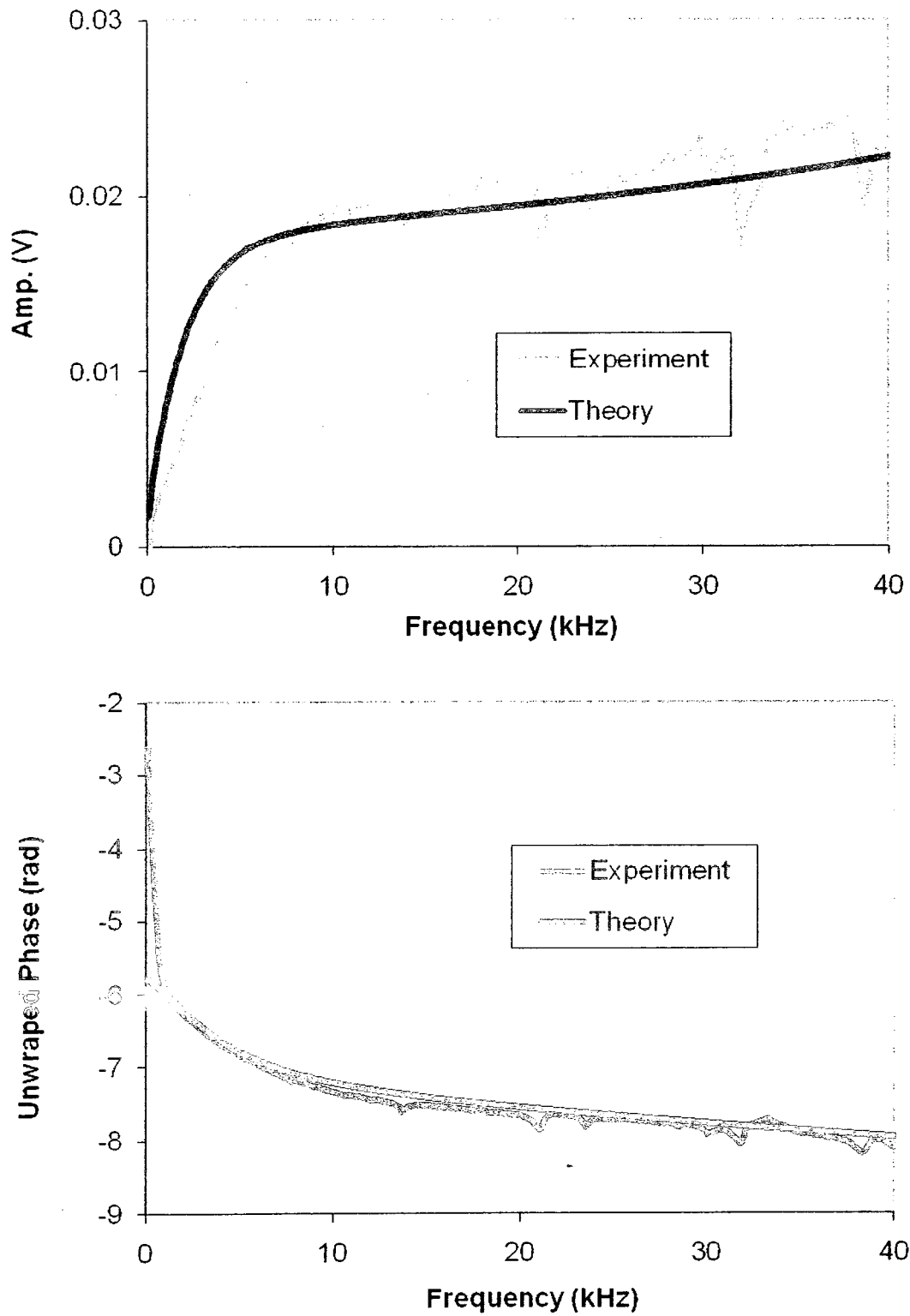


Figure 5.36 The comparison between the theoretical and experimental responses of frequency sweep excitation for the medium cantilever immersed in %16 PS/DEP solution.

responses of both long and medium cantilevers through the implementation of this suggestion. The results are shown in Figures 5.35 and 5.36. Referring to these figures, it can be seen that the theoretical results for the long cantilever showed a big deviation from the experimental results while the medium cantilever showed a surprisingly good agreement between experimental and theoretical results. The deviation that occurred in the results of the long cantilever was mainly due to the fact that the theory does not work very well for the long cantilevers when immersed in high viscous fluids, as explained in section 5.7. However, the agreement in results of the medium cantilever indicates the applicability of such suggestion for non-Newtonian fluids. It should be mentioned that this theory might be improved considerably if we applied a more accurate formula for the hydrodynamic force. Also the confirmation and applicability of this suggestion with the other solutions is left as a future work of this study.

It should be mentioned that the result of implementing this suggestion for extraction of the properties is exactly the same as the second approach of last section with the difference that for Newtonian fluids the average of properties over the frequency range is desired but for non-Newtonian fluids the results at each frequency is required. Moreover it can be assumed that the density of the fluid is known and as a result the amplitude and phase responses can be used separately for the determination of the viscosity. In this case it is expected that the phase response gives the property with less error.

The second suggestion would be to utilize the imaginary shear modulus of $G^* = i\omega\eta^*$, proposed by Belmiloud et al⁵². By substituting this function instead of the viscosity term in the hydrodynamic function and knowing that $G^* = G' + iG''$, we can derive two equations in terms of loss and storage modulus for the amplitude and phase

responses of the cantilever. Now by equalizing them with the experimentally obtained amplitude and phase responses, we can determine the G' and G'' at each frequency, which are the most important properties of non-Newtonian fluids. It should be mentioned that for this method, the density of the fluid should be considered as a constant known value.

Last but not least is to make use of the following hydrodynamic function derived by Frater⁷²:

$$\Gamma_{circ}(\omega) = 1 - \frac{4K_1(\alpha\sqrt{Re})}{K_1(\alpha\sqrt{Re}) + (\alpha\sqrt{Re})K_1'(\alpha\sqrt{Re})} \quad \text{Equation (5.9)}$$

where

$$\alpha^2 = i \left(\frac{1 + i\omega\lambda_1}{1 + i\omega\lambda_2} \right) \quad \text{Equation (5.10)}$$

and the constants of λ_1 and λ_2 are defined in the specific constitutive equation upon which the hydrodynamic function is derived. It should be mentioned that in order to utilize this hydrodynamic function, we must first check that the non-Newtonian fluids, which are to be tested, obey that constitutive equation.

At the end, the advantage of using the micro cantilever rheometer is that we can easily reach to the frequencies that are way beyond the limit of the available conventional rheometers. Moreover, this technique can solve the problem of inertia that we always had at high frequencies with the rotary rheometers. Finally even if the required range of frequency can be obtained by the conventional rheometers using the time-temperature super position principle, measuring the properties with this technique is still much faster. And as a result, more reliable results can be obtained for the cases that the fluid properties change over time.

Chapter 6

Conclusions, contributions and future works

6.1) Conclusions

In this thesis, an investigation has been made concerning the implementation of the atomic force microscope (AFM) for measuring the rheological properties of fluids, mainly liquids of high viscosity. Our analysis was divided into two parts. The first part involved a study of a few critical experimental issues, such as the one related to the fluid cell design. This evolved because the measured response had many unwanted peaks, which are not related to the actual cantilever response. We found that the regular fluid cell, that is widely used and provided commercially by the AFM manufacturers, is of poor quality in design. The main reason for this is that the piezo that is used to generate the displacement in this fluid cell is located on one of the fluid cell legs and in order to have ideal acoustic excitation it should be positioned exactly underneath the cantilever base. If it is not, in the response of the cantilever we will observe the interference of the vibration of the fluid cell with the vibration of the cantilever. There are also some issues of minor importance such as the large moving surface of the fluid cell, which generates a flow that also affects the cantilever response, and the specific design of the holding clip. Based on these draw backs, a regular tip holder, which is originally designed to be used in air, was modified to be suitable for working with liquids. Moreover, a study on two different mechanisms for piezo attachment to regular tip holders was done. It was found

that for the acoustic excitation experiments the tip holder, whose piezo is glued to its body, is suitable. As for the thermal noise experiment, the clamped piezo was found to give the response with the least noise.

In the second part of the thesis, we utilized the modified tip holder to obtain the responses of the different cantilevers in different fluids using thermal noise, frequency sweep and step excitations. The reason that the thermal noise method could not be used for high viscosity liquids is the existence of a noise floor which does not allow for the observation of the cantilever response. However, the frequency sweep and step excitations were offered to overcome this limitation. The theory for the frequency sweep was previously developed but the theory for step excitation was developed in this thesis. Although we showed that both frequency sweep and step excitation could be used for experimenting with high viscosity liquids, we proved that the step excitation theory had an advantage over the frequency sweep theory. This advantage was having an exact solution rather than a truncated series solution like the frequency sweep. We compared the theoretical results with the experimental results and possible experimental and theoretical sources of error were explained. For the theory, the main source of error was the assumption of 2D flow around the cantilever which is violated at the higher modes of vibration which is observed at low frequencies for high viscosity fluids. As for the experimental work, the main source of error was found to be the local heating of the fluid by the laser beam and viscous dissipation.

In addition, two approaches for the extraction of fluid properties from the experimental frequency sweep data were offered. One approach was based on the extraction of the properties from the whole range of frequency and the other one was to

determine these properties at each frequency of excitation. And finally since now we could find the properties of the fluid at each excitation frequency and also since the non-Newtonian fluids have properties that are frequency dependent, we applied this technique for some non-Newtonian fluids. The preliminary results were presented and the potential approaches for extending the AFM cantilever techniques are introduced as the future work.

6.2) Contributions

As a result of our study, there are three main contributions to such a field of work. First we managed to identify the key elements in the fluid cell design. These included the holding mechanism of cantilever chip in the fluid cell, the understanding of the fluid-borne excitation, the supporting of the piezo to the tip holder and most importantly the positioning of the piezo element, which must be directly located underneath of the cantilever. Second, we developed a technique that can be used for extracting the properties of the liquids from the frequency sweep data, which extended the applicability of the micro cantilever based rheometry to higher viscosity Newtonian liquids. We proposed three choices for such an extraction. The first two choices are to extract the properties from the whole frequency range of either the amplitude response or the phase response. And the third choice is to use both the amplitude and phase responses for the determination of the fluid properties at each frequency of excitation. Among the three previously mentioned extraction methods, the determination of properties from the phase response gave the closest results to the real values and therefore it was considered as the

most accurate method. Last but not least, we introduced the step excitation as a new method that can be used to excite the cantilever. We succeeded in producing a theoretical response for the cantilever that is excited acoustically by the step movement of its base. The main advantage for such theoretical analysis was that we have an exact solution for the theoretical response rather than a solution that is in series form and in this way the truncation error is eliminated completely.

6.3) Future work

Most of the intended future work of our study was already mentioned in detail in the text. They are summarized along with some other suggestions, in the following paragraphs.

Primary concerning the fluid cell design, we have to mention that although the main factor of the fluid cell design was determined in this work, still in order to get a very smooth response in the acoustic excitation, a very well designed holder is required so that it considers all the vibrational aspects of the holder. Therefore, the optimization and improvement of such a design to overcome this design limitation can be considered as a future work of our study.

The other topic is related to the inaccuracy of the theoretical models for predicting the cantilever response around its higher mode of vibration, while it is immersed in a Newtonian fluid. This inaccuracy is the result of implementing the 2D flow assumption for the surrounding fluid in the derivation of the hydrodynamic force. However recently, Eysden et al⁴⁷ developed an analytical model for the hydrodynamic force which considers

the axial flow as well. Therefore, implementing such a model in the governing equation of the cantilever deflection and then comparing the obtained results with the experimental response of the cantilever can be considered as the second recommendation for the future work.

Thirdly, in this work, we introduced the step excitation as a better alternative for the frequency sweep excitation. The theory for this type of excitation was developed and the results were compared with the experimental data. However the extraction of the fluid properties from experimental data for this type of excitation was left as a future work.

Last but not least, we proposed to extend the usage of the micro cantilever based rheometry for the non-Newtonian fluids because of the potential advantages that this technique offers in comparison to the traditional rheometers. Preliminary results were obtained for such continuation and some suggestions for developing the required theory were explained in chapter 5.

References

- [1] Binnig, G.; Quate, C.F.; Gerber, C. Atomic force microscope. *Phys. Rev. Lett.* 1986, 56, 930-933.
- [2] Giessibl, J.F. Atomic-resolution of the silicon (111)-(7x7) surface by atomic-force microscopy. *Science* 1995, 267, 68-71.
- [3] Ohnesorge, F.; Binnig, G. True atomic-resolution by atomic force microscopy through repulsive and attractive forces. *Science* 1993, 260, 1451-1456.
- [4] Putman, C.A.J.; Vanderwerf, K.O.; Degrooth, B.G.; Vanhulst, N.F.; Greve, J. Tapping mode atomic-force microscopy in liquid. *Appl. Phys. Lett* 1994, 64, 2454-2456.
- [5] Berger R.; Gerber C.; Lang H.P.; Gimzewski J.K. Micromechanics: A toolbox for femtoscale science: "Towards a laboratory on a tip". *Microelectronic Engineering* 1997, 35, 373-379.
- [6] Boskovic, S.; Chon, J.W.M.; Mulvaney, P.; Sader, J.E. Rheological measurements using microcantilevers. *J. Rheol.* 2002, 46, 891-899.
- [7] Hennemeyer, M.; Burghardt, S.; Stark, R.W. Cantilever micro-rheometer for the characterization of sugar solutions. *Sensors* 2008, 8, 1, 10-22.
- [8] Gannepalli, A.; Sebastian A.; Cleveland, J.; Salapaka, M. Thermally driven non-contact atomic force microscopy. *Appl. Phys. Lett.* 2005, 87, 111901.
- [9] Sader, J.E. Frequency response of cantilever beams immersed in viscous fluids with applications to the atomic force microscope. *J. Appl. Phys.* 1998, 84, 64-76.
- [10] Han, W.H.; Lindsay, S.M.; Jing, T.W. A magnetically driven oscillating probe microscope for operation in liquids. *Appl. Phys. Lett.* 1996, 69, 4111-4113.

- [11] Florin, E.L.; Radmacher, M.; Fleck, B.; Gaub, H.E. Atomic-force microscope with magnetic force modulation. *Rev. Sci. Instrum.* 1994, 65, 639-643.
- [12] Revenko, I.; Proksch, R. Magnetic and acoustic tapping mode microscopy of liquid phase phospholipid bilayers and DNA molecules. *J. Appl. Phys.* 2000, 87, 526-533.
- [13] Scherer, M.P.; Frank, G.; Gummer, A.W. Experimental determination of the mechanical impedance of atomic force microscopy cantilevers in fluids up to 70 kHz. *J. Appl. Phys.* 2000, 88, 2912-2920.
- [14] Degertekin, F.L.; Hadimioglu, B.; Sulchek, T.; Quate, C.F. Actuation and characterization of atomic force microscope cantilevers in fluids by acoustic radiation pressure. *Appl. Phys. Lett* 2001, 78, 1628-1630.
- [15] Buguin, A.; Du Roure, O.; Silberzan, P. Active atomic force microscopy cantilevers for imaging in liquids. *Appl. Phys. Lett.* 2001, 78, 2982-2984.
- [16] Ratcliff, G.C.; Erie, D.A.; Superfine, R. Photothermal modulation for oscillating mode atomic force microscopy in solution. *Appl. Phys. Lett* 1998, 72, 1911-1913.
- [17] Ramos, D.; Tamayo, J.; Mertens, J.; Calleja, M. Photothermal excitation of microcantilevers in liquids. *J. Appl. Phys.* 2006, 99, 124904.
- [18] Volkov, A.O.; Burnell-Gray, J.S.; Datta, P.K. Frequency response of atomic force microscope cantilever driven by fluid. *Appl. Phys. Lett* 2004, 85, 5397-5399.
- [19] Schaffer, T.E.; Cleveland, J.P.; Ohnesorge, F.; Walters, D.A.; Hansma, P.K. Studies of vibrating atomic force microscope cantilevers in liquid. *J. Appl. Phys.* 1996, 80, 3622-3627.

- [20] Kirstein S.; Mertesdorf M.; Schonhoff M. The influence of a viscous fluid on the vibration dynamics of scanning near-field optical microscopy fiber probes and atomic force microscopy cantilevers. *J. Appl. Phys.* 1998, 84, 1782-1790.
- [21] Bergaud C.; Nicu L. Viscosity measurements based on experimental investigations of composite cantilever beam eigenfrequencies in viscous media. *Rev. Sci. Instrum.* 2000, 71, 2487-2491.
- [22] Xu, X.; Raman, A. Comparative dynamics of magnetically, acoustically, and Brownian motion driven microcantilevers in liquids. *J. Appl. Phys.* 2007, 102, 3, 034303.
- [23] Tamayo, J.; Humphris, A.D.L.; Miles, M.J. Piconewton regime dynamic force microscopy in liquid. *Appl. Phys. Lett.* 2000, 77, 582-584.
- [24] Rogers B.; York D.; Whisman N.; Jones M.; Murray K.; Adams J.D.; Sulchek T.; Minne S.C.; Tapping mode atomic force microscopy in liquid with an insulated piezoelectric microactuator. *Rev. Sci. Instrum.* 2002, 73, 3242-3244.
- [25] Digital Instruments, 112 Robin Hill Road, Santa Barbara, CA 93117.
- [26] Weaver, W.; Timoshenko, S.P.; Young, D.H. *Vibration problems in engineering*, John Wiley and Son, New York, 1990.
- [27] Thomson, W.T.; Dahleh, M.D. *Theory of vibration with applications*, Prentice-Hall, New Jersey, 1998.
- [28] Rosenhead, L. *Laminar Boundary Layers*, Clarendon, Oxford, 1963.
- [29] Potter, M.C.; Wiggert, D.C. *Mechanics of Fluids*, Prentice-Hall, London, 1991.
- [30] Landau, L.D.; Lifshitz, E.M. *Fluid Mechanics*, Pergamon, Oxford, 1975.

- [31] Butt H.,J.; Siedle, P.; Seifert, K.; Fendler, K.; Seeger, T.; Bamberg, E.; Weisenhorn, A.L.; Goldie, K.; Engel, A. Scan speed limit in atomic force microscopy. *Journal of Microscopy-Oxford*. 1993,169, Part 1, 75-84.
- [32] Chen, G.Y.; Warmack, R.J.; Thundat, T.; Allison, D.P.; Huang, A. Resonance response of scanning force microscopy cantilevers. *Rev. Sci. Instrum.* 1994, 65, 8, 2532-2537.
- [33] Oden, P.I.; Chen, G.Y.; Steele, R.A.; Warmack, R.J.; Thundat, T. Viscous drag measurements utilizing microfabricated cantilevers. *Appl. Phys. Lett.* 1996, 68, 26, 3814-3816.
- [34] Kokubun, K.; Hirata, M.; Murakami, H.; Toda, Y.; Ono, M. A bending and stretching mode crystal-oscillator as a friction vacuum gauge. *Vacuum*. 1984, 34, 8-9, 731-735.
- [35] Hirai, Y.; Mori, R.; Kikuta, H.; Kato, N.; Inoue, K.; Tanaka, Y. Resonance characteristics of micro cantilever in liquid. *Japanese Journal of Applied Physics Part 1-Regular Papers Short Notes and Review Papers*. 1998, 37, 12B, 7064-7069.
- [36] Salapaka, M.V.; Bergh, H.S.; Lai, J.; Majumdar, A.; McFarland, E. Multi-mode noise analysis of cantilevers for scanning probe microscopy. *J. Appl. Phys.* 1997, 81, 6, 2480-2487.
- [37] Bergaud, C.; Nicu, N.; Martinez, A. Multi-mode air damping analysis of composite cantilever beams. *Japanese Journal of Applied Physics Part 1-Regular Papers Short Notes and Review Papers*. 1999, 38, 11, 6521-6525.

- [38] Blom, F.R.; Bouwstra, S.; Elwenspoek, M.; Fluitman, J.H.J. Dependence of the quality factor of micromachined silicon beam resonators on pressure and geometry. *Journal of Vacuum Science and Technology B*. 1992, 10, 1, 19-26.
- [39] Walters, D.A.; Cleveland, J.P.; Thomson, N.H.; Hansma, P.K.; Wendman, M.A.; Gurley, G.; Elings, V. Short cantilevers for atomic force microscopy. *Rev. Sci. Instrum.* 1996, 67, 10, 3583-3590.
- [40] Hosaka, H.; Itao, K.; Kuroda, S. Damping characteristics of beam-shaped micro-oscillators. *Sensors and Actuators A-Physical*. 1995, 49, 1-2, 87-95.
- [41] Weigert, S.; Dreier, M.; Hegner, M. Frequency shifts of cantilevers vibrating in various media. *Appl. Phys. Lett.* 1996, 69, 19, 2834-2836.
- [42] Elmer, F.J.; Dreier, M. Eigenfrequencies of a rectangular atomic force microscope cantilever in a medium. *J. Appl. Phys.* 1997, 81, 12, 7709-7714
- [43] Maali, A.; Hurth, C.; Boisgard, R.; Jai, C.; Cohen-Bouhacina, T.; Aime, J.P. Hydrodynamics of oscillating atomic force microscopy cantilevers in viscous fluids. *J. Appl. Phys.* 2005, 97, 7, 074907
- [44] Chon, J.W.M.; Mulvaney, P.; Sader J.E. Experimental validation of theoretical models for the frequency response of atomic force microscope cantilever beams immersed in fluids. *J. Appl. Phys.* 2000, 87, 8, 3978-3988.
- [45] Chu, W.H. Tech. Rep. No. 2 DTMB, Contract NObs-86396(X), South-west Research Institute, San Antonio, TX, 1963.
- [46] Green, C.P.; Sader, J.E. Torsional frequency response of cantilever beams immersed in viscous fluids with applications to the atomic force microscope. *J. Appl. Phys.* 2002, 92, 10, 6262-6274

- [47] Van Eysden, C.A.; Sader, J.E. Frequency response of cantilever beams immersed in viscous fluids with applications to the atomic force microscope: Arbitrary mode order. *J. Appl. Phys.* 2007, 101, 4, 044908
- [48] Green, C.P.; Sader, J.E. Frequency response of cantilever beams immersed in viscous fluids near a solid surface with applications to the atomic force microscope. *J. Appl. Phys.* 2005, 98, 11, 114913.
- [49] Jai, C.; Cohen-Bouhacina, T.; Maali, A. Analytical description of the motion of an acoustic-driven atomic force microscope cantilever in liquid. *Appl. Phys. Lett.* 2007, 90, 11, 113512.
- [50] Ahmed, N.; Nino, D.F.; Moy, V.T. Viscous drag measurements utilizing microfabricated cantilevers. *Rev. Sci. Instrum.* 2001, 72, 6, 2731-2734.
- [51] Belmiloud, N.; Dufour, I.; Colin, A.; Nicu, L. Rheological behavior probed by vibrating microcantilevers. *Appl. Phys. Lett.* 2008, 92, 4, 041907.
- [52] Belmiloud, N.; Dufour, I.; Colin, A.; Nicu, L. Vibrating Microcantilevers : Tools for Microrheology, XVth International Congress on Rheology, The Society of Rheology 80th Annual Meeting.
- [53] Lubarsky, G.V.; Hahner, G. Calibration of the normal spring constant of microcantilevers in a parallel fluid flow. *Rev. Sci. Instrum.* 2007, 78, 095102.
- [54] Tortonese, M.; Kirk, M. Characterization of application specific probes for SPMs. *Proc. SPIE* 3009, 53, 1997.
- [55] Sader, J.E.; Chon, J.W.M.; Mulvaney, P. Calibration of rectangular atomic force microscope cantilevers. *Rev. Sci. Instrum.* 1999, 70, 10, 3967-3969.

- [56] Papi, M.; Arcovito, G.; De Spirito, M.; Vassalli, M.; Tiribilli, B. Fluid viscosity determination by means of uncalibrated atomic force microscopy cantilevers. *Appl. Phys. Lett.* 2006, 88, 19, 194102
- [57] Papi, M.; Maulucci, G.; Arcovito, G.; Paoletti, P.; Vassalli, M.; De Spirito, M. Detection of microviscosity by using uncalibrated atomic force microscopy cantilevers. *Appl. Phys. Lett.* 2008, 93, 12, 124102.
- [58] Paul, M.R.; Cross, M.C. Stochastic dynamics of nanoscale mechanical oscillators immersed in a viscous fluid. *Appl. Phys. Lett.* 2004, 92, 23, 235501.
- [59] LabVIEW 8.2, M63X83171, LabVIEW Full Development System, National Instruments.
- [60] Ethanol 99%, Concordia chemical store (Code: C0029).
- [61] Glycerol (Certified ACS), Fisher Chemical (Cat. No. G33-4).
- [62] www.dow.com/glycerine/resources/table18.htm
- [63] www.dow.com/webapps/lit/litorder.asp?filepath=glycerine/pdfs/noreg/115-00656.pdf&pdf=true
- [64] PS 1301, NOVA, Dow Chemical Company.
- [65] Diethyl Phthalate 99%, Fisher Chemical (Cat. No. AC11452-0025, Acros Organics, No.:114520025).
- [66] Methylene Chloride (Stabilized/Certified ACS), Fisher Chemical (Cat. No. D37-4).
- [67] Rheometer Physica MCR 500 (Anton Paar).
- [68] GE Sealants and Adhesives, Huntersville, NC 28078.

- [69] Giacomin, A.J.; Dealy J.M. Large-amplitude oscillatory shear, in *Techniques in rheological measurement*, edited by Collyer, A.A. 99-121, Chapman and Hall, London, 1993.
- [70] Larson, R.G. *The structure and rheology of complex fluids*, Oxford University Press, New York, 1999.
- [71] Cox, W.P.; Merz, E.H. correlation of dynamic and steady flow viscosities. *J. Polym. Sci.* 1958, 28,619-621.
- [72] Frater, K.R. Drag on a circular cylinder oscillating in an elasto-viscous fluid. *Zeitschrift Fur Angewandte Mathematik Und Physik*, 1968, 19, 3, 510.

Appendix A

MATLAB code for the modal shapes and the α and β parameters:

```
=====
clc; clear all; close all;

L=10;
delta_x=0.00001*L; x=[0:delta_x:L];

landa(1)=1.8751/L; landa(2)=4.694/L; landa(3)=7.855/L; landa(4)=10.996/L; landa(5)=14.137/L;
landa(6)=17.279/L;

% deflection %%%
X1=(cos(landa(1)*x)-cosh(landa(1)*x)-
((cos(landa(1)*L)+cosh(landa(1)*L))/(sin(landa(1)*L)+sinh(landa(1)*L)))*(sin(landa(1)*x)-
sinh(landa(1)*x)));
X2=(cos(landa(2)*x)-cosh(landa(2)*x)-
((cos(landa(2)*L)+cosh(landa(2)*L))/(sin(landa(2)*L)+sinh(landa(2)*L)))*(sin(landa(2)*x)-
sinh(landa(2)*x)));
X3=(cos(landa(3)*x)-cosh(landa(3)*x)-
((cos(landa(3)*L)+cosh(landa(3)*L))/(sin(landa(3)*L)+sinh(landa(3)*L)))*(sin(landa(3)*x)-
sinh(landa(3)*x)));
X4=(cos(landa(4)*x)-cosh(landa(4)*x)-
((cos(landa(4)*L)+cosh(landa(4)*L))/(sin(landa(4)*L)+sinh(landa(4)*L)))*(sin(landa(4)*x)-
sinh(landa(4)*x)));
X5=(cos(landa(5)*x)-cosh(landa(5)*x)-
((cos(landa(5)*L)+cosh(landa(5)*L))/(sin(landa(5)*L)+sinh(landa(5)*L)))*(sin(landa(5)*x)-
sinh(landa(5)*x)));
X6=(cos(landa(6)*x)-cosh(landa(6)*x)-
((cos(landa(6)*L)+cosh(landa(6)*L))/(sin(landa(6)*L)+sinh(landa(6)*L)))*(sin(landa(6)*x)-
sinh(landa(6)*x)));

% inclination %%%
X11=landa(1)*((-sin(landa(1)*x)-sinh(landa(1)*x)-
((cos(landa(1)*L)+cosh(landa(1)*L))/(sin(landa(1)*L)+sinh(landa(1)*L)))*(cos(landa(1)*x)-
cosh(landa(1)*x)));
X12=landa(2)*((-sin(landa(2)*x)-sinh(landa(2)*x)-
((cos(landa(2)*L)+cosh(landa(2)*L))/(sin(landa(2)*L)+sinh(landa(2)*L)))*(cos(landa(2)*x)-
cosh(landa(2)*x)));
X13=landa(3)*((-sin(landa(3)*x)-sinh(landa(3)*x)-
((cos(landa(3)*L)+cosh(landa(3)*L))/(sin(landa(3)*L)+sinh(landa(3)*L)))*(cos(landa(3)*x)-
cosh(landa(3)*x)));
X14=landa(4)*((-sin(landa(4)*x)-sinh(landa(4)*x)-
((cos(landa(4)*L)+cosh(landa(4)*L))/(sin(landa(4)*L)+sinh(landa(4)*L)))*(cos(landa(4)*x)-
cosh(landa(4)*x)));
X15=landa(5)*((-sin(landa(5)*x)-sinh(landa(5)*x)-
((cos(landa(5)*L)+cosh(landa(5)*L))/(sin(landa(5)*L)+sinh(landa(5)*L)))*(cos(landa(5)*x)-
cosh(landa(5)*x)));
```

```
X16=landa(6)*((-sin(landa(6)*x)-sinh(landa(6)*x)-
((cos(landa(6)*L)+cosh(landa(6)*L))/(sin(landa(6)*L)+sinh(landa(6)*L)))*(cos(landa(6)*x)-
cosh(landa(6)*x)));
```

```
% normalization
```

```
X11=(X11/X1(length(X1)));
X12=(X12/X2(length(X2)));
X13=(X13/X3(length(X3)));
X14=(X14/X4(length(X4)));
X15=(X15/X5(length(X5)));
X16=(X16/X6(length(X6)));
X1=(X1/X1(length(X1)));
X2=(X2/X2(length(X2)));
X3=(X3/X3(length(X3)));
X4=(X4/X4(length(X4)));
X5=(X5/X5(length(X5)));
X6=(X6/X6(length(X6)));
```

```
% alpha & beta
```

```
alpha(1)=sum(X1.*X1)*delta_x/L; beta(1)=sum(X1)*delta_x/L;
alpha(2)=sum(X2.*X2)*delta_x/L; beta(2)=sum(X2)*delta_x/L;
alpha(3)=sum(X3.*X3)*delta_x/L; beta(3)=sum(X3)*delta_x/L;
alpha(4)=sum(X4.*X4)*delta_x/L; beta(4)=sum(X4)*delta_x/L;
alpha(5)=sum(X5.*X5)*delta_x/L; beta(5)=sum(X5)*delta_x/L;
alpha(6)=sum(X6.*X6)*delta_x/L; beta(6)=sum(X6)*delta_x/L;
```

```
figure; hold on; plot(x,(X1),'-b'); plot(x,(X2),'-g'); plot(x,(X3),'-r');
```

Appendix B

Maple code for detail derivation of hydrodynamic drag force and hydrodynamic function:

```
> restart; ln(e) := 1; nu := mu/rho;
> with(linalg):
```

$$\ln(e) := 1$$

$$v := \frac{\mu}{\rho}$$

```
> V[r@R] := U[0]*e^(I*omega*t)*cos(theta);
> V[theta@R] := -U[0]*e^(I*omega*t)*sin(theta);
> psi[1] := e^(I*omega*t)/r*sin(theta);
> psi[2] := BesselK(1, r*sqrt(I*omega/nu))*e^(I*omega*t)*sin(theta);
```

$$V_{r@R} := U_0 e^{(\omega t I)} \cos(\theta)$$

$$V_{\theta@R} := -U_0 e^{(\omega t I)} \sin(\theta)$$

$$\psi_1 := \frac{e^{(\omega t I)} \sin(\theta)}{r}$$

$$\psi_2 := \text{BesselK}\left(1, r \sqrt{\frac{\omega \rho I}{\mu}}\right) e^{(\omega t I)} \sin(\theta)$$

```
> A := simplify(subs(r=R, det(array([[R*V[r@R], diff(psi[2], theta)], [-V[theta@R], diff(psi[2], r)]])))/det(array([[diff(psi[1], theta), diff(psi[2], theta)], [diff(psi[1], r), diff(psi[2], r)]]])));
```

```
> B := simplify(subs(r=R, det(array([[diff(psi[1], theta), R*V[r@R]], [diff(psi[1], r), -V[theta@R]]])))/det(array([[diff(psi[1], theta), diff(psi[2], theta)], [diff(psi[1], r), diff(psi[2], r)]]])));
```

$$A := \frac{U_0 R \left(R \text{BesselK}\left(0, R \sqrt{\frac{\omega \rho I}{\mu}}\right) \sqrt{\frac{\omega \rho I}{\mu}} + 2 \text{BesselK}\left(1, R \sqrt{\frac{\omega \rho I}{\mu}}\right) \right)}{\text{BesselK}\left(0, R \sqrt{\frac{\omega \rho I}{\mu}}\right) \sqrt{\frac{\omega \rho I}{\mu}}}$$

$$B := -\frac{2 U_0}{\sqrt{\frac{\omega \rho I}{\mu}} \text{BesselK}\left(0, R \sqrt{\frac{\omega \rho I}{\mu}}\right)}$$

> psi:=simplify(A*psi[1]+B*psi[2]);

$$\psi := -U_0 e^{(\omega t)} \sin(\theta) \left(-R^2 \text{BesselK}\left(0, R \sqrt{\frac{\omega \rho I}{\mu}}\right) \sqrt{\frac{\omega \rho I}{\mu}} \right. \\ \left. - 2 R \text{BesselK}\left(1, R \sqrt{\frac{\omega \rho I}{\mu}}\right) + 2 \text{BesselK}\left(1, r \sqrt{\frac{\omega \rho I}{\mu}}\right) r \right) / \left(\right. \\ \left. \text{BesselK}\left(0, R \sqrt{\frac{\omega \rho I}{\mu}}\right) \sqrt{\frac{\omega \rho I}{\mu}} r \right)$$

> V[_r]:=simplify(diff(psi, theta)/r);

> V[_theta]:=simplify(-diff(psi, r));

$$V_{_r} := -U_0 e^{(\omega t)} \cos(\theta) \left(-R^2 \text{BesselK}\left(0, R \sqrt{\frac{\omega \rho I}{\mu}}\right) \sqrt{\frac{\omega \rho I}{\mu}} \right. \\ \left. - 2 R \text{BesselK}\left(1, R \sqrt{\frac{\omega \rho I}{\mu}}\right) + 2 \text{BesselK}\left(1, r \sqrt{\frac{\omega \rho I}{\mu}}\right) r \right) / \left(\right. \\ \left. \text{BesselK}\left(0, R \sqrt{\frac{\omega \rho I}{\mu}}\right) \sqrt{\frac{\omega \rho I}{\mu}} r^2 \right)$$

$$V_{_\theta} := U_0 e^{(\omega t)} \sin(\theta) \sqrt{\frac{\omega \rho I}{\mu}} \left(2 r^2 \sqrt{\frac{\omega \rho I}{\mu}} \text{BesselK}\left(0, r \sqrt{\frac{\omega \rho I}{\mu}}\right) \right. \\ \left. - R^2 \text{BesselK}\left(0, R \sqrt{\frac{\omega \rho I}{\mu}}\right) \sqrt{\frac{\omega \rho I}{\mu}} - 2 R \text{BesselK}\left(1, R \sqrt{\frac{\omega \rho I}{\mu}}\right) \right. \\ \left. + 2 \text{BesselK}\left(1, r \sqrt{\frac{\omega \rho I}{\mu}}\right) r \right) \mu I / \left(r^2 \omega \rho \text{BesselK}\left(0, R \sqrt{\frac{\omega \rho I}{\mu}}\right) \right)$$

> p:=int(rho*(nu*(diff(V[_r], '\$'(r,2))+diff(V[_r],r)/r+diff(V[_r], '\$'(theta,2))/(r^2)-V[_r]/(r^2)-2*diff(V[_theta], theta)/(r^2))-diff(V[_r],t)),r);

$$p := - \left(-\rho U_0 \omega e^{(\omega t)} \cos(\theta) R^2 \text{BesselK}\left(0, R \sqrt{\frac{\omega \rho I}{\mu}}\right) \sqrt{\frac{\omega \rho I}{\mu}} I \right. \\ \left. - 2 I \rho U_0 \omega e^{(\omega t)} \cos(\theta) R \text{BesselK}\left(1, R \sqrt{\frac{\omega \rho I}{\mu}}\right) \right) / \left(\right. \\ \left. \text{BesselK}\left(0, R \sqrt{\frac{\omega \rho I}{\mu}}\right) \sqrt{\frac{\omega \rho I}{\mu}} r \right)$$

> P[_r_r]:=simplify(subs(r=R,-p+2*mu*diff(V[_r],r)));

> P[_r_theta]:=simplify(subs(r=R,mu*(r*diff(V[_theta]/r,r)+diff(V[_r],theta)/r)));

$$P_{_r_r} := -I \rho U_0 \omega e^{(\omega t)} \cos(\theta)$$

$$\left(R \text{BesselK}\left(0, R \sqrt{\frac{\omega \rho I}{\mu}}\right) \sqrt{\frac{\omega \rho I}{\mu}} + 2 \text{BesselK}\left(1, R \sqrt{\frac{\omega \rho I}{\mu}}\right) \right) / \left(\right. \\ \left. \text{BesselK}\left(0, R \sqrt{\frac{\omega \rho I}{\mu}}\right) \sqrt{\frac{\omega \rho I}{\mu}} \right)$$

$$P_{r_theta} := \frac{2 I U_0 e^{(\omega t)} \sin(\theta) \omega \rho \text{BesselK}\left(1, R \sqrt{\frac{\omega \rho I}{\mu}}\right)}{\sqrt{\frac{\omega \rho I}{\mu}} \text{BesselK}\left(0, R \sqrt{\frac{\omega \rho I}{\mu}}\right)}$$

> F:=simplify(R*L*int(P[_r_r]*cos(theta)-P[_r_theta]*sin(theta), theta=0..2*Pi));

$$F := \frac{-I R L \rho U_0 \omega e^{(\omega t)} \pi \left(4 \text{BesselK}\left(1, R \sqrt{\frac{\omega \rho I}{\mu}}\right) + R \text{BesselK}\left(0, R \sqrt{\frac{\omega \rho I}{\mu}}\right) \sqrt{\frac{\omega \rho I}{\mu}} \right)}{\text{BesselK}\left(0, R \sqrt{\frac{\omega \rho I}{\mu}}\right) \sqrt{\frac{\omega \rho I}{\mu}}}$$

> HD[_omega]:=simplify(F/(-I*omega*U[0]*e^(I*omega*t))/(mu/nu*Pi*R^2*L));

$$HD_{-\omega} := \frac{4 \text{BesselK}\left(1, R \sqrt{\frac{\omega \rho I}{\mu}}\right) + R \text{BesselK}\left(0, R \sqrt{\frac{\omega \rho I}{\mu}}\right) \sqrt{\frac{\omega \rho I}{\mu}}}{R \text{BesselK}\left(0, R \sqrt{\frac{\omega \rho I}{\mu}}\right) \sqrt{\frac{\omega \rho I}{\mu}}}$$

Appendix C

MATLAB code for producing the theoretical response of the thermal excitation:

```
=====
clc; clear all; close all;

% cantilever properties %%%%%%%%%%
L=400e-6;
b=30e-6;
h=2e-6;
A=b*h; I=b*h^3/12;
ro_c=2330;
E=170e9;

% fluid properties %%%%%%%%%%
ro_f=997;
eta_f=0.8628e-3;

% mode shapes and related parameters %%%%%%%%%%
delta_x=0.00001*L; x=[0:delta_x:L];

landa(1)=1.8751/L; landa(2)=4.694/L; landa(3)=7.855/L; landa(4)=10.996/L;

X1=(cos(landa(1)*x)-cosh(landa(1)*x)-
((cos(landa(1)*L)+cosh(landa(1)*L))/(sin(landa(1)*L)+sinh(landa(1)*L)))*(sin(landa(1)*x)-
sinh(landa(1)*x)));
X2=(cos(landa(2)*x)-cosh(landa(2)*x)-
((cos(landa(2)*L)+cosh(landa(2)*L))/(sin(landa(2)*L)+sinh(landa(2)*L)))*(sin(landa(2)*x)-
sinh(landa(2)*x)));
X3=(cos(landa(3)*x)-cosh(landa(3)*x)-
((cos(landa(3)*L)+cosh(landa(3)*L))/(sin(landa(3)*L)+sinh(landa(3)*L)))*(sin(landa(3)*x)-
sinh(landa(3)*x)));
X4=(cos(landa(4)*x)-cosh(landa(4)*x)-
((cos(landa(4)*L)+cosh(landa(4)*L))/(sin(landa(4)*L)+sinh(landa(4)*L)))*(sin(landa(4)*x)-
sinh(landa(4)*x)));

X11=landa(1)*((-sin(landa(1)*x)-sinh(landa(1)*x)-
((cos(landa(1)*L)+cosh(landa(1)*L))/(sin(landa(1)*L)+sinh(landa(1)*L)))*(cos(landa(1)*x)-
cosh(landa(1)*x)));
X12=landa(2)*((-sin(landa(2)*x)-sinh(landa(2)*x)-
((cos(landa(2)*L)+cosh(landa(2)*L))/(sin(landa(2)*L)+sinh(landa(2)*L)))*(cos(landa(2)*x)-
cosh(landa(2)*x)));
X13=landa(3)*((-sin(landa(3)*x)-sinh(landa(3)*x)-
((cos(landa(3)*L)+cosh(landa(3)*L))/(sin(landa(3)*L)+sinh(landa(3)*L)))*(cos(landa(3)*x)-
cosh(landa(3)*x)));
X14=landa(4)*((-sin(landa(4)*x)-sinh(landa(4)*x)-
((cos(landa(4)*L)+cosh(landa(4)*L))/(sin(landa(4)*L)+sinh(landa(4)*L)))*(cos(landa(4)*x)-
cosh(landa(4)*x)));
```

```

X11=(X11/X1(length(X1)));
X12=(X12/X2(length(X2)));
X13=(X13/X3(length(X3)));
X14=(X14/X4(length(X4)));
X1=(X1/X1(length(X1)));
X2=(X2/X2(length(X2)));
X3=(X3/X3(length(X3)));
X4=(X4/X4(length(X4)));

alpha(1)=sum(X1.*X1)*delta_x/L; beta(1)=sum(X1)*delta_x/L;
alpha(2)=sum(X2.*X2)*delta_x/L; beta(2)=sum(X2)*delta_x/L;
alpha(3)=sum(X3.*X3)*delta_x/L; beta(3)=sum(X3)*delta_x/L;
alpha(4)=sum(X4.*X4)*delta_x/L; beta(4)=sum(X4)*delta_x/L;

% theoretical response of thermal noise %%%
f=[0.01:0.01:60];
omega=2*pi*f*1000;

Re = @(X) ro_f*X*b^2/4/eta_f;
GAMA_circ = @(X)1+(4*i*besselk(1,-i*sqrt(i*Re(X))))./(sqrt(i*Re(X)).*besselk(0,-i*sqrt(i*Re(X))));
tao = @(X)log10(Re(X));
OMEGA_r = @(X)(0.91324-0.48274*(tao(X))+0.46842*(tao(X)).^2-
0.12886*(tao(X)).^3+0.044055*(tao(X)).^4-0.0035117*(tao(X)).^5+0.00069085*(tao(X)).^6)/(1-
0.56964*(tao(X))+0.48690*(tao(X)).^2-0.13444*(tao(X)).^3+0.045155*(tao(X)).^4-
0.0035862*(tao(X)).^5+0.00069085*(tao(X)).^6);
OMEGA_i = @(X)(-0.024134-0.029256*(tao(X))+0.016294*(tao(X)).^2-
0.00010961*(tao(X)).^3+0.000064577*(tao(X)).^4-0.000044510*(tao(X)).^5)/(1-
0.597020*(tao(X))+0.551820*(tao(X)).^2-0.18357000*(tao(X)).^3+0.079156000*(tao(X)).^4-
0.014369000*(tao(X)).^5+0.0028361*(tao(X)).^6);
OMEGA = @(X)OMEGA_r(X) + OMEGA_i(X)*i;
GAMA_rect = @(X)OMEGA(X) .* GAMA_circ(X);

THE1=(4*(pi/4*ro_f*b^2*(omega).*imag(GAMA_rect(omega)))*beta(1)*L)./(E*I*(landa(1))^4*alpha(1)
*L-(omega.^2).*(ro_c*A+pi/4*ro_f*b^2*GAMA_rect(omega))*alpha(1)*L);
THE2=(4*(pi/4*ro_f*b^2*(omega).*imag(GAMA_rect(omega)))*beta(2)*L)./(E*I*(landa(2))^4*alpha(2)
*L-(omega.^2).*(ro_c*A+pi/4*ro_f*b^2*GAMA_rect(omega))*alpha(2)*L);
THE3=(4*(pi/4*ro_f*b^2*(omega).*imag(GAMA_rect(omega)))*beta(3)*L)./(E*I*(landa(3))^4*alpha(3)
*L-(omega.^2).*(ro_c*A+pi/4*ro_f*b^2*GAMA_rect(omega))*alpha(3)*L);
THE4=(4*(pi/4*ro_f*b^2*(omega).*imag(GAMA_rect(omega)))*beta(4)*L)./(E*I*(landa(4))^4*alpha(4)
*L-(omega.^2).*(ro_c*A+pi/4*ro_f*b^2*GAMA_rect(omega))*alpha(4)*L);

THE_response=[(abs(THE1*X11(length(X11))+THE2*X12(length(X12))+THE3*X13(length(X13))+THE
4*X14(length(X14))))];
figure; plot(f,THE_response,'-r');

```

Appendix D

MATLAB code for producing the theoretical response of the frequency sweep excitation:

```
=====
clc; clear all; close all;

% cantilever properties %%%%%%%%%%
L=400e-6;
b=30e-6;
h=2e-6;

A=b*h; I=b*h^3/12;
ro_c=2330;
E=170e9;
% fluid properties %%%%%%%%%%
ro_f=997;
eta_f=0.8628e-3;

% mode shapes and related parameters %%%%%%%%%%
delta_x=0.00001*L; x=[0:delta_x:L];

landa(1)=1.8751/L; landa(2)=4.694/L; landa(3)=7.855/L; landa(4)=10.996/L;

X1=(cos(landa(1)*x)-cosh(landa(1)*x)-
((cos(landa(1)*L)+cosh(landa(1)*L))/(sin(landa(1)*L)+sinh(landa(1)*L)))*(sin(landa(1)*x)-
sinh(landa(1)*x)));
X2=(cos(landa(2)*x)-cosh(landa(2)*x)-
((cos(landa(2)*L)+cosh(landa(2)*L))/(sin(landa(2)*L)+sinh(landa(2)*L)))*(sin(landa(2)*x)-
sinh(landa(2)*x)));
X3=(cos(landa(3)*x)-cosh(landa(3)*x)-
((cos(landa(3)*L)+cosh(landa(3)*L))/(sin(landa(3)*L)+sinh(landa(3)*L)))*(sin(landa(3)*x)-
sinh(landa(3)*x)));
X4=(cos(landa(4)*x)-cosh(landa(4)*x)-
((cos(landa(4)*L)+cosh(landa(4)*L))/(sin(landa(4)*L)+sinh(landa(4)*L)))*(sin(landa(4)*x)-
sinh(landa(4)*x)));

X11=landa(1)*((-sin(landa(1)*x)-sinh(landa(1)*x)-
((cos(landa(1)*L)+cosh(landa(1)*L))/(sin(landa(1)*L)+sinh(landa(1)*L)))*(cos(landa(1)*x)-
cosh(landa(1)*x)));
X12=landa(2)*((-sin(landa(2)*x)-sinh(landa(2)*x)-
((cos(landa(2)*L)+cosh(landa(2)*L))/(sin(landa(2)*L)+sinh(landa(2)*L)))*(cos(landa(2)*x)-
cosh(landa(2)*x)));
X13=landa(3)*((-sin(landa(3)*x)-sinh(landa(3)*x)-
((cos(landa(3)*L)+cosh(landa(3)*L))/(sin(landa(3)*L)+sinh(landa(3)*L)))*(cos(landa(3)*x)-
cosh(landa(3)*x)));
X14=landa(4)*((-sin(landa(4)*x)-sinh(landa(4)*x)-
((cos(landa(4)*L)+cosh(landa(4)*L))/(sin(landa(4)*L)+sinh(landa(4)*L)))*(cos(landa(4)*x)-
cosh(landa(4)*x)));
```

```

X11=(X11/X1(length(X1)));
X12=(X12/X2(length(X2)));
X13=(X13/X3(length(X3)));
X14=(X14/X4(length(X4)));
X1=(X1/X1(length(X1)));
X2=(X2/X2(length(X2)));
X3=(X3/X3(length(X3)));
X4=(X4/X4(length(X4)));

alpha(1)=sum(X1.*X1)*delta_x/L; beta(1)=sum(X1)*delta_x/L;
alpha(2)=sum(X2.*X2)*delta_x/L; beta(2)=sum(X2)*delta_x/L;
alpha(3)=sum(X3.*X3)*delta_x/L; beta(3)=sum(X3)*delta_x/L;
alpha(4)=sum(X4.*X4)*delta_x/L; beta(4)=sum(X4)*delta_x/L;

% theoretical response of frequency sweep %%%
f=[0.01:0.01:60];
omega=2*pi*f*1000;

Re = @(X) ro_f*X*b^2/4/eta_f;
GAMA_circ = @(X)1+(4*i*besselk(1,-i*sqrt(i*Re(X))))./(sqrt(i*Re(X)).*besselk(0,-i*sqrt(i*Re(X))));
tao = @(X)log10(Re(X));
OMEGA_r = @(X)(0.91324-0.48274*(tao(X))+0.46842*(tao(X)).^2-
0.12886*(tao(X)).^3+0.044055*(tao(X)).^4-0.0035117*(tao(X)).^5+0.00069085*(tao(X)).^6)/(1-
0.56964*(tao(X))+0.48690*(tao(X)).^2-0.13444*(tao(X)).^3+0.045155*(tao(X)).^4-
0.0035862*(tao(X)).^5+0.00069085*(tao(X)).^6);
OMEGA_i = @(X)(-0.024134-0.029256*(tao(X))+0.016294*(tao(X)).^2-
0.00010961*(tao(X)).^3+0.000064577*(tao(X)).^4-0.000044510*(tao(X)).^5)/(1-
0.597020*(tao(X))+0.551820*(tao(X)).^2-0.18357000*(tao(X)).^3+0.079156000*(tao(X)).^4-
0.014369000*(tao(X)).^5+0.0028361*(tao(X)).^6);
OMEGA = @(X)OMEGA_r(X) + OMEGA_i(X)*i;
GAMA_rect = @(X)OMEGA(X) .* GAMA_circ(X);

ACO1=((omega.^2).*(ro_c*A+pi/4*ro_f*b^2*GAMA_rect(omega))*beta(1)*L)./(E*I*(landa(1))^4*alpha(
1)*L-(omega.^2).*(ro_c*A+pi/4*ro_f*b^2*GAMA_rect(omega))*alpha(1)*L);
ACO2=((omega.^2).*(ro_c*A+pi/4*ro_f*b^2*GAMA_rect(omega))*beta(2)*L)./(E*I*(landa(2))^4*alpha(
2)*L-(omega.^2).*(ro_c*A+pi/4*ro_f*b^2*GAMA_rect(omega))*alpha(2)*L);
ACO3=((omega.^2).*(ro_c*A+pi/4*ro_f*b^2*GAMA_rect(omega))*beta(3)*L)./(E*I*(landa(3))^4*alpha(
3)*L-(omega.^2).*(ro_c*A+pi/4*ro_f*b^2*GAMA_rect(omega))*alpha(3)*L);
ACO4=((omega.^2).*(ro_c*A+pi/4*ro_f*b^2*GAMA_rect(omega))*beta(4)*L)./(E*I*(landa(4))^4*alpha(
4)*L-(omega.^2).*(ro_c*A+pi/4*ro_f*b^2*GAMA_rect(omega))*alpha(4)*L);

ACO_response=[(abs(ACO1*X11(length(X11))+ACO2*X12(length(X12))+ACO3*X13(length(X13))+A
CO4*X14(length(X14))))];
figure; plot(f,ACO_response,'-r');

```

Appendix E

MATLAB code for producing the theoretical response of a cantilever to step excitation and also for finding the damped resonant frequency and decaying coefficient:

```
=====
clc; clear all; %close all;

% cantilever properties %%%%%%%%%%%
cantilever='long'; cantilever_N=1;
L=400e-6;
b=30e-6;
h=2e-6;

A=b*h; I=b*h^3/12;
ro_c=2330;
E=170e9;
w_vac=(1.8751/L)^2*sqrt(E*I/ro_c/A);
% fluid properties %%%%%%%%%%%
ro_f=997;
eta_f=0.8628e-3;
%#####
%##### Non-inertial reference frame #####
%#####
% mode shapes and related parameters %%%%%%%%%%%
delta_x=0.00001*L; x=[0:delta_x:L];

landa(1)=1.8751/L;      landa(2)=4.694/L;      landa(3)=7.855/L;
landa(4)=10.996/L;     landa(5)=14.137/L;     landa(6)=17.279/L;
landa(7)=(7-0.5)*pi/L; landa(8)=(8-0.5)*pi/L; landa(9)=(9-0.5)*pi/L;
landa(10)=(10-0.5)*pi/L; landa(11)=(11-0.5)*pi/L; landa(12)=(12-
0.5)*pi/L;

X1=(cos(landa(1)*x)-cosh(landa(1)*x)-
((cos(landa(1)*L)+cosh(landa(1)*L))/(sin(landa(1)*L)+sinh(landa(1)*L)))
*(sin(landa(1)*x)-sinh(landa(1)*x));
X2=(cos(landa(2)*x)-cosh(landa(2)*x)-
((cos(landa(2)*L)+cosh(landa(2)*L))/(sin(landa(2)*L)+sinh(landa(2)*L)))
*(sin(landa(2)*x)-sinh(landa(2)*x));
X3=(cos(landa(3)*x)-cosh(landa(3)*x)-
((cos(landa(3)*L)+cosh(landa(3)*L))/(sin(landa(3)*L)+sinh(landa(3)*L)))
*(sin(landa(3)*x)-sinh(landa(3)*x));
X4=(cos(landa(4)*x)-cosh(landa(4)*x)-
((cos(landa(4)*L)+cosh(landa(4)*L))/(sin(landa(4)*L)+sinh(landa(4)*L)))
*(sin(landa(4)*x)-sinh(landa(4)*x));
X5=(cos(landa(5)*x)-cosh(landa(5)*x)-
((cos(landa(5)*L)+cosh(landa(5)*L))/(sin(landa(5)*L)+sinh(landa(5)*L)))
*(sin(landa(5)*x)-sinh(landa(5)*x));
```

```

X6=(cos(landa(6)*x)-cosh(landa(6)*x)-
((cos(landa(6)*L)+cosh(landa(6)*L))/(sin(landa(6)*L)+sinh(landa(6)*L)))
*(sin(landa(6)*x)-sinh(landa(6)*x)));
X7=(cos(landa(7)*x)-cosh(landa(7)*x)-
((cos(landa(7)*L)+cosh(landa(7)*L))/(sin(landa(7)*L)+sinh(landa(7)*L)))
*(sin(landa(7)*x)-sinh(landa(7)*x)));
X8=(cos(landa(8)*x)-cosh(landa(8)*x)-
((cos(landa(8)*L)+cosh(landa(8)*L))/(sin(landa(8)*L)+sinh(landa(8)*L)))
*(sin(landa(8)*x)-sinh(landa(8)*x)));
X9=(cos(landa(9)*x)-cosh(landa(9)*x)-
((cos(landa(9)*L)+cosh(landa(9)*L))/(sin(landa(9)*L)+sinh(landa(9)*L)))
*(sin(landa(9)*x)-sinh(landa(9)*x)));

X11=landa(1)*((-sin(landa(1)*x)-sinh(landa(1)*x)-
((cos(landa(1)*L)+cosh(landa(1)*L))/(sin(landa(1)*L)+sinh(landa(1)*L)))
*(cos(landa(1)*x)-cosh(landa(1)*x))));
X12=landa(2)*((-sin(landa(2)*x)-sinh(landa(2)*x)-
((cos(landa(2)*L)+cosh(landa(2)*L))/(sin(landa(2)*L)+sinh(landa(2)*L)))
*(cos(landa(2)*x)-cosh(landa(2)*x))));
X13=landa(3)*((-sin(landa(3)*x)-sinh(landa(3)*x)-
((cos(landa(3)*L)+cosh(landa(3)*L))/(sin(landa(3)*L)+sinh(landa(3)*L)))
*(cos(landa(3)*x)-cosh(landa(3)*x))));
X14=landa(4)*((-sin(landa(4)*x)-sinh(landa(4)*x)-
((cos(landa(4)*L)+cosh(landa(4)*L))/(sin(landa(4)*L)+sinh(landa(4)*L)))
*(cos(landa(4)*x)-cosh(landa(4)*x))));
X15=landa(5)*((-sin(landa(5)*x)-sinh(landa(5)*x)-
((cos(landa(5)*L)+cosh(landa(5)*L))/(sin(landa(5)*L)+sinh(landa(5)*L)))
*(cos(landa(5)*x)-cosh(landa(5)*x))));
X16=landa(6)*((-sin(landa(6)*x)-sinh(landa(6)*x)-
((cos(landa(6)*L)+cosh(landa(6)*L))/(sin(landa(6)*L)+sinh(landa(6)*L)))
*(cos(landa(6)*x)-cosh(landa(6)*x))));
X17=landa(7)*((-sin(landa(7)*x)-sinh(landa(7)*x)-
((cos(landa(7)*L)+cosh(landa(7)*L))/(sin(landa(7)*L)+sinh(landa(7)*L)))
*(cos(landa(7)*x)-cosh(landa(7)*x))));
X18=landa(8)*((-sin(landa(8)*x)-sinh(landa(8)*x)-
((cos(landa(8)*L)+cosh(landa(8)*L))/(sin(landa(8)*L)+sinh(landa(8)*L)))
*(cos(landa(8)*x)-cosh(landa(8)*x))));
X19=landa(9)*((-sin(landa(9)*x)-sinh(landa(9)*x)-
((cos(landa(9)*L)+cosh(landa(9)*L))/(sin(landa(9)*L)+sinh(landa(9)*L)))
*(cos(landa(9)*x)-cosh(landa(9)*x))));

X11=(X11/X1(length(X1)));
X12=(X12/X2(length(X2)));
X13=(X13/X3(length(X3)));
X14=(X14/X4(length(X4)));
X15=(X15/X5(length(X5)));
X16=(X16/X6(length(X6)));
X17=(X17/X7(length(X7)));
X18=(X18/X8(length(X8)));
X19=(X19/X9(length(X9)));
X1=(X1/X1(length(X1)));
X2=(X2/X2(length(X2)));
X3=(X3/X3(length(X3)));
X4=(X4/X4(length(X4)));
X5=(X5/X5(length(X5)));
X6=(X6/X6(length(X6)));
X7=(X7/X7(length(X7)));

```



```

X8=(X8/X8(length(X8)));
X9=(X9/X9(length(X9)));

alpha(1)=sum(X1.*X1)*delta_x/L; beta(1)=sum(X1)*delta_x/L;
alpha(2)=sum(X2.*X2)*delta_x/L; beta(2)=sum(X2)*delta_x/L;
alpha(3)=sum(X3.*X3)*delta_x/L; beta(3)=sum(X3)*delta_x/L;
alpha(4)=sum(X4.*X4)*delta_x/L; beta(4)=sum(X4)*delta_x/L;
alpha(5)=sum(X5.*X5)*delta_x/L; beta(5)=sum(X5)*delta_x/L;
alpha(6)=sum(X6.*X6)*delta_x/L; beta(6)=sum(X6)*delta_x/L;
alpha(7)=sum(X7.*X7)*delta_x/L; beta(7)=sum(X7)*delta_x/L;
alpha(8)=sum(X8.*X8)*delta_x/L; beta(8)=sum(X8)*delta_x/L;
alpha(9)=sum(X9.*X9)*delta_x/L; beta(9)=sum(X9)*delta_x/L;

clear X1 X2 X3 X4 X5 X6 X7 X8 X9;
% theoretical response of frequency sweep %%%%%%%%%%%
f=[0.01:0.01:500];
omega=2*pi*f*1000;

Re = @(X) ro_f*X*b^2/4/eta_f;
GAMA_circ = @(X) 1+(4*i*besselk(1,(-i*sqrt(i*Re(X)))))/(sqrt(i*Re(X)).*besselk(0,(-i*sqrt(i*Re(X)))));
tao = @(X) log10(Re(X));
OMEGA_r = @(X) (0.91324-0.48274*(tao(X))+0.46842*(tao(X)).^2-
0.12886*(tao(X)).^3+0.044055*(tao(X)).^4-
0.0035117*(tao(X)).^5+0.00069085*(tao(X)).^6)/(1-
0.56964*(tao(X))+0.48690*(tao(X)).^2-
0.13444*(tao(X)).^3+0.045155*(tao(X)).^4-
0.0035862*(tao(X)).^5+0.00069085*(tao(X)).^6);
OMEGA_i = @(X) (-0.024134-0.029256*(tao(X))+0.016294*(tao(X)).^2-
0.00010961*(tao(X)).^3+0.000064577*(tao(X)).^4-
0.000044510*(tao(X)).^5)/(1-0.597020*(tao(X))+0.551820*(tao(X)).^2-
0.18357000*(tao(X)).^3+0.079156000*(tao(X)).^4-
0.014369000*(tao(X)).^5+0.0028361*(tao(X)).^6);
OMEGA = @(X) OMEGA_r(X) + OMEGA_i(X)*i;
GAMA_rect = @(X) OMEGA(X) .* GAMA_circ(X);

ACO1=((omega.^2).*(ro_c*A+pi/4*ro_f*b^2*GAMA_rect(omega))*beta(1)*L)/((
E*I*(landa(1))^4*alpha(1)*L-
(omega.^2).*(ro_c*A+pi/4*ro_f*b^2*GAMA_rect(omega))*alpha(1)*L);
ACO2=((omega.^2).*(ro_c*A+pi/4*ro_f*b^2*GAMA_rect(omega))*beta(2)*L)/((
E*I*(landa(2))^4*alpha(2)*L-
(omega.^2).*(ro_c*A+pi/4*ro_f*b^2*GAMA_rect(omega))*alpha(2)*L);
ACO3=((omega.^2).*(ro_c*A+pi/4*ro_f*b^2*GAMA_rect(omega))*beta(3)*L)/((
E*I*(landa(3))^4*alpha(3)*L-
(omega.^2).*(ro_c*A+pi/4*ro_f*b^2*GAMA_rect(omega))*alpha(3)*L);
ACO4=((omega.^2).*(ro_c*A+pi/4*ro_f*b^2*GAMA_rect(omega))*beta(4)*L)/((
E*I*(landa(4))^4*alpha(4)*L-
(omega.^2).*(ro_c*A+pi/4*ro_f*b^2*GAMA_rect(omega))*alpha(4)*L);
ACO5=((omega.^2).*(ro_c*A+pi/4*ro_f*b^2*GAMA_rect(omega))*beta(5)*L)/((
E*I*(landa(5))^4*alpha(5)*L-
(omega.^2).*(ro_c*A+pi/4*ro_f*b^2*GAMA_rect(omega))*alpha(5)*L);
ACO6=((omega.^2).*(ro_c*A+pi/4*ro_f*b^2*GAMA_rect(omega))*beta(6)*L)/((
E*I*(landa(6))^4*alpha(6)*L-
(omega.^2).*(ro_c*A+pi/4*ro_f*b^2*GAMA_rect(omega))*alpha(6)*L);
ACO7=((omega.^2).*(ro_c*A+pi/4*ro_f*b^2*GAMA_rect(omega))*beta(7)*L)/((
E*I*(landa(7))^4*alpha(7)*L-
(omega.^2).*(ro_c*A+pi/4*ro_f*b^2*GAMA_rect(omega))*alpha(7)*L);

```

```

ACO8=((omega.^2).*(ro_c*A+pi/4*ro_f*b^2*GAMA_rect(omega))*beta(8)*L)./(
E*I*(landa(8))^4*alpha(8)*L-
(omega.^2).*(ro_c*A+pi/4*ro_f*b^2*GAMA_rect(omega))*alpha(8)*L);
ACO9=((omega.^2).*(ro_c*A+pi/4*ro_f*b^2*GAMA_rect(omega))*beta(9)*L)./(
E*I*(landa(9))^4*alpha(9)*L-
(omega.^2).*(ro_c*A+pi/4*ro_f*b^2*GAMA_rect(omega))*alpha(9)*L);
ACO_response9=[(-
i./omega).*(ACO1*X11(length(X11))+ACO2*X12(length(X12))+ACO3*X13(length
(X13))+ACO4*X14(length(X14))+ACO5*X15(length(X15))+ACO6*X16(length(X16)
)+ACO7*X17(length(X17))+ACO8*X18(length(X18))+ACO9*X19(length(X19)))]';

for ppp=1:length(ACO_response9)
    YY_x_omega(ppp,1)=ACO_response9(ppp);
    YY_x_omega(2*length(ACO_response9)-ppp+1,1)=ACO_response9(ppp);
end

y_x_time=ifft(YY_x_omega);

t=[1e-6:1e-6:0.1]';

figure;
subplot(2,1,1); plot(f,abs(ACO_response9),'k'); xlabel('Frequency
(kHz)'); ylabel('Amplitude');
subplot(2,1,2); plot(t,real(y_x_time),'k'); xlabel('time (s)');
ylabel('Amplitude');
%#####
%##### Inertial reference frame #####
%#####
landa(1)=1.8751/L;

f=[0.01:0.01:500]; omega=2*pi*f*1000;

Re = @(X) ro_f*X*b^2/4/eta_f;
GAMA_circ = @(X)1+(4*i*besselk(1,(-
i*sqrt(i*Re(X)))))./(sqrt(i*Re(X)).*besselk(0,(-i*sqrt(i*Re(X)))));
tao = @(X) log10(Re(X));
OMEGA_r = @(X) (0.91324-0.48274*(tao(X))+0.46842*(tao(X)).^2-
0.12886*(tao(X)).^3+0.044055*(tao(X)).^4-
0.0035117*(tao(X)).^5+0.00069085*(tao(X)).^6)/(1-
0.56964*(tao(X))+0.48690*(tao(X)).^2-
0.13444*(tao(X)).^3+0.045155*(tao(X)).^4-
0.0035862*(tao(X)).^5+0.00069085*(tao(X)).^6);
OMEGA_i = @(X) (-0.024134-0.029256*(tao(X))+0.016294*(tao(X)).^2-
0.00010961*(tao(X)).^3+0.000064577*(tao(X)).^4-
0.000044510*(tao(X)).^5)/(1-0.597020*(tao(X))+0.551820*(tao(X)).^2-
0.18357000*(tao(X)).^3+0.079156000*(tao(X)).^4-
0.014369000*(tao(X)).^5+0.0028361*(tao(X)).^6);
OMEGA = @(X)OMEGA_r(X) + OMEGA_i(X)*i;
GAMA_rect = @(X)OMEGA(X) .* GAMA_circ(X);

B_omega=landa(1).*sqrt(omega/w_vac).*(1+(pi*ro_f*b^2)/(4*ro_c*A)*GAMA_r
ect(omega)).^(1/4);

A1=dirac(omega)/(8*pi)-i./(2*omega);
A2=-
A1.*(sin(B_omega*L).*sinh(B_omega*L))./(1+cos(B_omega*L).*cosh(B_omega*
L));

```

```

A3=0;
A4=A1.*(sin(B_omega*L).*cosh(B_omega*L)+cos(B_omega*L).*sinh(B_omega*L)
)./(1+cos(B_omega*L).*cosh(B_omega*L));
Y_x_omega=B_omega.*(A1.*(-sin(B_omega*L)+sinh(B_omega*L))+A2.*(-
sin(B_omega*L)-
sinh(B_omega*L))+A3.*(cos(B_omega*L)+cosh(B_omega*L))+A4.*(cos(B_omega*
L)-cosh(B_omega*L)));

for ppp=1:length(Y_x_omega)
    YY_x_omega(ppp,1)=Y_x_omega(ppp);
    YY_x_omega(2*length(Y_x_omega)-ppp+1,1)=Y_x_omega(ppp);
end

y_x_time=ifft(YY_x_omega);

t=[1e-6:1e-6:0.1]';

figure;
subplot(2,1,1); plot(f,abs(Y_x_omega),'k'); xlabel('Frequency (kHz)');
ylabel('Amplitude');
subplot(2,1,2); plot(t,real(y_x_time),'k'); xlabel('time (s)');
ylabel('Amplitude');

```

Appendix F

Properties of glycerin-water solutions at different temperatures and concentrations:

Viscosity of aqueous glycerin solutions in mPa s:

Glycerin (wt%)	Temperature (°C)										
	0	10	20	30	40	50	60	70	80	90	100
0	1.792	1.308	1.005	0.8007	0.656	0.5494	0.4688	0.4061	0.3565	0.3165	0.2838
10	2.44	1.74	1.31	1.03	0.826	0.68	0.575	0.5	-	-	-
20	3.44	2.41	1.76	1.35	1.07	0.879	0.731	0.635	-	-	-
30	5.14	3.49	2.5	1.87	1.46	1.16	0.956	0.816	0.69	-	-
40	8.25	5.37	3.72	2.72	2.07	1.62	1.3	1.09	0.918	0.763	0.668
50	14.6	9.01	6	4.21	3.1	2.37	1.86	1.53	1.25	1.05	0.91
60	29.9	17.4	10.8	7.19	5.08	3.76	2.85	2.29	1.84	1.52	1.28
65	45.7	25.3	15.2	9.85	6.8	4.89	3.66	2.91	2.28	1.86	1.55
67	55.5	29.9	17.7	11.3	7.73	5.5	4.09	3.23	2.5	2.03	1.68
70	76	38.8	22.5	14.1	9.4	6.61	4.86	3.78	2.9	2.34	1.93
75	132	65.2	35.5	21.2	13.6	9.25	6.61	5.01	3.8	3	2.43
80	255	116	60.1	33.9	20.8	13.6	9.42	6.94	5.13	4.03	3.18
85	540	223	109	58	33.5	21.2	14.2	10	7.28	5.52	4.24
90	1310	498	219	109	60	35.5	22.5	15.5	11	7.93	6
91	1590	592	259	127	68.1	39.8	25.1	17.1	11.9	8.62	6.4
92	1950	729	310	147	78.3	44.8	28	19	13.1	9.46	6.82
93	2400	860	367	172	89	51.5	31.6	21.2	14.4	10.3	7.54
94	2930	1040	437	202	105	58.4	35.4	23.6	15.8	11.2	8.19
95	3690	1270	523	237	121	67	39.9	26.4	17.5	12.4	9.08
96	4600	1580	624	281	142	77.8	45.4	29.7	19.6	13.6	10.1
97	5770	1950	765	340	166	88.9	51.9	33.6	21.9	15.1	10.9
98	7370	2460	939	409	196	104	59.8	38.5	24.8	17	12.2
99	9420	3090	1150	500	235	122	69.1	43.6	27.8	19	13.3
100	12070	3900	1410	612	284	142	81.3	50.6	31.9	21.3	14.8

Density of aqueous glycerin solutions in g/cm³:

Glycerin (wt%)	Temperature (°C)					Glycerin (wt%)	Temperature (°C)				
	15	15.5	20	25	30		15	15.5	20	25	30
100	1.26415	1.26381	1.26108	1.25802	1.25495	50	1.1287	1.12845	1.1263	1.12375	1.1211
99	1.2616	1.26125	1.2585	1.25545	1.25235	49	1.126	1.12575	1.1236	1.1211	1.11845
98	1.259	1.25865	1.2559	1.2529	1.24975	48	1.12325	1.12305	1.1209	1.1184	1.1158
97	1.25645	1.2561	1.25335	1.2503	1.2471	47	1.12055	1.1203	1.1182	1.11575	1.1132
96	1.25385	1.2535	1.2508	1.2477	1.2445	46	1.1178	1.1176	1.1155	1.1131	1.11055
95	1.2513	1.25095	1.24825	1.24515	1.2419	45	1.1151	1.1149	1.1128	1.1104	1.10795
94	1.24865	1.2483	1.2456	1.2425	1.2393	44	1.11235	1.11215	1.1101	1.10775	1.1053
93	1.246	1.24565	1.243	1.23985	1.2367	43	1.1096	1.10945	1.1074	1.1051	1.10265
92	1.2434	1.24305	1.24035	1.23725	1.2341	42	1.1069	1.1067	1.1047	1.1024	1.10005
91	1.24075	1.2404	1.2377	1.2346	1.2315	41	1.10415	1.104	1.102	1.09975	1.0974
90	1.2381	1.23775	1.2351	1.232	1.2289	40	1.10145	1.1013	1.0993	1.0971	1.09475
89	1.23545	1.2351	1.23245	1.22935	1.22625	39	1.09875	1.0986	1.09665	1.09445	1.09215
88	1.2328	1.23245	1.22975	1.22665	1.2236	38	1.09605	1.0959	1.094	1.0918	1.08955
87	1.23015	1.2298	1.2271	1.224	1.22095	37	1.0934	1.0932	1.09135	1.08915	1.0869
86	1.2275	1.2271	1.22445	1.22135	1.2183	36	1.0907	1.0905	1.08865	1.08655	1.0843
85	1.22485	1.22445	1.2218	1.2187	1.21565	35	1.088	1.0878	1.086	1.0839	1.08165
84	1.2222	1.2218	1.21915	1.21605	1.213	34	1.0853	1.08515	1.08335	1.08125	1.07905
83	1.21955	1.21915	1.2165	1.2134	1.21035	33	1.08265	1.08245	1.0807	1.0786	1.07645
82	1.2169	1.2165	1.2138	1.21075	1.2077	32	1.07995	1.07975	1.078	1.076	1.0738
81	1.21425	1.21385	1.21115	1.2081	1.20505	31	1.07725	1.07705	1.07535	1.07335	1.0712
80	1.2116	1.2112	1.2085	1.20545	1.2024	30	1.07455	1.07435	1.0727	1.0707	1.06855
79	1.20885	1.20845	1.20575	1.20275	1.1997	29	1.07195	1.07175	1.0701	1.06815	1.06605
78	1.2061	1.2057	1.20305	1.20005	1.19705	28	1.06935	1.06915	1.06755	1.0656	1.06355
77	1.20335	1.203	1.2003	1.19735	1.19435	27	1.0667	1.06655	1.06495	1.06305	1.06105
76	1.2006	1.20025	1.1976	1.19465	1.1917	26	1.0641	1.0639	1.0624	1.06055	1.05855
75	1.19785	1.1975	1.19485	1.19195	1.189	25	1.0615	1.0613	1.0598	1.058	1.05605
74	1.1951	1.1948	1.19215	1.18925	1.18635	24	1.05885	1.0587	1.0572	1.05545	1.0535
73	1.19235	1.19205	1.1894	1.1865	1.18365	23	1.05625	1.0561	1.05465	1.0529	1.051
72	1.18965	1.1893	1.1867	1.1838	1.181	22	1.05365	1.0535	1.05205	1.05035	1.0485
71	1.1869	1.18655	1.18395	1.1811	1.1783	21	1.051	1.0509	1.0495	1.0478	1.046
70	1.18415	1.18385	1.18125	1.1784	1.17565	20	1.0484	1.04825	1.0469	1.04525	1.0435
69	1.18135	1.18105	1.1785	1.17565	1.1729	19	1.0459	1.04575	1.0444	1.0428	1.04105
68	1.1786	1.1783	1.17575	1.17295	1.1702	18	1.04335	1.04325	1.04195	1.04035	1.0386
67	1.17585	1.17555	1.173	1.1702	1.16745	17	1.04085	1.04075	1.03945	1.0379	1.03615
66	1.17305	1.17275	1.17025	1.16745	1.1647	16	1.03835	1.03825	1.03695	1.03545	1.0337
65	1.1703	1.17	1.1675	1.16475	1.16195	15	1.0358	1.0357	1.0345	1.033	1.0313
64	1.16755	1.16725	1.16475	1.162	1.15925	14	1.0333	1.0332	1.032	1.03055	1.02885
63	1.1648	1.16445	1.16205	1.15925	1.1565	13	1.0308	1.0307	1.02955	1.02805	1.0264
62	1.162	1.1617	1.1593	1.15655	1.15375	12	1.0283	1.0282	1.02705	1.0256	1.02395
61	1.15925	1.15895	1.15655	1.1538	1.151	11	1.02575	1.02565	1.02455	1.02315	1.0215
60	1.1565	1.15615	1.1538	1.15105	1.1483	10	1.02325	1.02315	1.0221	1.0207	1.01905
59	1.1537	1.1534	1.15105	1.14835	1.14555	9	1.02085	1.02075	1.0197	1.01835	1.0167
58	1.15095	1.15065	1.1483	1.1456	1.14285	8	1.0184	1.01835	1.0173	1.016	1.0144
57	1.14815	1.14785	1.14555	1.14285	1.1401	7	1.016	1.0159	1.01495	1.0136	1.01205
56	1.14535	1.1451	1.1428	1.14015	1.1374	6	1.0136	1.0135	1.01255	1.01125	1.0097
55	1.1426	1.1423	1.14005	1.1374	1.1347	5	1.0112	1.0111	1.01015	1.0089	1.00735
54	1.1398	1.13955	1.1373	1.13465	1.13195	4	1.00875	1.0087	1.0078	1.00655	1.00505
53	1.13705	1.1368	1.13455	1.13195	1.12925	3	1.00635	1.0063	1.0054	1.00415	1.0027
52	1.13425	1.134	1.1318	1.1292	1.1265	2	1.00395	1.00385	1.003	1.0018	1.00035
51	1.1315	1.13125	1.12905	1.1265	1.1238	1	1.00155	1.00145	1.0006	0.99945	0.998
						0	0.99913	0.99905	0.99823	0.99708	0.99568

Appendix G

The values of shifting factors a_T and b_T , used to generate the master curve for each concentration

Concentration (wt %)	8.5% PS/DEP	12% PS/DEP	16% PS/DEP	25% PS/DEP
a_T (-45 °C)	-	-	27413.61	-
b_T (-45 °C)	-	-	0.588842	-

Concentration (wt %)	8.5% PS/DEP	12% PS/DEP	16% PS/DEP	25% PS/DEP
a_T (-30 °C)	-	-	441.2482	-
b_T (-30 °C)	-	-	0.767568	-

Concentration (wt %)	8.5% PS/DEP	12% PS/DEP	16% PS/DEP	25% PS/DEP
a_T (-25 °C)	175.6454	-	-	-
b_T (-25 °C)	0.537061	-	-	-

Concentration (wt %)	8.5% PS/DEP	12% PS/DEP	16% PS/DEP	25% PS/DEP
$a_T (-20\text{ }^\circ\text{C})$	-	-	-	191.8246
$b_T (-20\text{ }^\circ\text{C})$	-	-	-	0.868963

Concentration (wt %)	8.5% PS/DEP	12% PS/DEP	16% PS/DEP	25% PS/DEP
$a_T (-15\text{ }^\circ\text{C})$	-	36.43693	40.71392	-
$b_T (-15\text{ }^\circ\text{C})$	-	0.609097	0.776458	-

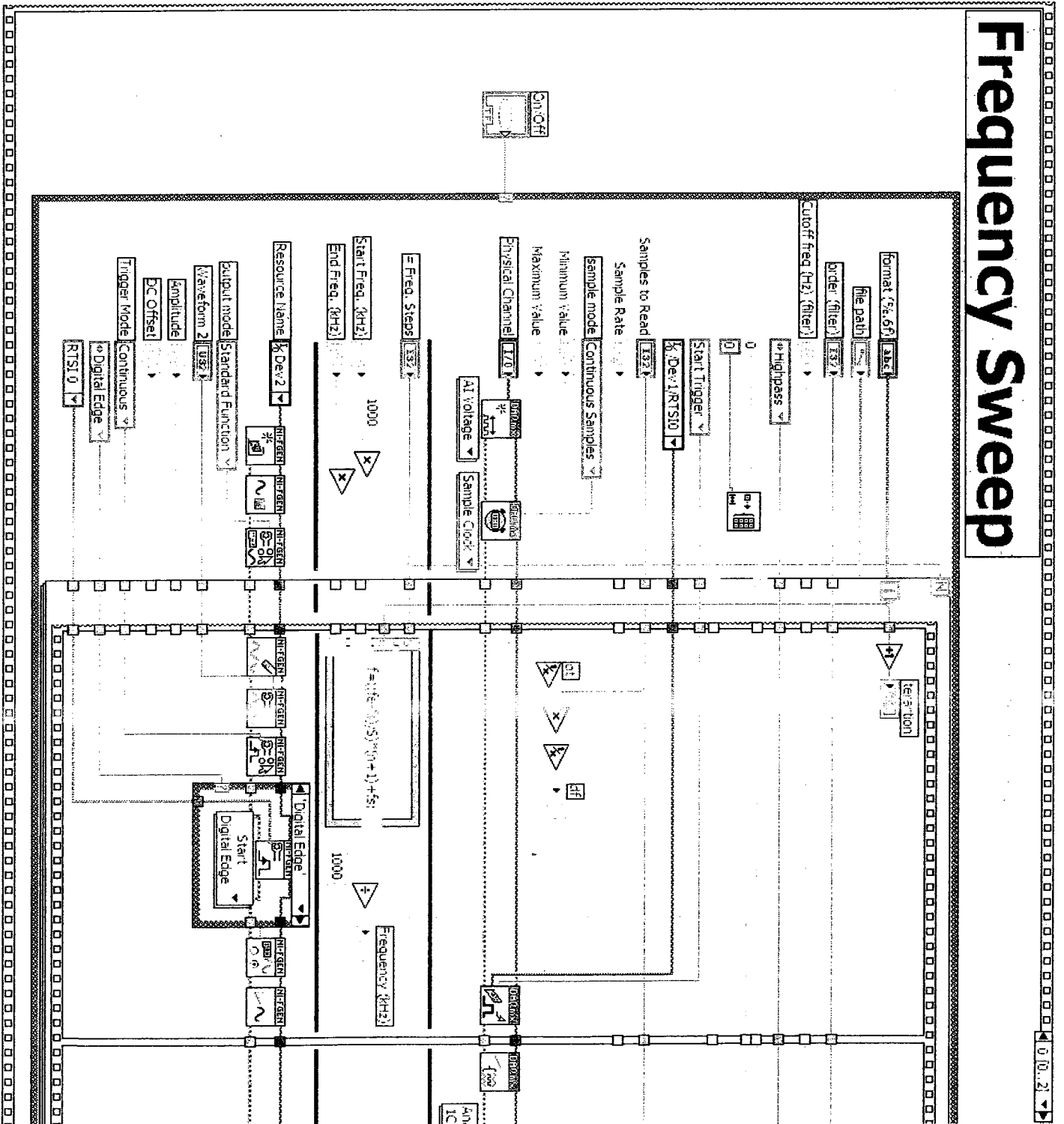
Concentration (wt %)	8.5% PS/DEP	12% PS/DEP	16% PS/DEP	25% PS/DEP
$a_T (5\text{ }^\circ\text{C})$	5.052725*	4.73894	4.562384	7.345386
$b_T (5\text{ }^\circ\text{C})$	1*	0.686828	0.853523	0.905225

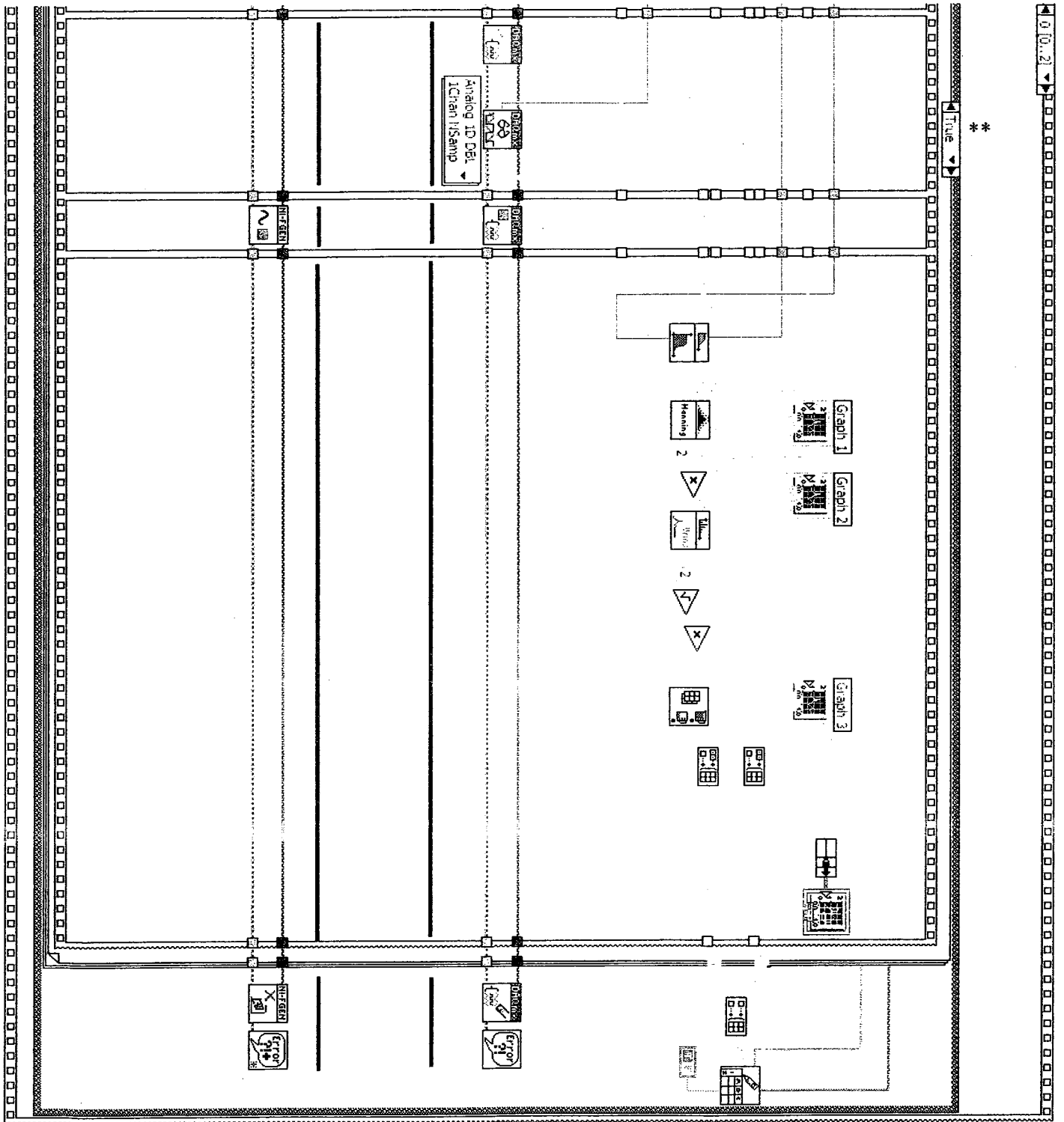
Concentration (wt %)	8.5% PS/DEP	12% PS/DEP	16% PS/DEP	25% PS/DEP
$a_T (15\text{ }^\circ\text{C})$	-	-	1.94798	2.443513
$b_T (15\text{ }^\circ\text{C})$	-	-	0.968404	0.968404

* No experiment was performed for 8.5% PS/DEP at 25 °C, however the zero shear viscosity at this temperature was determined using the exponential Arrhenius relation.

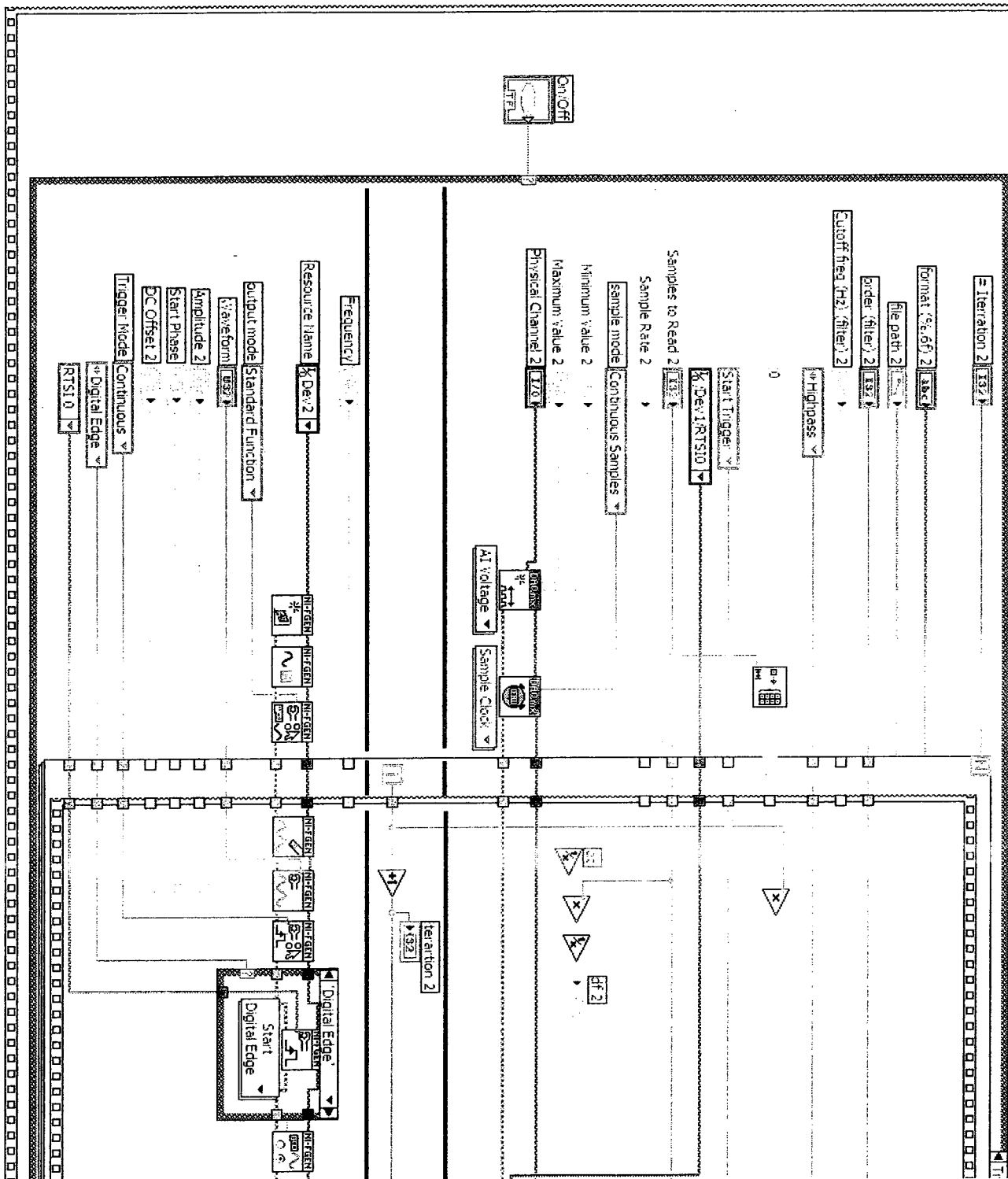
Appendix H

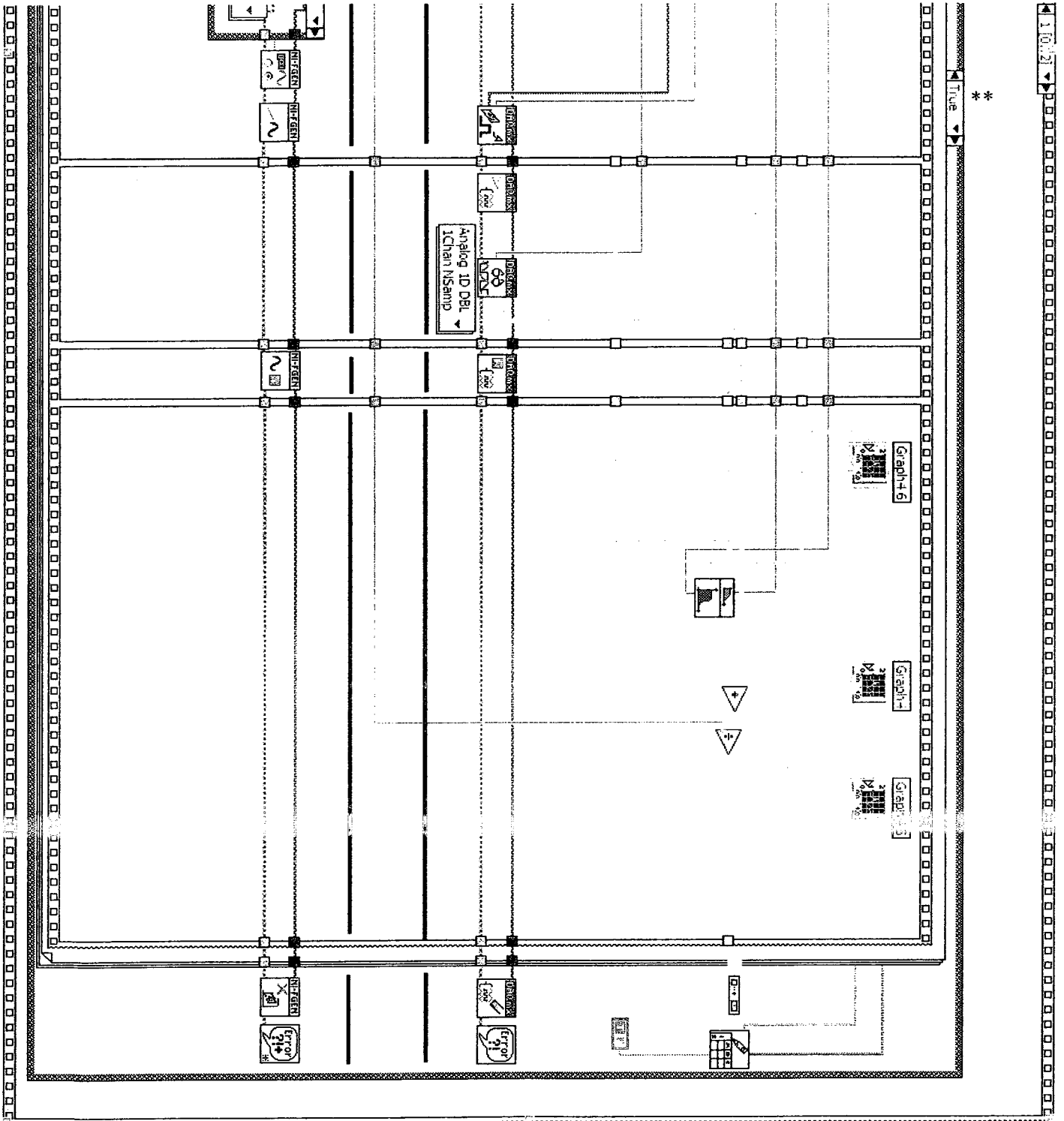
LabVIEW code written for controlling the SG and DAQ hardware and also for analyzing the recorded data.



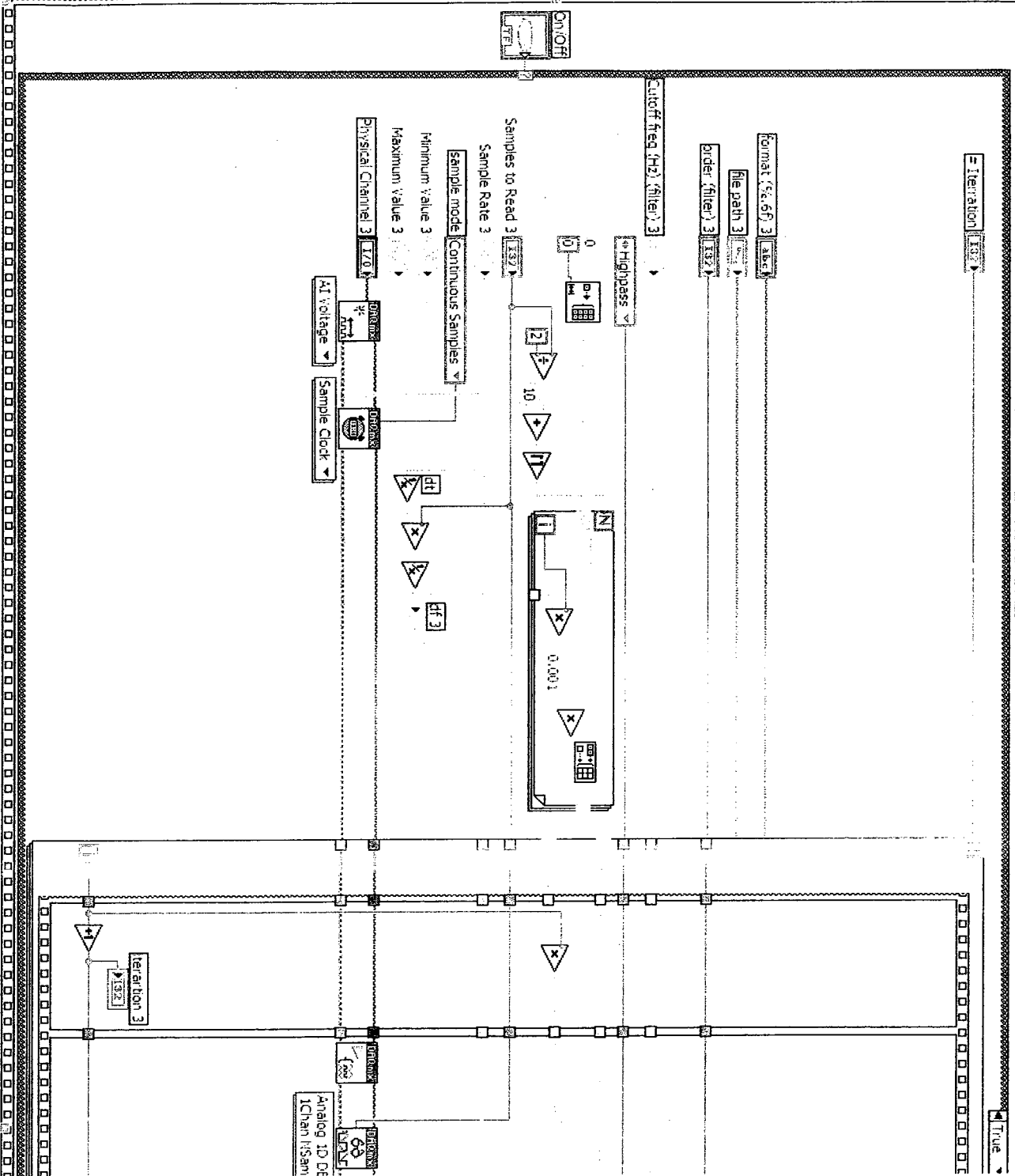


Step Excitation

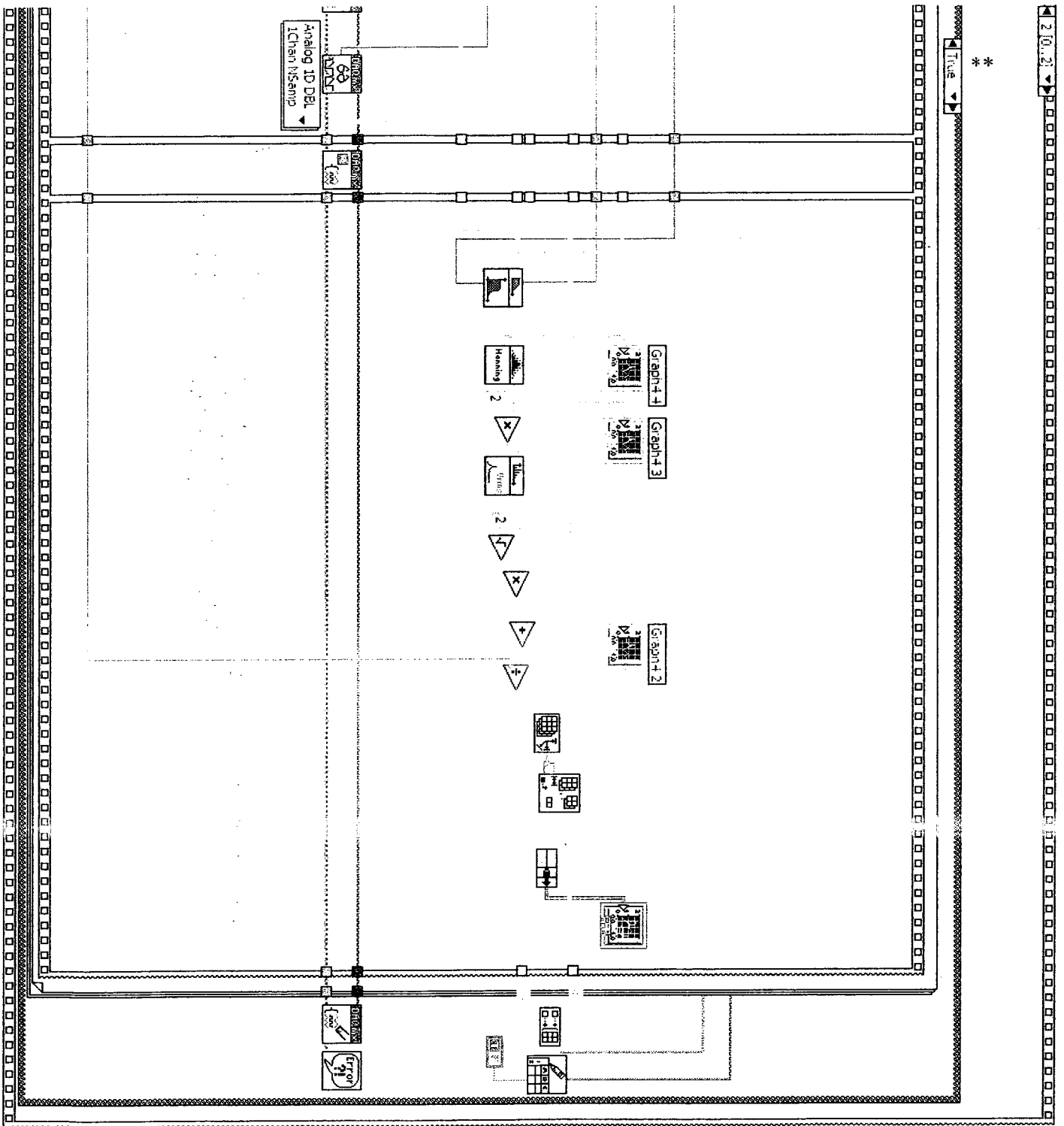




Thermal Excitation



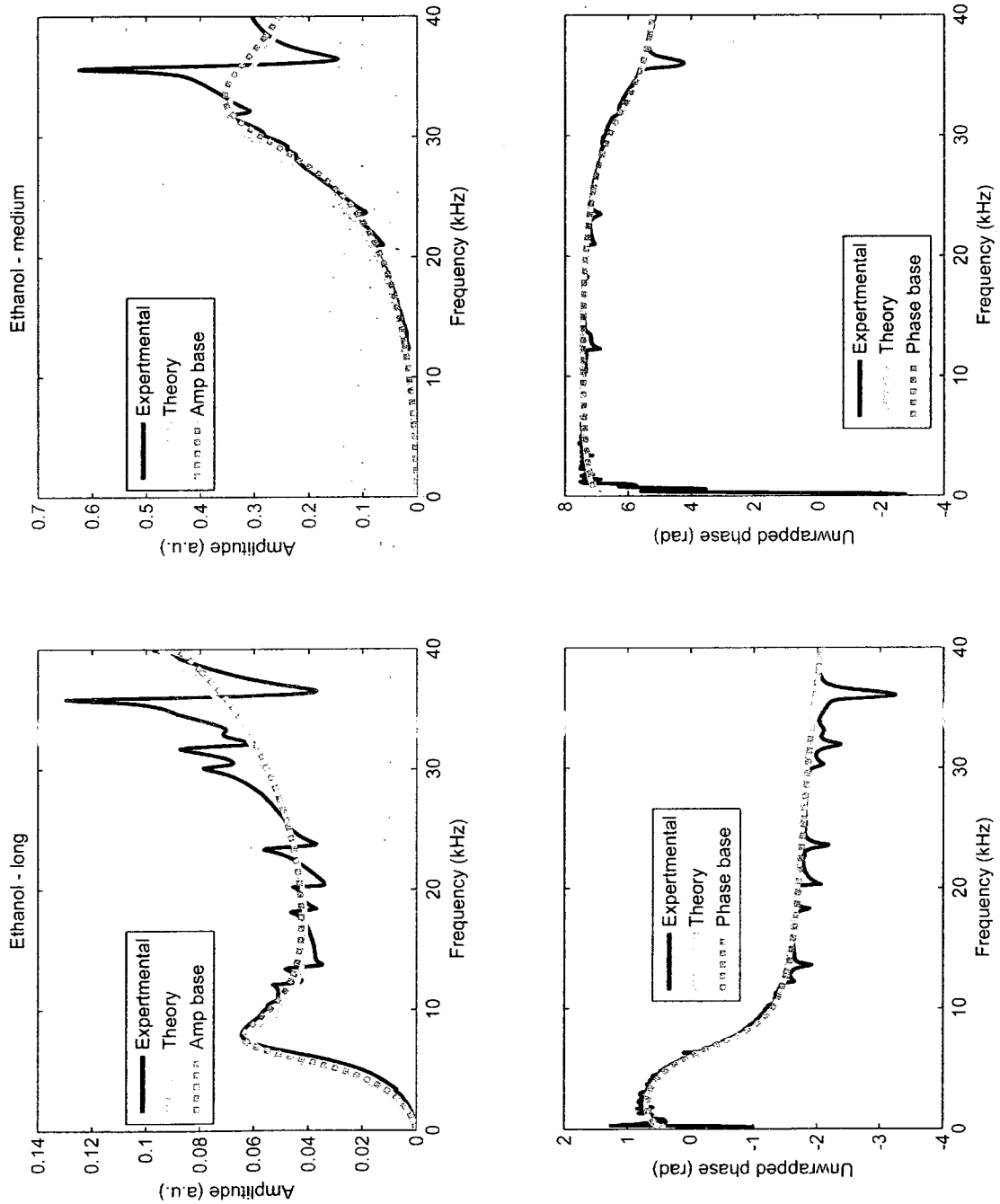
**

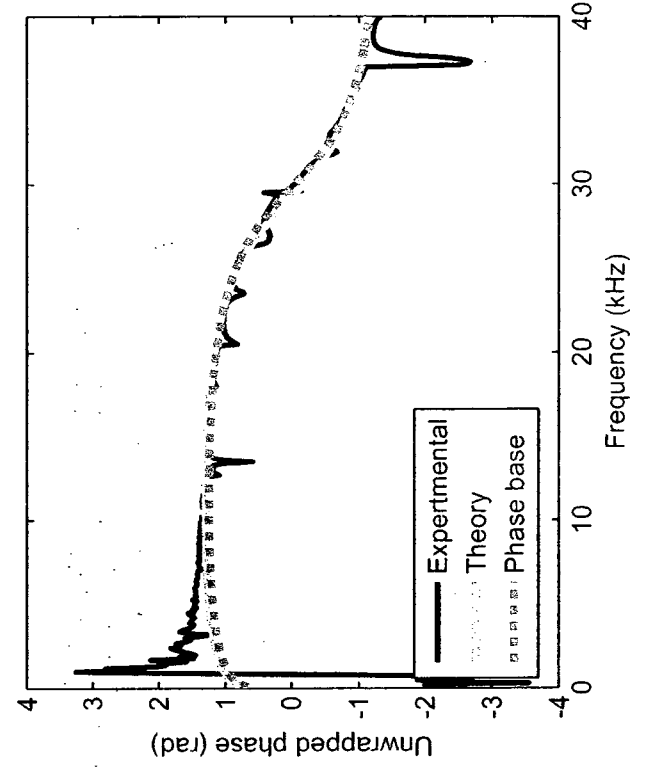
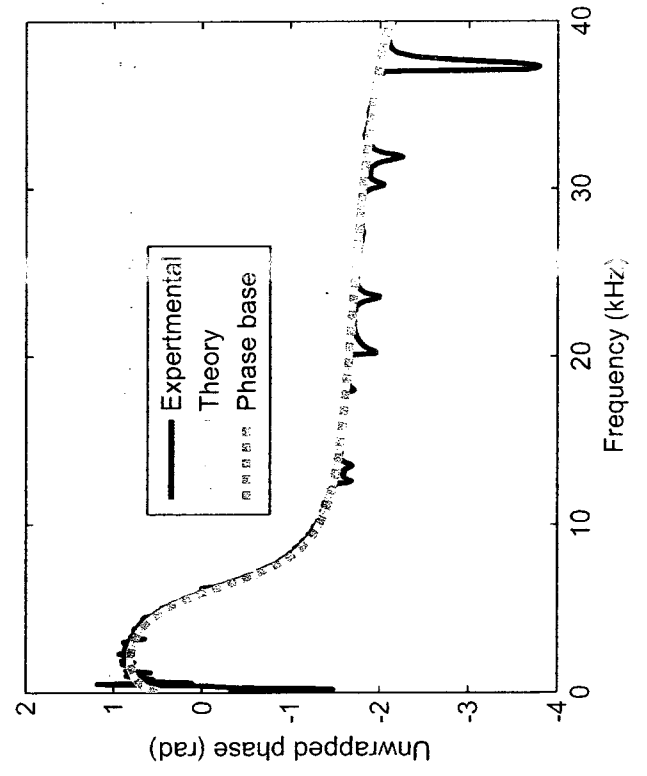
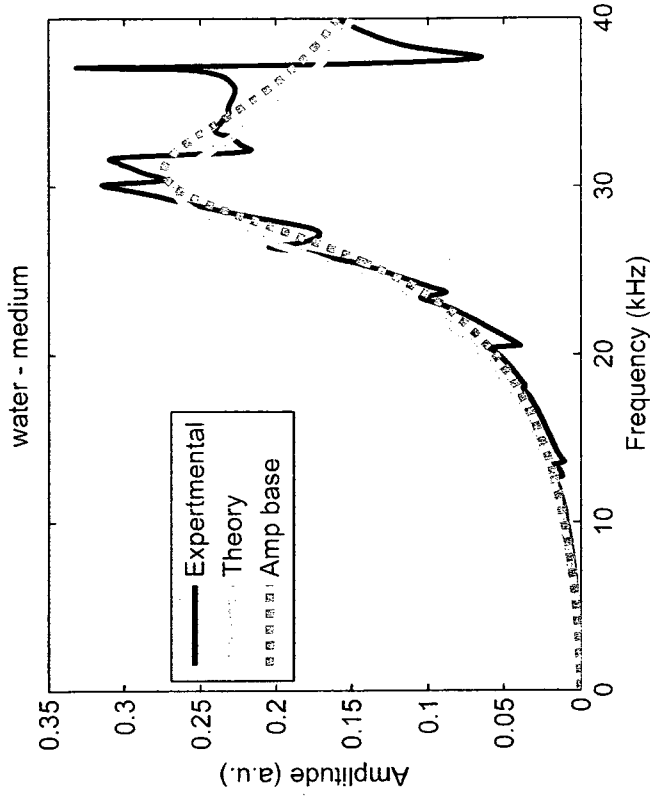
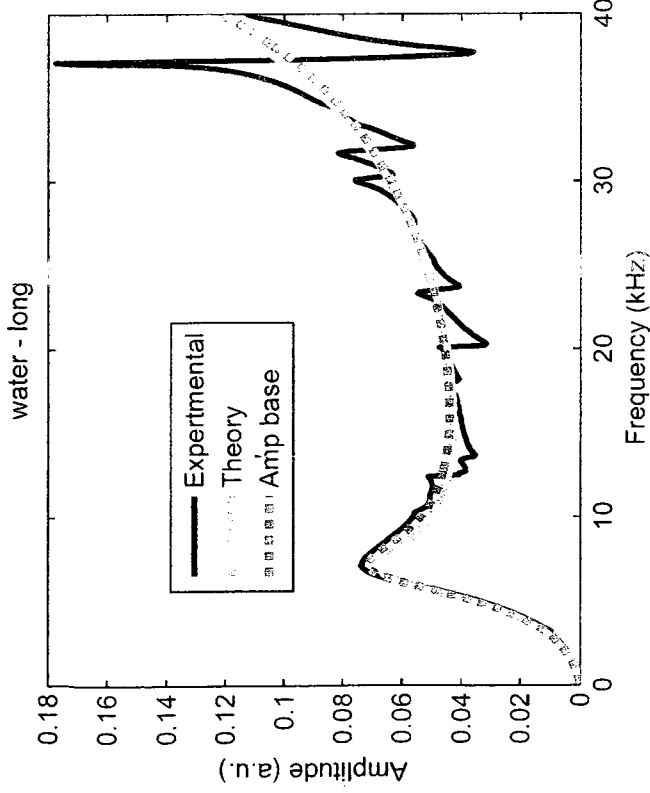


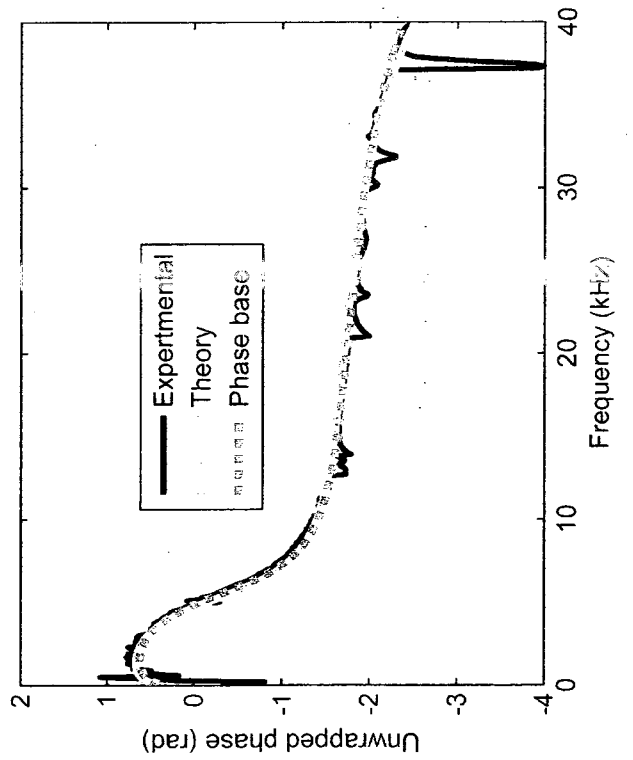
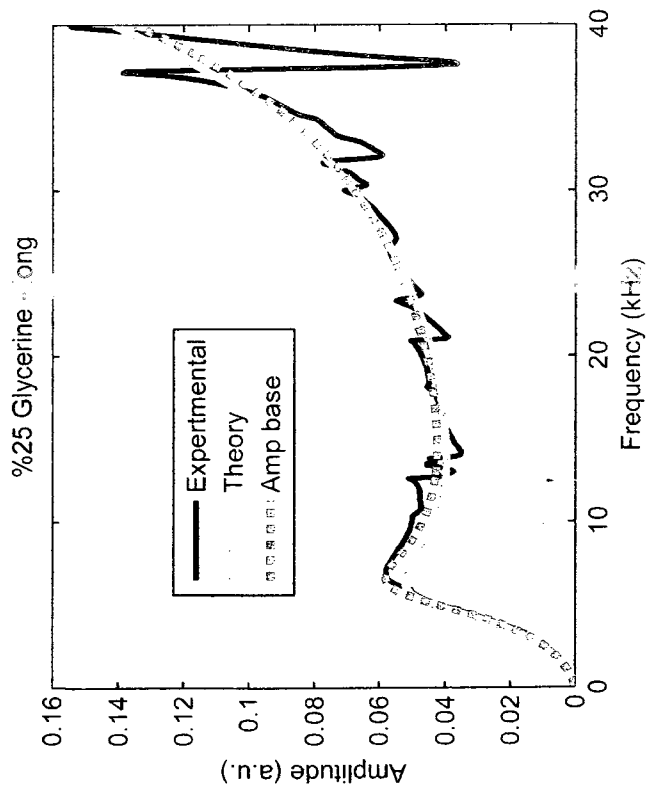
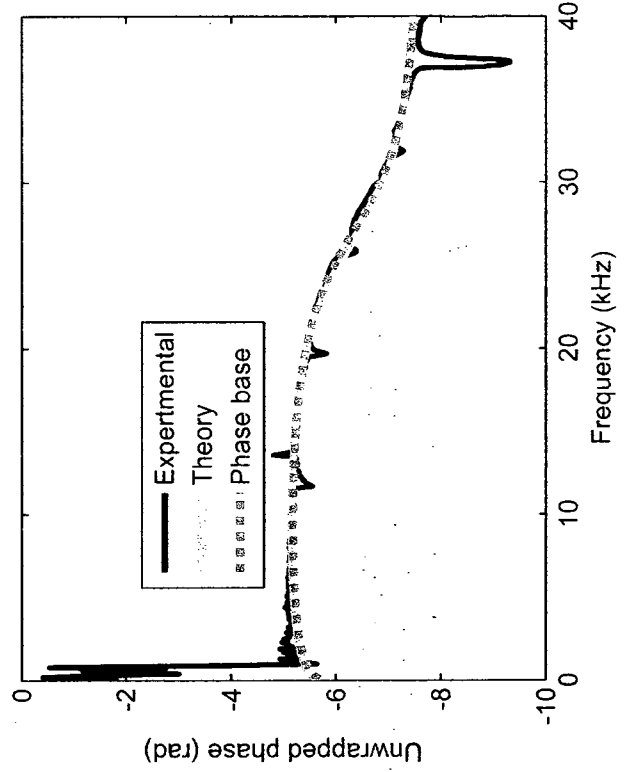
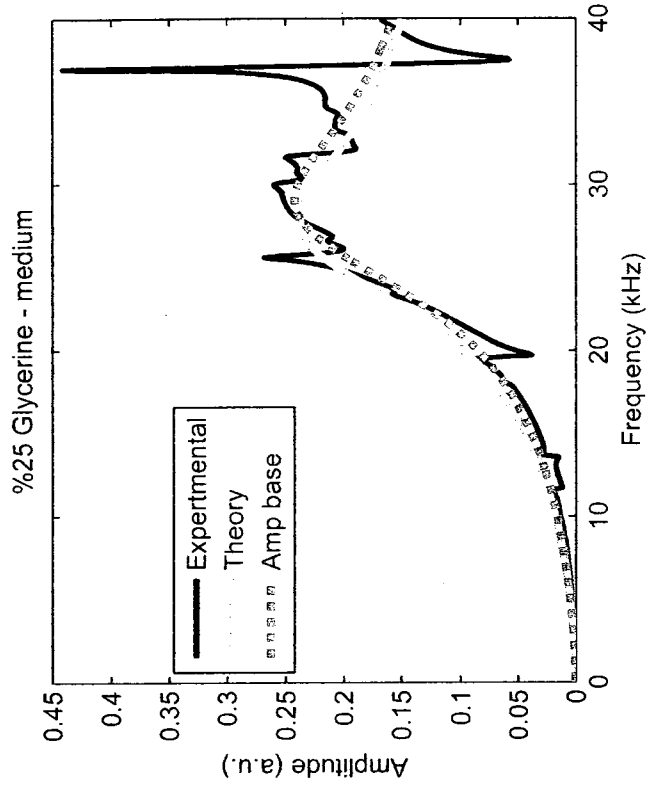
** The false cases for all the frames are empty.

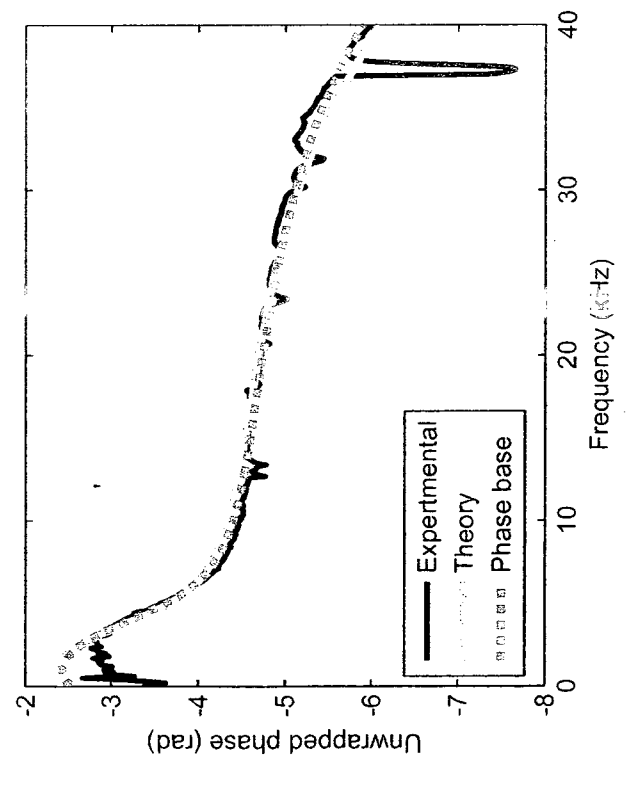
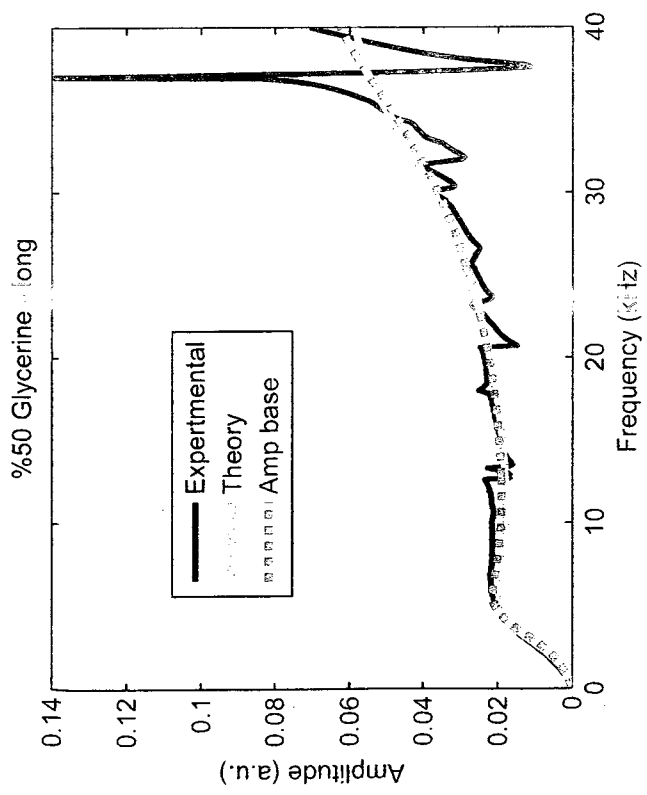
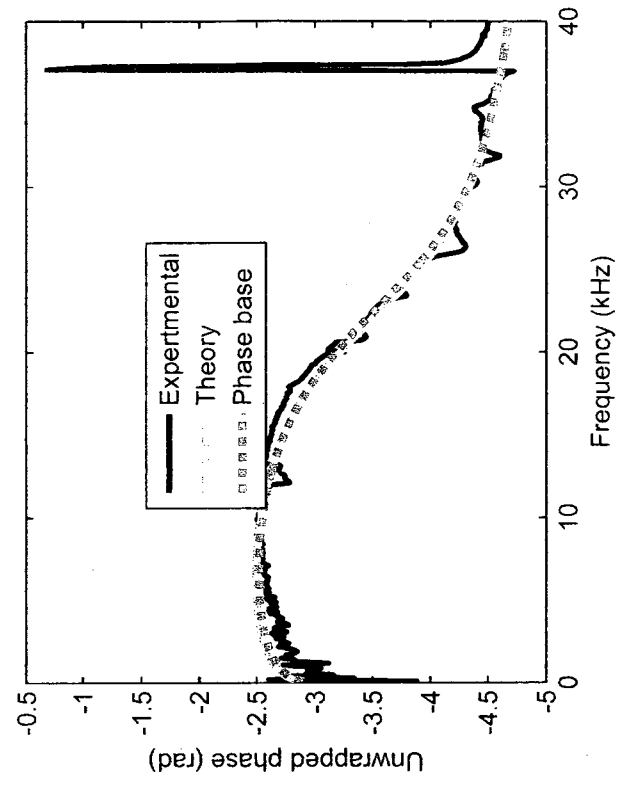
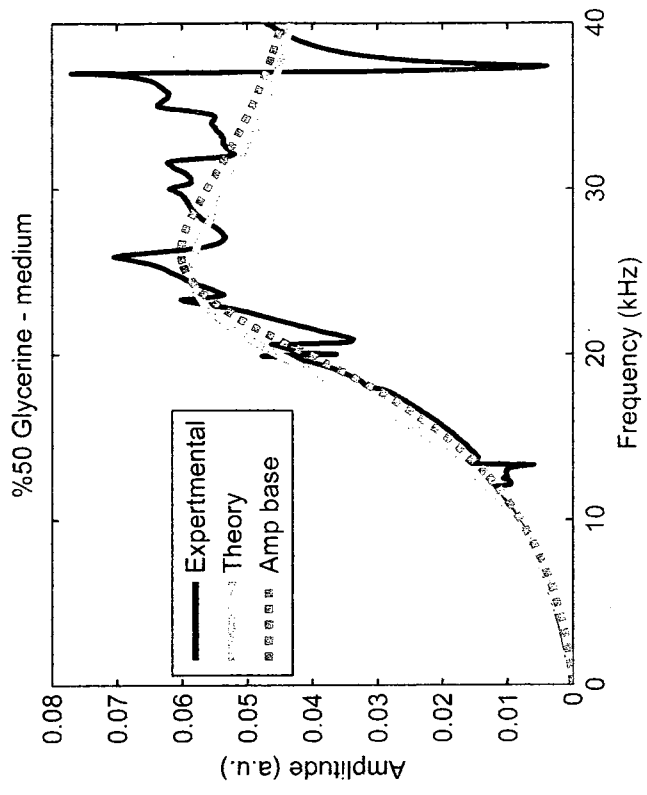
Appendix I

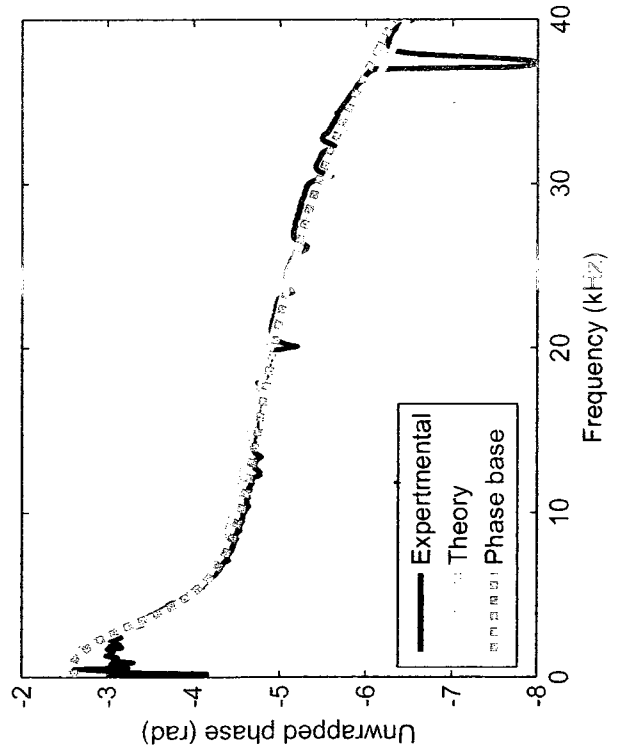
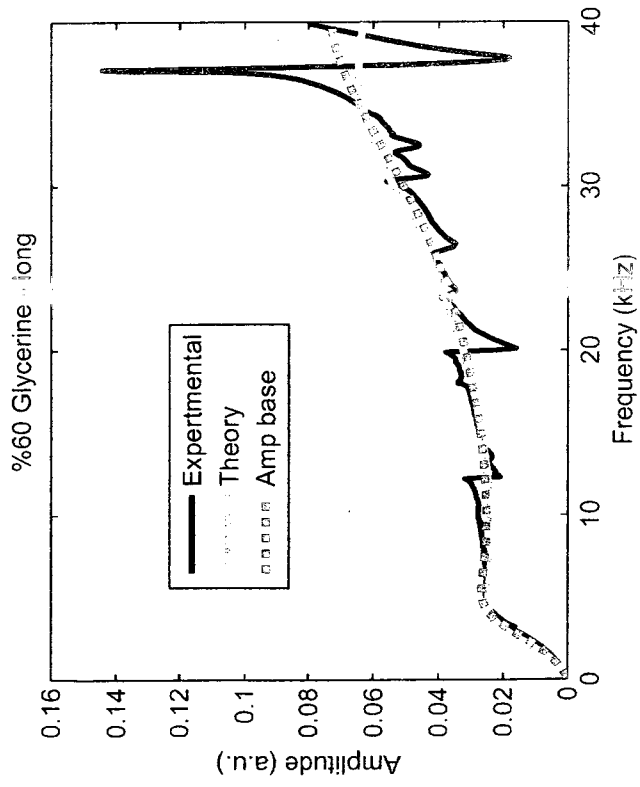
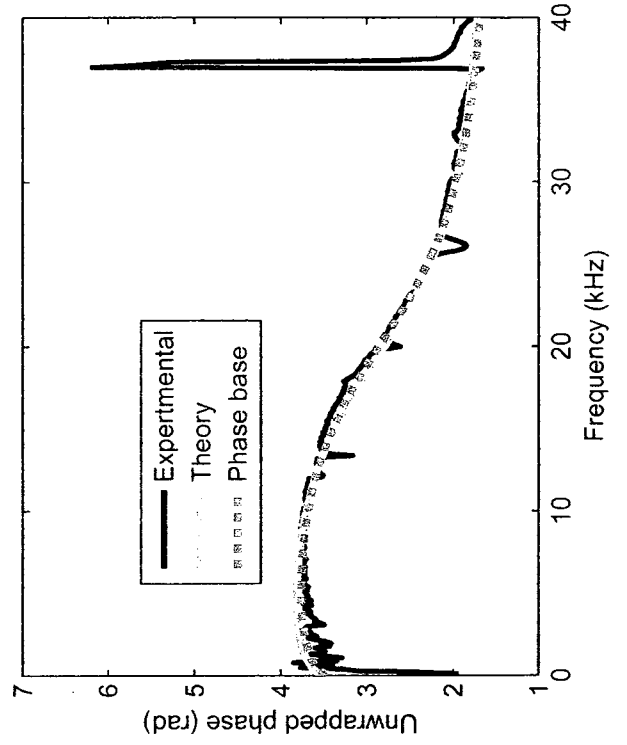
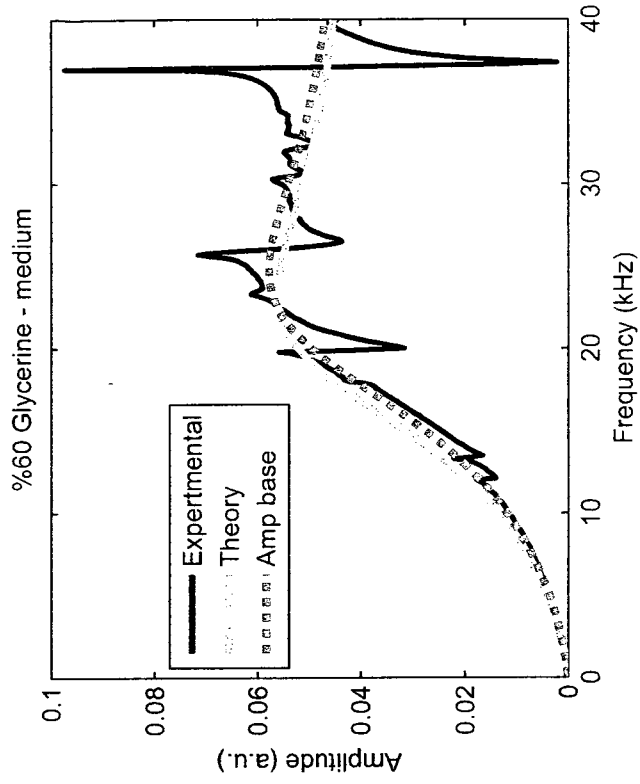
Amplitude and phase responses for frequency sweep excitation. The best fit for theoretical response with known properties (Theory), with unknown properties for amplitude response (amp base) and with unknown properties for amplitude response (phase base) are also presented:



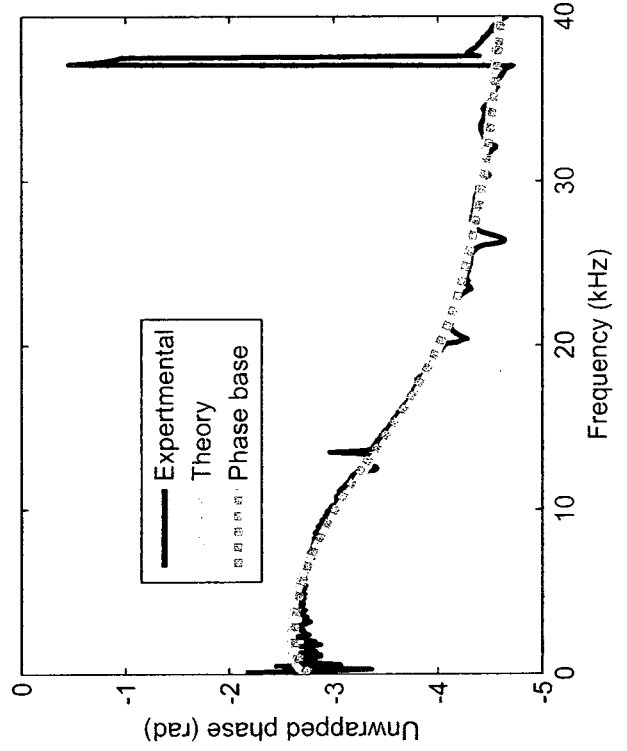
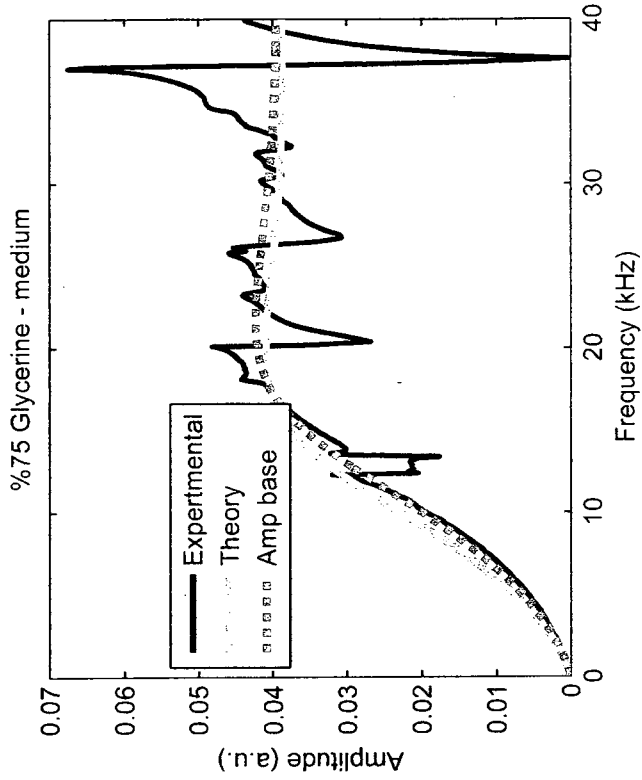




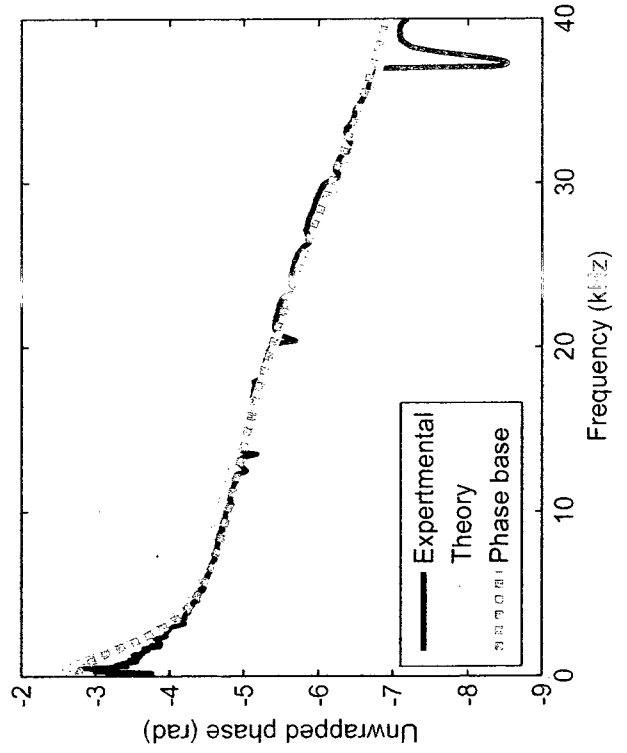
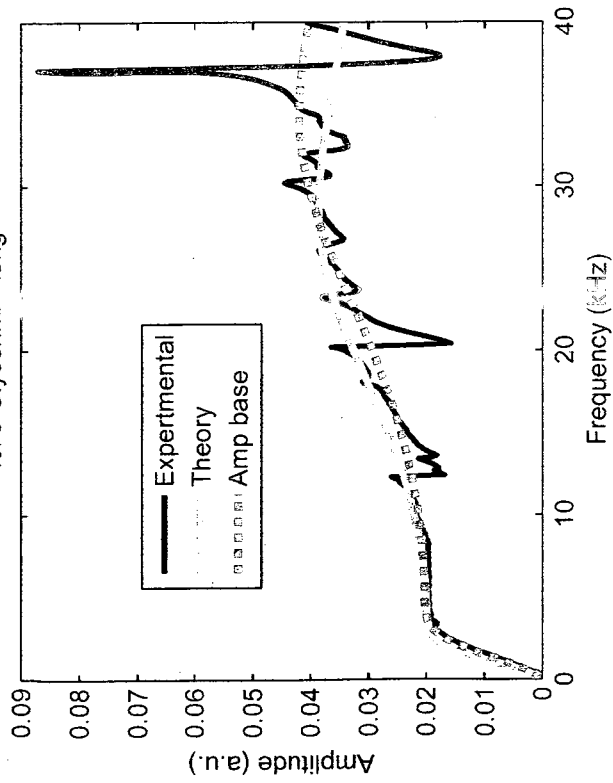


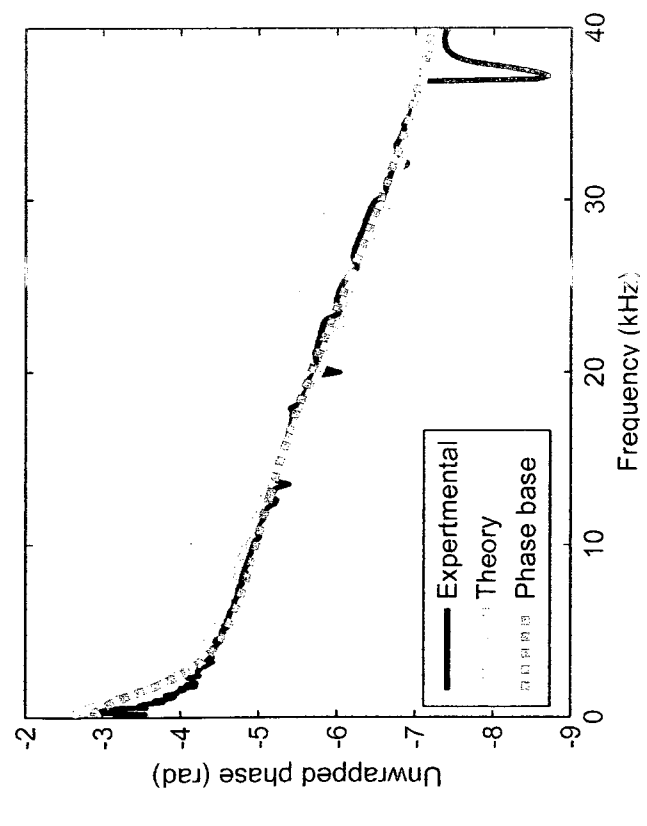
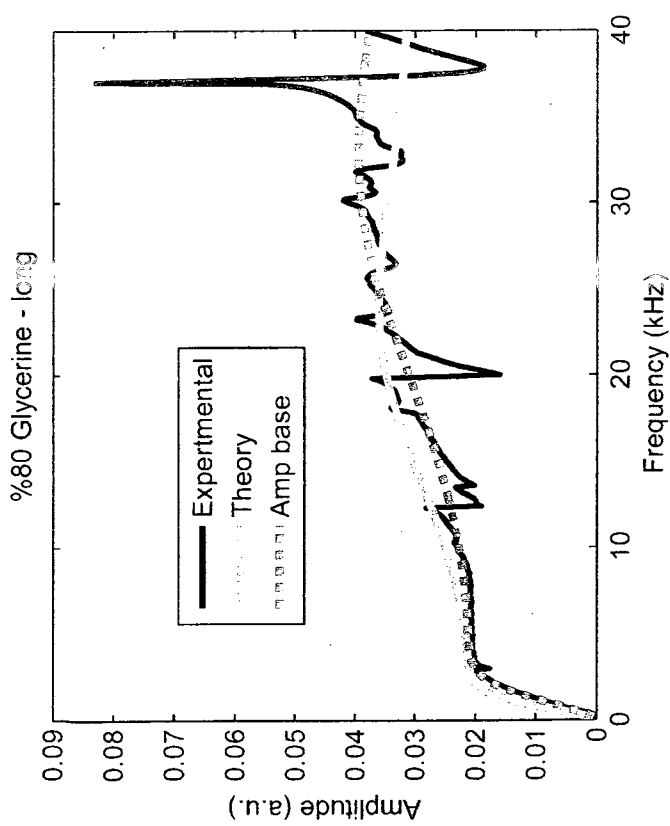
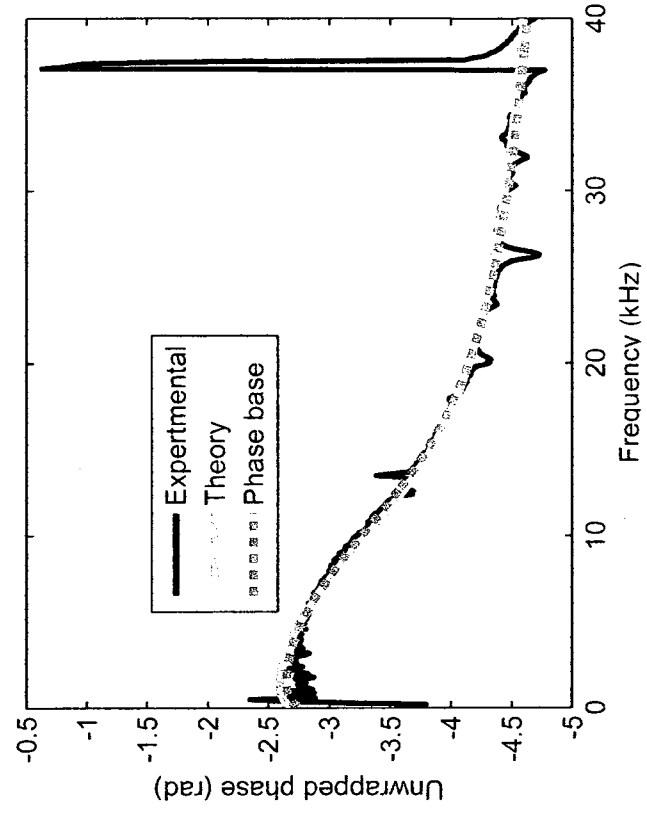
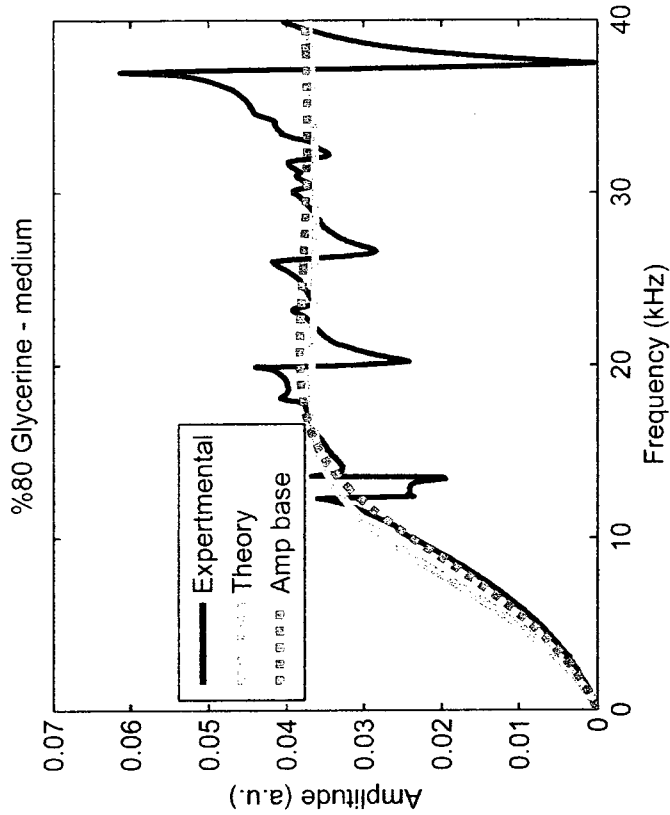


%75 Glycerine - medium

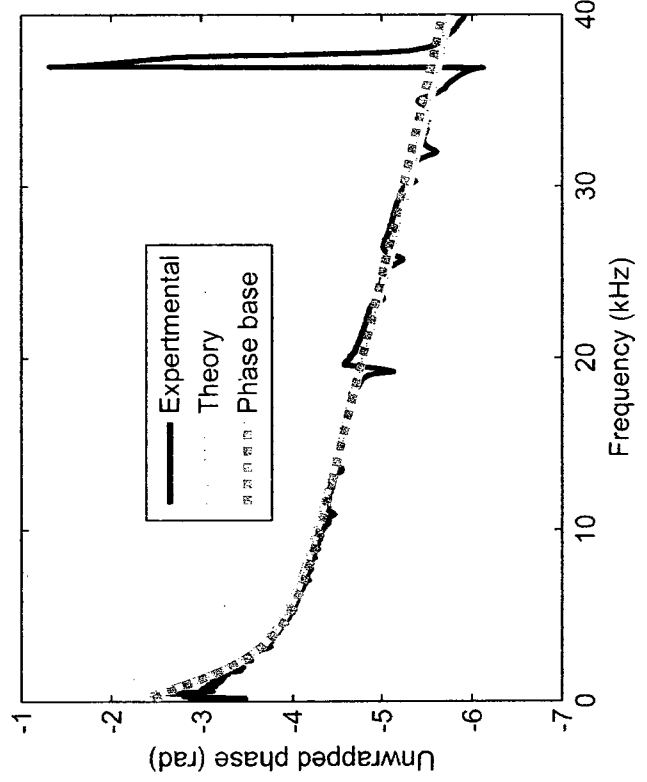
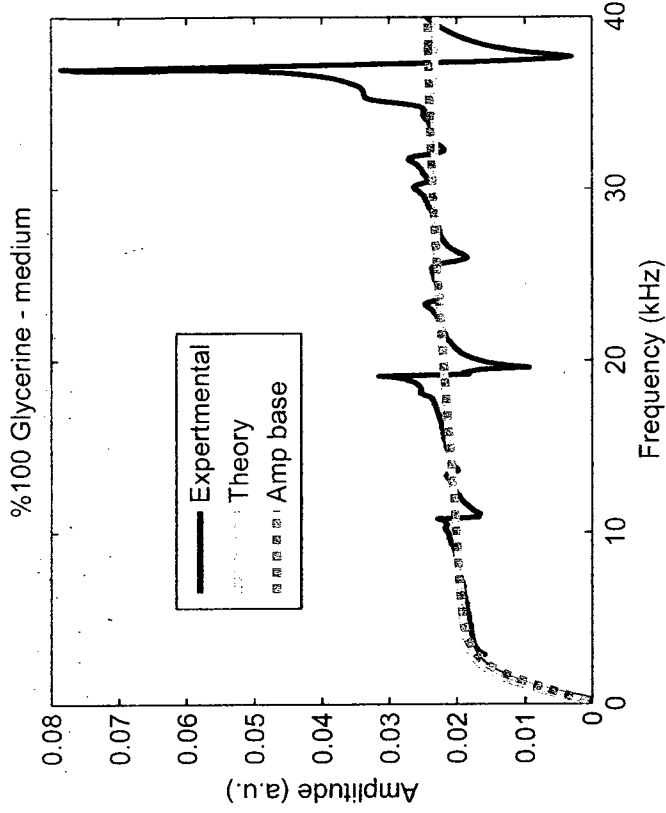


%75 Glycerine - long

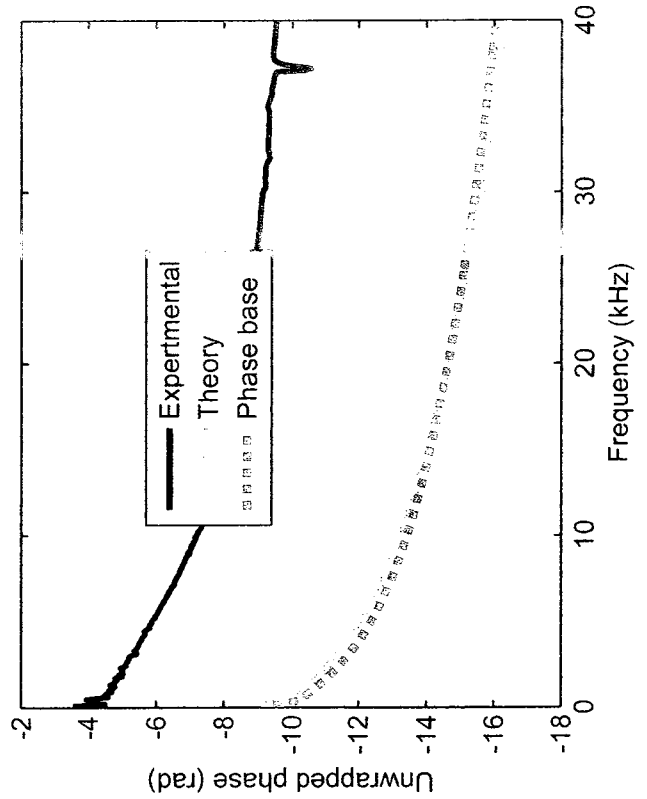
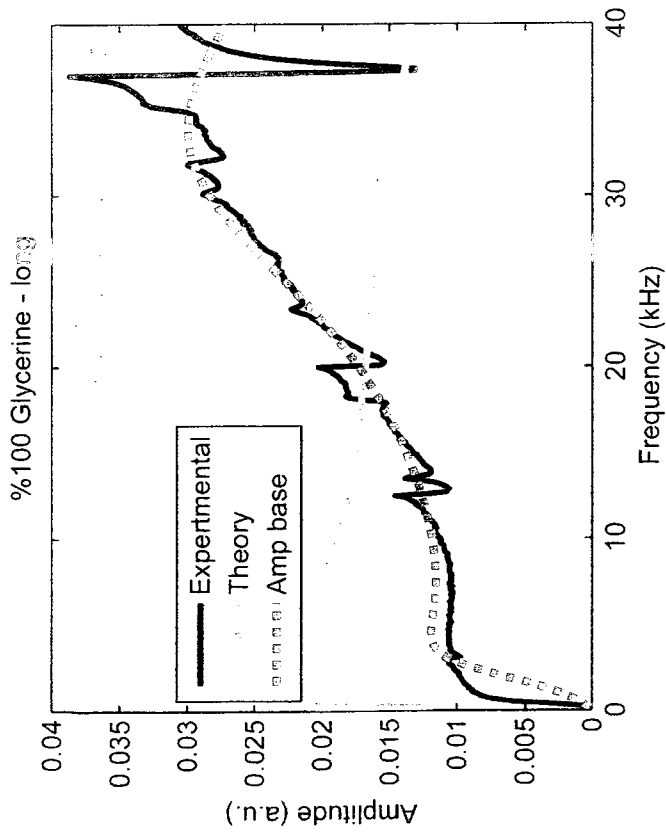




%100 Glycerine - medium

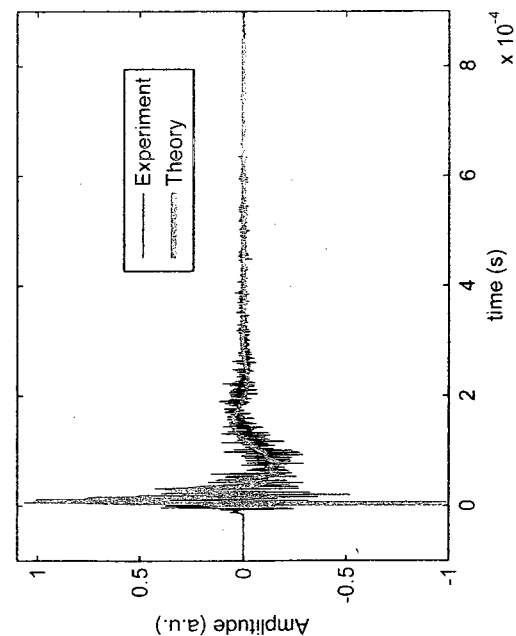
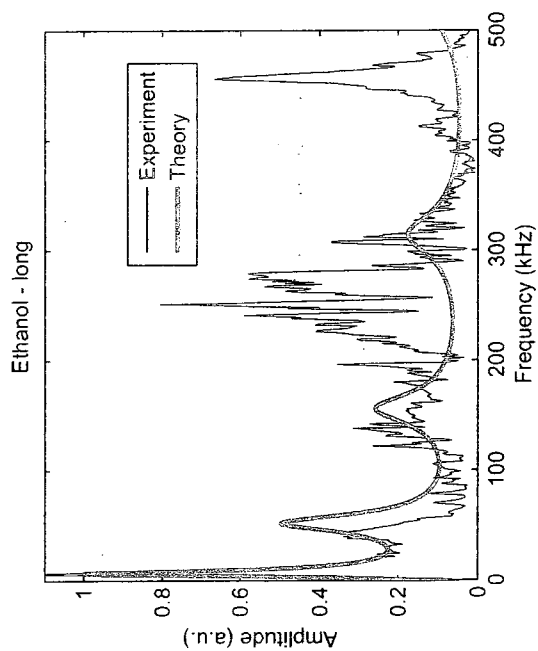
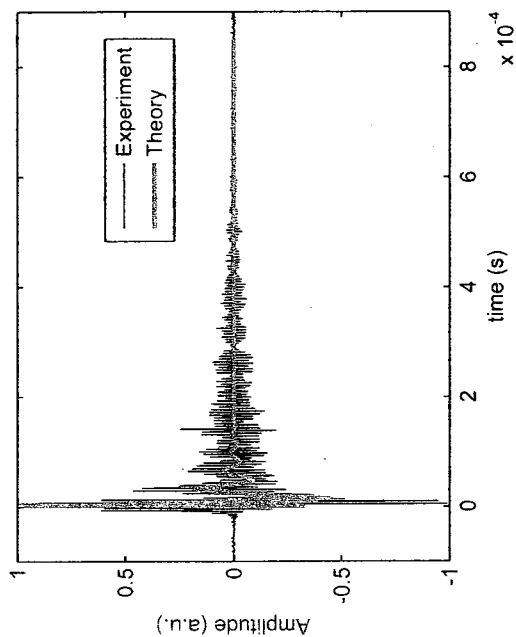
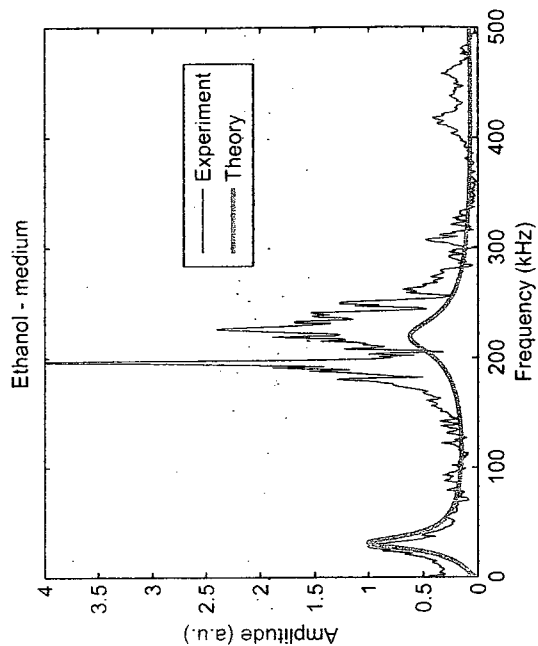


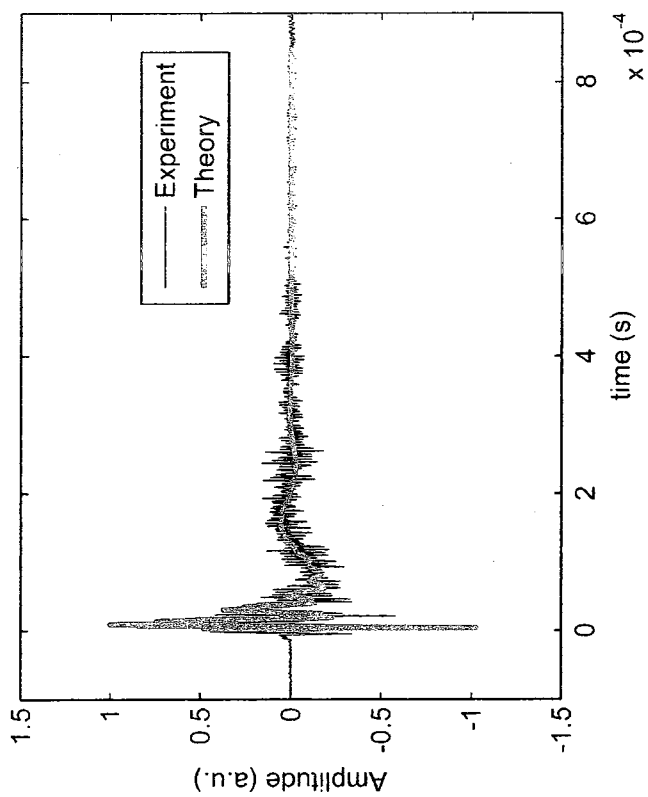
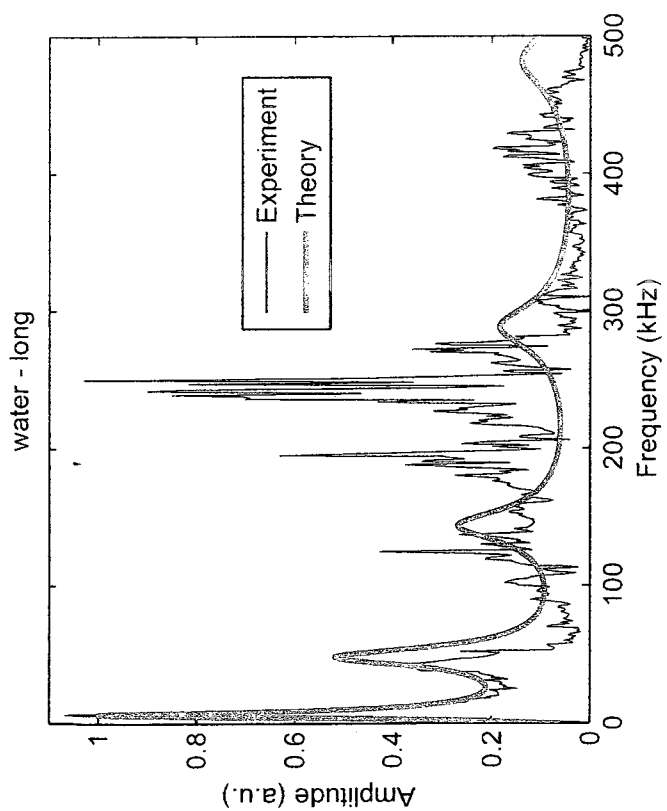
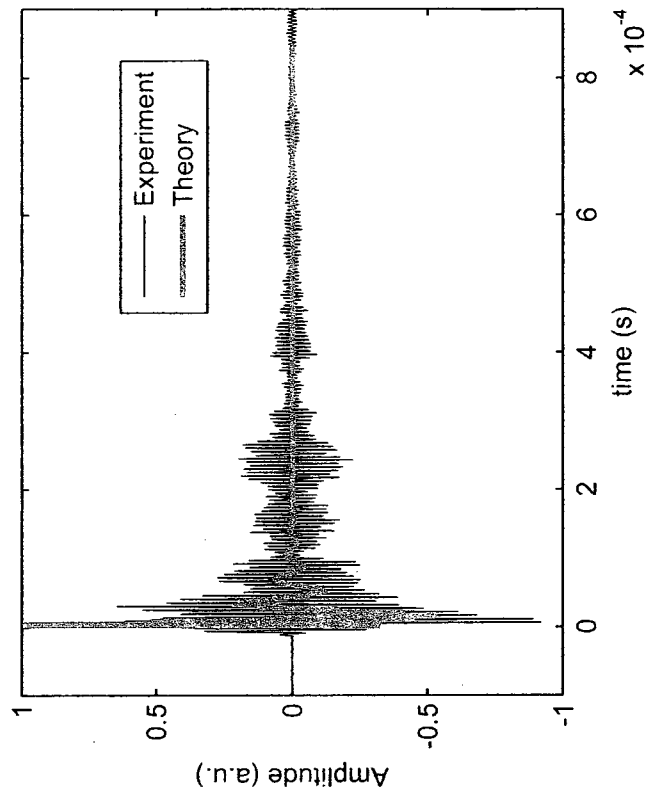
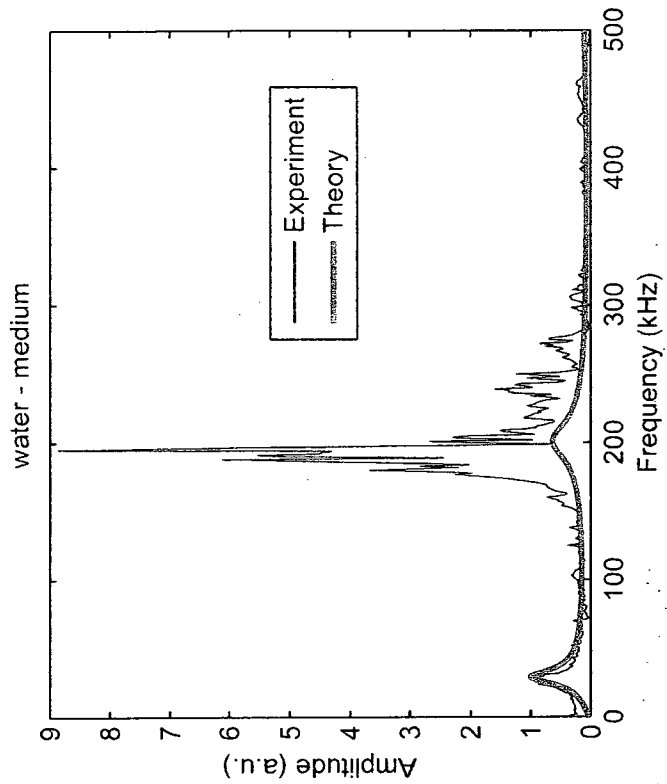
%100 Glycerine - long



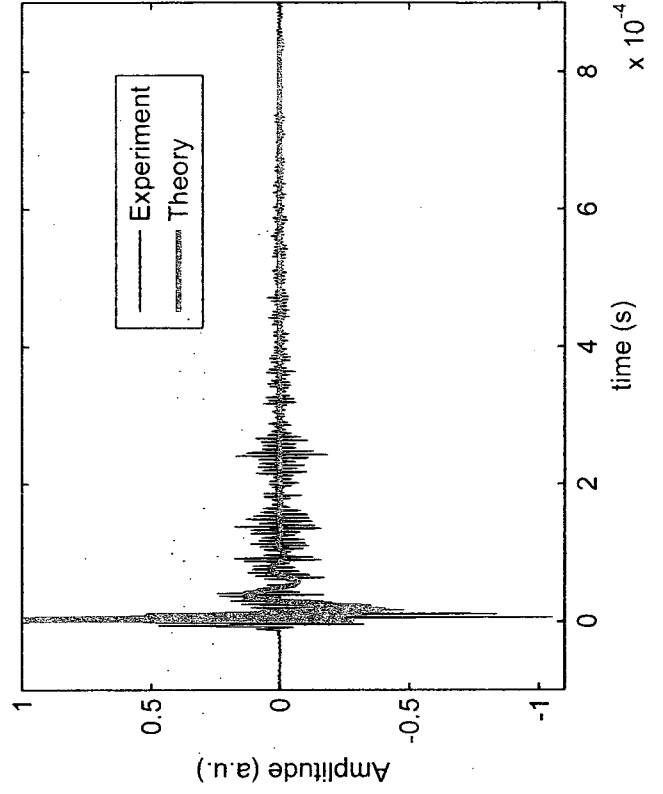
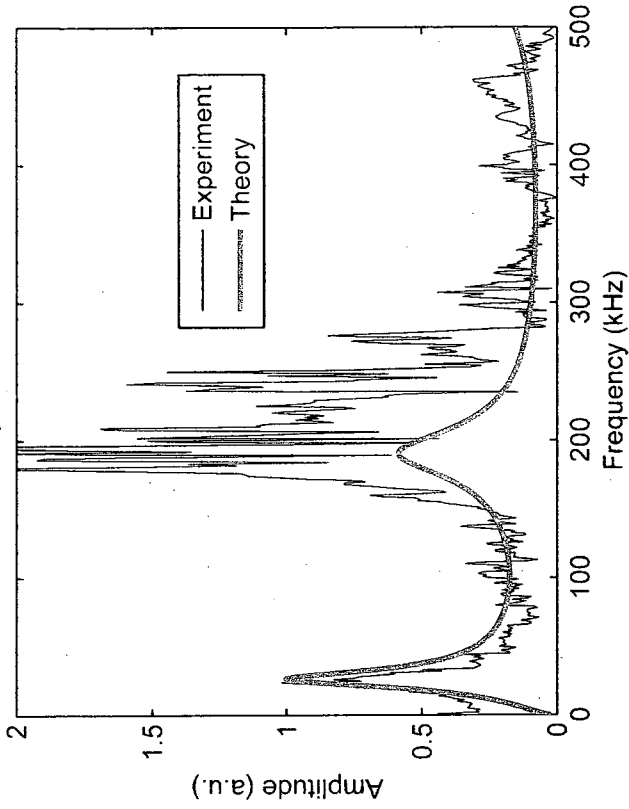
Appendix J

Experimental and theoretical responses of the cantilevers in the time and frequency domain. The amplitudes are normalized with the magnitude of the first peak:

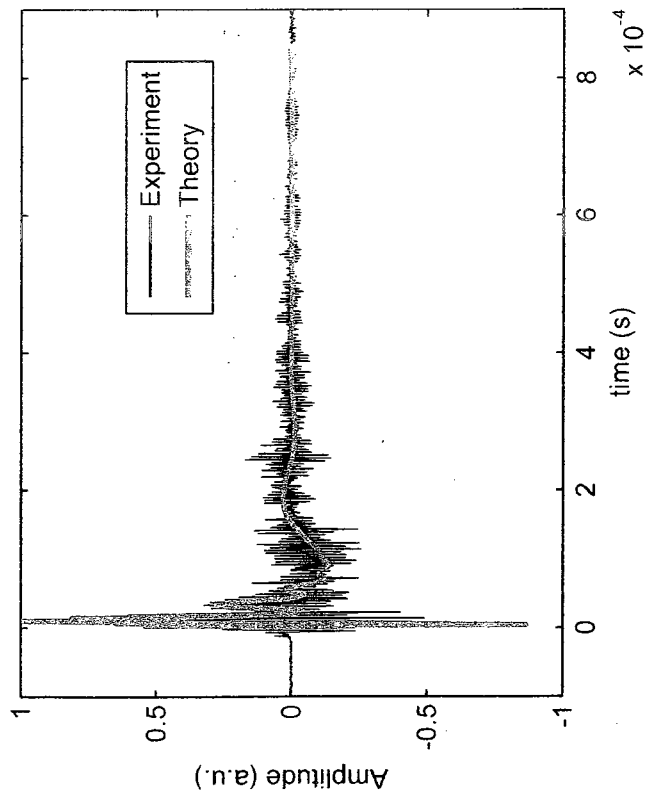
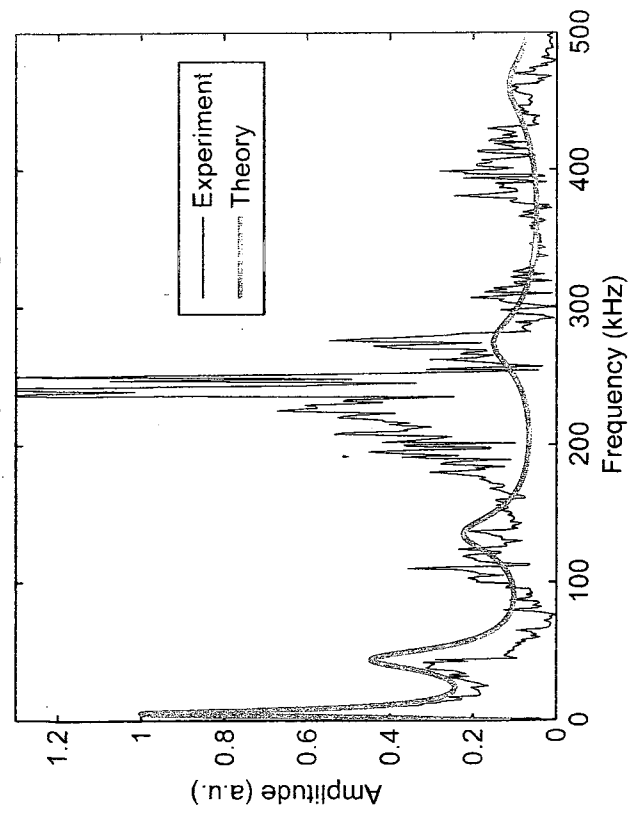




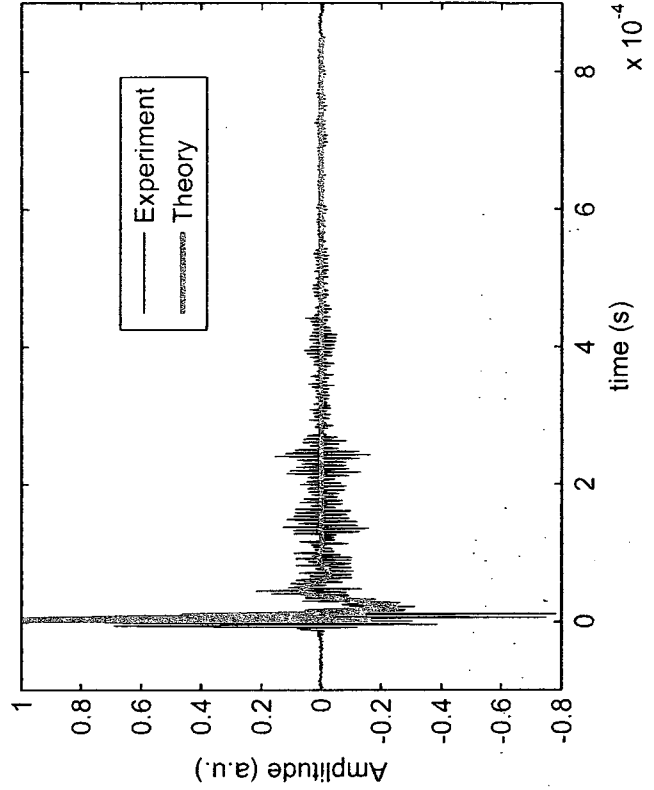
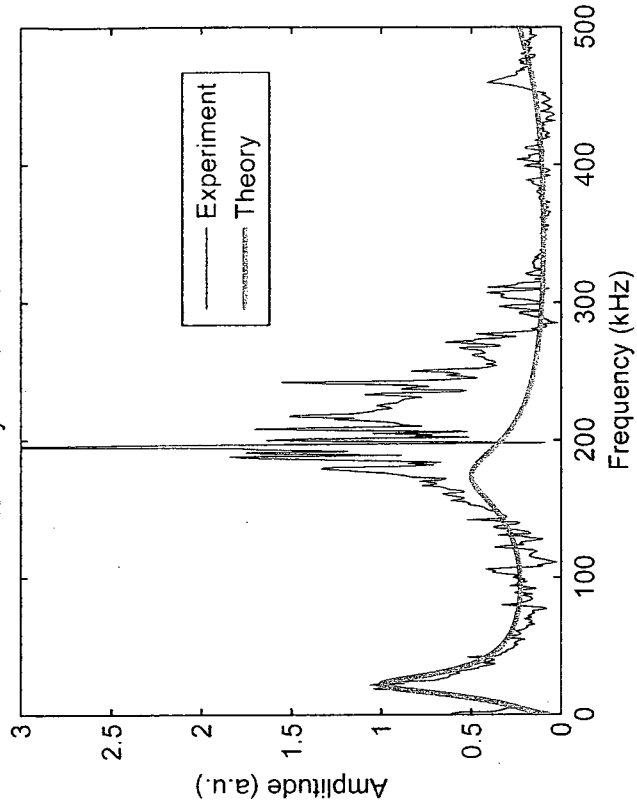
%25 Glycerine - medium



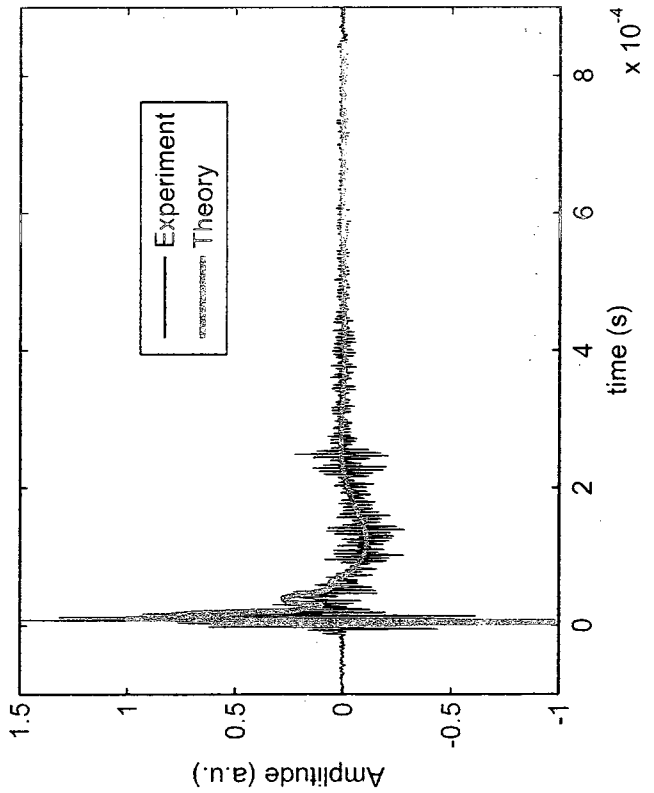
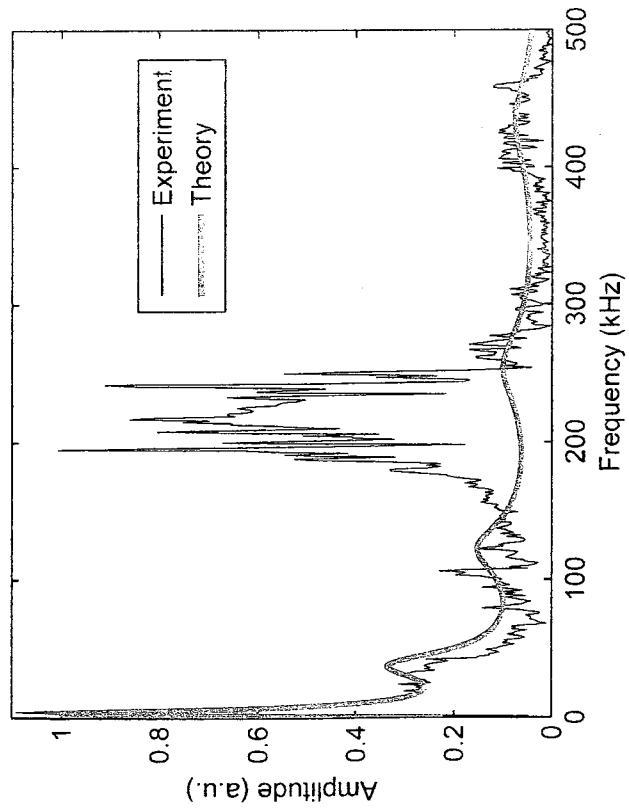
%25 Glycerine - long



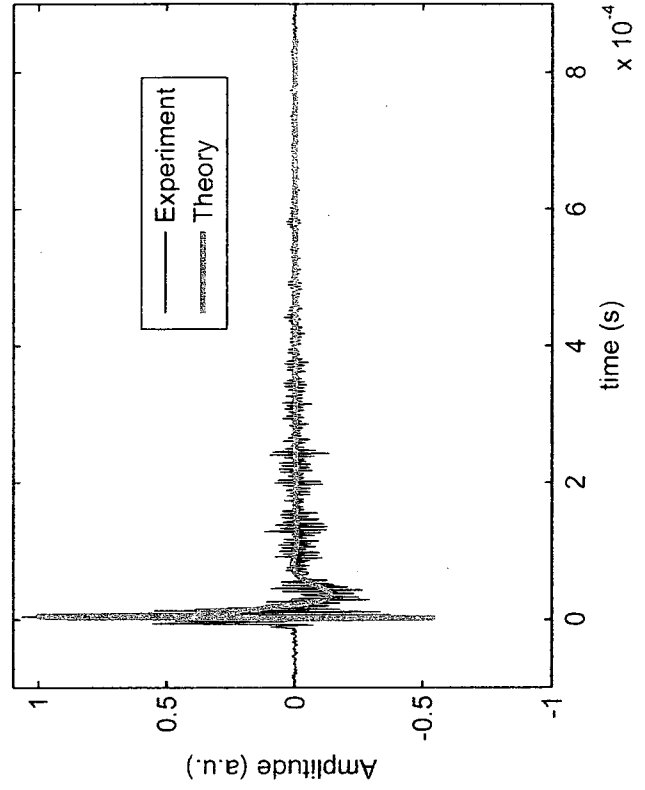
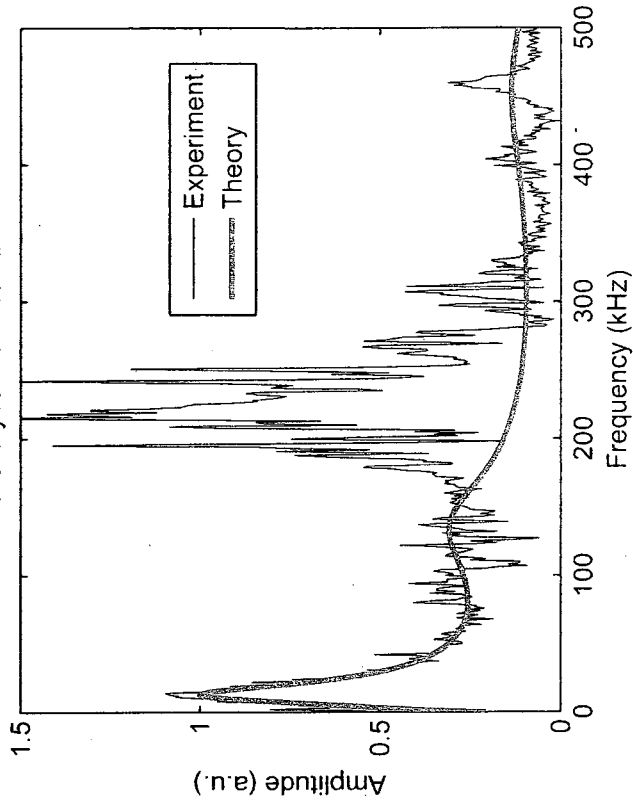
%50 Glycerine - medium



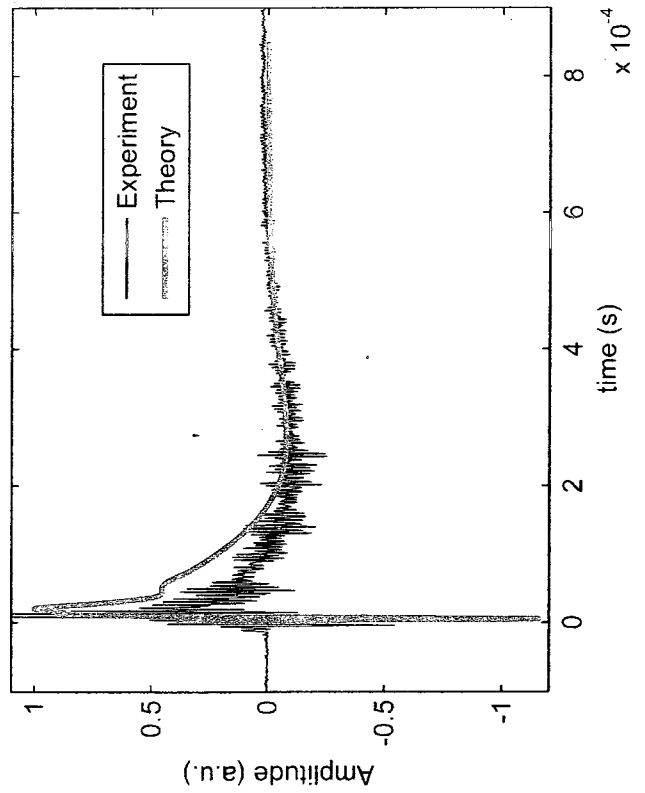
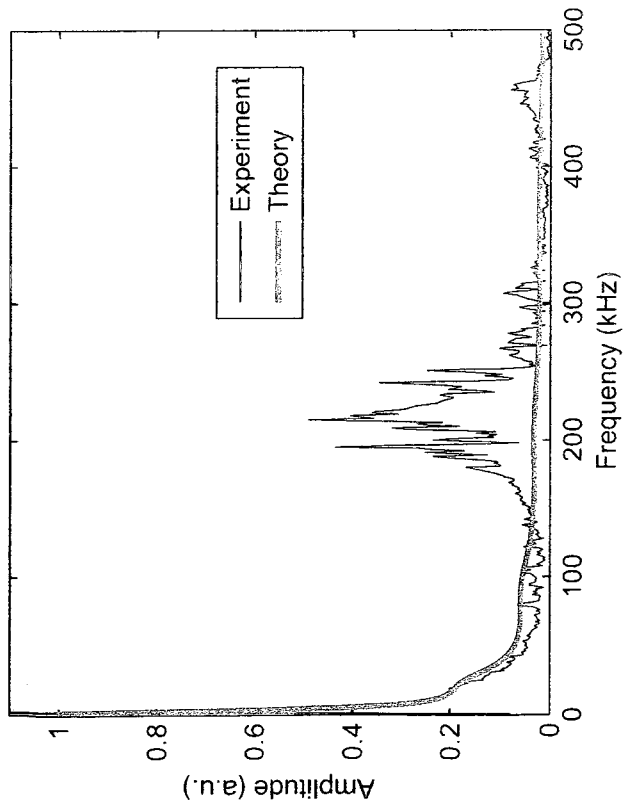
%50 Glycerine - long

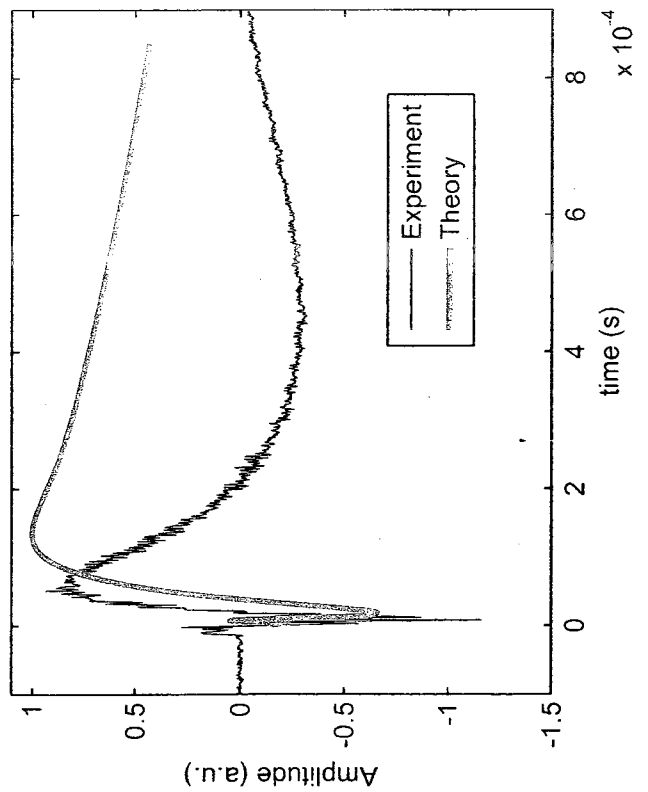
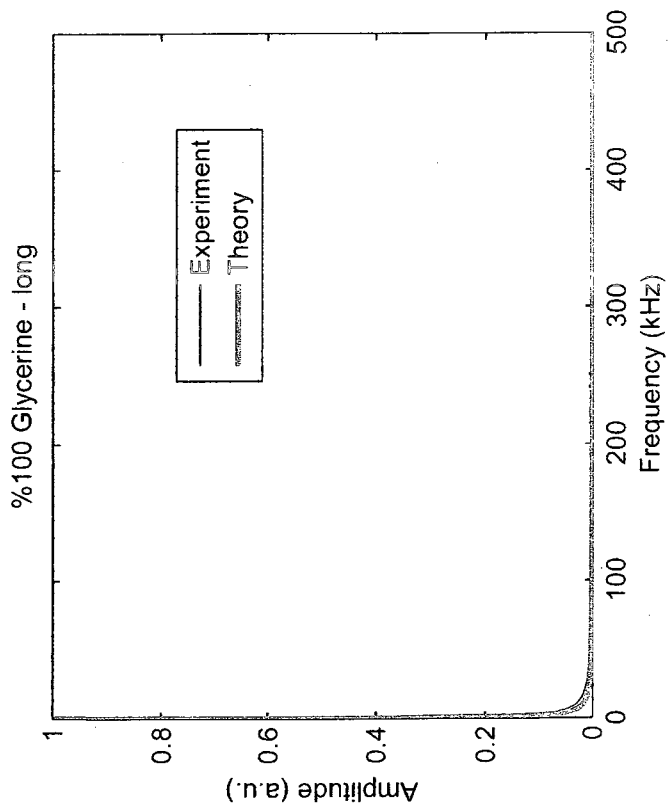
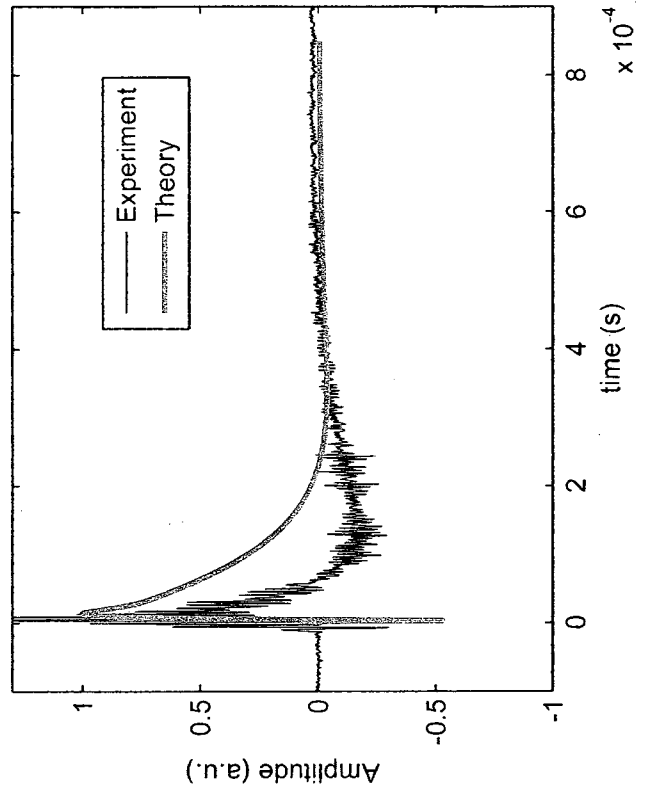
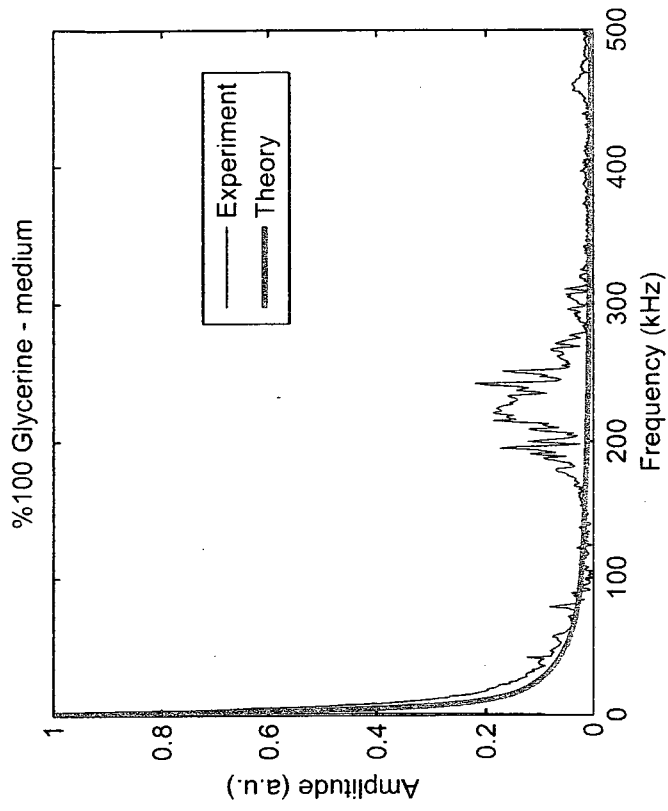


%75 Glycerine - medium



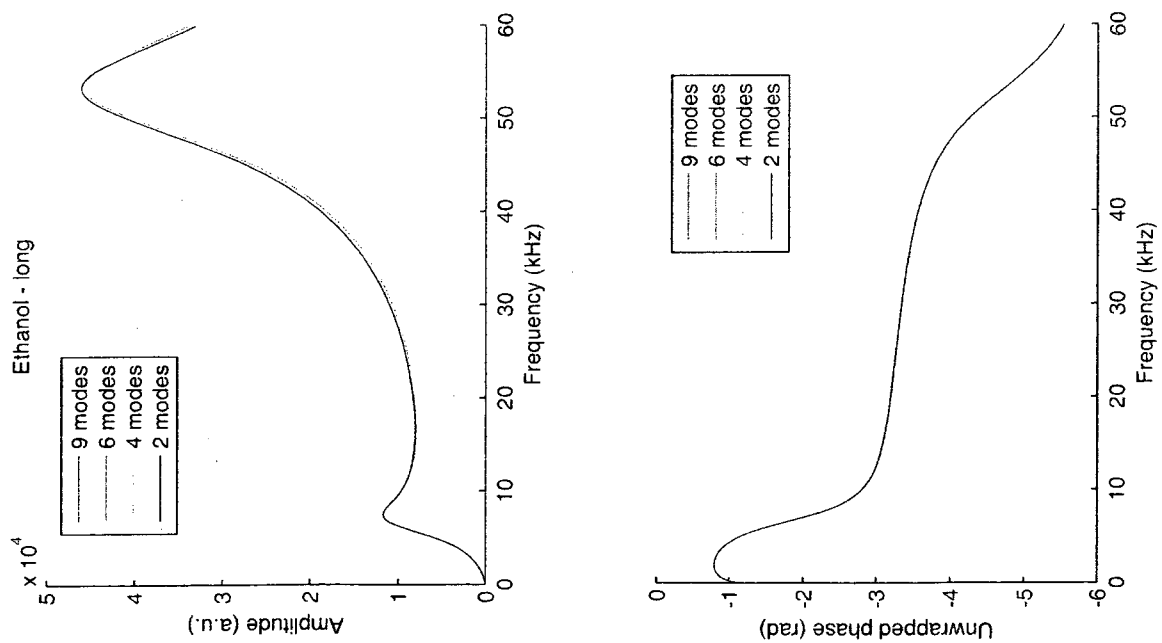
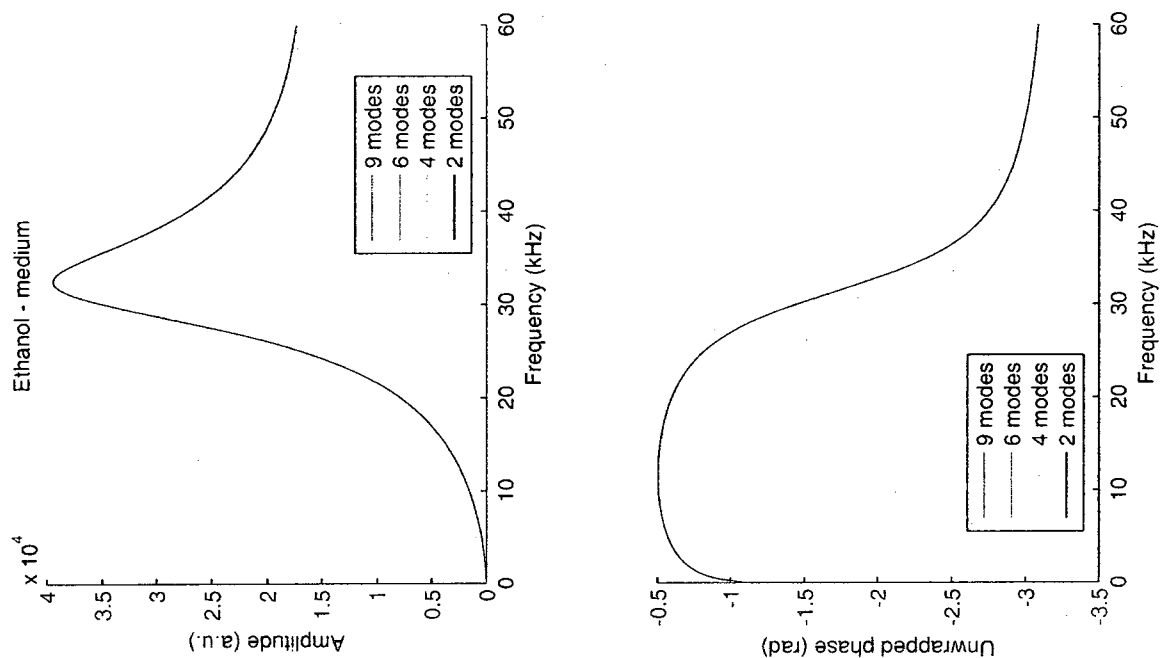
%75 Glycerine - long

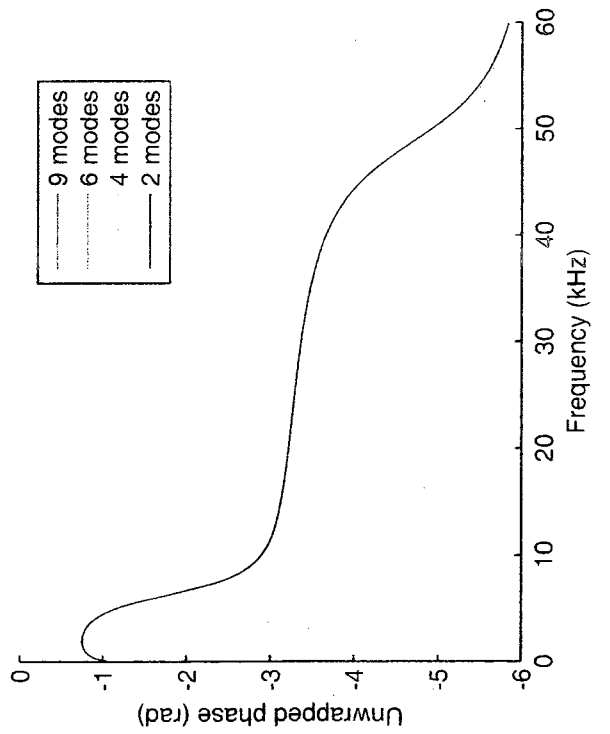
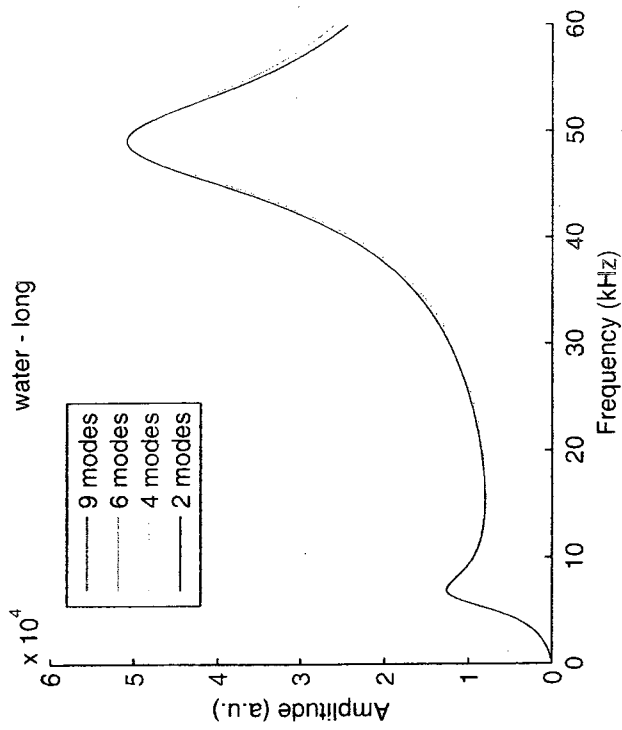
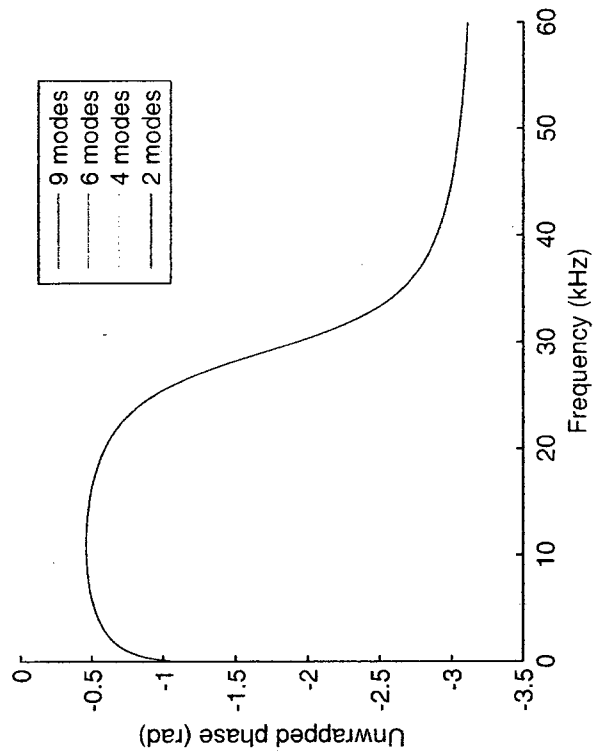
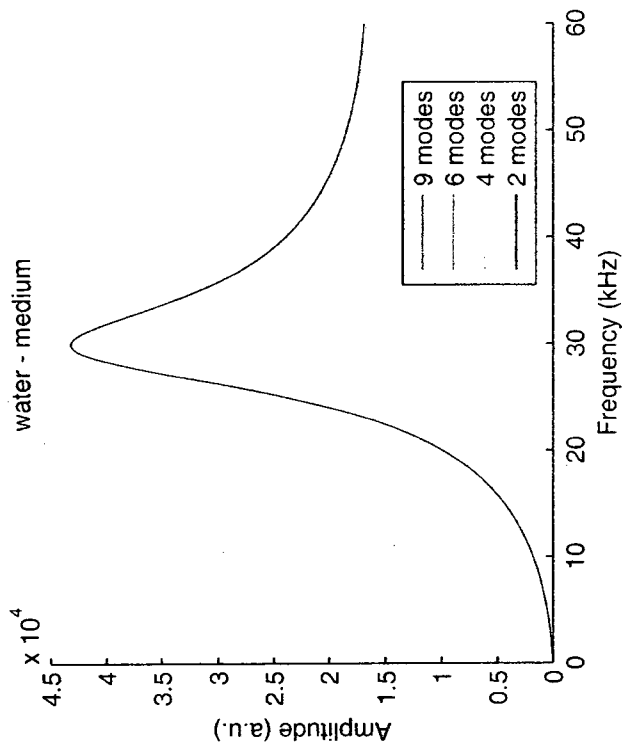


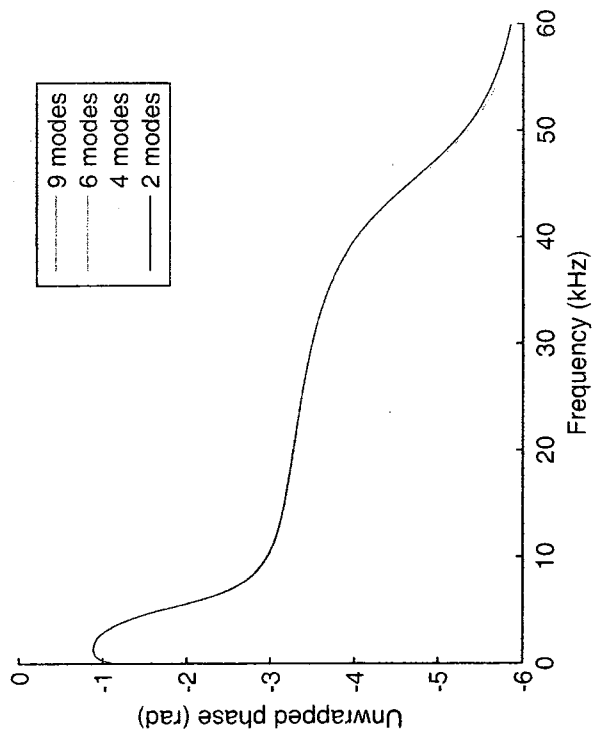
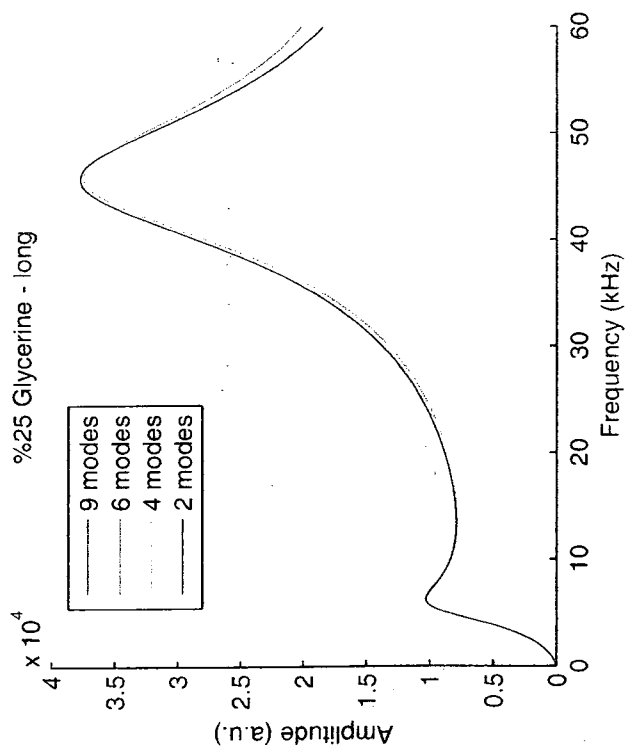
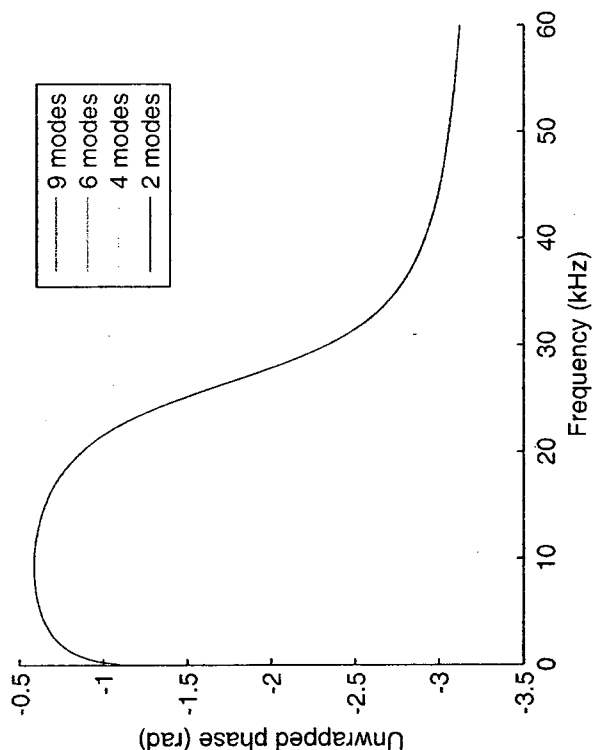
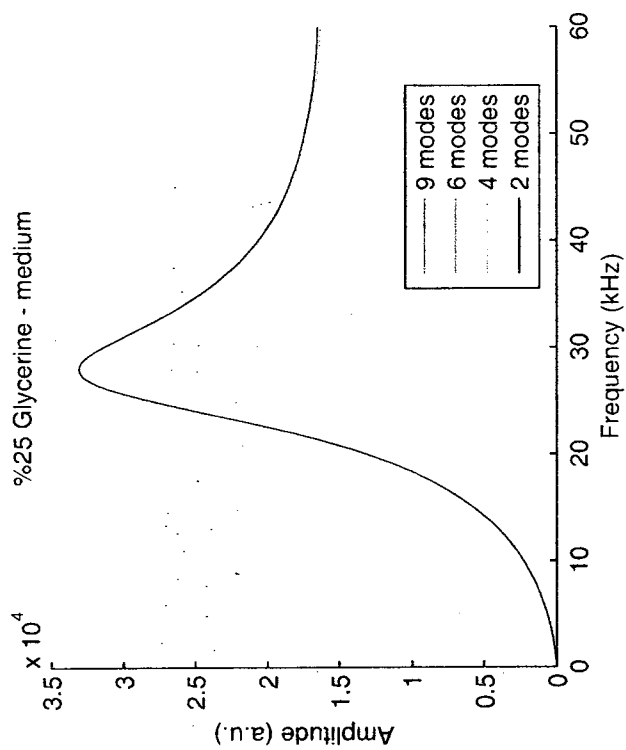


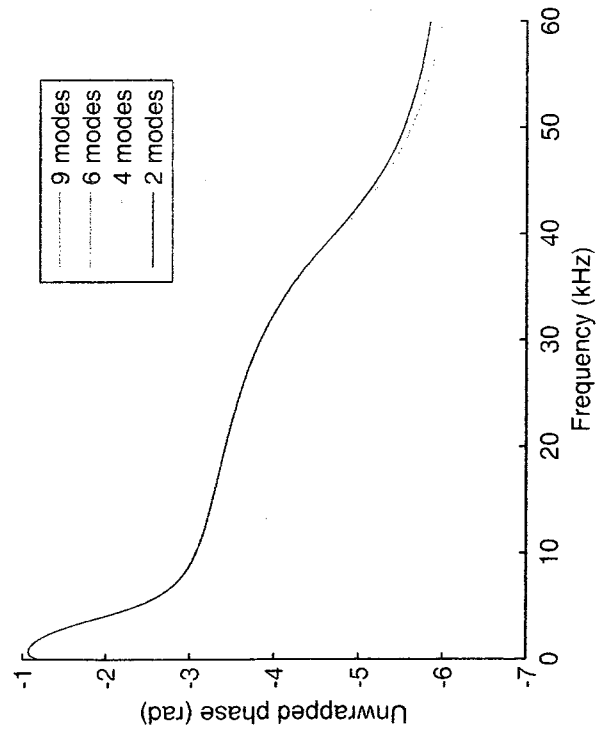
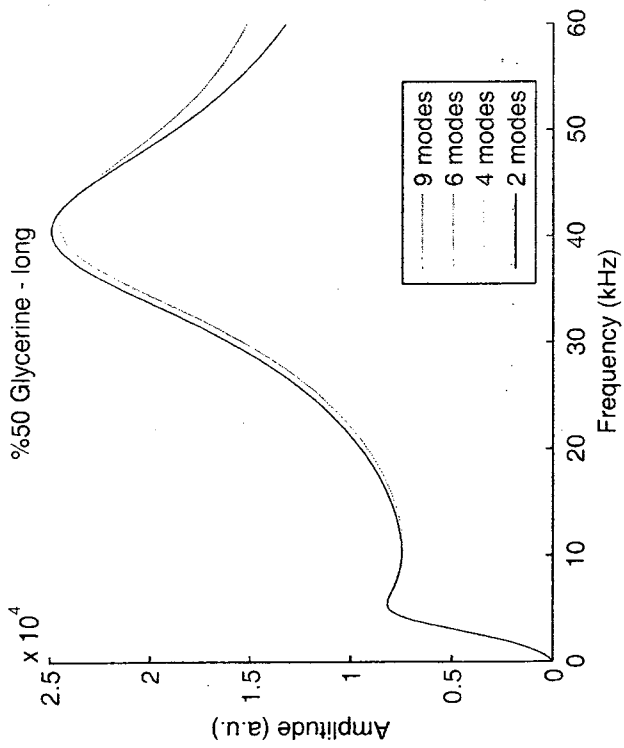
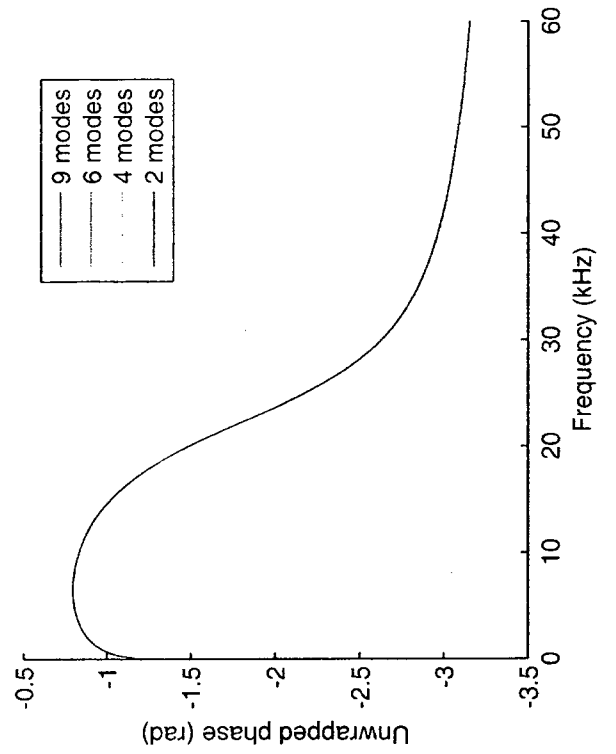
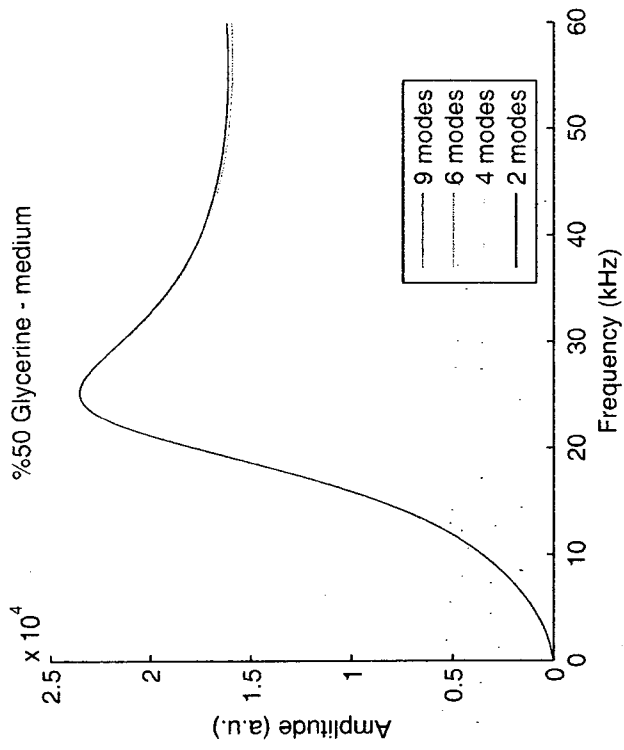
Appendix K

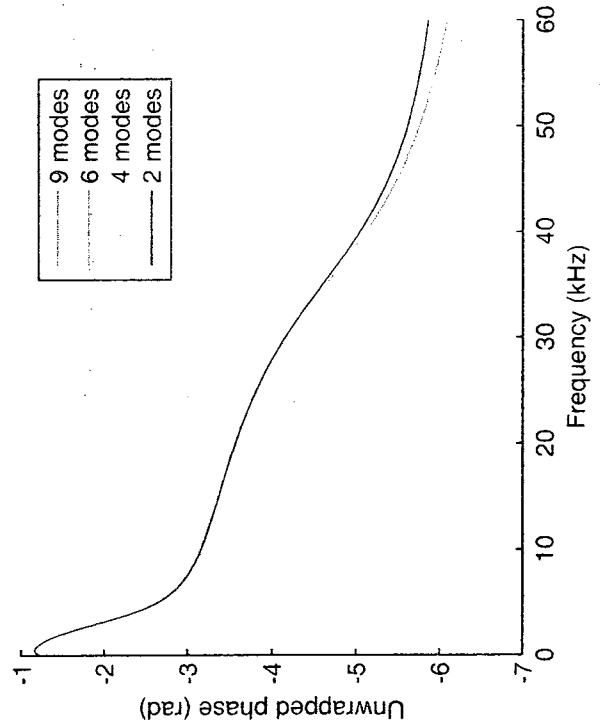
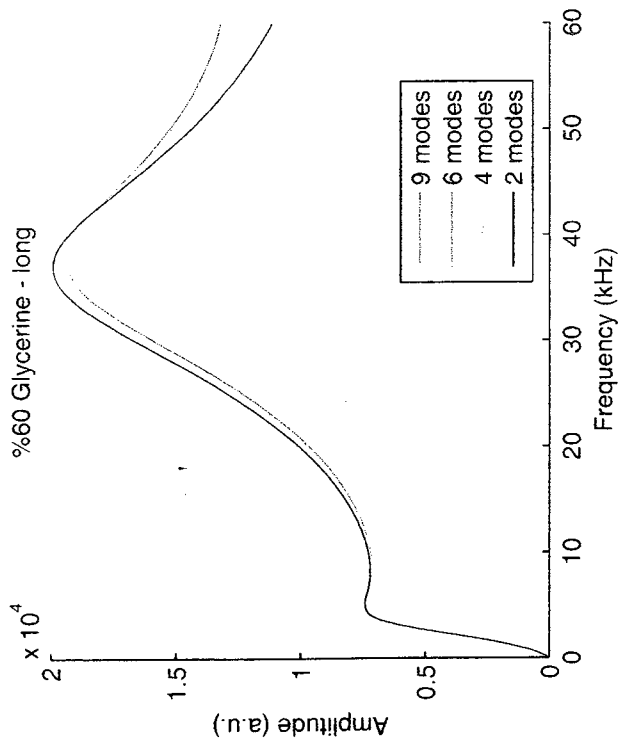
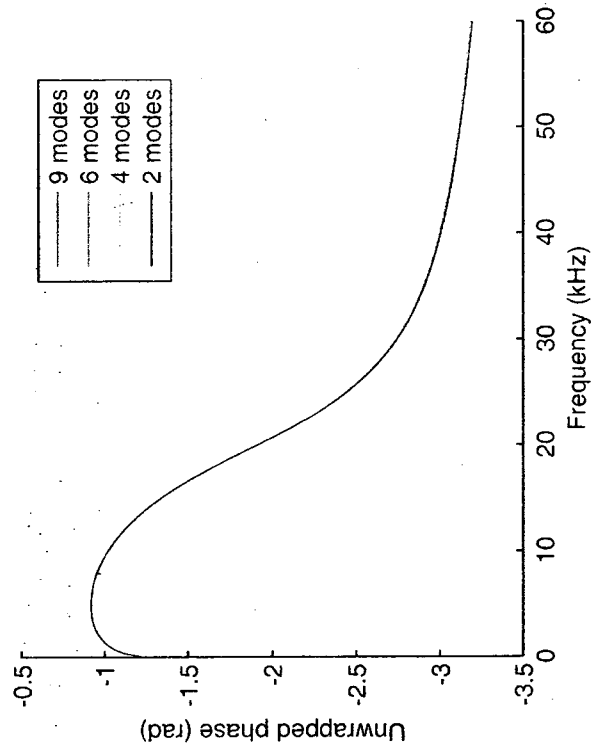
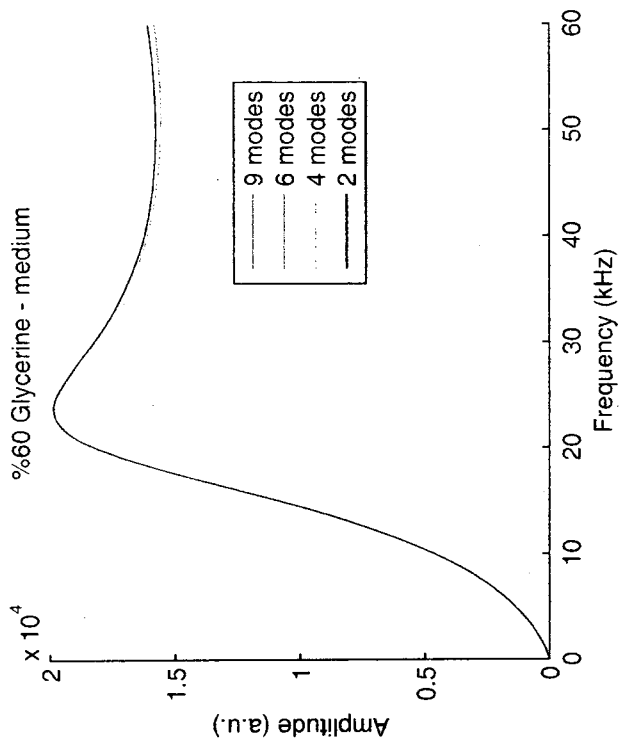
The effect of using different number of modes on the calculation of theoretical response:

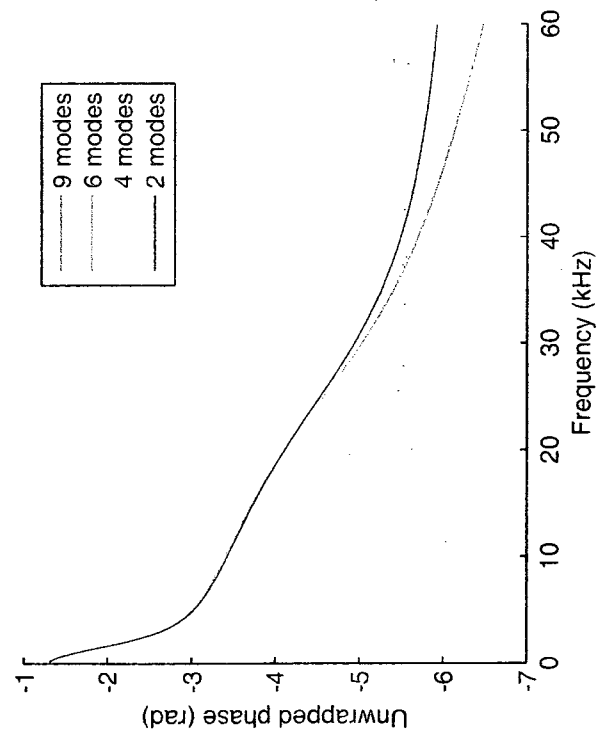
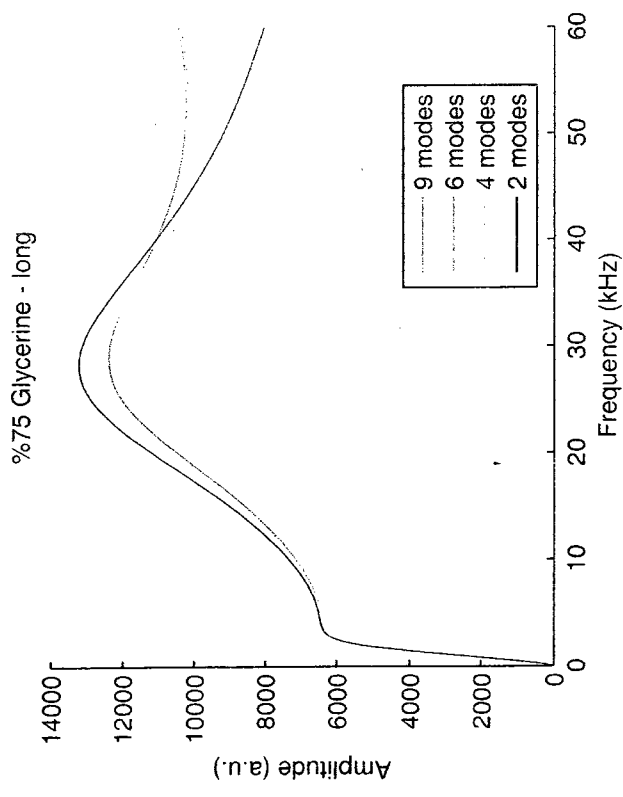
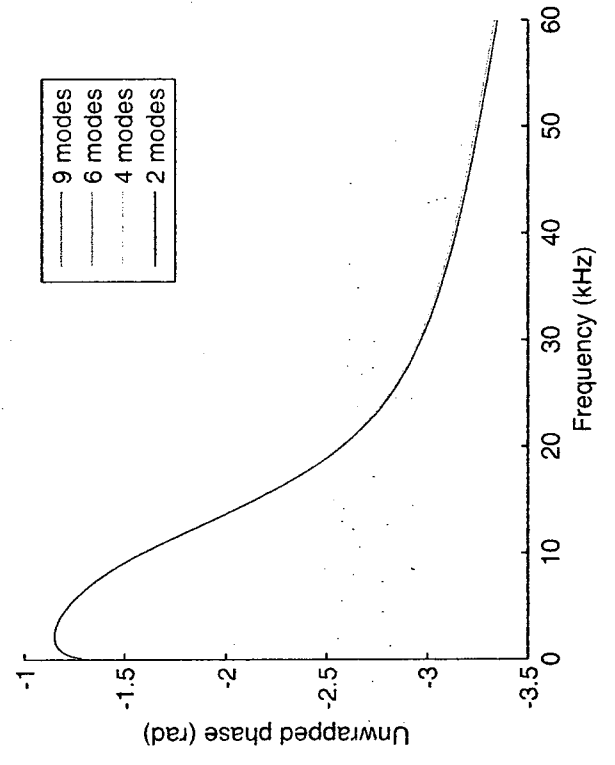
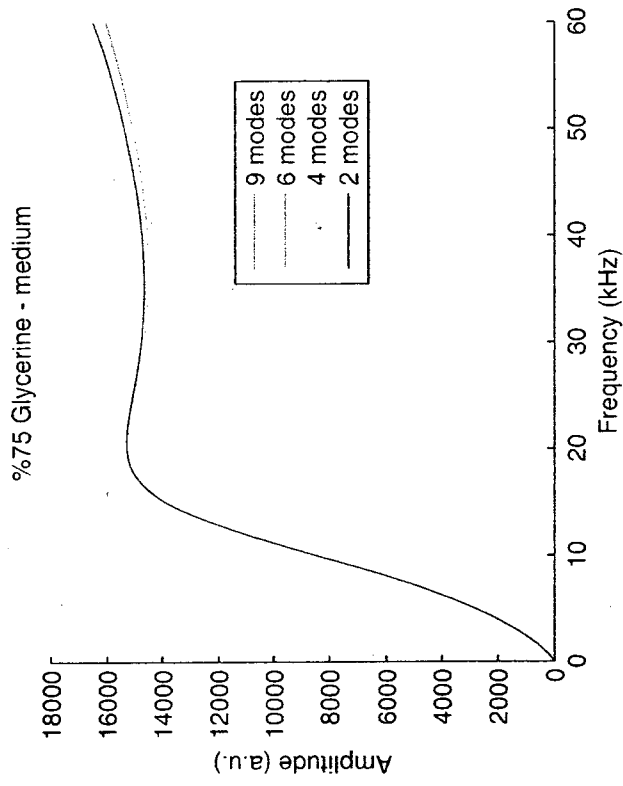


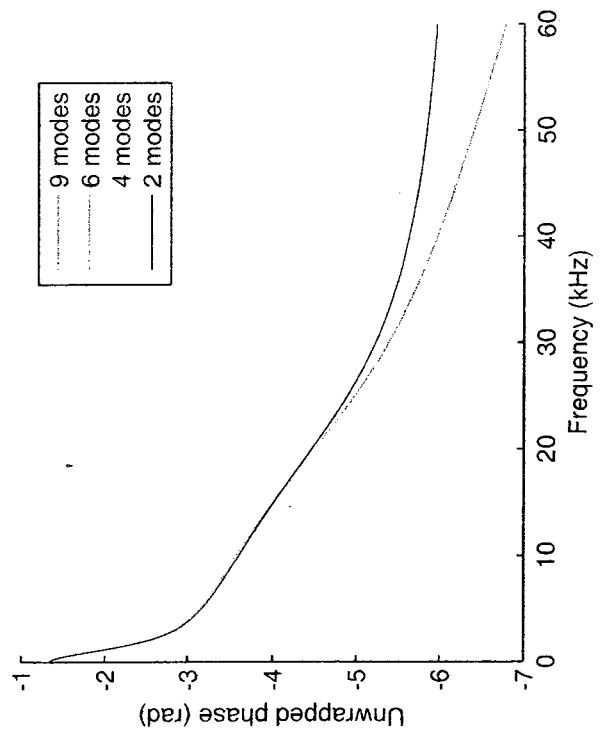
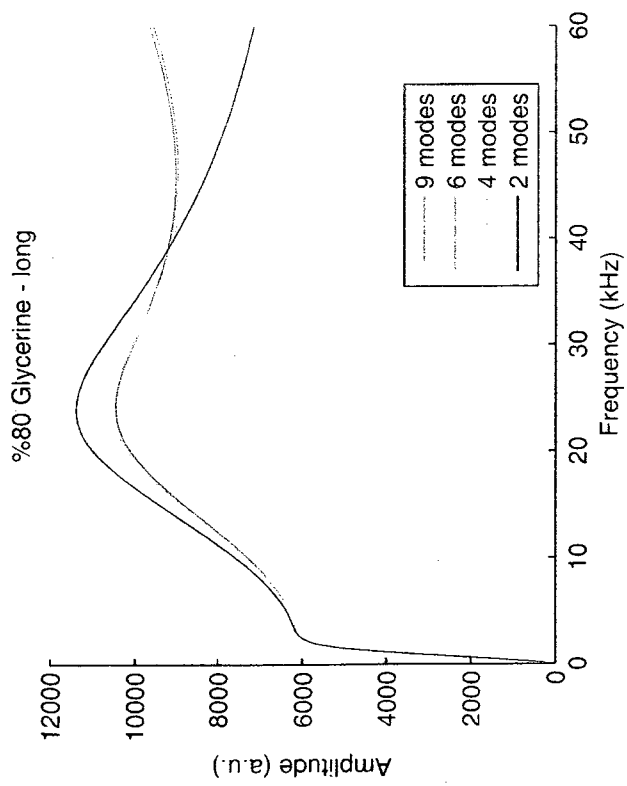
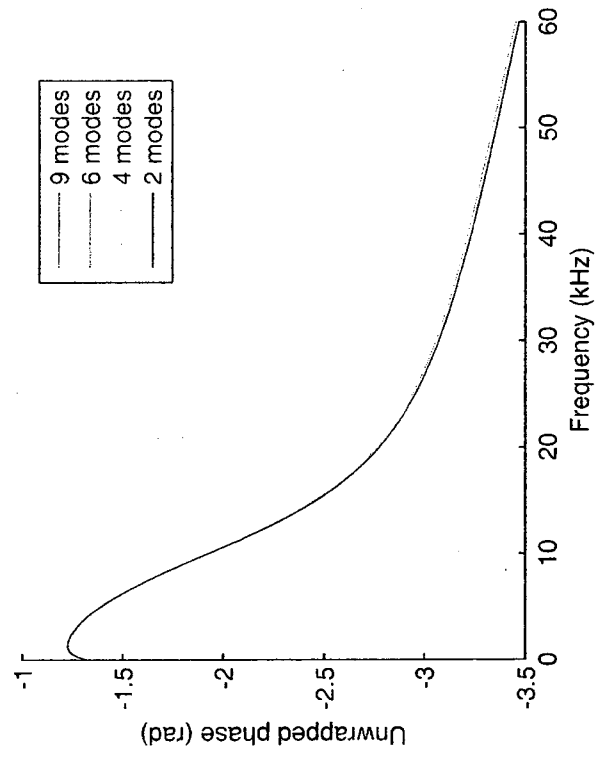
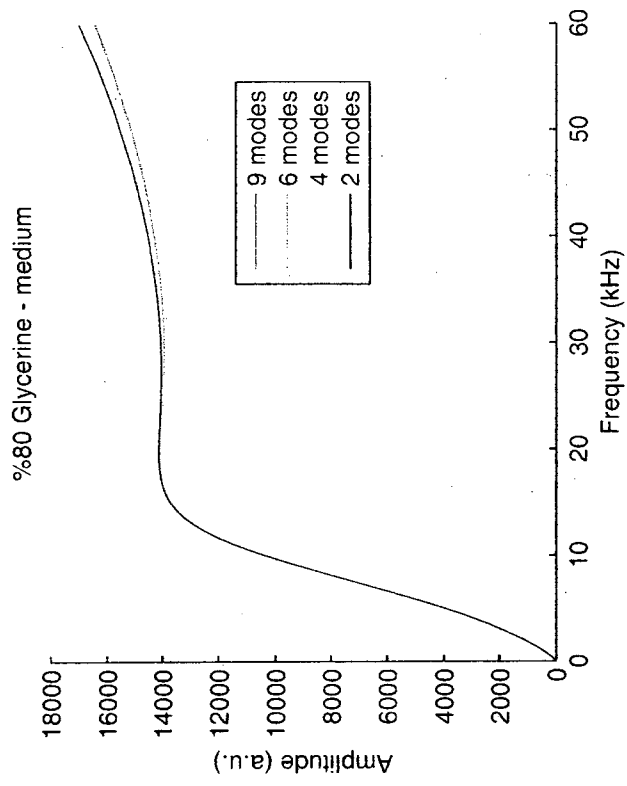


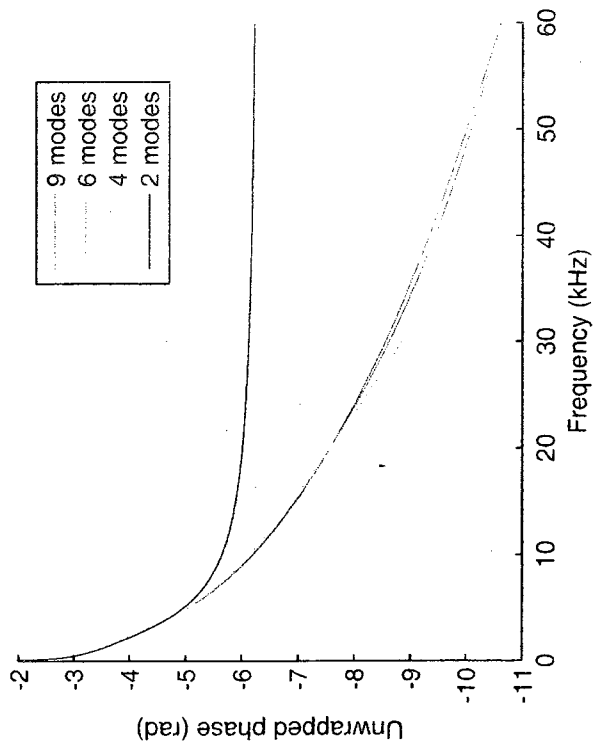
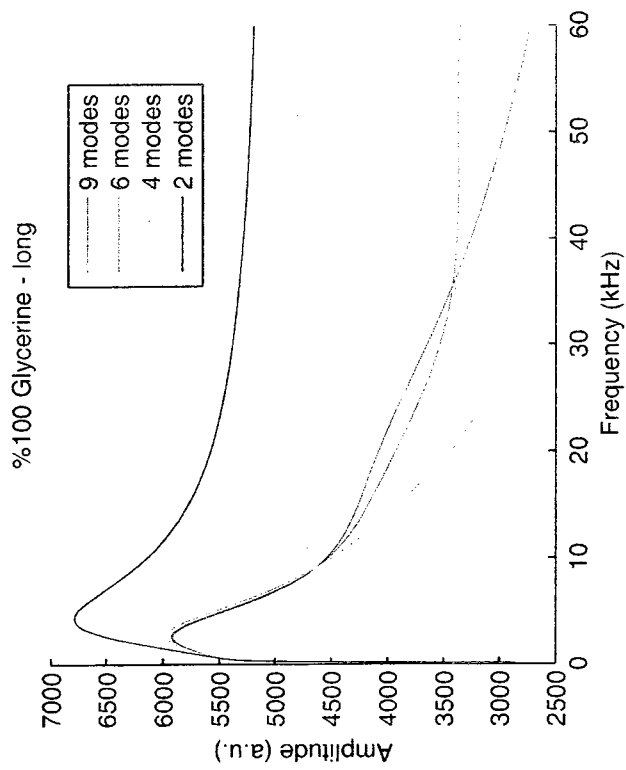
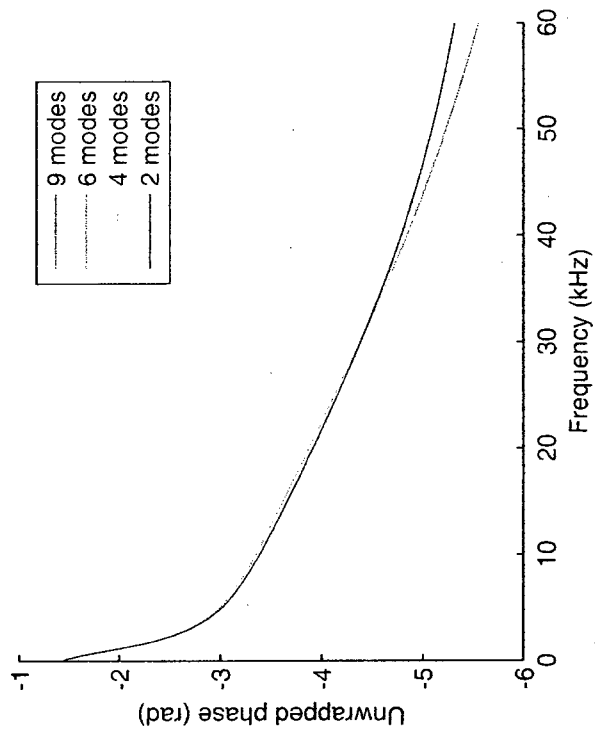
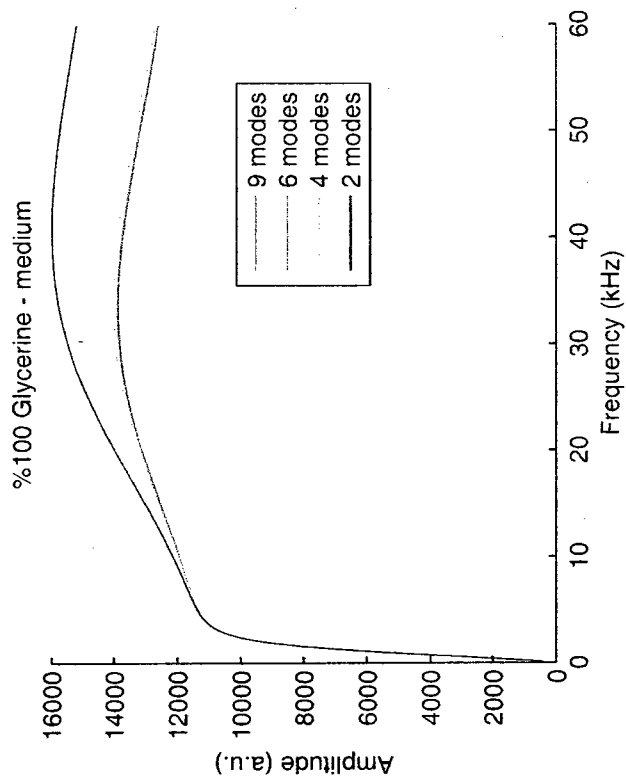












Appendix L

MATLAB code for determining the fluid's properties using the whole frequency range:

```

=====
% this code needs the files in these folders:
%           _CoUP - CaUP
%           _CoUP - CaUP_NDP
%#####
%#####
%#####
clc; clear all; close all;

cutoff_freq=40;
amps='_amp 8';
%#####
%##### cantilever properties #####
%#####
cantilever='long';
L=397e-6;
b=29e-6;
h=2.33e-6;

% cantilever='medium';
% L=197e-6;
% b=29e-6;
% h=2.255e-6;

A=b*h; I=b*h^3/12;
ro_c=2330;
E=170e9;
w_vac=(1.8751/L)^2*sqrt(E*I/ro_c/A);
%#####
%##### fluid properties #####
%#####
fluid_cel=['air      '; 'Ethanol    '; 'water      '; '%25 Glycerine '; '%50 Glycerine '; '%60 Glycerine '; '%75
Glycerine '; '%80 Glycerine '; '%100 Glycerine'];
filename_cel=['FS_air_   '; 'FS_ethanol_ '; 'FS_GW00_   '; 'FS_GW25_   '; 'FS_GW50_
'; 'FS_GW60_   '; 'FS_GW75_   '; 'FS_GW80_   '; 'FS_GW100_  '];
fluid_cel=cellstr(fluid_cel);
filename_cel=cellstr(filename_cel);

      % (1) (2) (3) (4) (5) (6) (7) (8) (9)
      % air ethanol water %25 %50 %60 %75 %80 %100
g_ro_f_cel=[ 1.184 785 997 1058 1123 1151 1191 1205 1257 ];
g_eta_f_cel=[ 0.018 1.078 0.88242 1.818 4.926 8.634 26.92 44.38 931.2 ]*1e-3;
g_scal_cel=[ 1 1 1 1 1 1 1 1 1 ]*1e5;
g_angl_cel=[ 0 0 0 0 0 0 0 0 0 ];

%#####

```

```

##### mode shapes and related parameters #####
%#####
delta_x=0.00001*L; x=[0:delta_x:L];

```

```

landa(1)=1.8751/L;   landa(2)=4.694/L;   landa(3)=7.855/L;   landa(4)=10.996/L;
landa(5)=14.137/L;   landa(6)=17.279/L;
landa(7)=(7-0.5)*pi/L; landa(8)=(8-0.5)*pi/L; landa(9)=(9-0.5)*pi/L; landa(10)=(10-0.5)*pi/L;
landa(11)=(11-0.5)*pi/L; landa(12)=(12-0.5)*pi/L;

```

```

X1=(cos(landa(1)*x)-cosh(landa(1)*x)-
((cos(landa(1)*L)+cosh(landa(1)*L))/(sin(landa(1)*L)+sinh(landa(1)*L)))*(sin(landa(1)*x)-
sinh(landa(1)*x)));

```

```

X2=(cos(landa(2)*x)-cosh(landa(2)*x)-
((cos(landa(2)*L)+cosh(landa(2)*L))/(sin(landa(2)*L)+sinh(landa(2)*L)))*(sin(landa(2)*x)-
sinh(landa(2)*x)));

```

```

X3=(cos(landa(3)*x)-cosh(landa(3)*x)-
((cos(landa(3)*L)+cosh(landa(3)*L))/(sin(landa(3)*L)+sinh(landa(3)*L)))*(sin(landa(3)*x)-
sinh(landa(3)*x)));

```

```

X4=(cos(landa(4)*x)-cosh(landa(4)*x)-
((cos(landa(4)*L)+cosh(landa(4)*L))/(sin(landa(4)*L)+sinh(landa(4)*L)))*(sin(landa(4)*x)-
sinh(landa(4)*x)));

```

```

X5=(cos(landa(5)*x)-cosh(landa(5)*x)-
((cos(landa(5)*L)+cosh(landa(5)*L))/(sin(landa(5)*L)+sinh(landa(5)*L)))*(sin(landa(5)*x)-
sinh(landa(5)*x)));

```

```

X6=(cos(landa(6)*x)-cosh(landa(6)*x)-
((cos(landa(6)*L)+cosh(landa(6)*L))/(sin(landa(6)*L)+sinh(landa(6)*L)))*(sin(landa(6)*x)-
sinh(landa(6)*x)));

```

```

X7=(cos(landa(7)*x)-cosh(landa(7)*x)-
((cos(landa(7)*L)+cosh(landa(7)*L))/(sin(landa(7)*L)+sinh(landa(7)*L)))*(sin(landa(7)*x)-
sinh(landa(7)*x)));

```

```

X8=(cos(landa(8)*x)-cosh(landa(8)*x)-
((cos(landa(8)*L)+cosh(landa(8)*L))/(sin(landa(8)*L)+sinh(landa(8)*L)))*(sin(landa(8)*x)-
sinh(landa(8)*x)));

```

```

X9=(cos(landa(9)*x)-cosh(landa(9)*x)-
((cos(landa(9)*L)+cosh(landa(9)*L))/(sin(landa(9)*L)+sinh(landa(9)*L)))*(sin(landa(9)*x)-
sinh(landa(9)*x)));

```

```

X11=landa(1)*((-sin(landa(1)*x)-sinh(landa(1)*x)-
((cos(landa(1)*L)+cosh(landa(1)*L))/(sin(landa(1)*L)+sinh(landa(1)*L)))*(cos(landa(1)*x)-
cosh(landa(1)*x)));

```

```

X12=landa(2)*((-sin(landa(2)*x)-sinh(landa(2)*x)-
((cos(landa(2)*L)+cosh(landa(2)*L))/(sin(landa(2)*L)+sinh(landa(2)*L)))*(cos(landa(2)*x)-
cosh(landa(2)*x)));

```

```

X13=landa(3)*((-sin(landa(3)*x)-sinh(landa(3)*x)-
((cos(landa(3)*L)+cosh(landa(3)*L))/(sin(landa(3)*L)+sinh(landa(3)*L)))*(cos(landa(3)*x)-
cosh(landa(3)*x)));

```

```

X14=landa(4)*((-sin(landa(4)*x)-sinh(landa(4)*x)-
((cos(landa(4)*L)+cosh(landa(4)*L))/(sin(landa(4)*L)+sinh(landa(4)*L)))*(cos(landa(4)*x)-
cosh(landa(4)*x)));

```

```

X15=landa(5)*((-sin(landa(5)*x)-sinh(landa(5)*x)-
((cos(landa(5)*L)+cosh(landa(5)*L))/(sin(landa(5)*L)+sinh(landa(5)*L)))*(cos(landa(5)*x)-
cosh(landa(5)*x)));

```

```

X16=landa(6)*((-sin(landa(6)*x)-sinh(landa(6)*x)-
((cos(landa(6)*L)+cosh(landa(6)*L))/(sin(landa(6)*L)+sinh(landa(6)*L)))*(cos(landa(6)*x)-
cosh(landa(6)*x)));

```

```

X17=landa(7)*((-sin(landa(7)*x)-sinh(landa(7)*x)-
((cos(landa(7)*L)+cosh(landa(7)*L))/(sin(landa(7)*L)+sinh(landa(7)*L)))*(cos(landa(7)*x)-
cosh(landa(7)*x)));
X18=landa(8)*((-sin(landa(8)*x)-sinh(landa(8)*x)-
((cos(landa(8)*L)+cosh(landa(8)*L))/(sin(landa(8)*L)+sinh(landa(8)*L)))*(cos(landa(8)*x)-
cosh(landa(8)*x)));
X19=landa(9)*((-sin(landa(9)*x)-sinh(landa(9)*x)-
((cos(landa(9)*L)+cosh(landa(9)*L))/(sin(landa(9)*L)+sinh(landa(9)*L)))*(cos(landa(9)*x)-
cosh(landa(9)*x)));

```

```

X11=(X11/X1(length(X1)));
X12=(X12/X2(length(X2)));
X13=(X13/X3(length(X3)));
X14=(X14/X4(length(X4)));
X15=(X15/X5(length(X5)));
X16=(X16/X6(length(X6)));
X17=(X17/X7(length(X7)));
X18=(X18/X8(length(X8)));
X19=(X19/X9(length(X9)));
X1=(X1/X1(length(X1)));
X2=(X2/X2(length(X2)));
X3=(X3/X3(length(X3)));
X4=(X4/X4(length(X4)));
X5=(X5/X5(length(X5)));
X6=(X6/X6(length(X6)));
X7=(X7/X7(length(X7)));
X8=(X8/X8(length(X8)));
X9=(X9/X9(length(X9)));

```

```

alpha(1)=sum(X1.*X1)*delta_x/L; beta(1)=sum(X1)*delta_x/L;
alpha(2)=sum(X2.*X2)*delta_x/L; beta(2)=sum(X2)*delta_x/L;
alpha(3)=sum(X3.*X3)*delta_x/L; beta(3)=sum(X3)*delta_x/L;
alpha(4)=sum(X4.*X4)*delta_x/L; beta(4)=sum(X4)*delta_x/L;
alpha(5)=sum(X5.*X5)*delta_x/L; beta(5)=sum(X5)*delta_x/L;
alpha(6)=sum(X6.*X6)*delta_x/L; beta(6)=sum(X6)*delta_x/L;
alpha(7)=sum(X7.*X7)*delta_x/L; beta(7)=sum(X7)*delta_x/L;
alpha(8)=sum(X8.*X8)*delta_x/L; beta(8)=sum(X8)*delta_x/L;
alpha(9)=sum(X9.*X9)*delta_x/L; beta(9)=sum(X9)*delta_x/L;

```

```

clear delta_x X1 X2 X3 X4 X5 X6 X7 X8 X9;
%#####
%#####
%#####
for fluid_N=2:2
tic
fluid=char(fluid_cel(fluid_N))
filename=char(filename_cel(fluid_N));
g_ro_f=g_ro_f_cel(fluid_N);
g_eta_f=g_eta_f_cel(fluid_N);
g_scal=g_scal_cel(fluid_N);
g_angl=g_angl_cel(fluid_N);
%#####
%##### finding the proper fitting parameters of modified file #####
%#####
% data management %%%

```

```

filename_NDP=[filename cantilever amps '_CoUP - CaUP_NDP.dat'];
exp_data=load(filename_NDP);
indices = find(cutoff_freq<exp_data(:,1) & exp_data(:,1)<=100); exp_data(indices,:)=[];
f_3=exp_data(:,1)'; exp_amp=exp_data(:,2); exp_ang=exp_data(:,3);
omega_3=2*pi*f_3*1000; omega2_3=omega_3.^2;
clear filename_NDP exp_data.indices;

% finding the best scal & angl %%%
g_Tb=(g_ro_f*b)/(ro_c*h);
g_Reb=(g_ro_f*w_vac*b^2)/(4*g_eta_f);
Ya_0=[g_scal];
Yp_0=[g_angl];

Re = @(X,Xf) X*Xf/w_vac;
GAMA_circ = @(X,Xf)1+(4*i*besselk(1,(-i*sqrt(i*Re(X,Xf)))))/(sqrt(i*Re(X,Xf)).*besselk(0,(-i*sqrt(i*Re(X,Xf)))));
tao = @(X,Xf)log10(Re(X,Xf));
OMEGA_r = @(X,Xf)(0.91324-0.48274*(tao(X,Xf))+0.46842*(tao(X,Xf)).^2-0.12886*(tao(X,Xf)).^3+0.044055*(tao(X,Xf)).^4-0.0035117*(tao(X,Xf)).^5+0.00069085*(tao(X,Xf)).^6)/(1-0.56964*(tao(X,Xf))+0.48690*(tao(X,Xf)).^2-0.13444*(tao(X,Xf)).^3+0.045155*(tao(X,Xf)).^4-0.0035862*(tao(X,Xf)).^5+0.00069085*(tao(X,Xf)).^6);
OMEGA_i = @(X,Xf)(-0.024134-0.029256*(tao(X,Xf))+0.016294*(tao(X,Xf)).^2-0.00010961*(tao(X,Xf)).^3+0.000064577*(tao(X,Xf)).^4-0.000044510*(tao(X,Xf)).^5)/(1-0.597020*(tao(X,Xf))+0.551820*(tao(X,Xf)).^2-0.18357000*(tao(X,Xf)).^3+0.079156000*(tao(X,Xf)).^4-0.014369000*(tao(X,Xf)).^5+0.0028361*(tao(X,Xf)).^6);
OMEGA = @(X,Xf)OMEGA_r(X,Xf) + OMEGA_i(X,Xf)*i;
GAMA_rect = @(X,Xf)OMEGA(X,Xf) .* GAMA_circ(X,Xf);
ACO1=@(X,Xf)(omega2_3.*(1+(pi*X(1)/4)*GAMA_rect(X(2),Xf))*beta(1))./(w_vac^2*(landa(1)/landa(1))^4*alpha(1)-omega2_3.*(1+(pi*X(1)/4)*GAMA_rect(X(2),Xf))*alpha(1));
ACO2=@(X,Xf)(omega2_3.*(1+(pi*X(1)/4)*GAMA_rect(X(2),Xf))*beta(2))./(w_vac^2*(landa(2)/landa(1))^4*alpha(2)-omega2_3.*(1+(pi*X(1)/4)*GAMA_rect(X(2),Xf))*alpha(2));
ACO3=@(X,Xf)(omega2_3.*(1+(pi*X(1)/4)*GAMA_rect(X(2),Xf))*beta(3))./(w_vac^2*(landa(3)/landa(1))^4*alpha(3)-omega2_3.*(1+(pi*X(1)/4)*GAMA_rect(X(2),Xf))*alpha(3));
ACO4=@(X,Xf)(omega2_3.*(1+(pi*X(1)/4)*GAMA_rect(X(2),Xf))*beta(4))./(w_vac^2*(landa(4)/landa(1))^4*alpha(4)-omega2_3.*(1+(pi*X(1)/4)*GAMA_rect(X(2),Xf))*alpha(4));
ACO5=@(X,Xf)(omega2_3.*(1+(pi*X(1)/4)*GAMA_rect(X(2),Xf))*beta(5))./(w_vac^2*(landa(5)/landa(1))^4*alpha(5)-omega2_3.*(1+(pi*X(1)/4)*GAMA_rect(X(2),Xf))*alpha(5));
ACO6=@(X,Xf)(omega2_3.*(1+(pi*X(1)/4)*GAMA_rect(X(2),Xf))*beta(6))./(w_vac^2*(landa(6)/landa(1))^4*alpha(6)-omega2_3.*(1+(pi*X(1)/4)*GAMA_rect(X(2),Xf))*alpha(6));
ACO7=@(X,Xf)(omega2_3.*(1+(pi*X(1)/4)*GAMA_rect(X(2),Xf))*beta(7))./(w_vac^2*(landa(7)/landa(1))^4*alpha(7)-omega2_3.*(1+(pi*X(1)/4)*GAMA_rect(X(2),Xf))*alpha(7));
ACO8=@(X,Xf)(omega2_3.*(1+(pi*X(1)/4)*GAMA_rect(X(2),Xf))*beta(8))./(w_vac^2*(landa(8)/landa(1))^4*alpha(8)-omega2_3.*(1+(pi*X(1)/4)*GAMA_rect(X(2),Xf))*alpha(8));
ACO9=@(X,Xf)(omega2_3.*(1+(pi*X(1)/4)*GAMA_rect(X(2),Xf))*beta(9))./(w_vac^2*(landa(9)/landa(1))^4*alpha(9)-omega2_3.*(1+(pi*X(1)/4)*GAMA_rect(X(2),Xf))*alpha(9));
ACO_response9=@(X,Xf)
[ACO1(X,Xf)*X11(length(X11))+ACO2(X,Xf)*X12(length(X12))+ACO3(X,Xf)*X13(length(X13))+ACO4(X,Xf)*X14(length(X14))+ACO5(X,Xf)*X15(length(X15))+ACO6(X,Xf)*X16(length(X16))+ACO7(X,Xf)*X17(length(X17))+ACO8(X,Xf)*X18(length(X18))+ACO9(X,Xf)*X19(length(X19))];
AAA=@(X,Xf) abs(ACO_response9([g_Tb g_Reb],Xf))/X;
BBB=@(X,Xf)angle(ACO_response9(X,Xf));
CCC=@(X,Xf)unwrap(BBB([g_Tb g_Reb],Xf))-X;

```

```

[Ya,ra,Ja] = nlinfit(omega_3,exp_amp,AAA,Ya_0); clear ra Ja;
[Yp,rp,Ip] = nlinfit(omega_3,exp_ang,CCC,Yp_0); clear rp Ip;

scal_best=Ya;
angl_best=Yp;
clear g Tb g_Reb Ya_0 Yp_0 Ya Yp Re GAMA_circ tao OMEGA_r OMEGA_i OMEGA GAMA_rect
ACO1 ACO2 ACO3 ACO4 ACO5 ACO6 ACO7 ACO8 ACO9 ACO_response9 AAA BBB CCC;

% finding the best ro and eta for amplitude and phase responses %%%
g_Tb=(g_ro_f*b)/(ro_c*h);
g_Reb=(g_ro_f*w_vac*b^2)/(4*g_eta_f);
Ya_0=[g_Tb g_Reb scal_best];
Yp_0=[g_Tb g_Reb angl_best];

Re = @(X,Xf) X*Xf/w_vac;
GAMA_circ = @(X,Xf)1+(4*i*besselk(1,(-i*sqrt(i*Re(X,Xf)))))/(sqrt(i*Re(X,Xf)).*besselk(0,(-i*sqrt(i*Re(X,Xf)))));
tao = @(X,Xf)log10(Re(X,Xf));
OMEGA_r = @(X,Xf)(0.91324-0.48274*(tao(X,Xf))+0.46842*(tao(X,Xf)).^2-0.12886*(tao(X,Xf)).^3+0.044055*(tao(X,Xf)).^4-0.0035117*(tao(X,Xf)).^5+0.00069085*(tao(X,Xf)).^6)/(1-0.56964*(tao(X,Xf))+0.48690*(tao(X,Xf)).^2-0.13444*(tao(X,Xf)).^3+0.045155*(tao(X,Xf)).^4-0.0035862*(tao(X,Xf)).^5+0.00069085*(tao(X,Xf)).^6);
OMEGA_i = @(X,Xf)(-0.024134-0.029256*(tao(X,Xf))+0.016294*(tao(X,Xf)).^2-0.00010961*(tao(X,Xf)).^3+0.000064577*(tao(X,Xf)).^4-0.000044510*(tao(X,Xf)).^5)/(1-0.597020*(tao(X,Xf))+0.551820*(tao(X,Xf)).^2-0.18357000*(tao(X,Xf)).^3+0.079156000*(tao(X,Xf)).^4-0.014369000*(tao(X,Xf)).^5+0.0028361*(tao(X,Xf)).^6);
OMEGA = @(X,Xf)OMEGA_r(X,Xf) + OMEGA_i(X,Xf)*i;
GAMA_rect = @(X,Xf)OMEGA(X,Xf) .* GAMA_circ(X,Xf);
ACO1=@(X,Xf)(omega2_3.*(1+(pi*X(1)/4)*GAMA_rect(X(2),Xf)*beta(1))./(w_vac^2*(landa(1)/landa(1))^4*alpha(1)-omega2_3.*(1+(pi*X(1)/4)*GAMA_rect(X(2),Xf)*alpha(1)));
ACO2=@(X,Xf)(omega2_3.*(1+(pi*X(1)/4)*GAMA_rect(X(2),Xf)*beta(2))./(w_vac^2*(landa(2)/landa(1))^4*alpha(2)-omega2_3.*(1+(pi*X(1)/4)*GAMA_rect(X(2),Xf)*alpha(2)));
ACO3=@(X,Xf)(omega2_3.*(1+(pi*X(1)/4)*GAMA_rect(X(2),Xf)*beta(3))./(w_vac^2*(landa(3)/landa(1))^4*alpha(3)-omega2_3.*(1+(pi*X(1)/4)*GAMA_rect(X(2),Xf)*alpha(3)));
ACO4=@(X,Xf)(omega2_3.*(1+(pi*X(1)/4)*GAMA_rect(X(2),Xf)*beta(4))./(w_vac^2*(landa(4)/landa(1))^4*alpha(4)-omega2_3.*(1+(pi*X(1)/4)*GAMA_rect(X(2),Xf)*alpha(4)));
ACO5=@(X,Xf)(omega2_3.*(1+(pi*X(1)/4)*GAMA_rect(X(2),Xf)*beta(5))./(w_vac^2*(landa(5)/landa(1))^4*alpha(5)-omega2_3.*(1+(pi*X(1)/4)*GAMA_rect(X(2),Xf)*alpha(5)));
ACO6=@(X,Xf)(omega2_3.*(1+(pi*X(1)/4)*GAMA_rect(X(2),Xf)*beta(6))./(w_vac^2*(landa(6)/landa(1))^4*alpha(6)-omega2_3.*(1+(pi*X(1)/4)*GAMA_rect(X(2),Xf)*alpha(6)));
ACO7=@(X,Xf)(omega2_3.*(1+(pi*X(1)/4)*GAMA_rect(X(2),Xf)*beta(7))./(w_vac^2*(landa(7)/landa(1))^4*alpha(7)-omega2_3.*(1+(pi*X(1)/4)*GAMA_rect(X(2),Xf)*alpha(7)));
ACO8=@(X,Xf)(omega2_3.*(1+(pi*X(1)/4)*GAMA_rect(X(2),Xf)*beta(8))./(w_vac^2*(landa(8)/landa(1))^4*alpha(8)-omega2_3.*(1+(pi*X(1)/4)*GAMA_rect(X(2),Xf)*alpha(8)));
ACO9=@(X,Xf)(omega2_3.*(1+(pi*X(1)/4)*GAMA_rect(X(2),Xf)*beta(9))./(w_vac^2*(landa(9)/landa(1))^4*alpha(9)-omega2_3.*(1+(pi*X(1)/4)*GAMA_rect(X(2),Xf)*alpha(9)));
ACO_response9=@(X,Xf)
[ACO1(X,Xf)*X11(length(X11))+ACO2(X,Xf)*X12(length(X12))+ACO3(X,Xf)*X13(length(X13))+ACO4(X,Xf)*X14(length(X14))+ACO5(X,Xf)*X15(length(X15))+ACO6(X,Xf)*X16(length(X16))+ACO7(X,Xf)*X17(length(X17))+ACO8(X,Xf)*X18(length(X18))+ACO9(X,Xf)*X19(length(X19))];
AAA=@(X,Xf) abs(ACO_response9(X(1:2),Xf))/X(3);
BBB=@(X,Xf)angle(ACO_response9(X,Xf));
CCC=@(X,Xf)unwrap(BBB(X(1:2),Xf))-X(3);

```



```

[Ya,ra,Ja] = nlinfit(omega_3,exp_amp,AAA,Ya_0); clear ra Ja;
[Yp,rp,Ip] = nlinfit(omega_3,exp_ang,CCC,Yp_0); clear rp Ip;

Tb_a=Ya(1); Reb_a=Ya(2); scal=Ya(3);
Tb_p=Yp(1); Reb_p=Yp(2); angl=Yp(3);

ro_a_f=Tb_a*ro_c*h/b; eta_a_f=(ro_a_f*w_vac*b^2)/(4*Reb_a);
ro_p_f=Tb_p*ro_c*h/b; eta_p_f=(ro_p_f*w_vac*b^2)/(4*Reb_p);

error_ro_a=(ro_a_f-g_ro_f)/g_ro_f*100; error_eta_a=(eta_a_f-g_eta_f)/g_eta_f*100;
error_ro_p=(ro_p_f-g_ro_f)/g_ro_f*100; error_eta_p=(eta_p_f-g_eta_f)/g_eta_f*100;

error_scal=(scal-scal_best)/scal_best*100;
error_angl=(angl-angl_best)/angl_best*100;

format short e;
eta_ro_scal=[eta_a_f error_eta_a ro_a_f error_ro_a scal error_scal];
eta_ro_angl=[eta_p_f error_eta_p ro_p_f error_ro_p angl error_angl];
summary_of_fitting_params(fluid_N,:)= [eta_ro_scal scal_best eta_ro_angl angl_best];

clear g Tb_g Reb Ya_0 Yp_0 Ya Yp Re GAMA_circ tao OMEGA_r OMEGA_i OMEGA GAMA_rect
ACO1 ACO2 ACO3 ACO4 ACO5 ACO6 ACO7 ACO8 ACO9 ACO_response9 AAA BBB CCC;
clear Tb_a Tb_p Reb_a Reb_p error_ro_a error_ro_p error_scal error_angl error_eta_a error_eta_p;
clear f_3 omega_3 omega2_3 exp_amp exp_ang eta_ro_scal eta_ro_angl;
#####
##### determining the theoretical amplitude and phase responses #####
#####
f_4=[1:1000]/10; omega_4=2*pi*f_4*1000;

% determining the best theoretical response %%%
ro_f=g_ro_f;
eta_f=g_eta_f;
scal_t=scal_best;
angl_t=angl_best;

Re = @(X) ro_f*X*b^2/4/eta_f;
GAMA_circ = @(X) 1+(4*i*besselk(1,(-i*sqrt(i*Re(X)))))/(sqrt(i*Re(X)).*besselk(0,(-i*sqrt(i*Re(X)))));
tao = @(X) log10(Re(X));
OMEGA_r = @(X) (0.91324-0.48274*(tao(X))+0.46842*(tao(X)).^2-
0.12886*(tao(X)).^3+0.044055*(tao(X)).^4-0.0035117*(tao(X)).^5+0.00069085*(tao(X)).^6)/(1-
0.56964*(tao(X))+0.48690*(tao(X)).^2-0.13444*(tao(X)).^3+0.045155*(tao(X)).^4-
0.0035862*(tao(X)).^5+0.00069085*(tao(X)).^6);
OMEGA_i = @(X) (-0.024134-0.029256*(tao(X))+0.016294*(tao(X)).^2-
0.00010961*(tao(X)).^3+0.000064577*(tao(X)).^4-0.000044510*(tao(X)).^5)/(1-
0.597020*(tao(X))+0.551820*(tao(X)).^2-0.18357000*(tao(X)).^3+0.079156000*(tao(X)).^4-
0.014369000*(tao(X)).^5+0.0028361*(tao(X)).^6);
OMEGA = @(X) OMEGA_r(X) + OMEGA_i(X)*i;
GAMA_rect = @(X) OMEGA(X) .* GAMA_circ(X);
GAMA_rect_value=GAMA_rect(omega_4);
ACO1=((omega_4.^2).*(ro_c*A+pi/4*ro_f*b^2*GAMA_rect_value)*beta(1)*L)/(E*I*(landa(1))^4*alpha
(1)*L-(omega_4.^2).*(ro_c*A+pi/4*ro_f*b^2*GAMA_rect_value)*alpha(1)*L);
ACO2=((omega_4.^2).*(ro_c*A+pi/4*ro_f*b^2*GAMA_rect_value)*beta(2)*L)/(E*I*(landa(2))^4*alpha
(2)*L-(omega_4.^2).*(ro_c*A+pi/4*ro_f*b^2*GAMA_rect_value)*alpha(2)*L);

```

```

ACO3=((omega_4.^2).*(ro_c*A+pi/4*ro_f*b^2*GAMA_rect_value)*beta(3)*L)./(E*I*(landa(3))^4*alpha
(3)*L-(omega_4.^2).*(ro_c*A+pi/4*ro_f*b^2*GAMA_rect_value)*alpha(3)*L);
ACO4=((omega_4.^2).*(ro_c*A+pi/4*ro_f*b^2*GAMA_rect_value)*beta(4)*L)./(E*I*(landa(4))^4*alpha
(4)*L-(omega_4.^2).*(ro_c*A+pi/4*ro_f*b^2*GAMA_rect_value)*alpha(4)*L);
ACO5=((omega_4.^2).*(ro_c*A+pi/4*ro_f*b^2*GAMA_rect_value)*beta(5)*L)./(E*I*(landa(5))^4*alpha
(5)*L-(omega_4.^2).*(ro_c*A+pi/4*ro_f*b^2*GAMA_rect_value)*alpha(5)*L);
ACO6=((omega_4.^2).*(ro_c*A+pi/4*ro_f*b^2*GAMA_rect_value)*beta(6)*L)./(E*I*(landa(6))^4*alpha
(6)*L-(omega_4.^2).*(ro_c*A+pi/4*ro_f*b^2*GAMA_rect_value)*alpha(6)*L);
ACO7=((omega_4.^2).*(ro_c*A+pi/4*ro_f*b^2*GAMA_rect_value)*beta(7)*L)./(E*I*(landa(7))^4*alpha
(7)*L-(omega_4.^2).*(ro_c*A+pi/4*ro_f*b^2*GAMA_rect_value)*alpha(7)*L);
ACO8=((omega_4.^2).*(ro_c*A+pi/4*ro_f*b^2*GAMA_rect_value)*beta(8)*L)./(E*I*(landa(8))^4*alpha
(8)*L-(omega_4.^2).*(ro_c*A+pi/4*ro_f*b^2*GAMA_rect_value)*alpha(8)*L);
ACO9=((omega_4.^2).*(ro_c*A+pi/4*ro_f*b^2*GAMA_rect_value)*beta(9)*L)./(E*I*(landa(9))^4*alpha
(9)*L-(omega_4.^2).*(ro_c*A+pi/4*ro_f*b^2*GAMA_rect_value)*alpha(9)*L);
ACO_response9=[ACO1*X11(length(X11))+ACO2*X12(length(X12))+ACO3*X13(length(X13))+ACO4
*X14(length(X14))+ACO5*X15(length(X15))+ACO6*X16(length(X16))+ACO7*X17(length(X17))+AC
O8*X18(length(X18))+ACO9*X19(length(X19))];
AAA_t=abs(ACO_response9)/scal_t; CCC_t=unwrap(angle(ACO_response9))-angl_t;
clear ro_f eta_f scal_t angl_t Re GAMA_circ tao OMEGA_r OMEGA_i OMEGA GAMA_rect
GAMA_rect_value ACO1 ACO2 ACO3 ACO4 ACO5 ACO6 ACO7 ACO8 ACO9 ACO_response9;

```

% determining the best theoretical response for the amplitude %%%%%%%%%%

```

ro_f=ro_a_f;
eta_f=eta_a_f;
scal_a=scal;
angl_a=angl;

```

```

Re = @(X) ro_f*X*b^2/4/eta_f;
GAMA_circ = @(X)1+(4*i*besselk(1,(-i*sqrt(i*Re(X)))))./(sqrt(i*Re(X)).*besselk(0,(-i*sqrt(i*Re(X)))));
tao = @(X)log10(Re(X));
OMEGA_r = @(X)(0.91324-0.48274*(tao(X))+0.46842*(tao(X)).^2-
0.12886*(tao(X)).^3+0.044055*(tao(X)).^4-0.0035117*(tao(X)).^5+0.00069085*(tao(X)).^6)/(1-
0.56964*(tao(X))+0.48690*(tao(X)).^2-0.13444*(tao(X)).^3+0.045155*(tao(X)).^4-
0.0035862*(tao(X)).^5+0.00069085*(tao(X)).^6);
OMEGA_i = @(X)(-0.024134-0.029256*(tao(X))+0.016294*(tao(X)).^2-
0.00010961*(tao(X)).^3+0.000064577*(tao(X)).^4-0.000044510*(tao(X)).^5)/(1-
0.597020*(tao(X))+0.551820*(tao(X)).^2-0.18357000*(tao(X)).^3+0.079156000*(tao(X)).^4-
0.014369000*(tao(X)).^5+0.0028361*(tao(X)).^6);
OMEGA = @(X)OMEGA_r(X) + OMEGA_i(X)*i;
GAMA_rect = @(X)OMEGA(X) .* GAMA_circ(X);
GAMA_rect_value=GAMA_rect(omega_4);
ACO1=((omega_4.^2).*(ro_c*A+pi/4*ro_f*b^2*GAMA_rect_value)*beta(1)*L)./(E*I*(landa(1))^4*alpha
(1)*L-(omega_4.^2).*(ro_c*A+pi/4*ro_f*b^2*GAMA_rect_value)*alpha(1)*L);
ACO2=((omega_4.^2).*(ro_c*A+pi/4*ro_f*b^2*GAMA_rect_value)*beta(2)*L)./(E*I*(landa(2))^4*alpha
(2)*L-(omega_4.^2).*(ro_c*A+pi/4*ro_f*b^2*GAMA_rect_value)*alpha(2)*L);
ACO3=((omega_4.^2).*(ro_c*A+pi/4*ro_f*b^2*GAMA_rect_value)*beta(3)*L)./(E*I*(landa(3))^4*alpha
(3)*L-(omega_4.^2).*(ro_c*A+pi/4*ro_f*b^2*GAMA_rect_value)*alpha(3)*L);
ACO4=((omega_4.^2).*(ro_c*A+pi/4*ro_f*b^2*GAMA_rect_value)*beta(4)*L)./(E*I*(landa(4))^4*alpha
(4)*L-(omega_4.^2).*(ro_c*A+pi/4*ro_f*b^2*GAMA_rect_value)*alpha(4)*L);
ACO5=((omega_4.^2).*(ro_c*A+pi/4*ro_f*b^2*GAMA_rect_value)*beta(5)*L)./(E*I*(landa(5))^4*alpha
(5)*L-(omega_4.^2).*(ro_c*A+pi/4*ro_f*b^2*GAMA_rect_value)*alpha(5)*L);
ACO6=((omega_4.^2).*(ro_c*A+pi/4*ro_f*b^2*GAMA_rect_value)*beta(6)*L)./(E*I*(landa(6))^4*alpha
(6)*L-(omega_4.^2).*(ro_c*A+pi/4*ro_f*b^2*GAMA_rect_value)*alpha(6)*L);
ACO7=((omega_4.^2).*(ro_c*A+pi/4*ro_f*b^2*GAMA_rect_value)*beta(7)*L)./(E*I*(landa(7))^4*alpha
(7)*L-(omega_4.^2).*(ro_c*A+pi/4*ro_f*b^2*GAMA_rect_value)*alpha(7)*L);

```

```

ACO8=((omega_4.^2).*(ro_c*A+pi/4*ro_f*b^2*GAMA_rect_value)*beta(8)*L)/(E*I*(landa(8))^4*alpha
(8)*L-(omega_4.^2).*(ro_c*A+pi/4*ro_f*b^2*GAMA_rect_value)*alpha(8)*L);
ACO9=((omega_4.^2).*(ro_c*A+pi/4*ro_f*b^2*GAMA_rect_value)*beta(9)*L)/(E*I*(landa(9))^4*alpha
(9)*L-(omega_4.^2).*(ro_c*A+pi/4*ro_f*b^2*GAMA_rect_value)*alpha(9)*L);
ACO_response9=[ACO1*X11(length(X11))+ACO2*X12(length(X12))+ACO3*X13(length(X13))+ACO4
*X14(length(X14))+ACO5*X15(length(X15))+ACO6*X16(length(X16))+ACO7*X17(length(X17))+AC
O8*X18(length(X18))+ACO9*X19(length(X19))];
AAA_a=abs(ACO_response9)/scal_a; CCC_a=unwrap(angle(ACO_response9))-angl_a;
clear ro_f eta_f scal_a angl_a Re GAMA_circ tao OMEGA_r OMEGA_i OMEGA GAMA_rect
GAMA_rect_value ACO1 ACO2 ACO3 ACO4 ACO5 ACO6 ACO7 ACO8 ACO9 ACO_response9;

```

```

% determining the best theoretical response for the phase %%%%%%%%%%%%%%%%%%%%%%%%%%%%%%%%%%%
ro_f=ro_p_f;
eta_f=eta_p_f;
scal_p=scal;
angl_p=angl;

```

```

Re = @(X) ro_f*X*b^2/4/eta_f;
GAMA_circ = @(X)1+(4*i*besselk(1,-i*sqrt(i*Re(X))))/(sqrt(i*Re(X)).*besselk(0,-i*sqrt(i*Re(X))));
tao = @(X)log10(Re(X));
OMEGA_r = @(X)(0.91324-0.48274*(tao(X))+0.46842*(tao(X)).^2-
0.12886*(tao(X)).^3+0.044055*(tao(X)).^4-0.0035117*(tao(X)).^5+0.00069085*(tao(X)).^6)/(1-
0.56964*(tao(X))+0.48690*(tao(X)).^2-0.13444*(tao(X)).^3+0.045155*(tao(X)).^4-
0.0035862*(tao(X)).^5+0.00069085*(tao(X)).^6);
OMEGA_i = @(X)(-0.024134-0.029256*(tao(X))+0.016294*(tao(X)).^2-
0.00010961*(tao(X)).^3+0.000064577*(tao(X)).^4-0.000044510*(tao(X)).^5)/(1-
0.597020*(tao(X))+0.551820*(tao(X)).^2-0.18357000*(tao(X)).^3+0.079156000*(tao(X)).^4-
0.014369000*(tao(X)).^5+0.0028361*(tao(X)).^6);
OMEGA = @(X)OMEGA_r(X) + OMEGA_i(X)*i;
GAMA_rect = @(X)OMEGA_r(X) .* GAMA_circ(X);
GAMA_rect_value=GAMA_rect(omega_4);
ACO1=((omega_4.^2).*(ro_c*A+pi/4*ro_f*b^2*GAMA_rect_value)*beta(1)*L)/(E*I*(landa(1))^4*alpha
(1)*L-(omega_4.^2).*(ro_c*A+pi/4*ro_f*b^2*GAMA_rect_value)*alpha(1)*L);
ACO2=((omega_4.^2).*(ro_c*A+pi/4*ro_f*b^2*GAMA_rect_value)*beta(2)*L)/(E*I*(landa(2))^4*alpha
(2)*L-(omega_4.^2).*(ro_c*A+pi/4*ro_f*b^2*GAMA_rect_value)*alpha(2)*L);
ACO3=((omega_4.^2).*(ro_c*A+pi/4*ro_f*b^2*GAMA_rect_value)*beta(3)*L)/(E*I*(landa(3))^4*alpha
(3)*L-(omega_4.^2).*(ro_c*A+pi/4*ro_f*b^2*GAMA_rect_value)*alpha(3)*L);
ACO4=((omega_4.^2).*(ro_c*A+pi/4*ro_f*b^2*GAMA_rect_value)*beta(4)*L)/(E*I*(landa(4))^4*alpha
(4)*L-(omega_4.^2).*(ro_c*A+pi/4*ro_f*b^2*GAMA_rect_value)*alpha(4)*L);
ACO5=((omega_4.^2).*(ro_c*A+pi/4*ro_f*b^2*GAMA_rect_value)*beta(5)*L)/(E*I*(landa(5))^4*alpha
(5)*L-(omega_4.^2).*(ro_c*A+pi/4*ro_f*b^2*GAMA_rect_value)*alpha(5)*L);
ACO6=((omega_4.^2).*(ro_c*A+pi/4*ro_f*b^2*GAMA_rect_value)*beta(6)*L)/(E*I*(landa(6))^4*alpha
(6)*L-(omega_4.^2).*(ro_c*A+pi/4*ro_f*b^2*GAMA_rect_value)*alpha(6)*L);
ACO7=((omega_4.^2).*(ro_c*A+pi/4*ro_f*b^2*GAMA_rect_value)*beta(7)*L)/(E*I*(landa(7))^4*alpha
(7)*L-(omega_4.^2).*(ro_c*A+pi/4*ro_f*b^2*GAMA_rect_value)*alpha(7)*L);
ACO8=((omega_4.^2).*(ro_c*A+pi/4*ro_f*b^2*GAMA_rect_value)*beta(8)*L)/(E*I*(landa(8))^4*alpha
(8)*L-(omega_4.^2).*(ro_c*A+pi/4*ro_f*b^2*GAMA_rect_value)*alpha(8)*L);
ACO9=((omega_4.^2).*(ro_c*A+pi/4*ro_f*b^2*GAMA_rect_value)*beta(9)*L)/(E*I*(landa(9))^4*alpha
(9)*L-(omega_4.^2).*(ro_c*A+pi/4*ro_f*b^2*GAMA_rect_value)*alpha(9)*L);
ACO_response9=[ACO1*X11(length(X11))+ACO2*X12(length(X12))+ACO3*X13(length(X13))+ACO4
*X14(length(X14))+ACO5*X15(length(X15))+ACO6*X16(length(X16))+ACO7*X17(length(X17))+AC
O8*X18(length(X18))+ACO9*X19(length(X19))];
AAA_p=abs(ACO_response9)/scal_p; CCC_p=unwrap(angle(ACO_response9))-angl_p;
clear ro_f eta_f scal_p angl_p Re GAMA_circ tao OMEGA_r OMEGA_i OMEGA GAMA_rect
GAMA_rect_value ACO1 ACO2 ACO3 ACO4 ACO5 ACO6 ACO7 ACO8 ACO9 ACO_response9;

```



```

plot(Fig_ORI(:,1),Fig_ORI(:,6),'k','LineWidth',2); hold on;
plot(Fig_ORI(:,1),Fig_ORI(:,7),'g','LineWidth',3);
plot(Fig_ORI(:,1),Fig_ORI(:,9),'b','LineWidth',3);
legend('Experimental','Theory','Phase base','Location','Best'); hold off;

beep

clear scal_best scal_angl_best angl_ro_p_f ro_a_f eta_p_f eta_a_f
clear indices_ORI indices_NDP fluid filename g_ro_f g_eta_f g_scal g_angl
clear exp_data_NDP exp_data_ORI Fig_NDP Fig_ORI
clear AAA_a AAA_p AAA_t CCC_a CCC_p CCC_t

toc
end

```

Appendix M

MATLAB code for determining the fluid's properties at each frequency of excitation:

```

=====

% this code needs the files in these folders:
%                               _CoUP - CaUP_NDP

%#####
%#####
%#####
clc; clear all; close all; format compact;

cutoff_freq=40;
amps=' amp 8';
%#####
%##### cantilever properties #####
%#####
cantilever='long'; cantilever_N=1;
L=397e-6;
b=29e-6;
h=2.33e-6;

% cantilever='medium'; cantilever_N=2;
% L=197e-6;
% b=29e-6;
% h=2.255e-6;

A=b*h; I=b*h^3/12;
ro_c=2330;
E=170e9;
w_vac=(1.8751/L)^2*sqrt(E*I/ro_c/A);
%#####
%##### fluid properties #####
%#####

fluid_cel=['air      '; 'Ethanol  '; 'water    '; '%25 Glycerine '; '%50 Glycerine '; '%60 Glycerine
'; '%75 Glycerine '; '%80 Glycerine '; '%100 Glycerine'];
filename0_cel=['FS_air_   '; 'FS_ethanol_ '; 'FS_GW00_   '; 'FS_GW25_   '; 'FS_GW50_
'; 'FS_GW60_   '; 'FS_GW75_   '; 'FS_GW80_   '; 'FS_GW100_  '];
fluid_cel=cellstr(fluid_cel);
filename0_cel=cellstr(filename0_cel);

      % (1)  (2)  (3)  (4)  (5)  (6)  (7)  (8)  (9)
      %air  ethanol water  %25  %50  %60  %75  %80  %100
      g_ro_f_cel=[ 1.184 785 997 1058 1123 1151 1191 1205 1257 ];
      g_eta_f_cel=[ 0.018 1.078 0.88242 1.818 4.926 8.634 26.92 44.38 931.2 ]*1e-3;
      f_ref_cel(1,:)= [ 22 8 7.5 7 6 5 5 5 5 ];
      f_ref_cel(2,:)= [ 80 16 16 16 10 10 10 9 8 ];
%#####

```

```

%##### mode shapes and related parameters #####
%#####
delta_x=0.00001*L; x=[0:delta_x:L];

```

```

landa(1)=1.8751/L;   landa(2)=4.694/L;   landa(3)=7.855/L;   landa(4)=10.996/L;
landa(5)=14.137/L;  landa(6)=17.279/L;
landa(7)=(7-0.5)*pi/L; landa(8)=(8-0.5)*pi/L; landa(9)=(9-0.5)*pi/L; landa(10)=(10-0.5)*pi/L;
landa(11)=(11-0.5)*pi/L; landa(12)=(12-0.5)*pi/L;

```

```

X1=(cos(landa(1)*x)-cosh(landa(1)*x)-
((cos(landa(1)*L)+cosh(landa(1)*L))/(sin(landa(1)*L)+sinh(landa(1)*L)))*(sin(landa(1)*x)-
sinh(landa(1)*x)));

```

```

X2=(cos(landa(2)*x)-cosh(landa(2)*x)-
((cos(landa(2)*L)+cosh(landa(2)*L))/(sin(landa(2)*L)+sinh(landa(2)*L)))*(sin(landa(2)*x)-
sinh(landa(2)*x)));

```

```

X3=(cos(landa(3)*x)-cosh(landa(3)*x)-
((cos(landa(3)*L)+cosh(landa(3)*L))/(sin(landa(3)*L)+sinh(landa(3)*L)))*(sin(landa(3)*x)-
sinh(landa(3)*x)));

```

```

X4=(cos(landa(4)*x)-cosh(landa(4)*x)-
((cos(landa(4)*L)+cosh(landa(4)*L))/(sin(landa(4)*L)+sinh(landa(4)*L)))*(sin(landa(4)*x)-
sinh(landa(4)*x)));

```

```

X5=(cos(landa(5)*x)-cosh(landa(5)*x)-
((cos(landa(5)*L)+cosh(landa(5)*L))/(sin(landa(5)*L)+sinh(landa(5)*L)))*(sin(landa(5)*x)-
sinh(landa(5)*x)));

```

```

X6=(cos(landa(6)*x)-cosh(landa(6)*x)-
((cos(landa(6)*L)+cosh(landa(6)*L))/(sin(landa(6)*L)+sinh(landa(6)*L)))*(sin(landa(6)*x)-
sinh(landa(6)*x)));

```

```

X7=(cos(landa(7)*x)-cosh(landa(7)*x)-
((cos(landa(7)*L)+cosh(landa(7)*L))/(sin(landa(7)*L)+sinh(landa(7)*L)))*(sin(landa(7)*x)-
sinh(landa(7)*x)));

```

```

X8=(cos(landa(8)*x)-cosh(landa(8)*x)-
((cos(landa(8)*L)+cosh(landa(8)*L))/(sin(landa(8)*L)+sinh(landa(8)*L)))*(sin(landa(8)*x)-
sinh(landa(8)*x)));

```

```

X9=(cos(landa(9)*x)-cosh(landa(9)*x)-
((cos(landa(9)*L)+cosh(landa(9)*L))/(sin(landa(9)*L)+sinh(landa(9)*L)))*(sin(landa(9)*x)-
sinh(landa(9)*x)));

```

```

X11=landa(1)*((-sin(landa(1)*x)-sinh(landa(1)*x)-
((cos(landa(1)*L)+cosh(landa(1)*L))/(sin(landa(1)*L)+sinh(landa(1)*L)))*(cos(landa(1)*x)-
cosh(landa(1)*x)));

```

```

X12=landa(2)*((-sin(landa(2)*x)-sinh(landa(2)*x)-
((cos(landa(2)*L)+cosh(landa(2)*L))/(sin(landa(2)*L)+sinh(landa(2)*L)))*(cos(landa(2)*x)-
cosh(landa(2)*x)));

```

```

X13=landa(3)*((-sin(landa(3)*x)-sinh(landa(3)*x)-
((cos(landa(3)*L)+cosh(landa(3)*L))/(sin(landa(3)*L)+sinh(landa(3)*L)))*(cos(landa(3)*x)-
cosh(landa(3)*x)));

```

```

X14=landa(4)*((-sin(landa(4)*x)-sinh(landa(4)*x)-
((cos(landa(4)*L)+cosh(landa(4)*L))/(sin(landa(4)*L)+sinh(landa(4)*L)))*(cos(landa(4)*x)-
cosh(landa(4)*x)));

```

```

X15=landa(5)*((-sin(landa(5)*x)-sinh(landa(5)*x)-
((cos(landa(5)*L)+cosh(landa(5)*L))/(sin(landa(5)*L)+sinh(landa(5)*L)))*(cos(landa(5)*x)-
cosh(landa(5)*x)));

```

```

X16=landa(6)*((-sin(landa(6)*x)-sinh(landa(6)*x)-
((cos(landa(6)*L)+cosh(landa(6)*L))/(sin(landa(6)*L)+sinh(landa(6)*L)))*(cos(landa(6)*x)-
cosh(landa(6)*x)));

```

```

X17=landa(7)*((-sin(landa(7)*x)-sinh(landa(7)*x)-
((cos(landa(7)*L)+cosh(landa(7)*L))/(sin(landa(7)*L)+sinh(landa(7)*L)))*(cos(landa(7)*x)-
cosh(landa(7)*x)));
X18=landa(8)*((-sin(landa(8)*x)-sinh(landa(8)*x)-
((cos(landa(8)*L)+cosh(landa(8)*L))/(sin(landa(8)*L)+sinh(landa(8)*L)))*(cos(landa(8)*x)-
cosh(landa(8)*x)));
X19=landa(9)*((-sin(landa(9)*x)-sinh(landa(9)*x)-
((cos(landa(9)*L)+cosh(landa(9)*L))/(sin(landa(9)*L)+sinh(landa(9)*L)))*(cos(landa(9)*x)-
cosh(landa(9)*x)));

```

```

X11=(X11/X1(length(X1)));
X12=(X12/X2(length(X2)));
X13=(X13/X3(length(X3)));
X14=(X14/X4(length(X4)));
X15=(X15/X5(length(X5)));
X16=(X16/X6(length(X6)));
X17=(X17/X7(length(X7)));
X18=(X18/X8(length(X8)));
X19=(X19/X9(length(X9)));
X1=(X1/X1(length(X1)));
X2=(X2/X2(length(X2)));
X3=(X3/X3(length(X3)));
X4=(X4/X4(length(X4)));
X5=(X5/X5(length(X5)));
X6=(X6/X6(length(X6)));
X7=(X7/X7(length(X7)));
X8=(X8/X8(length(X8)));
X9=(X9/X9(length(X9)));

```

```

alpha(1)=sum(X1.*X1)*delta_x/L; beta(1)=sum(X1)*delta_x/L;
alpha(2)=sum(X2.*X2)*delta_x/L; beta(2)=sum(X2)*delta_x/L;
alpha(3)=sum(X3.*X3)*delta_x/L; beta(3)=sum(X3)*delta_x/L;
alpha(4)=sum(X4.*X4)*delta_x/L; beta(4)=sum(X4)*delta_x/L;
alpha(5)=sum(X5.*X5)*delta_x/L; beta(5)=sum(X5)*delta_x/L;
alpha(6)=sum(X6.*X6)*delta_x/L; beta(6)=sum(X6)*delta_x/L;
alpha(7)=sum(X7.*X7)*delta_x/L; beta(7)=sum(X7)*delta_x/L;
alpha(8)=sum(X8.*X8)*delta_x/L; beta(8)=sum(X8)*delta_x/L;
alpha(9)=sum(X9.*X9)*delta_x/L; beta(9)=sum(X9)*delta_x/L;

```

```

clear delta_x X1 X2 X3 X4 X5 X6 X7 X8 X9;
%%%%%%%%%%%%%%%%%%%%%%%%%%%%%%%%%%%%%%%%%%%%%%%%%%%%%%%%%%%%%%%%%%%%%%%%
%%%%%%%%%%%%%%%%%%%%%%%%%%%%%%%%%%%%%%%%%%%%%%%%%%%%%%%%%%%%%%%%%%%%%%%%
%%%%%%%%%%%%%%%%%%%%%%%%%%%%%%%%%%%%%%%%%%%%%%%%%%%%%%%%%%%%%%%%%%%%%%%%
for fluid_N=2:9
tic
fluid=char(fluid_cel(fluid_N))
filename0=char(filename0_cel(fluid_N));
g_ro_f=g_ro_f_cel(fluid_N);
g_eta_f=g_eta_f_cel(fluid_N);
f_ref=f_ref_cel(cantilever_N,fluid_N);
% data management %%%%%%%%%%
filename=[filename0 cantilever amps ' _CoUP - CaUP_NDP.dat'];
exp_data=load(filename);
indices = find(cutoff_freq<exp_data(:,1) & exp_data(:,1)<=100); exp_data(indices,:)=[];

```



```

f=exp_data(:,1);    i_ref = find(f==f_ref); f(i_ref)=[];    omega_ref=2*pi*f_ref*1000;
omega=2*pi*f*1000;
exp_amp=exp_data(:,2); amp_ref=exp_amp(i_ref); exp_amp(i_ref)=[];
exp_ang=exp_data(:,3); ang_ref=exp_ang(i_ref); exp_ang(i_ref)=[];

clear filename exp_data indices i_ref f_ref;
%%%%%%%%%%%%%%%%%%%%%%%%%%%%%%%%%%%%%%%%%%%%%%%%%%%%%%%%%%
g_Tb=(g_ro_f*b)/(ro_c*h);
g_Reb=(g_ro_f*w_vac*b^2)/(4*g_eta_f);

for i_f=1:length(f)

    Y_0=[g_Tb g_Reb];

    Re = @(X,Xf) X*Xf/w_vac;
    GAMA_circ = @(X,Xf)1+(4*i*besselk(1,(-i*sqrt(i*Re(X,Xf)))))/(sqrt(i*Re(X,Xf)).*besselk(0,(-
i*sqrt(i*Re(X,Xf)))));
    tao = @(X,Xf)log10(Re(X,Xf));
    OMEGA_r=@(X,Xf)(0.91324-0.48274*(tao(X,Xf))+0.46842*(tao(X,Xf)).^2-
0.12886*(tao(X,Xf)).^3+0.044055*(tao(X,Xf)).^4-
0.0035117*(tao(X,Xf)).^5+0.00069085*(tao(X,Xf)).^6)/(1-0.56964*(tao(X,Xf))+0.48690*(tao(X,Xf)).^2-
0.13444*(tao(X,Xf)).^3+0.045155*(tao(X,Xf)).^4-
0.0035862*(tao(X,Xf)).^5+0.00069085*(tao(X,Xf)).^6);
    OMEGA_i=@(X,Xf)(-0.024134-0.029256*(tao(X,Xf))+0.016294*(tao(X,Xf)).^2-
0.00010961*(tao(X,Xf)).^3+0.000064577*(tao(X,Xf)).^4-0.000044510*(tao(X,Xf)).^5)/(1-
0.597020*(tao(X,Xf))+0.551820*(tao(X,Xf)).^2-
0.18357000*(tao(X,Xf)).^3+0.079156000*(tao(X,Xf)).^4-
0.014369000*(tao(X,Xf)).^5+0.0028361*(tao(X,Xf)).^6);
    OMEGA = @(X,Xf)OMEGA_r(X,Xf) + OMEGA_i(X,Xf)*i;
    GAMA_rect = @(X,Xf)OMEGA(X,Xf) .* GAMA_circ(X,Xf);

    ACO1=@(X,Xf)(Xf^2*(1+(pi*X(1)/4)*GAMA_rect(X(2),Xf))*beta(1))/(w_vac^2*(landa(1)/landa(1))^4*
alpha(1)-Xf^2*(1+(pi*X(1)/4)*GAMA_rect(X(2),Xf))*alpha(1));

    ACO2=@(X,Xf)(Xf^2*(1+(pi*X(1)/4)*GAMA_rect(X(2),Xf))*beta(2))/(w_vac^2*(landa(2)/landa(1))^4*
alpha(2)-Xf^2*(1+(pi*X(1)/4)*GAMA_rect(X(2),Xf))*alpha(2));

    ACO3=@(X,Xf)(Xf^2*(1+(pi*X(1)/4)*GAMA_rect(X(2),Xf))*beta(3))/(w_vac^2*(landa(3)/landa(1))^4*
alpha(3)-Xf^2*(1+(pi*X(1)/4)*GAMA_rect(X(2),Xf))*alpha(3));

    ACO4=@(X,Xf)(Xf^2*(1+(pi*X(1)/4)*GAMA_rect(X(2),Xf))*beta(4))/(w_vac^2*(landa(4)/landa(1))^4*
alpha(4)-Xf^2*(1+(pi*X(1)/4)*GAMA_rect(X(2),Xf))*alpha(4));

    ACO5=@(X,Xf)(Xf^2*(1+(pi*X(1)/4)*GAMA_rect(X(2),Xf))*beta(5))/(w_vac^2*(landa(5)/landa(1))^4*
alpha(5)-Xf^2*(1+(pi*X(1)/4)*GAMA_rect(X(2),Xf))*alpha(5));

    ACO6=@(X,Xf)(Xf^2*(1+(pi*X(1)/4)*GAMA_rect(X(2),Xf))*beta(6))/(w_vac^2*(landa(6)/landa(1))^4*
alpha(6)-Xf^2*(1+(pi*X(1)/4)*GAMA_rect(X(2),Xf))*alpha(6));

    ACO7=@(X,Xf)(Xf^2*(1+(pi*X(1)/4)*GAMA_rect(X(2),Xf))*beta(7))/(w_vac^2*(landa(7)/landa(1))^4*
alpha(7)-Xf^2*(1+(pi*X(1)/4)*GAMA_rect(X(2),Xf))*alpha(7));

    ACO8=@(X,Xf)(Xf^2*(1+(pi*X(1)/4)*GAMA_rect(X(2),Xf))*beta(8))/(w_vac^2*(landa(8)/landa(1))^4*
alpha(8)-Xf^2*(1+(pi*X(1)/4)*GAMA_rect(X(2),Xf))*alpha(8));

```

```

ACO9=@(X,Xf)(Xf^2*(1+(pi*X(1)/4)*GAMA_rect(X(2),Xf))*beta(9))/(w_vac^2*(landa(9)/landa(1))^4*
alpha(9)-Xf^2*(1+(pi*X(1)/4)*GAMA_rect(X(2),Xf))*alpha(9));
ACO_response9=@(X,Xf)
[ACO1(X,Xf)*X11(length(X11))+ACO2(X,Xf)*X12(length(X12))+ACO3(X,Xf)*X13(length(X13))+AC
O4(X,Xf)*X14(length(X14))+ACO5(X,Xf)*X15(length(X15))+ACO6(X,Xf)*X16(length(X16))+ACO7(
X,Xf)*X17(length(X17))+ACO8(X,Xf)*X18(length(X18))+ACO9(X,Xf)*X19(length(X19))];
AAA=@(X,Xf) abs(ACO_response9(X,Xf));
BBB=@(X,Xf)angle(ACO_response9(X,Xf));
CCC=@(X,Xf)unwrap(BBB(X,Xf));

root_function=@(X)[AAA(X,omega(i_f))/AAA(X,omega_ref); CCC(X,omega(i_f))-
CCC(X,omega_ref)]-[exp_amp(i_f)/amp_ref; exp_ang(i_f)-ang_ref];

options = optimset('MaxFunEvals',200,'MaxIter',100,'TolFun',1e-10,'TolX',1e-8);
[Y,fval,exitflag,output] = fsolve(root_function,Y_0,options);

i_f
M_Tb(i_f,1)=Y(1);
M_Reb(i_f,1)=Y(2);
control(i_f,:)= [exitflag output.funcCount output.iterations fval(1) fval(2)];

clear Y_0 Re GAMA_circ tao OMEGA_r OMEGA_i OMEGA GAMA_rect ACO1 ACO2 ACO3 ACO4
ACO5 ACO6 ACO7 ACO8 ACO9 ACO_response9 AAA BBB CCC root_function options Y fval exitflag
output;

end

clear i_f g_Tb g_Reb omega exp_amp exp_ang omega_ref amp_ref ang_ref
%%%%%%%%%%%%%%%%%%%%%%%%%%%%%%%%%%%%%%%%%%%%%%%%%%%%%%%%%%%%%%%%%%%%%%%%%%%%%%
%%%%%%%%%%%%%%%%%%%%%%%%%%%%%%%%%%%%%%%%%%%%%%%%%%%%%%%%%%%%%%%%%%%%%%%%%%%%%% saving results %%%%%%%%%%%%%%%%%%%%%%%%%%%%%%%%%%%%%%%%%%%%%%%%%%%%%%%%%%%%%%%%%%%%%%%%%%%%%%%
%%%%%%%%%%%%%%%%%%%%%%%%%%%%%%%%%%%%%%%%%%%%%%%%%%%%%%%%%%%%%%%%%%%%%%%%%%%%%%
M_ro_f=M_Tb*ro_c*h/b;
M_eta_f=(M_ro_f*w_vac*b^2)/(4*M_Reb);
M_error_ro=(M_ro_f-g_ro_f)/g_ro_f*100;
M_error_eta=(M_eta_f-g_eta_f)/g_eta_f*100;

ro_eta_control=[f M_ro_f M_error_ro M_eta_f M_error_eta control];

filename_save=[filename0 cantilever amps '_CoUP - CaUP_NDP_ro_eta_control.dat'];
save(filename_save,'ro_eta_control','-ascii');

clear M_ro_f M_eta_f M_Tb M_Reb M_error_ro M_error_eta control filename_save
%%%%%%%%%%%%%%%%%%%%%%%%%%%%%%%%%%%%%%%%%%%%%%%%%%%%%%%%%%%%%%%%%%%%%%%%%%%%%%
%%%%%%%%%%%%%%%%%%%%%%%%%%%%%%%%%%%%%%%%%%%%%%%%%%%%%%%%%%%%%%%%%%%%%%%%%%%%%% figures %%%%%%%%%%%%%%%%%%%%%%%%%%%%%%%%%%%%%%%%%%%%%%%%%%%%%%%%%%%%%%%%%%%%%%%%%%%%%%%
%%%%%%%%%%%%%%%%%%%%%%%%%%%%%%%%%%%%%%%%%%%%%%%%%%%%%%%%%%%%%%%%%%%%%%%%%%%%%%
figure;
subplot(2,2,1); hold on;
plot(ro_eta_control(:,1),g_ro_f*ones(length(f)),'g','LineWidth',2);
plot(ro_eta_control(:,1),mean(ro_eta_control(:,2))*ones(length(f)),'r','LineWidth',2);
plot(ro_eta_control(:,1),ro_eta_control(:,2),'k','LineWidth',2);
legend('Known','Average','Measured','Location','Best'); title(['Density of ' fluid ' - ' cantilever]); hold off;

subplot(2,2,2); hold on;

```

```

plot(ro_eta_control(:,1),g_eta_f*ones(length(f)), 'g', 'LineWidth',2);
plot(ro_eta_control(:,1),mean(ro_eta_control(:,4))*ones(length(f)), 'r', 'LineWidth',2);
plot(ro_eta_control(:,1),ro_eta_control(:,4), 'k', 'LineWidth',2);
legend('Known','Average','Measured','Location','Best'); title(['Viscosity of ' fluid ' - ' cantilever]); hold off;

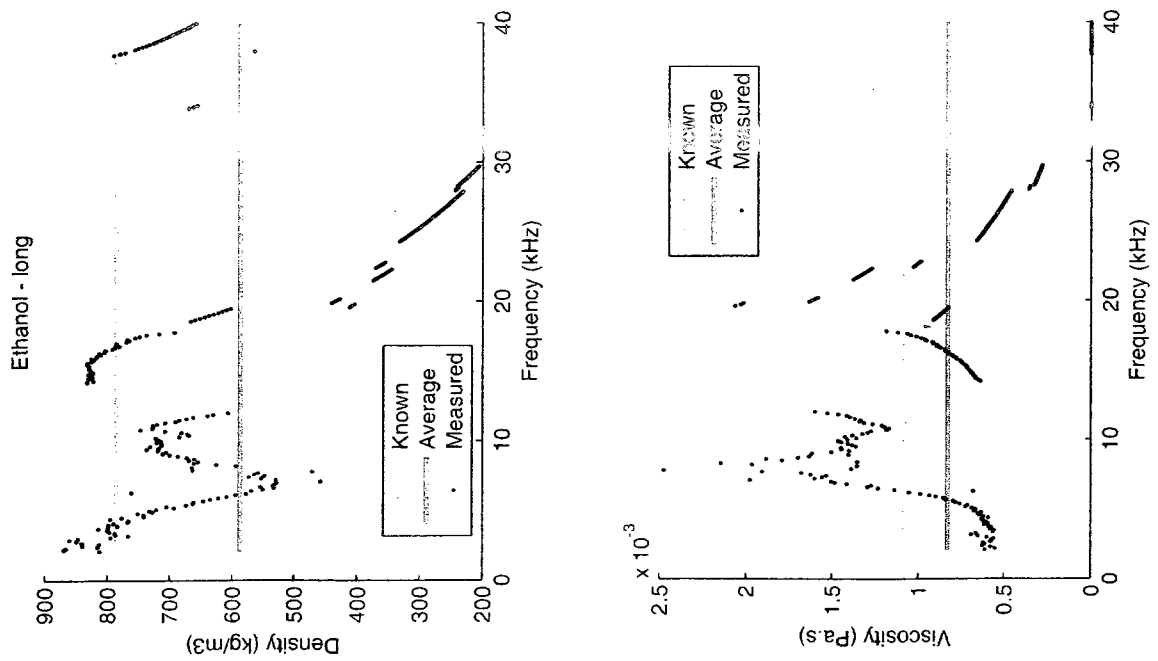
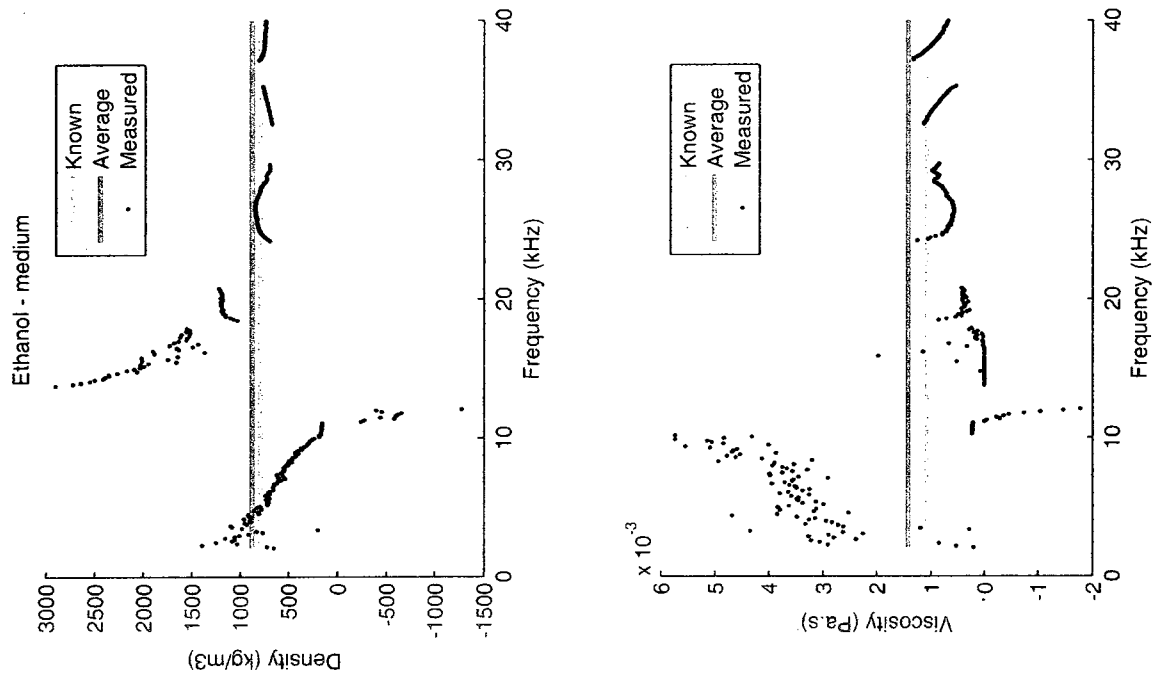
subplot(2,2,3); hold on;
plot(ro_eta_control(:,1),mean(ro_eta_control(:,3))*ones(length(f)), 'r', 'LineWidth',2);
plot(ro_eta_control(:,1),ro_eta_control(:,3), 'k', 'LineWidth',2);
legend('Average','Error','Location','Best'); title('Density error'); hold off;

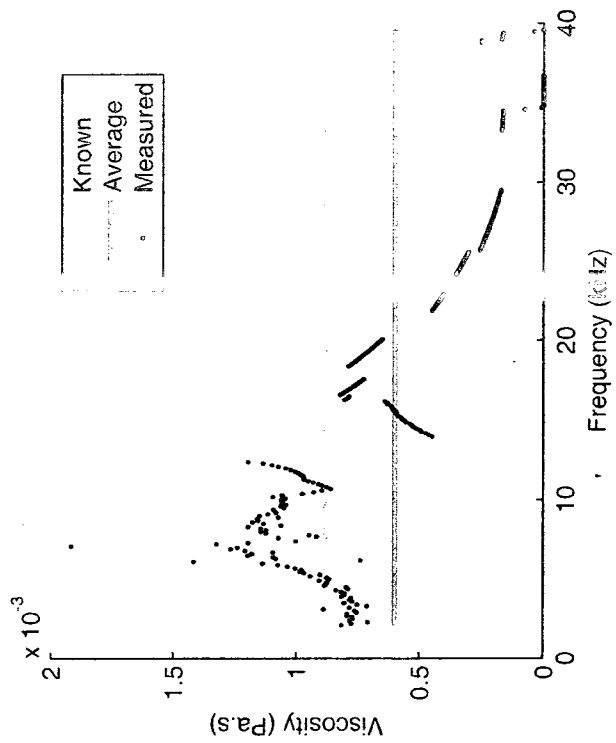
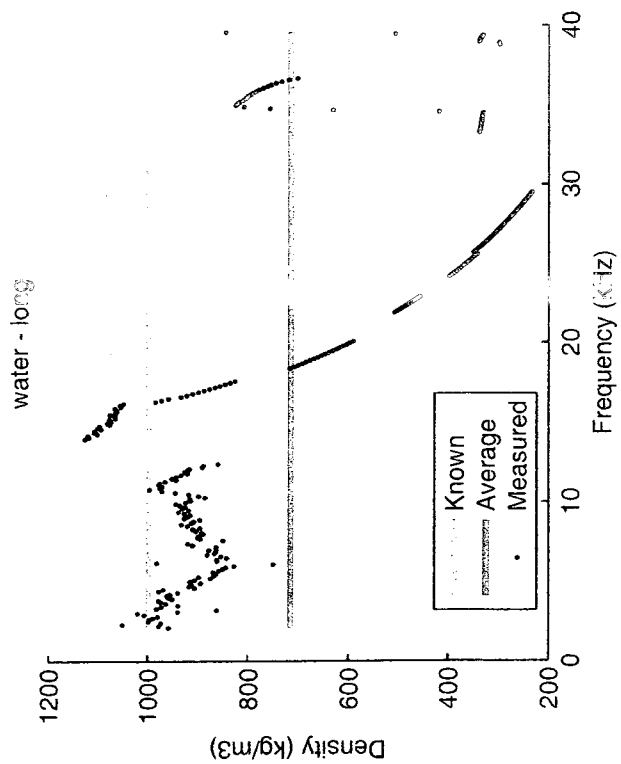
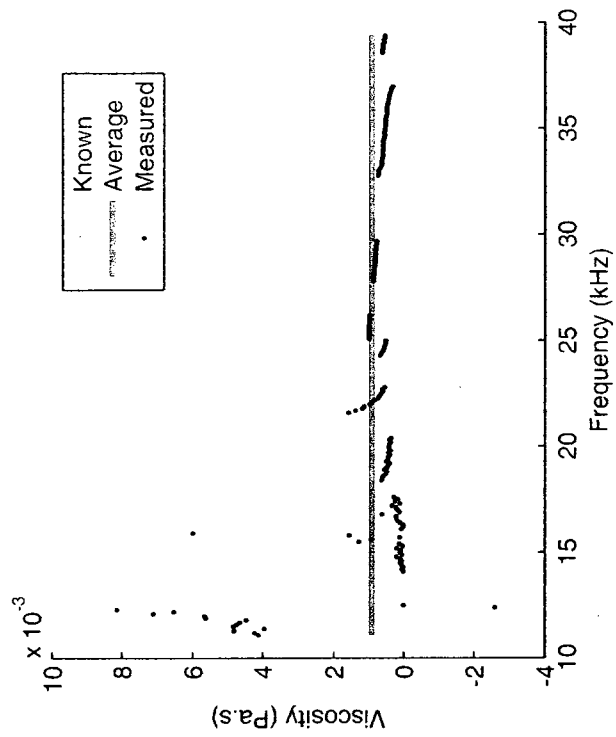
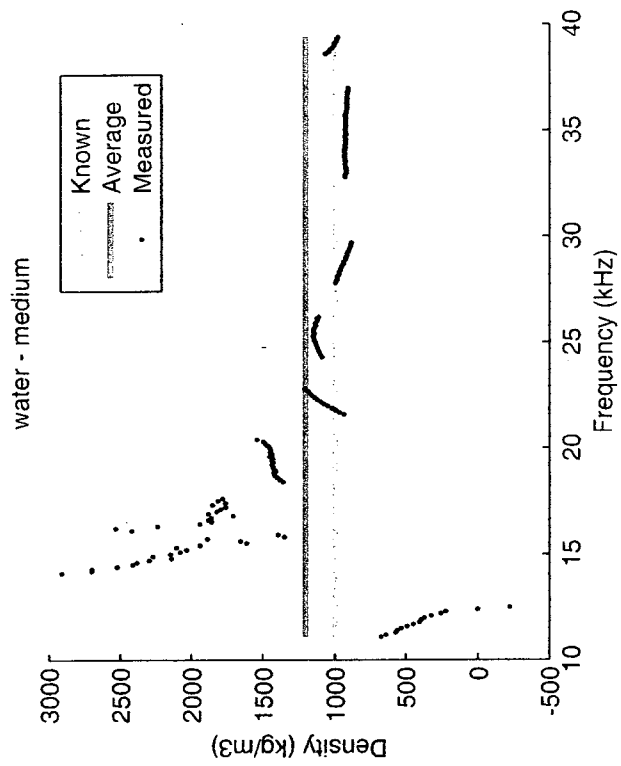
subplot(2,2,4); hold on;
plot(ro_eta_control(:,1),mean(ro_eta_control(:,5))*ones(length(f)), 'r', 'LineWidth',2);
plot(ro_eta_control(:,1),ro_eta_control(:,5), 'k', 'LineWidth',2);
legend('Average','Error','Location','Best'); title('Viscosity error'); hold off;
%#####
%#####
%#####
clear f fluid filename0 g_ro_f g_eta_f ro_eta_control
toc
end

```

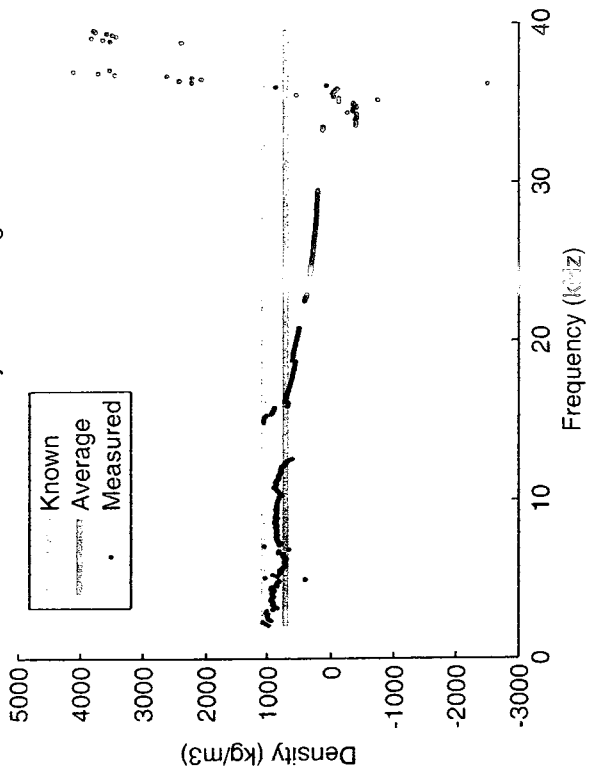
Appendix N

The effect of using different number of modes on the calculation of theoretical response:

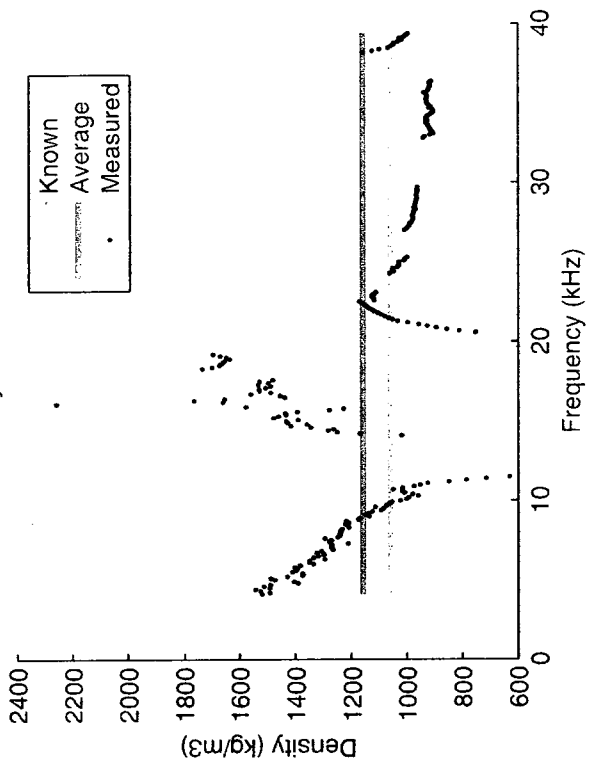




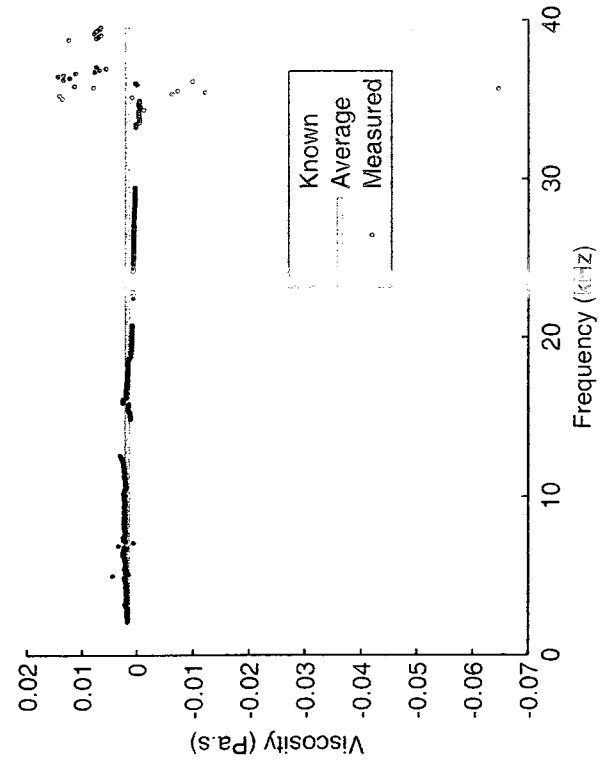
%25 Glycerine - long



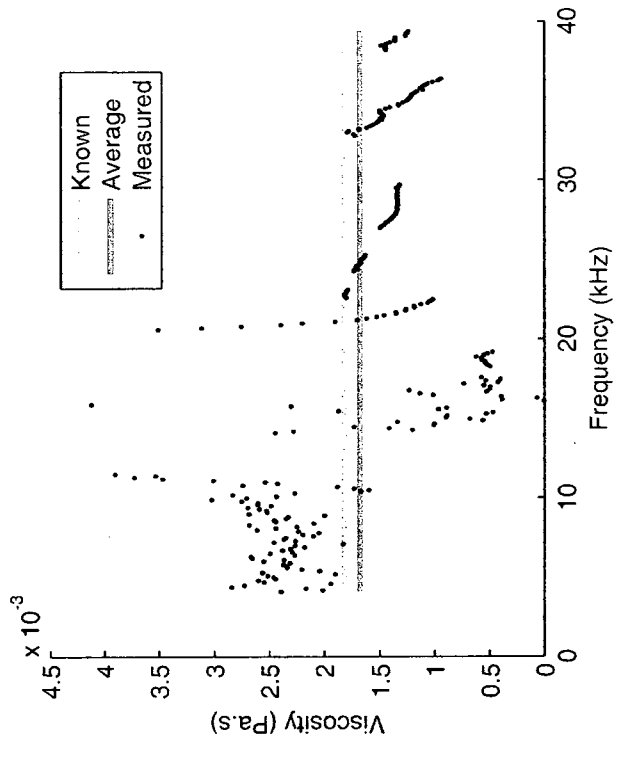
%25 Glycerine - medium



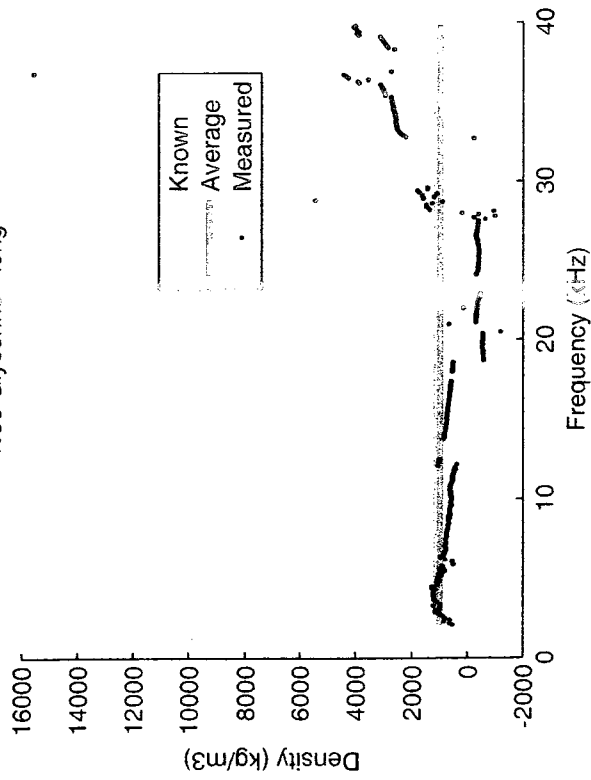
%25 Glycerine - long



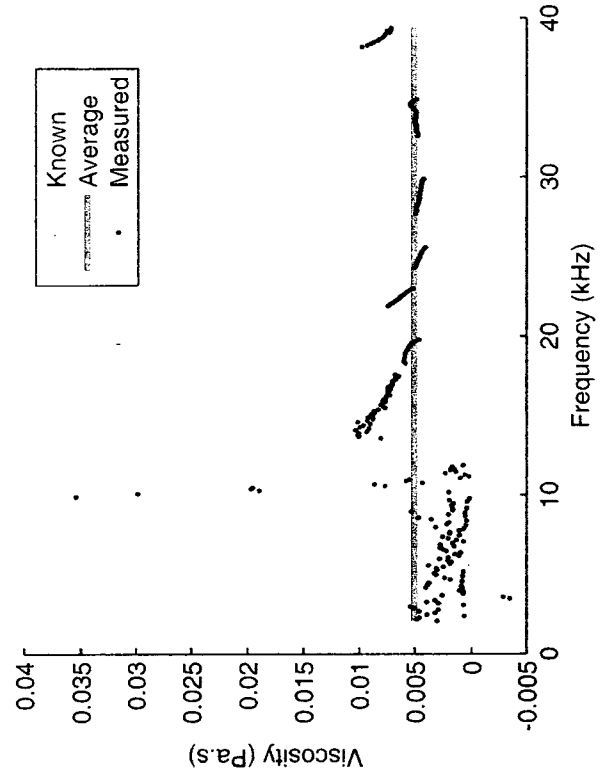
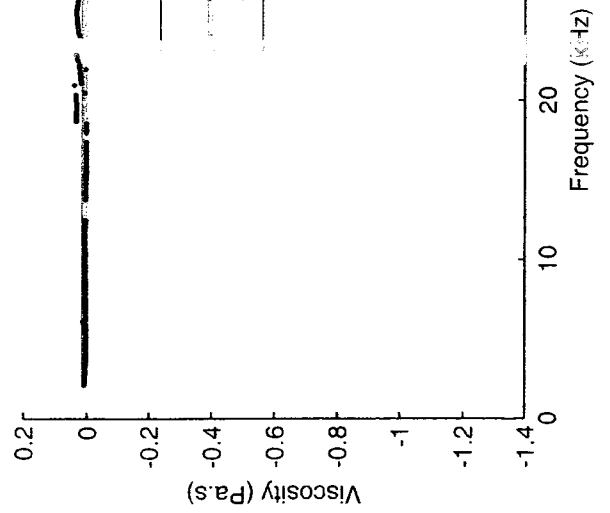
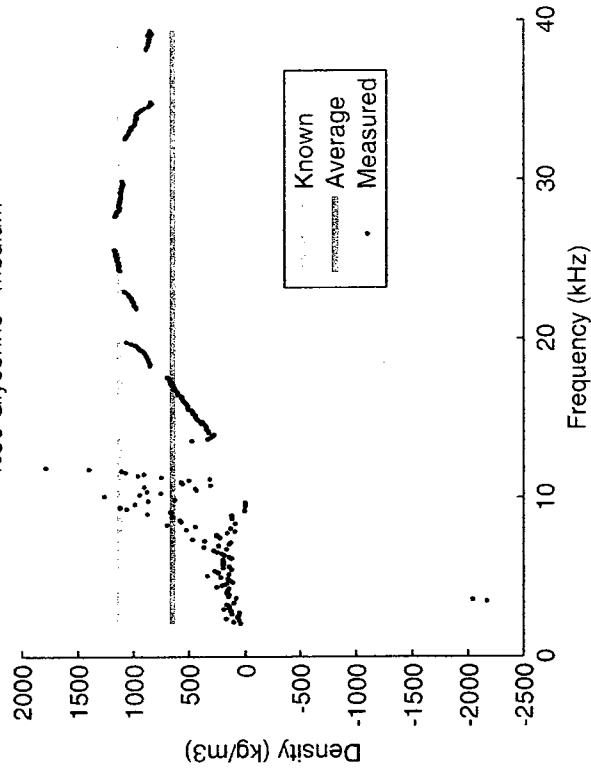
%25 Glycerine - medium

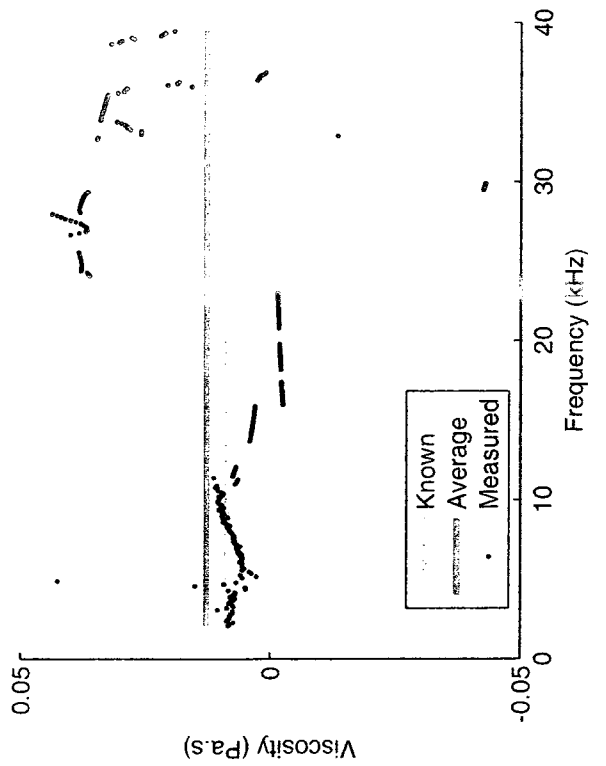
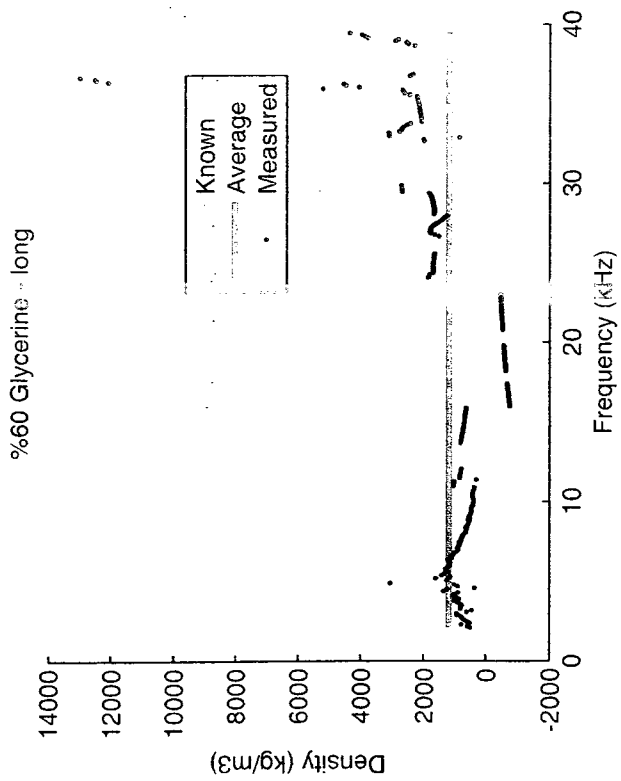
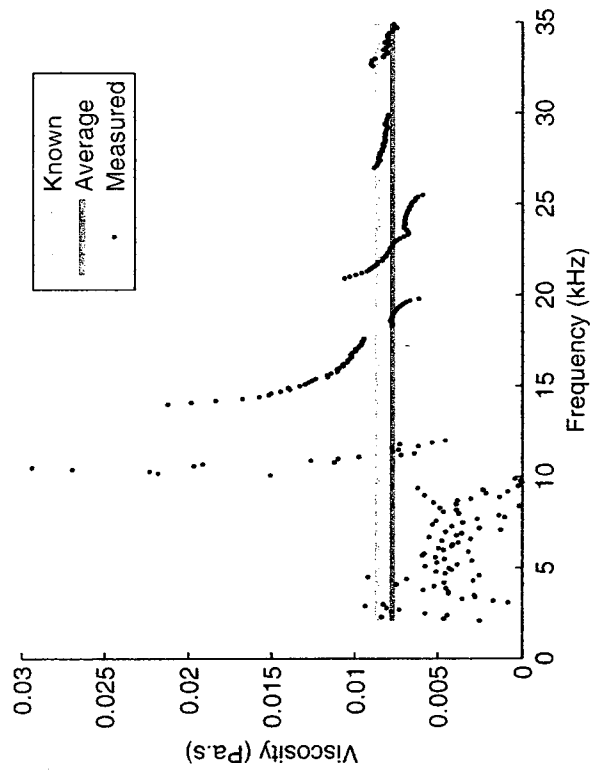
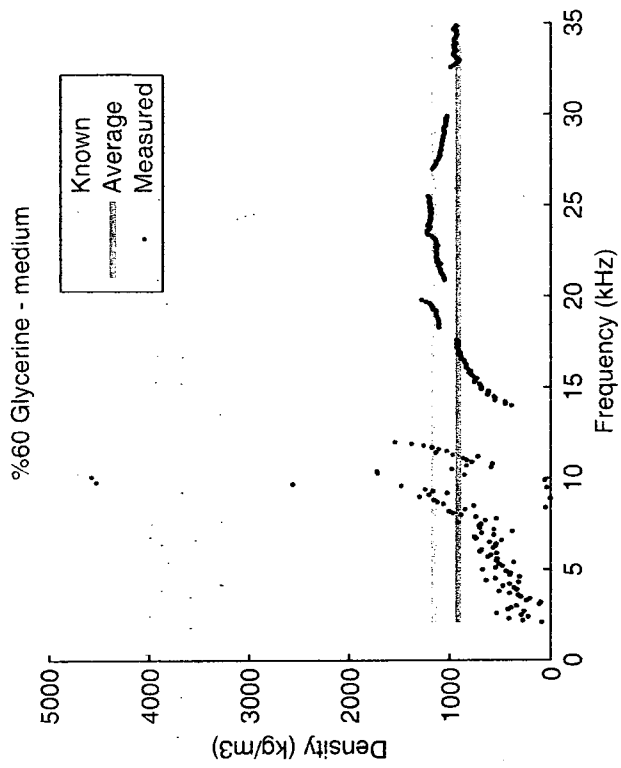


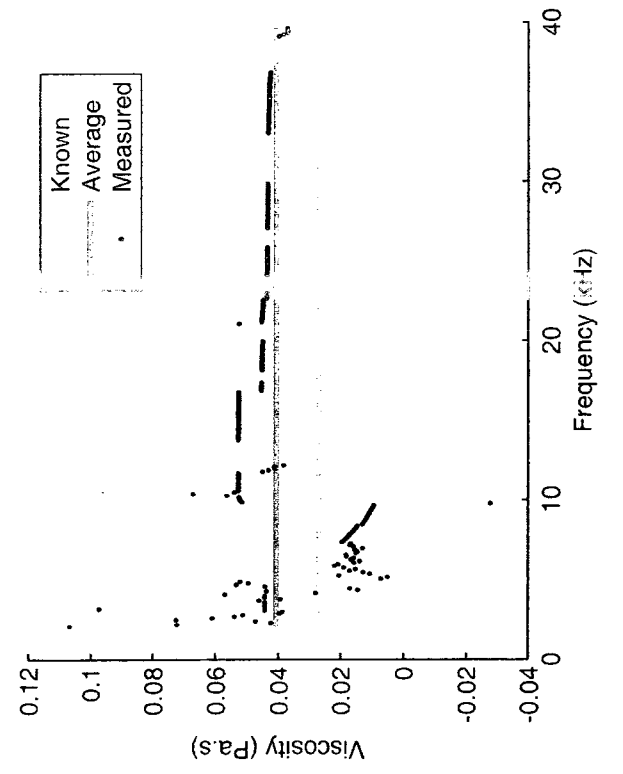
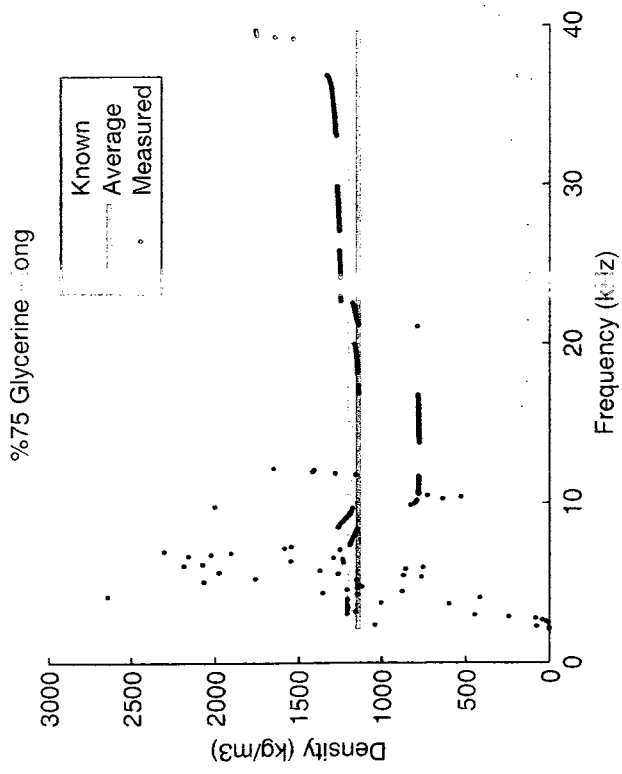
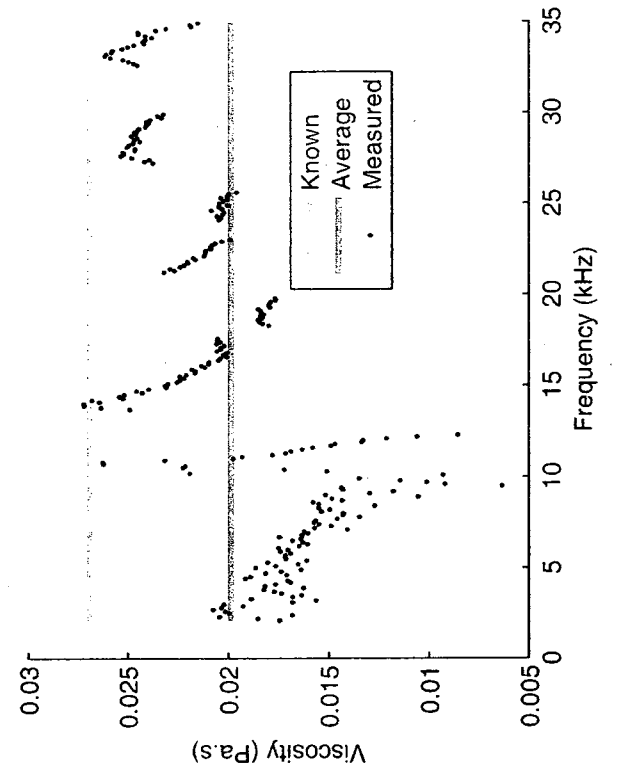
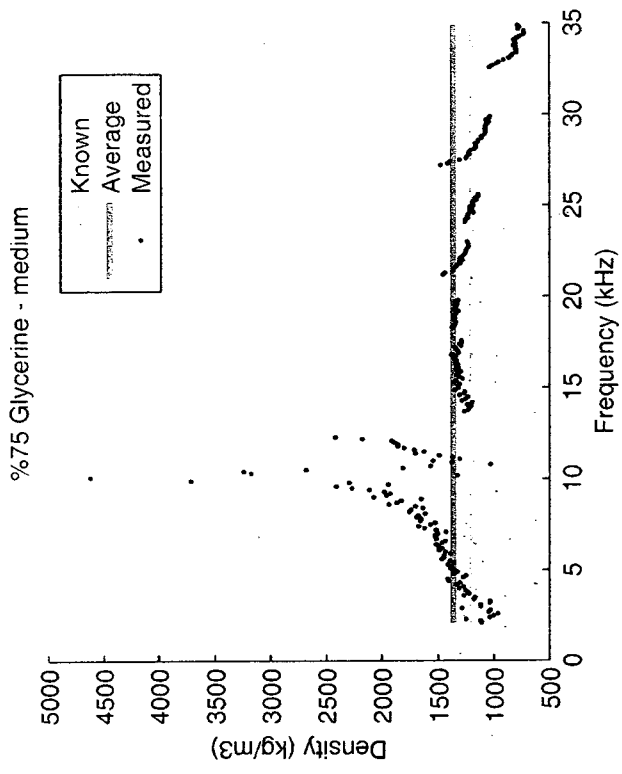
%50 Glycerino - long

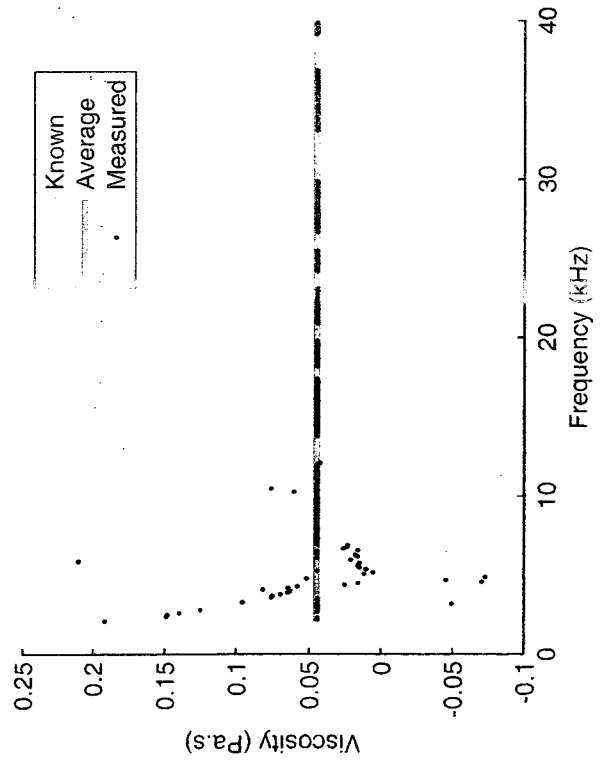
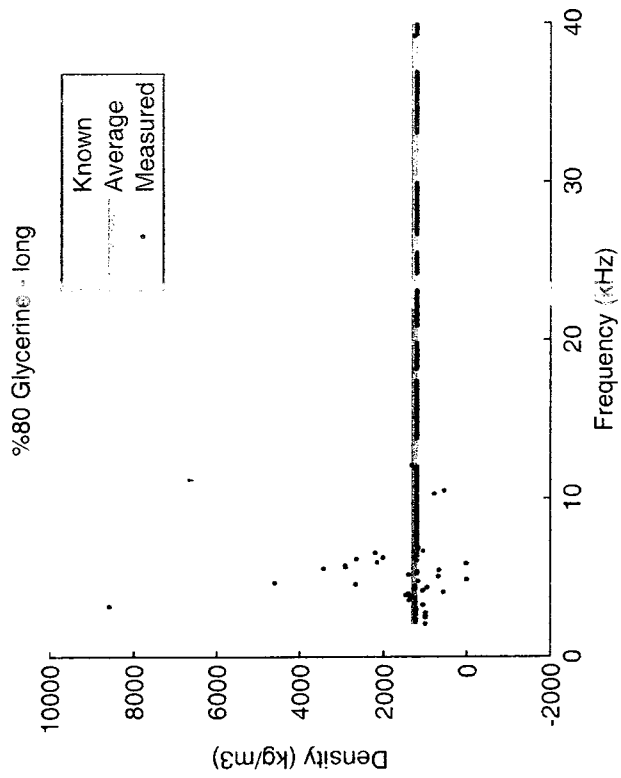
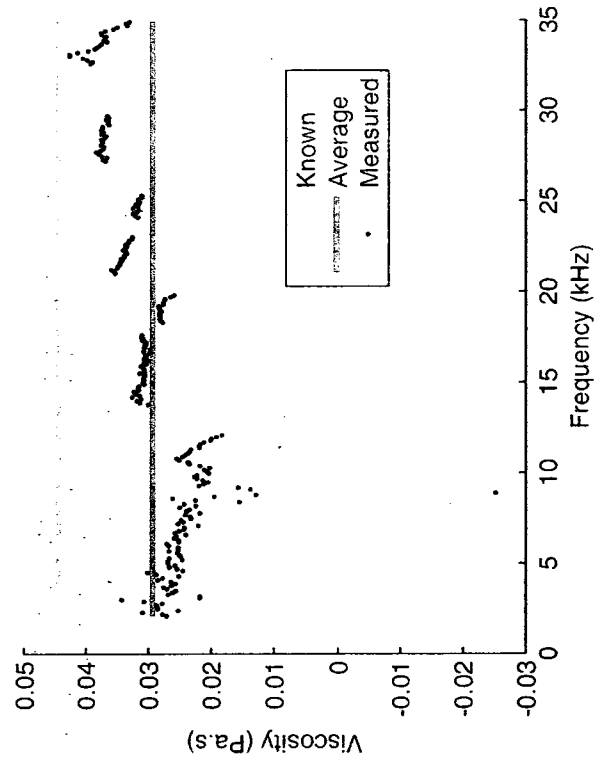
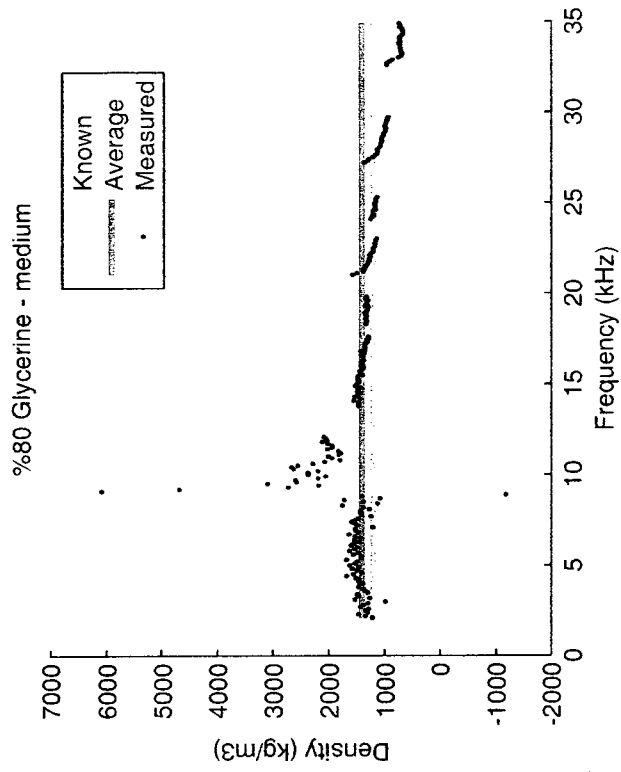


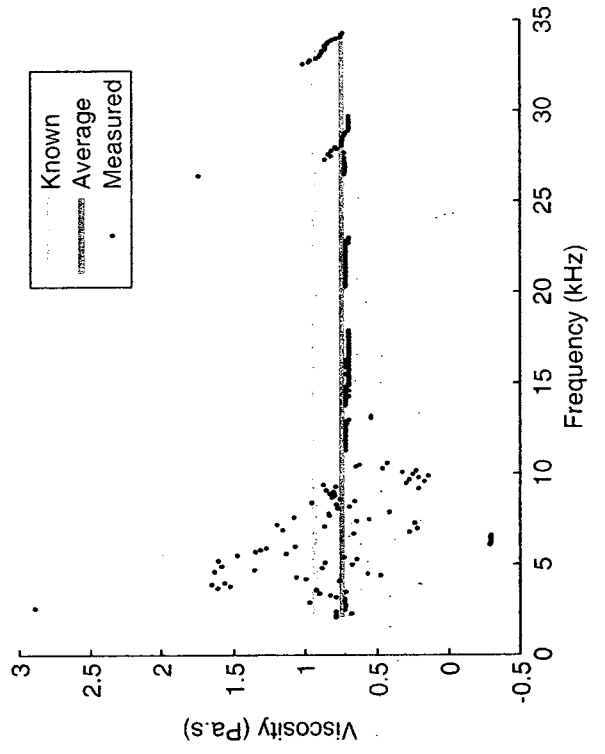
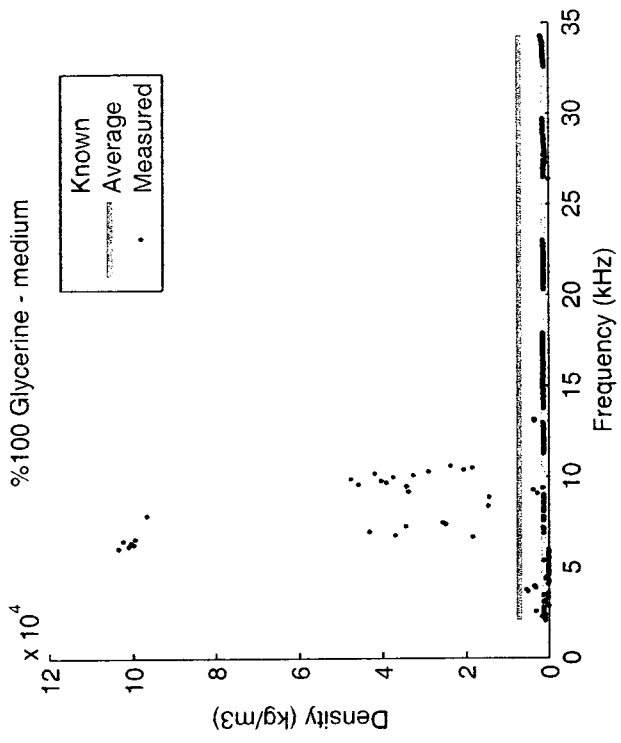
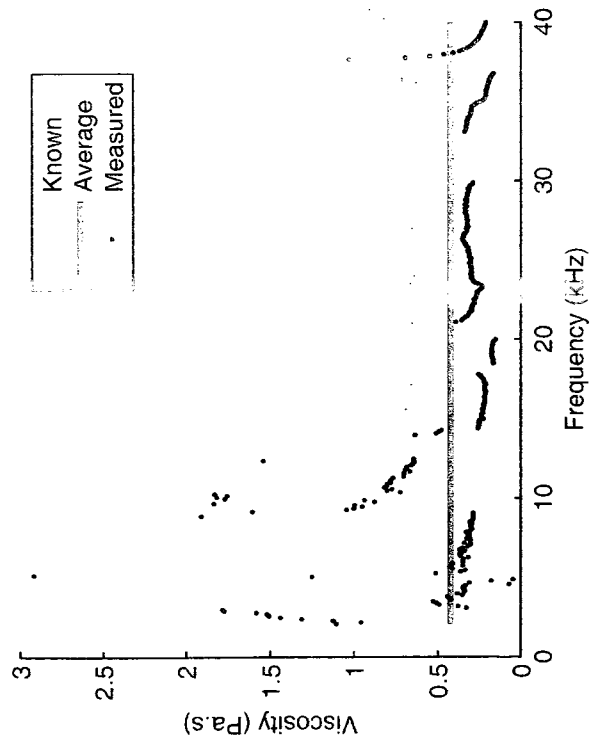
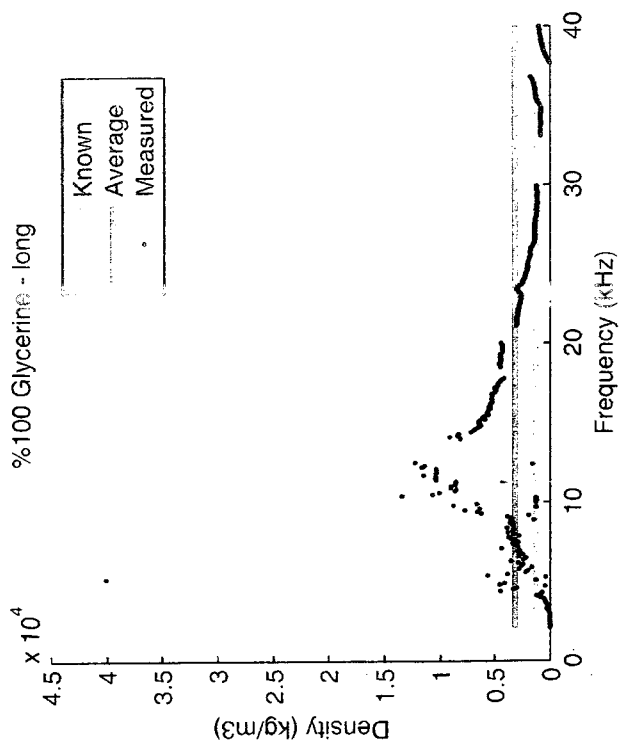
%50 Glycerine - medium





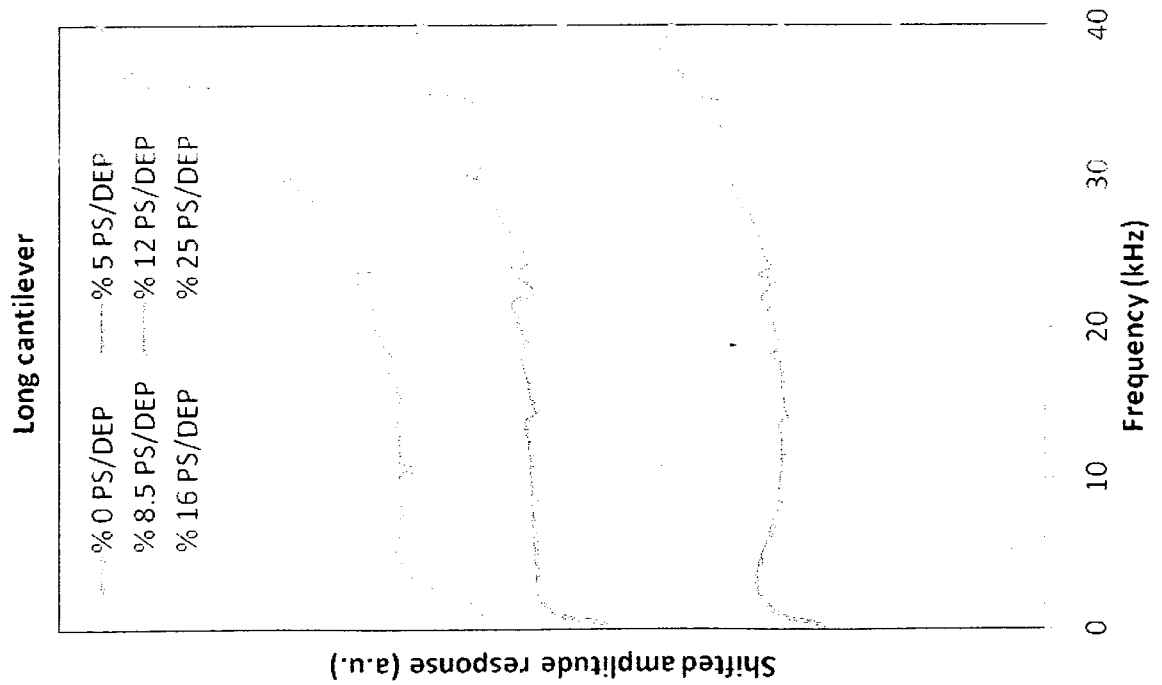
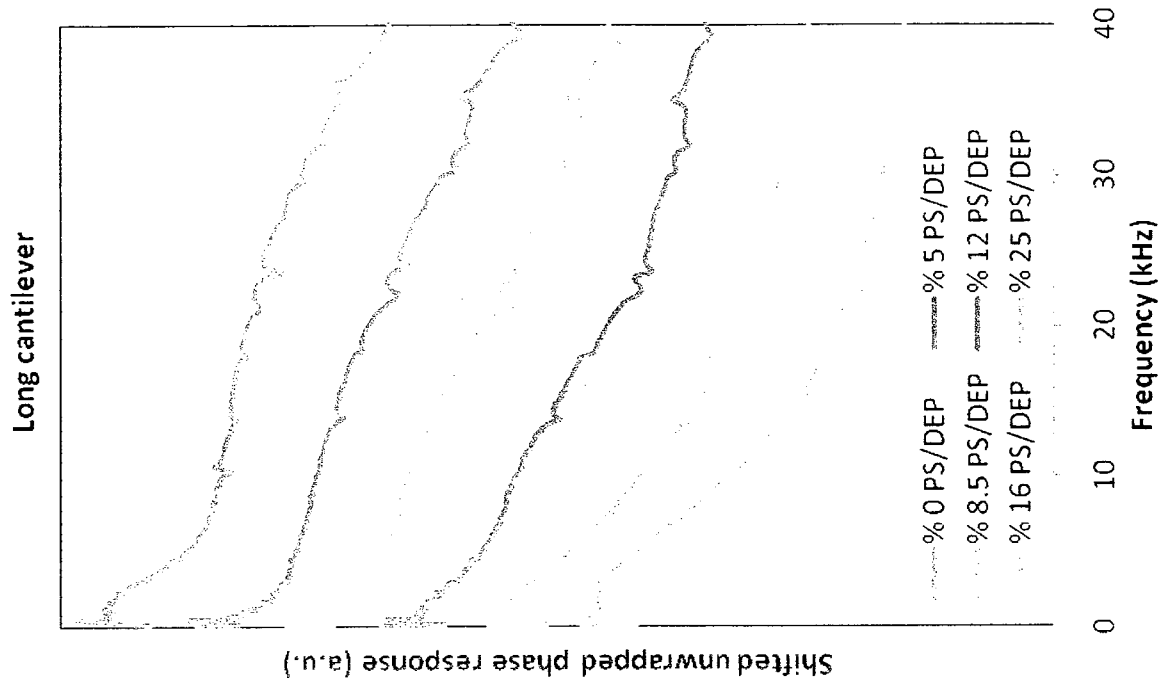




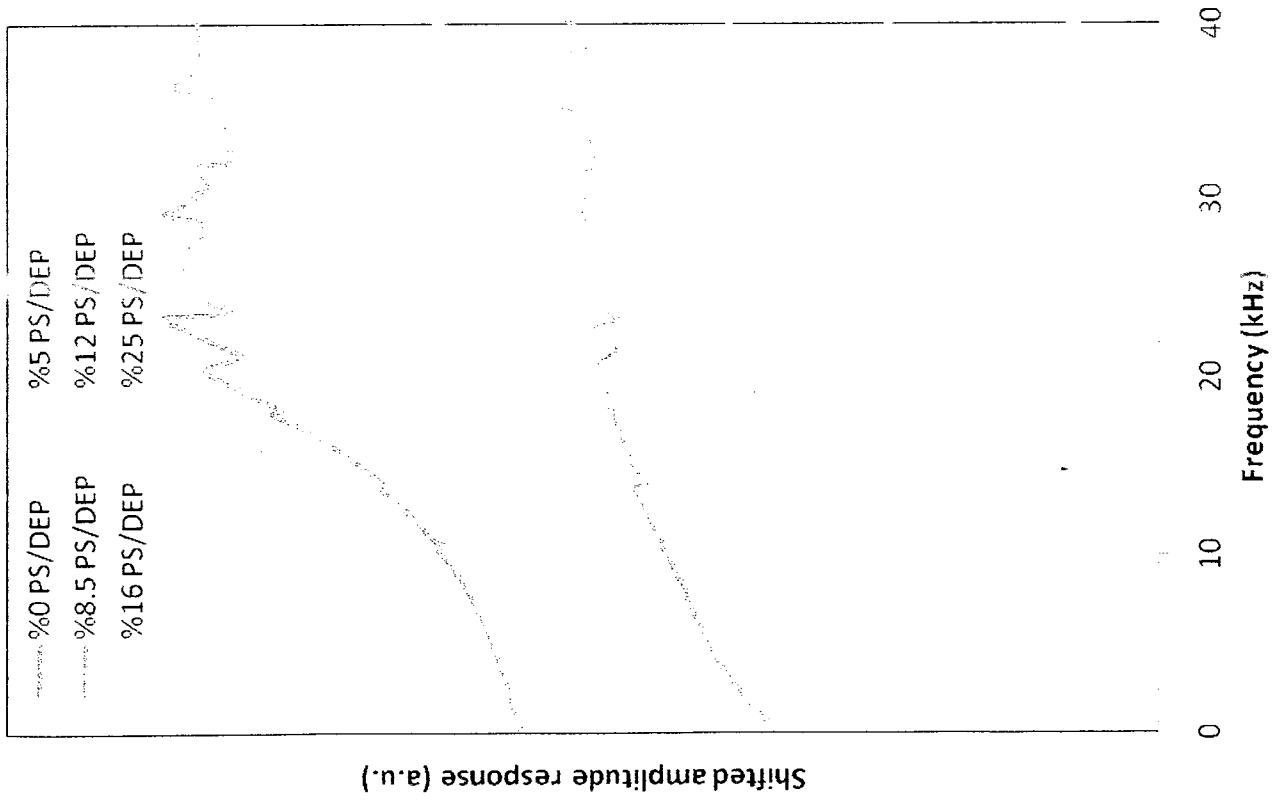


Appendix O

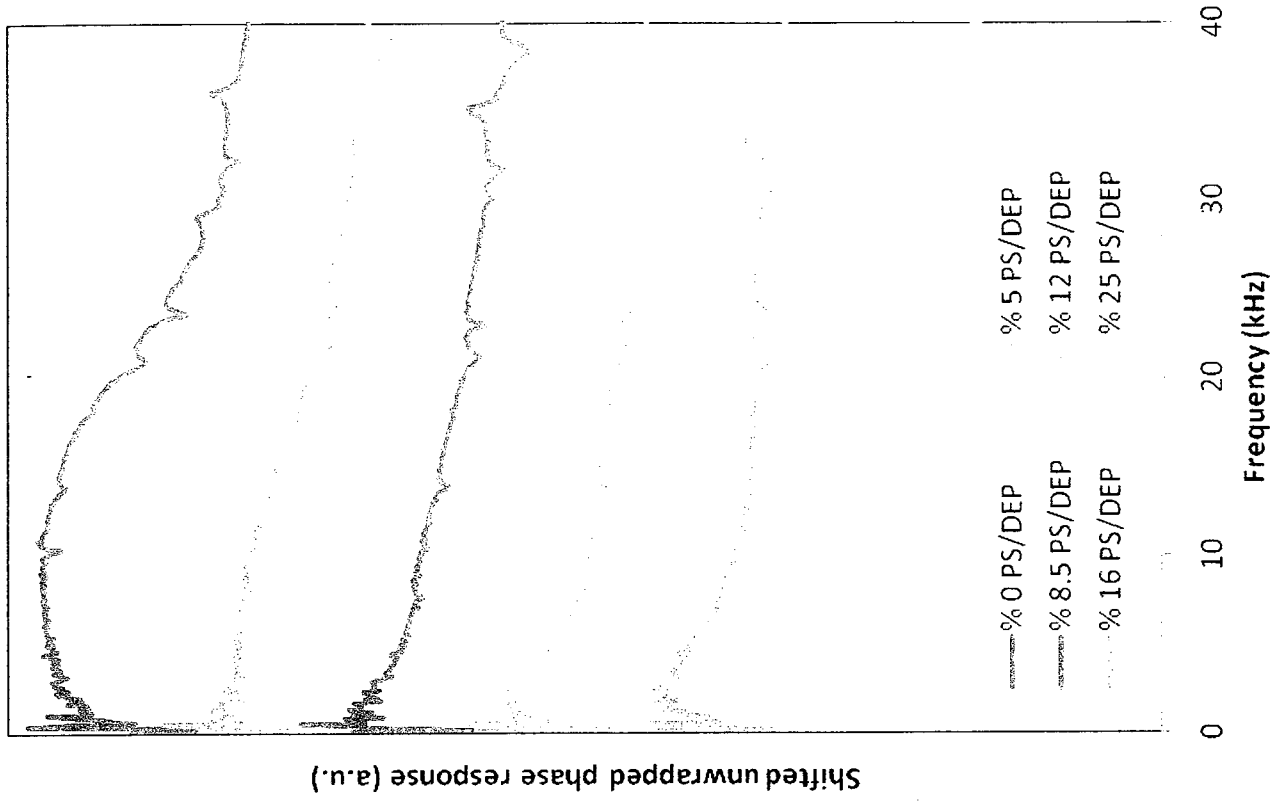
The responses of long and medium cantilevers in the non-Newtonian fluids:



Medium cantilever



Medium cantilever



REPORT OF EXTERNAL EXAMINER

A. Jeffrey Giacomin
Professor of Mechanical Engineering
Chair, Rheology Research Center
University of Wisconsin
Madison, WI

September 1, 2009

Micro Cantilever Based Rheology of Liquids
Ramin Motamedi, Ph.D.
Concordia University, 2009

I've been examining PhD theses in Mechanical Engineering generally, and in rheology in particular, since 1986. I've been doing so the Rheology Research Center at the University of Wisconsin since 1994. Motamedi's thesis stands out. The high quality of his Chapter 2 "Theory" earns him my respect as an engineer and as a scholar. Chapter 1 fearlessly introduces the rather formidable problems associated with interpreting the response of a tiny vibrating beams immersed in a fluid, and in terms of the density and rheology of this surrounding fluid. Chapter 2 then skillfully ploughs through the many problems with which others have grappled and capably arrives at a novel improvement to existing methods for the measuring the Newtonian viscosity of tiny quantities of precious liquids. Figure 5.31 is a substantial contribution to experimental engineering science. He has also capably mapped out the future for his research area, by preparing the extension of his work to tiny quantities of precious non-Newtonian fluids. The thesis leaves the reader yearning for the next student's installment of future work.

This thesis easily matches the highest quality theses defended in my own Mechanical Engineering Department at the University of Wisconsin. I would also place it among the top 5% of the theses defended in rheology, all disciplines, at the University of Wisconsin.

Typographical Errors

1. Page 1: "Noble" should be "Nobel".
2. Page 3: "reviewed in details." should be "reviewed in detail."
3. Page 21: "this error respect" should be "this error with respect".
4. Page 33: "Combing" should be "Combining".
5. Page 54: "Furrier" should be "Fourier".
6. Page 77: "spectra leakage" should be "spectral leakage".
7. Page 146: "Cox-Mertz" should be "Cox-Merz". Also, include the Cox-Merz reference here.
8. Page 154: "et al" should be "et al.". Correct throughout.